

Characterisation of Novel Genetic Variants of Amyotrophic Lateral Sclerosis

By

Tobias Alexander Moll



Sheffield Institute for Translational Neuroscience

A thesis submitted for the degree of
Doctor of Philosophy (PhD)

June 2020

Abstract

Background: Amyotrophic lateral sclerosis (ALS) is an invariably fatal and relatively common neurodegenerative disorder without effective therapy. Identified genetic variants cluster in biological pathways including RNA processing, axonal transport, and protein homeostasis. Discovery of new genetic variants within new biological pathways highlights new disease biology, and can lead to novel therapeutic targets. This project will focus on the development of cell and animal models to characterise novel ALS-associated mutations associated with GLT8D1, CAV1 and CAV2.

Aims and objectives: **i)** To evaluate the relative toxicity of ALS-associated GLT8D1 mutations in neuronal and non-neuronal cell lines via MTT and lactate dehydrogenase assays. **ii)** To investigate the effect of mutations on the enzyme activity of GLT8D1 using a UDP-Glo™ glycosyltransferase assay. **iii)** To test whether mutant GLT8D1 causes fragmentation of the Golgi network using immunocytochemistry. **iv)** To model GLT8D1 mutations in zebrafish larvae via RNA microinjection. **v)** To model CAV1/CAV2 enhancer mutations in neuronal and non-neuronal cells via CRISPR/Cas9 genome editing. **vi)** To measure ganglioside expression in human cells expressing GLT8D1, CAV1 and CAV2 mutations using live cell imaging.

Results: I studied in detail two ALS-associated GLT8D1 mutations: R92C and G78W. The relative toxicity of the mutations in model systems mirrors the clinical severity. Mutated GLT8D1 exhibits *in vitro* cytotoxicity and induces motor deficits in zebrafish larvae consistent with ALS. Identified GLT8D1 mutations are proximal to the substrate-binding site; both R92C and G78W mutations impair GLT8D1 enzyme activity. An R92C mutation reduces membrane ganglioside expression, which is indicative of dysregulated neurotrophic signalling. Ganglioside biosynthesis occurs in the Golgi; GLT8D1 localises to the Golgi in neuronal and non-neuronal cells, and preliminary data suggests an R92C mutation causes Golgi fragmentation. The second stage of this project follows the identification of ALS-associated variation within an enhancer linked to expression of CAV1/CAV2. CAV1 and CAV2 encode major components of caveolae, which organise membrane lipid rafts (MLR) important for neurotrophic signalling. Gangliosides are a key component of MLR. Discovered enhancer mutations reduce CAV1/CAV2 expression and disrupt ganglioside expression within MLR in patient-derived cells; and CRISPR/Cas9 perturbation proximate to a patient-mutation is sufficient to reduce CAV1/CAV2 expression in neurons.

Conclusions: These results place dysregulated ganglioside metabolism upstream in the pathogenesis of ALS. I propose that GLT8D1 and CAV1/CAV2 share a common pathway of pathogenesis in ALS via disruption of ganglioside recruitment to MLR and impaired neurotrophic signalling.

Declaration

I, Tobias Moll, confirm that this thesis is my own work. I am aware of the University's Guidance on the Use of Unfair Means (www.sheffield.ac.uk/ssid/unfair-means). This work has not been previously been presented for an award at this, or any other, university.

Where stated, sections of this thesis are comprised of the following published papers:

- **Chapter 1: Introduction** – Moll et al., 2020. Disrupted glycosylation of lipids and proteins is a cause of neurodegeneration. *Brain*. awz358. In addition to Moll et al., 2020, there is further discussion in Chapter 1 that is not published.
- **Chapter 3: ALS-linked G78W and R92C variants in GLT8D1 are toxic to HEK293 and N2A cells and impair enzyme activity** – Cooper-Knock et al., 2019. Mutations in the glycosyltransferase domain of GLT8D1 are associated with familial amyotrophic lateral sclerosis. *Cell Reports*. 26(9):2298-2306. In addition to Cooper-Knock et al., 2019, further results are presented in Chapter 3 that are not published.
- **Chapter 4: Knockdown of endogenous glt8d1 and overexpression of mutant GLT8D1 produces motor impairment in zebrafish larvae** – Cooper-Knock et al., 2019. Mutations in the glycosyltransferase domain of GLT8D1 are associated with familial amyotrophic lateral sclerosis. *Cell Reports*. 26(9):2298-2306. In addition to Cooper-Knock et al., 2019, further results are presented in Chapter 4 that are not published.

In addition, the following experimental chapter includes a paper currently in submission:

- **Chapter 6: Characterisation of ALS-associated CAV1/CAV2 enhancer variants** – Rare variant burden analysis within enhancers identifies *CAV1* as a new ALS risk gene. Available at: https://papers.ssrn.com/sol3/papers.cfm?abstract_id=3606796

At the start of each chapter, a full acknowledgment and reference of the publication is given, in addition to my contribution, as well as that of my co-authors and collaborators. Some chapters contain additional data and commentary that is not in the published/submitted manuscripts.

Dedication

This thesis is dedicated to Mr Lee Newton. The generous contribution from the Newton family has made this work possible, and I hope that this research will aid in the fight against motor neurone disease.

I would also like to dedicate this thesis to my father, Victor Moll. Your vision and work ethic inspired me from a young age. I hope I have made you proud.

Acknowledgements

I am highly indebted to the enthusiasm, commitment, and above all, friendship of Dr Johnathan Cooper-Knock, who has provided me with every opportunity to develop as a researcher. His passion and dedication have driven me to achieve things I did not think were possible. A very special mention goes to Professor Dame Pamela Shaw, for her continual guidance and support throughout this PhD, and for believing in my ability as a scientist. I would also like to thank Dr Janine Kirby for providing me with so much academic and personal support over the past five years.

This PhD would not have been as successful without the help of some very important people at SITraN, particularly Dr Adrian Higginbottom, who has been extremely generous with his time and has shown unprecedented levels of patience when helping me to develop my technical skills and my ability to think critically. I was extremely fortunate to have the support of the Hautbergue lab, who always found the time to explain protocols and help me with performing challenging experiments. I would like to extend my gratitude to Dr Tennore Ramesh for his help with the zebrafish work.

To all my friends and colleagues who have given me support, laughter and happiness along the way: John, Sam, Ramya, Helia, Dave, Andre, Robin, Toby, Osman, Mirinda, Emily, Charlotte, Ale, Matt, Nikita, Erica, Cleide, Allan, Alex...I love you all!

I would be in trouble if I did not mention my wonderful girlfriend, Anna, who is without question one of the most understanding and supportive people I have known. Thank you for putting up with my working evenings and weekends over the past three years!

Finally, this PhD would not have been possible without the love and support of my amazing family, particularly my mother, who has provided me with every opportunity in life, and has continually tried her hardest to understand what I do for a living. I would not have achieved half of what I have without the support of my amazing sister and best friend, Poppy. To the rest of the Moll family: Victor, Max, and Leo – I have always looked up to you boys and I hope I have made you as proud as I am of you.

Table of contents

List of figures.....	XII
List of tables.....	XIV
List of abbreviations.....	XV
Chapter 1. Introduction.....	1
1.1. Introduction to amyotrophic lateral sclerosis.....	1
1.2. Clinical presentation and disease management.....	1
1.3. Genetics of ALS.....	2
1.3.1. <i>SOD1</i>	3
1.3.2. <i>TARDBP</i>	3
1.3.3. <i>FUS</i>	4
1.3.4. <i>C9ORF72</i>	4
1.4. ALS pathological mechanisms.....	5
1.4.1. <i>Oxidative stress</i>	5
1.4.2. <i>Mitochondrial dysfunction</i>	6
1.4.3. <i>Impaired axonal transport</i>	6
1.4.4. <i>Dysregulated RNA metabolism</i>	6
1.4.5. <i>Impaired protein homeostasis</i>	7
1.4.6. <i>Non-cell autonomous toxicity and neuroinflammation</i>	7
1.5. Animal models of ALS.....	8
1.5.1. <i>Mouse models</i>	8
1.5.2. <i>Zebrafish models</i>	9
1.6. A literature review in the context of the present study: disrupted glycosyltransferase function is a cause of neurodegeneration.....	11
1.6.1. <i>Genetic mutations in glycosyltransferases are associated with neurodegeneration</i>	11
1.6.1.1. <i>UDP glycosyltransferase 8 (UGT8)</i>	13
1.6.1.2. <i>ST6 Beta-Galactoside Alpha-2,6-Sialyltransferase 1 (ST6GAL1)</i>	13
1.6.2. <i>Glycosyltransferases regulate ganglioside synthesis</i>	13
1.6.3. <i>Gangliosides are differentially distributed in the mammalian CNS</i>	14
1.6.4. <i>Gangliosides regulate neuroinflammation and neurotrophic action</i>	15
1.6.5. <i>Impaired ganglioside synthesis is linked to neurodegeneration</i>	17
1.6.5.1. <i>Parkinson's disease</i>	17
1.6.5.2. <i>Huntington's disease</i>	17

1.6.5.3. Alzheimer's disease.....	18
1.6.5.4. Amyotrophic lateral sclerosis	18
1.6.6. Gangliosides as a therapeutic target	19
1.6.6.1. Alzheimer's disease.....	19
1.6.6.2. Parkinson's disease.....	20
1.6.6.3. Amyotrophic lateral sclerosis	21
1.6.7. Glycosyltransferase O-GlcNAcylation: a key regulator of neurodegeneration?	24
1.6.7.1. O-GlcNAcylation is implicated in neurodegenerative disease.....	24
1.6.7.2. ALS-associated genetic variants within O-GlcNAcylation pathway enzymes.....	27
1.6.8. Summary	27
1.7. Work leading up to this study: GLT8D1	29
1.7.1. Exome sequencing in an autosomal dominant ALS pedigree identifies candidate deleterious variants	29
1.7.2. Targeted sequencing supports pathogenicity of variants within exon 4 of GLT8D1	29
1.7.3. Exon 4 of GLT8D1 is significantly enriched with ALS-associated rare deleterious variants affecting conserved amino acids.....	32
1.7.4. Clinical characteristics of patients with mutated GLT8D1	33
1.8. Work leading up to this study: CAV1 and CAV2	35
1.8.1. Discovery of ALS-linked CAV1/CAV2 enhancer mutations.....	35
1.8.2. Genetic variation within CAV1 coding sequence is associated with ALS.....	36
1.8.3. CAV1/CAV2 function and association with ALS	36
1.9. Overall objectives and hypotheses	38
1.9.1. Hypotheses:	38
1.9.2. Overall objectives:.....	38
Chapter 2. Materials and Methods	39
2.1. Materials.....	39
2.1.1. General materials.....	39
2.1.2. General buffers and solutions	39
2.1.3. Cell culture materials	39
2.1.4. Molecular biology materials	40
2.2. Methods	48
2.2.1. Cell culture	48
2.2.1.1. HEK293, Neuro-2A and SH-SY5Y cell line maintenance	48
2.2.1.2. HEK293 Sham and HEK293_GLT8D1-WT/R92C cell line generation ..	48

2.2.1.3. HEK293 Sham and HEK293_GLT8D1-WT/R92C stable cell line maintenance.....	49
2.2.1.4. Fibroblast cell maintenance	49
2.2.1.5. Lymphoblastoid cell maintenance.....	49
2.2.1.6. Generation of induced neural progenitor cells (iNPCs) from human fibroblasts	49
2.2.1.7. iNPC maintenance.....	50
2.2.1.8. Differentiation of iNPCs into iNeurons.....	50
2.2.1.9. Differentiation of iNPCs into iAstrocytes	51
2.2.1.10. SH-SY5Y neuronal differentiation	51
2.2.1.11. Cryopreservation of Cell Lines	51
2.2.1.12. Tetracycline induction of stable HEK293 cell lines	52
2.2.1.13. Preparation and maintenance of dissociated primary mouse cortical neurons.....	52
2.2.1.14. CRISPR editing of mammalian cell lines	52
2.2.1.15. Determining CRISPR editing efficiency	53
2.2.1.16. Liposome-mediated cell transfection.....	53
2.2.1.17. Electroporation-mediated cell transfection	54
2.2.2. Molecular cloning	56
2.2.2.1. Plasmid cloning by polymerase chain reaction (PCR).....	56
2.2.2.2. Agarose gel electrophoresis	56
2.2.2.3. DNA extraction from agarose gels	57
2.2.2.4. Restriction digests for PCR insert	57
2.2.2.5. Phenol-chloroform extraction for DNA purification	57
2.2.2.6. Plasmid ligation	58
2.2.2.7. Site-directed mutagenesis.....	58
2.2.2.8. LB agar plates	59
2.2.2.9. Plasmid transformation into competent <i>E. coli</i>	59
2.2.2.10. DNA extraction and purification from bacterial cultures	60
2.2.2.11. Restriction digests for plasmid characterisation	61
2.2.2.12. Quantitative Real-Time PCR (qRT-PCR)	61
2.2.3. Biochemical methods	61
2.2.3.1. Sodium dodecyl sulphate-polyacrylamide gel preparation.....	61
2.2.3.2. Cell lysis for immunoblotting	62
2.2.3.3. SDS-polyacrylamide gel electrophoresis	63
2.2.3.4. Immunoblotting.....	64

2.2.3.5. Coomassie blue staining	64
2.2.3.6. Immunoprecipitation (IP) of FLAG-tagged GLT8D1	64
2.2.3.7. Glycosyltransferase activity assay	65
2.2.3.8. Immunocytochemistry	66
2.2.3.9. Multiphoton and confocal microscopy imaging and image analysis	67
2.2.3.10. Live-cell imaging using fluorescent molecular probes	67
2.2.3.11. MTT cell viability assay	67
2.2.3.12. Lactate dehydrogenase assay	68
2.2.4. Modelling in zebrafish (<i>Danio rerio</i>)	68
2.2.4.1. RNA Synthesis for zebrafish embryo microinjection	68
2.2.4.2. Generation of a morpholino for zebrafish embryo microinjection	69
2.2.4.3. Zebrafish maintenance and breeding	70
2.2.4.4. Zebrafish embryo microinjection	70
2.2.4.5. Behavioural analysis	70
2.2.4.6. Zebrafish RT-PCR	71
2.2.4.7. Zebrafish immunoblotting	72
2.2.6. Statistical analysis	72
Chapter 3. ALS-linked G78W and R92C variants in GLT8D1 are toxic to HEK293 and N2A cells and impair enzyme activity	73
3.1. Introduction	73
3.2. Aims and objectives for characterising ALS-linked G78W and R92C mutations in GLT8D1	74
3.3. Results	74
3.3.1. Generation and characterisation of pEGFP-N1_GLT8D1-eGFP and pcDNA5/FRT/TO_3xFLAG-GLT8D1 expression vectors	74
3.3.2. Flp-In™ T-REx™ GLT8D1 isogenic HEK293 cell line generation	75
3.3.3. Generation of microRNA plasmids targeting human GLT8D1	76
3.3.4. Structural-based sequence alignment identifies 5GVV (<i>S. pneumonia</i> glycosyltransferase glyE) as a structural homologue of GLT8D1	79
3.3.5. A GLT8D1-R92C mutation reduces viability and increases cytotoxicity of HEK293 and N2A cells	81
3.3.6. An ALS-linked R92C mutation impairs the glycosyltransferase activity of GLT8D1	85
3.3.7. ALS-linked G78W and R92C mutations impair the glycosyltransferase activity of GLT8D1	90
3.4. Discussion	94
3.4.1. Generation of pEGFP-N1_GLT8D1-eGFP and pcDNA5/FRT/TO_3xFLAG-GLT8D1 plasmid constructs	94

3.4.2. Generation of the Flp-In T-REx TM GLT8D1 host cell lines	95
3.4.3. Structural-based sequence alignment identifies 5GVV as a homologue of GLT8D1	96
3.4.4. ALS-linked GLT8D1 mutations are toxic to HEK293 and N2A cells	96
3.4.5. ALS-linked GLT8D1 mutations impair glycosyltransferase activity.....	99
3.4.6. Clinicopathological characterisation of patients with ALS-linked GLT8D1 mutations	100
3.4.7. Ganglioside signalling as a GLT8D1-ALS pathological mechanism.....	101
3.4.8. Summary	101
Chapter 4. Knockdown of endogenous <i>glt8d1</i> and overexpression of mutant GLT8D1 produces motor impairment in zebrafish larvae	103
4.1. Introduction	103
4.2. Aims and objectives to investigate whether knockdown of endogenous <i>glt8d1</i> , or overexpression of mutant GLT8D1 mRNA, cause motor impairment in zebrafish larvae.....	104
4.3. Results	105
4.3.1. Knockdown of endogenous <i>glt8d1</i> impairs motor function in zebrafish larvae.....	105
4.3.2. Overexpression of GLT8D1-G78W and GLT8D1-R92C mRNA impairs motor function in zebrafish larvae, compared to overexpression of GLT8D1-WT mRNA.....	108
4.4. Discussion	115
4.4.1. Zebrafish as a neurodegenerative disease model.....	115
4.4.2. Advantages and limitations concerning the use of AMOs	118
4.4.3. Transient knockdown of endogenous <i>glt8d1</i> causes motor impairment in zebrafish larvae	119
4.4.4. Overexpression of mutant human GLT8D1 mRNA produces motor impairment in zebrafish larvae	121
4.4.5. Summary	122
Chapter 5. Membrane ganglioside concentration is dependent on GLT8D1 enzyme activity	123
5.1. Introduction.....	123
5.2. Aims and objectives for investigating the effects of an R92C variant in GLT8D1 on ganglioside expression and Golgi fragmentation	124
5.3. Results	124
5.3.1. An R92C variant in GLT8D1 reduces the expression of sialic acid and N-Acetylglucosamine (GlcNAc) residues in isogenic HEK293-GLT8D1 cell membranes	124
5.3.2. Overexpression of mutant GLT8D1 reduces membrane and cytoplasmic GM1 expression in isogenic HEK293-GLT8D1 cells.....	128

5.3.3. <i>GLT8D1-ALS patient fibroblasts did not successfully re-programme into induced neural progenitor cells</i>	130
5.3.4. <i>Membrane GlcNAc and sialic acid residue expression is unchanged in GLT8D1-ALS patient fibroblasts compared to an age- and sex-matched control</i>	131
5.3.5. <i>GLT8D1 is localised to the Golgi network when transiently overexpressed in HEK293 and N2A cells</i>	133
5.3.6. <i>Overexpression of an R92C variant in GLT8D1 causes fragmentation of the Golgi network in isogenic HEK293-GLT8D1 cells</i>	135
5.4. Discussion	138
5.4.1. <i>An R92C variant in GLT8D1 reduces the expression of sialic acid and N-Acetylglucosamine (GlcNAc) residues in isogenic HEK293 cell membranes</i> ...	138
5.4.2. <i>Overexpression of mutant GLT8D1 reduces membrane and cytoplasmic GM1 expression in isogenic HEK293 cells</i>	140
5.4.3. <i>GLT8D1-ALS patient fibroblasts did not successfully re-programme into induced neural progenitor cells</i>	142
5.4.4. <i>Membrane GlcNAc and sialic acid residue expression is unchanged in GLT8D1-ALS patient fibroblasts compared to an age- and sex-matched control</i>	143
5.4.5. <i>GLT8D1 is localised to the Golgi network when overexpressed in HEK293 and N2A cells</i>	144
5.4.6. <i>Overexpression of an R92C variant in GLT8D1 may cause fragmentation of the Golgi network in HEK293 cells</i>	145
5.4.7. <i>Summary</i>	148
Chapter 6. Characterisation of ALS-associated CAV1/CAV2 enhancer variants	149
6.1. Introduction	149
6.2. Aims and objectives for experimentally evaluating ALS-associated CAV1/CAV2 enhancer variants.....	152
6.3. Results	153
6.3.1. <i>CAV1 and CAV2 expression is reduced in patient-derived cells carrying an ALS-associated enhancer variant</i>	153
6.3.4. <i>An ALS-associated CAV1/CAV2 enhancer variant impairs MLR integrity in LCLs</i>	157
6.3.5. <i>CRISPR/Cas9 enhancer editing reduces CAV1/CAV2 expression in differentiated SH-SY5Y cells</i>	161
6.4. Discussion	168
6.4.1. <i>CAV1 and CAV2 expression are reduced in patient-derived cells carrying an ALS-associated enhancer variant</i>	168
6.4.2. <i>Patient-derived LCLs carrying an ALS-associated CAV enhancer variant have disrupted MLR</i>	170
6.4.3. <i>CRISPR/Cas9 genome editing of human cells</i>	171

6.4.4. <i>Generation of a CRISPR-edited neuronal model</i>	173
6.4.5. <i>Summary</i>	175
Chapter 7. <i>Conclusions and future directions</i>	177
7.1. <i>Conclusions</i>	177
7.1.1. <i>ALS-associated GLT8D1 mutations act via a dominant-negative mechanism</i>	177
7.1.2. <i>GLT8D1 mutations fragment the Golgi and disrupt ganglioside-containing membrane lipid rafts</i>	179
7.1.3. <i>CAV1/CAV2 enhancer mutations also disrupt membrane lipid rafts</i>	182
7.1.4. <i>Identified genetic risk factors converge on disruption of neurotrophic signalling</i>	183
7.2. <i>Future directions</i>	185
References	188
Appendices.....	224
Research outputs from the work of my PhD	242

List of figures

Figure 1.1. Schematic overview of the biosynthesis and function of major gangliosides within the mammalian brain	16
Figure 1.2. Timeline of the key events in the characterisation of gangliosides and their role in neurodegenerative disease.	23
Figure 1.3. O-GlcNAcylation is implicated the pathophysiology of neurodegenerative disease	26
Figure 1.4. Discovery of ALS-Associated Mutations within Exon 4 of GLT8D1 in Close Proximity to the Putative Substrate Binding Site	31
Figure 1.5. Significant enrichment of ALS genetic-risk within enhancers and coding regions linked to CAV1 and CAV2.....	37
Figure 3.1. Construction and validation of pEGFP-N1_GLT8D1 and pcDNA5/FRT/TO_3xFLAG_GLT8D1 plasmids.....	77
Figure 3.2. Flp-In™ and T-REx™ systems used to generate isogenic HEK293 cell lines with tetracycline-inducible expression of WT and mutated GLT8D1	78
Figure 3.3. Structural-based sequence alignment identifies 5GVV (<i>S. pneumoniae</i> glycosyltransferase glyE) as a related homologue of GLT8D1	80
Figure 3.4. Overexpression of mutated GLT8D1 causes cytotoxicity and reduces viability in HEK293 and N2A cells compared to overexpression of the WT protein.....	82
Figure 3.5. Immunoblotting shows similar expression levels of WT and mutant GLT8D1 in HEK293 and N2A cells	84
Figure 3.6. Immunoblotting confirms tetracycline-inducible expression of GLT8D1-WT and GLT8D1-R92C in isogenic HEK293 cells.....	86
Figure 3.7. Immunopurification of GLT8D1-WT and GLT8D1-R92C from tetracycline-induced isogenic HEK293 cells	87
Figure 3.8. Validating the linear range for determination of accurate UDP concentration measurements for the UDP-Glo™ glycosyltransferase assay.....	88
Figure 3.9. ALS-linked GLT8D1-R92C mutation impairs glycosyltransferase activity	89
Figure 3.10. Immunopurification of GLT8D1-WT, GLT8D1-G78W and GLT8D1-R92C recombinant proteins from HEK293 cells	91
Figure 3.11. ALS-linked GLT8D1-G78W and GLT8D1-R92C mutations impair glycosyltransferase activity	93
Figure 4.1. Agarose gel electrophoresis showing a reduction in the expression of zebrafish GLT8D1 RNA following microinjection of ~1.5ng splice blocking AMO.....	105
Figure 4.2. Knockdown of endogenous <i>glt8d1</i> correlates with a reduction in the velocity and distance moved by zebrafish larvae at 5dpf.....	107
Figure 4.3. Generation of GLT8D1-WT, GLT8D1-G78W and GLT8D1-R92C mRNA for zebrafish embryo microinjection	109
Figure 4.4. Overexpression of GLT8D1-WT and GLT8D1-R92C in zebrafish embryos is confirmed via immunoblotting at 2dpf.....	110
Figure 4.5. Survival of zebrafish embryos following microinjection of human mRNA encoding GLT8D1-WT, GLT8D1-G78W and GLT8D1-R92C.....	112
Figure 4.6. Overexpression of GLT8D1-G78W and GLT8D1-R92C mRNA produces motor impairment in zebrafish larvae, compared to overexpression of GLT8D1-WT	114

Figure 5.1. GLT8D1-R92C expression is enhanced in isogenic HEK293-GLT8D1 cell lines compared to WT	126
Figure 5.2. ALS-linked R92C mutation in GLT8D1 reduces membrane sialic acid and N-Acetylglucosamine (GlcNAc) expression in isogenic HEK293-GLT8D1 cells.....	127
Figure 5.3. ALS-linked R92C mutation reduces membrane GM1 expression in isogenic HEK293-GLT8D1 cells	129
Figure 5.4. Poor growth rate was possibly a key factor preventing the direct conversion of GLT8D1-ALS patient fibroblasts into iNeurons	130
Figure 5.5. Membrane sialic acid and N-Acetylglucosamine (GlcNAc) expression is unchanged in GLT8D1-ALS patient fibroblasts compared to an age- and sex-matched control.....	132
Figure 5.6. When transiently over-expressed in HEK293 and N2A cells, GLT8D1 is localised to the Golgi network.....	134
Figure 5.7. Preliminary data suggest that overexpression of GLT8D1-R92C causes fragmentation of the trans-Golgi network in isogenic HEK293 cells.....	136
Figure 5.8. Preliminary data suggest that overexpression of GLT8D1-R92C causes fragmentation of the cis-Golgi network in isogenic HEK293 cells	137
Figure 6.1. An ALS-associated CAV1/CAV2-enhancer variant reduces CAV1 protein expression in LCLs	155
Figure 6.2. An ALS-associated CAV1/CAV2-enhancer variant reduces CAV1 and CAV2 mRNA expression in LCLs.....	156
Figure 6.3. A CellMask™ plasma membrane stain was not suitable for determining cell area in LCLs	157
Figure 6.4. Patient-derived LCLs carrying an ALS-associated CAV1/CAV2 enhancer variant have disrupted MLR.....	159
Figure 6.5. CTxB fluorescence intensity and CAV1 protein expression are positively correlated	160
Figure 6.6. CRISPR-directed perturbation of a CAV-enhancer region proximate to a patient mutation in LCLs	162
Figure 6.7. CRISPR-directed perturbation of a CAV-enhancer region proximate to a patient mutation in SH-SY5Y cells.....	164
Figure 6.8. Increased dendrite length and altered PAX6 expression suggests successful neuronal differentiation of SH-SY5Y cells	166
Figure 6.9. qPCR measurement of CAV1 mRNA and CAV2 mRNA reveals reduced expression in CAV-enhancer and CAV1-exon CRISPR-edited neurons, compared to CRISPR editing of HPRT	167
Figure 6.10. Schematic representation of the generation of a neuronal model of CAV-associated ALS	174
Figure 7.1. Graphical summary of key findings from the characterisation of pathogenic variants in GLT8D1	181
Figure 7.2. Graphical summary of key findings from the characterisation of pathogenic enhancer variants in CAV1 and CAV2, and a proposed ALS disease pathway	185
Figure 7.3. ALS-associated GLT8D1 and CAV1/CAV2 enhancer variants likely converge on the same pathological mechanism of disrupted neurotrophic signalling	187

List of tables

Table 1.1. Defects affecting specific glycosyltransferase enzymes observed in neurodegenerative disease	12
Table 1.2. Mutations identified with exon 4 of GLT8D1	33
Table 1.3. Phenotype information for patients carrying ALS-associated mutations in GLT8D1	34
Table 2.1. Molecular biology kit product details	41
Table 2.2. Primary antibodies used for immunoblotting (WB) and immunocytochemistry (ICC).....	41
Table 2.3. Secondary antibodies and molecular probes.....	42
Table 2.4. PCR primer sequences for molecular cloning and site-directed mutagenesis.....	43
Table 2.5. Media compositions	43
Table 2.6. Plasmid manipulations and origins.....	44
Table 2.7. Oligonucleotide sequences for GLT8D1 cloning and knockdown in zebrafish	45
Table 2.8. Transfection conditions according to plate size, experiment, cell type and cell density	54
Table 2.9. Nucleofection conditions using the Neon® Transfection System.....	55
Table 2.10. PCR programme for I.M.A.G.E clone amplification.	56
Table 2.11. PCR programme for site-directed mutagenesis.....	58
Table 2.12. Composition of 12% resolving and 5% stacking polyacrylamide gels.....	62
Table 2.13. PCR programme for zebrafish RT-PCR.....	72
Table 4.1. Zebrafish ALS models recapitulate pathological and phenotypic disease traits .	118
Table 6.1. Summary of the LCLs used for characterising the relative expression of CAV1/CAV2 in patients carrying ALS-associated enhancer variants.....	153

List of abbreviations

AD	Alzheimer's disease
ALS	Amyotrophic lateral sclerosis
AMO	Antisense morpholino oligonucleotide
C9ORF72	Chromosome 9 open reading frame 72
Cas9	Caspase 9
CAV1	Caveolin 1
CAV2	Caveolin 2
CNS	Central nervous system
CRISPR	Clustered regularly interspaced short palindromic repeats
CSF	Cerebrospinal fluid
CTxB	Cholera toxin subunit B
eGFP	Enhanced green fluorescent protein
EOGT	EGF Domain Specific O-Linked N-Acetylglucosamine Transferase
ER	Endoplasmic reticulum
fALS	Familial amyotrophic lateral sclerosis
FRT	Flippase recognition target
FTD	Frontotemporal dementia
FUS	Fused in sarcoma
GFP	Green fluorescence protein
GlcNAc	N-Acetylglucosamine transferase
GLT8D1	Glycosyltransferase 8 domain containing 1
GM1	Ganglioside mono-sialic acid 1
GSL	Glycosphingolipid
HEK293	Human embryonic kidney 293
ICE	Inference of CRISPR edits
iNPC	Induced neural progenitor cell
kDa	Kilo Dalton
Km	Michaelis constant
LCL	Lymphoblastoid cell line
miRNA	Micro ribonucleic acid

MLR	Membrane lipid raft
mRNA	Messenger ribonucleic acid
N2A	Neuro-2A (mouse neuroblastoma line)
OGT	O-linked N-Acetylglucosamine transferase
OPTN	Optineurin
PAM	Protospacer adjacent motif
PD	Parkinson's disease
PLS	Primary lateral sclerosis
sALS	Sporadic amyotrophic lateral sclerosis
SOD1	Cu/Zn super oxide dismutase 1
TBK1	TANK-binding kinase 1
TDP-43	TAR DNA binding protein 43kDa
TIDE	Tracking indels by decomposition
UDP	Uridine diphosphate
WGA	Wheat germ agglutinin
WT	Wild type

Chapter 1. Introduction

1.1. Introduction to amyotrophic lateral sclerosis

Amyotrophic lateral sclerosis (ALS) is the most common form of motor neuron disease, accounting for roughly 66% of all cases (Gordon, 2013). It is a relentlessly progressive and incurable neurodegenerative disorder characterised by the loss of both upper and lower motor neurons within the brainstem and spinal cord. Death and injury to motor neurons leads to a breakdown of neuromuscular junctions resulting in muscular atrophy, paralysis, and death usually by respiratory failure within 2-5 years of the first symptom (Yang et al., 2014, Renton et al., 2014). ALS is a multifactorial disorder with a number of described genetic and environmental risk factors. Although phenotypically indistinguishable from one another, 10% of cases are familial (fALS), usually with an autosomal dominant inheritance pattern, whilst the remaining 90% are sporadic (sALS), defined as having no family history of the disease (Renton et al., 2014). It is notable that even sALS is significantly heritable; twin studies estimate the broad sense heritability of sALS to be as high as 61% (Al-Chalabi et al., 2010).

ALS is an age-related disorder with an incidence of 1-2 per 100,000 people worldwide and an estimated lifetime risk of 1 in 400 (Barber et al., 2006, Ingre et al., 2015), although some estimates are as high as 1 in 350 (Alonso et al., 2009, Al-Chalabi and Hardiman, 2013). There are geographical variations in the number of ALS cases, with prevalence rates significantly lower in non-European countries; however, this may be due to a lack of reliable epidemiological data (Chio et al., 2013).

1.2. Clinical presentation and disease management

The presentation of ALS varies greatly between individuals depending on the population of neurons first affected: disease can be limb- or bulbar-onset and may affect upper or lower motor neurons to differing degrees (Hardiman et al., 2017). While traditionally regarded as a pure motor system disease, cognitive decline and behavioural disturbance are increasingly recognised as cardinal features of ALS. Indeed, as many as 30% of ALS patients meet the diagnostic criteria for frontotemporal dementia (FTD) (Hinz and Geschwind, 2017). There is a significant genetic overlap between ALS and FTD, and both disorders are heterogeneous at the clinical, neuropathological, and genetic levels (Ferrari et al., 2011). FTD is a collection of

neurocognitive syndromes characterised by the impairment of executive functioning, behavioural changes, and reduced language proficiency (Young et al., 2018). Diagnosis of ALS is clinical and is based on the El Escorial criteria. Neurophysiology and laboratory studies are used to exclude alternative diagnoses, particularly reversible ALS mimics such as entrapment neuropathies and multifocal motor neuropathy with conduction block (Hardiman et al., 2017).

There is currently no cure for ALS; therefore, clinical management is largely supportive and requires a multidisciplinary approach. Symptoms such as dysphagia, spasticity, cramping, and sialorrhea are managed on an individual basis. Two disease-modifying medications are currently licensed by the Food and Drugs Administration. Riluzole, a sodium channel blocking agent, has been shown to modestly prolong survival by approximately three months, and has been used for many years (Hardiman et al., 2017). The more recent, Edaravone, is an antioxidant that has been shown to mildly prolong functional independence in selected patients (Abe et al., 2014, Hardiman and van den Berg, 2017). It is expected that significant advancements in the treatment of the disease will require personalised approaches to target specific causative genes and proteins. For example, Tofersen, an antisense oligonucleotide for SOD1 fALS, is currently undergoing phase III trials having shown promise in phase I and II studies (NCT02623699).

1.3. Genetics of ALS

The first discovered ALS-associated gene, SOD1, was first identified almost three decades ago, and since then over 50 ALS-associated genes have been described (Taylor et al., 2016). Despite this, a genetic cause still cannot be identified in many families; the search for new ALS genes is ongoing. The cause of sALS is not fully elucidated, but genetic and environmental factors are both predicted to be important. Indeed, a genetic cause can be observed in many sporadic patients, although genetic screening of these patients is not in widespread clinical practice at present. Environmental factors including diet, physical activity and toxins have been postulated as risk factors, but definitive proof for these has yet to emerge (Hardiman et al., 2017). Described genetic variants are associated with >68% fALS and >11% sALS cases (Renton et al., 2014). Whilst more than 50 potentially causative or disease-modifying genes have been identified, mutations in *SOD1*, *TARDBP*, *FUS*, and *C9ORF72* are most frequently associated with ALS (Boylan, 2015). The discovery and characterisation of new genetic risk factors for ALS helps to illuminate the upstream mechanisms leading to neuronal death and can identify new therapeutic targets.

1.3.1. *SOD1*

The first ALS-causative mutation was identified in 1993 in the Cu/Zn superoxide dismutase gene (*SOD1*). Due to the role of *SOD1* in converting superoxide radicals into oxygen and hydrogen peroxide, it was initially thought that mutations within this gene caused ALS via a loss-of-function mechanism resulting in a decrease in radical scavenging activity (Rosen, 1993). However, this was soon disputed as different *SOD1* mutants show varying degrees of enzyme activity, and *SOD1* knockout mice do not develop ALS (Reaume et al., 1996, Yim et al., 1996, Al-Chalabi et al., 2012, Saccon et al., 2013). Moreover, correlations were not found between *SOD1* dismutase activity and the aggressiveness of clinical phenotypes (Ratovitski et al., 1999). The fact that *SOD1* mutations are autosomal dominant is most consistent with a gain-of-function mechanism. ALS-causing *SOD1* mutations increase the protein's propensity to misfold, which leads to the accumulation of *SOD1* protein aggregates that induce neurotoxicity through mechanisms including oxidative stress and mitochondrial dysfunction (Rakhit et al., 2004, Vassall et al., 2006, Stathopoulos et al., 2006, Joyce et al., 2011, Magrane et al., 2012). Since its discovery, *SOD1* mutations have been shown to account for 15-20% of fALS cases and ~2% sALS cases, although there is significant variability between populations with the highest incidence in Scandinavia. More than 170 missense mutations have been identified which affect each of the five exons of *SOD1* (Da Cruz et al., 2017). It is notable that *SOD1*-ALS is clinically and pathologically distinct from the majority of ALS cases. Familial *SOD1*-ALS patients lack TDP-43 pathology and are less likely to have significant cognitive changes (Mackenzie et al., 2007, Wicks et al., 2009), which may explain the failure to translate findings from *SOD1*-ALS mice into clinical treatments.

1.3.2. *TARDBP*

In 2008, it was demonstrated that mutations within transactive response DNA binding protein 43kDa (*TARDBP*), which encodes the TDP-43 protein (Sreedharan et al., 2008), are a cause of ALS. TDP-43 is a ubiquitously expressed ribonucleoprotein that is predominantly localised in the nucleus, where it performs a range of functions linked to RNA metabolism including transcription, mRNA splicing, mRNA stability, RNA transport, miRNA biogenesis, and stress granule dynamics (Buratti and Baralle, 2012). There are over 50 known ALS-causing mutations in *TARDBP*, which contribute to 4-5% of fALS cases and 1% of sALS cases (Millecamps et al., 2010, Buratti, 2015). The mislocalisation of TDP-43 from the nucleus to the cytoplasm and the formation of TDP-43-positive cytoplasmic inclusions is recognised as the pathological hallmark of ~97% of ALS cases, including patients with mutated *TARDBP* (Neumann et al., 2006). The discovery that mutations within this protein are a cause of ALS

was a powerful argument that this almost universal pathology is an upstream cause of disease and not simply a downstream consequence.

It is unclear whether TDP-43 aggregates cause toxicity through gain-of-function and/or loss-of-function mechanisms. Several lines of evidence have shown that loss of nuclear TDP-43 causes splicing defects in cellular and animal models, as well as in motor neurons from TARDBP-ALS patients (De Conti et al., 2015, Highley et al., 2014, Ling et al., 2015). However, other lines of evidence suggest that the key change is loss of autoregulation leading to overexpression (White et al., 2018).

1.3.3. *FUS*

The following year, in 2009, ALS-causing mutations were identified within fused in sarcoma (*FUS*) (Kwiatkowski et al., 2009, Vance et al., 2009). *FUS* has a functional role in a range of metabolic processes including transcription, mRNA splicing, mRNA transport, stress granule formation, miRNA biogenesis, and genome integrity (Deng et al., 2014b). Similar to TDP-43, *FUS* is predominantly localised in the nucleus, but also shuttles between the nucleus and cytoplasm (Zinszner et al., 1997). Cytoplasmic aggregations of *FUS* are described; however, like TDP-43, it is unknown how these aggregates cause motor neuron toxicity. Although, there is strong evidence for a dominant negative mechanism of *FUS* mislocalisation, misfolding and aggregation, leading to depleted nuclear function (Deng et al., 2014a). Currently, there are more than 50 *FUS* mutations associated with 4-5% fALS and <1% sALS cases, and the majority of these mutations present with an autosomal dominant mode of inheritance. Clinically *FUS*-ALS patients are younger than most, and importantly TDP-43 pathology is absent from degenerating neurons (Deng et al., 2014a).

1.3.4. *C9ORF72*

At 39% of fALS cases and 8% of sALS cases, the most common genetic cause of ALS was identified in 2011 as a (G4C2)_n hexanucleotide repeat expansion in intron 1 of chromosome 9 open reading frame 72 (*C9ORF72*) (DeJesus-Hernandez et al., 2011, Renton et al., 2011, Majounie et al., 2012). Whilst >30 (G4C2)_n repeats are considered pathogenic (Byrne et al., 2014, Beer et al., 2015), expansions of 500-2000 repeats are common in ALS patients (Cooper-Knock et al., 2014). It remains unclear as to how the (G4C2)_n repeat expansion causes ALS, although it is thought to be a result of three mutually-inclusive mechanisms: *C9ORF72* haploinsufficiency, dipeptide repeat protein toxicity, and RNA toxicity (Donnelly et al., 2013, Waite et al., 2014, Mori et al., 2013, Zu et al., 2013). The weight of evidence

suggests *C9ORF72* repeat expansions cause ALS via a gain-of-function mechanism, whilst loss-of-function mechanisms are more likely to modulate the disease phenotype through dysregulated autophagy (Zhu et al., 2020). Patients with hexanucleotide-repeat expansions in the *C9ORF72* gene tend to have aggressive disease and a higher prevalence of cognitive involvement and overlap with FTD (Hardiman et al., 2017). Crucially, C9ORF72-ALS overlaps clinically and pathologically with the more common sporadic disease (Cooper-Knock et al., 2012), suggesting that study of C9ORF72-ALS may lead to discoveries applicable for the vast majority of ALS patients. This fact together with the relative frequency of C9ORF72-ALS cases, made this discovery a landmark in the ALS literature.

1.4. ALS pathological mechanisms

ALS is a multifactorial disorder with various mechanisms implicated in the disease pathogenesis. In most cases of ALS, it is difficult to separate the initial toxic insult and exacerbating secondary pathways that drive disease progression. Associated pathological mechanisms include oxidative stress, mitochondrial dysfunction, dysregulated axonal transport, aberrant RNA processing, and impaired protein homeostasis, as well as a non-cell autonomous toxicity.

1.4.1. Oxidative stress

Oxidative stress is a result of an imbalance in the production and removal of reactive oxygen species (ROS), and/or the inability to repair oxidative damage. Oxidative stress promotes tissue damage by interacting with other pathological mechanisms that promote the degeneration of motor neurons (Pollari et al., 2014). Oxidative stress in the form of free radical damage and abnormal free radical metabolism is well described in ALS patients (Shaw et al., 1995, Ferrante et al., 1997, Smith et al., 1998, Chang et al., 2008). In certain SOD1-ALS mouse models, oxidative stress is shown to originate from the distal muscles in advance of disease onset (Kraft et al., 2007). ROS are shown to inhibit the release of neurotransmitters, thus interfering with synaptic transmission. Moreover, a rise in the level of ROS is demonstrated to inhibit the function of neuromuscular junctions (Naumenko et al., 2011), suggesting that oxidative damage may originate in peripheral tissues and progress in a retrograde manner to neurons. Indeed, the ALS gene most commonly associated with oxidative damage is SOD1 (Wiedau-Pazos et al., 1996, Crow et al., 1997), although mutant TDP-43 has also been implicated in this pathway (Duan et al., 2010).

1.4.2. Mitochondrial dysfunction

The mitochondrion is a membrane-bound organelle that functions as the major hub to convert energy for cellular processes (Liu et al., 2020b). Impaired mitochondrial morphology and function are well-known phenomena of ALS and neurodegeneration more broadly (Johri and Beal, 2012). Mitochondrial dysfunction has been described in ALS patient spinal motor neurons and in various cell and animal models of the disease. These models have identified impaired ATP production, calcium buffering, redox balance, respiratory complexes and mitochondria-dependent apoptosis (Bowling et al., 1993, Dal Canto and Gurney, 1994, Fujita et al., 1996, Menzies et al., 2002, Ferri et al., 2006, Sasaki et al., 2007, Grosskreutz et al., 2010, Shi et al., 2010, Cozzolino and Carri, 2012). Indeed, motor neurons have a high metabolic demand, making them particularly susceptible to dysregulated ATP production (Menzies et al., 2002). Moreover, impaired mitochondrial function has been shown to increase ROS production, resulting in a positive feedback loop characterised by enhanced oxidative damage to mitochondrial components and greater mitochondrial dysfunction. This process could be central to motor neuron degeneration in ALS (Kaal et al., 2000, Robberecht, 2000).

1.4.3. Impaired axonal transport

Motor neurons have extremely long axons extending from the CNS to the muscles in which they innervate. Any hypothesis to explain ALS needs to account for the specific vulnerability of motor neurons, and their anatomy is the most obvious candidate. These axons rely on the efficient transport of protein, lipids, RNA and organelles via the cytoskeleton and associated motor proteins. Various genes implicated in ALS including *FUS*, *TARBP*, and *C9ORF72*, are associated with axonal transport and the cytoskeleton, suggesting impaired axonal transport is a feature of ALS pathogenesis. Impaired axonal transport has been described in several different genetic models of ALS (Alami et al., 2014, De Vos et al., 2007, Morotz et al., 2012), and is proposed to occur early in the disease pathogenesis (De Vos et al., 2008). Indeed, axonal transport defects have been reported in pre-symptomatic *SOD1*^{G93A} ALS mice (Bilsland et al., 2010).

1.4.4. Dysregulated RNA metabolism

It has become increasingly clear that aberrant RNA metabolism is central to ALS pathogenesis. The four major ALS genes: *SOD1*, *TARDBP*, *FUS*, and *C9ORF72*, have functional roles in aspects of RNA metabolism including mRNA transcription, alternative splicing, RNA transport, mRNA stabilization, and miRNA biogenesis (Butti and Patten, 2018).

In particular, TDP-43, which forms the characteristic cytoplasmic inclusions seen in the majority of ALS patients, is reported to regulate the expression of hundreds of mRNAs and the splicing of >1000 mRNAs (Polymenidou et al., 2011). Moreover, TDP-43 is transported along axons and co-localises with axonal mRNA binding proteins at synaptic terminals (Wang et al., 2008, Narayanan et al., 2013). TDP-43-mediated regulation of cytoplasmic mRNA in motor neurons is shown to influence axonal outgrowth (Fallini et al., 2012). Similarly, FUS is crucial for mRNA transport within axons and this function is disrupted in ALS (Butti and Patten, 2018). Furthermore, the (G4C2)_n repeat expansion in C9ORF72 is thought to directly exert RNA toxicity by disrupting RNA metabolism. Transcription of the repeat expansion leads to accumulations of RNA foci, which facilitate the recruitment, mislocalisation, and impaired function of RNA binding proteins (Gendron et al., 2013, Simon-Sanchez et al., 2012, Donnelly et al., 2013, Lee et al., 2013).

1.4.5. Impaired protein homeostasis

Insoluble protein aggregates are a hallmark neuropathological feature of ALS (Webster et al., 2017). Protein inclusions have been identified in degenerating neurons and glial cells of the brainstem, spinal cord, cerebellum, hippocampus, as well as the frontal and temporal lobes (Piao et al., 2003, Nishihira et al., 2008, Zhang et al., 2008, Al-Chalabi et al., 2012). These inclusions are ubiquitinated, implying that the ubiquitin-proteasome and autophagy systems are impaired, which is suggestive of defects in protein turnover (Neumann et al., 2006, Blokhuis et al., 2013). Multiple lines of evidence implicate ER stress in ALS pathogenesis, suggesting an inability to manage misfolded proteins (Matus et al., 2013). A large number of ALS associated genes including *VCP*, *OPTN*, *SOD1*, *TARDBP*, *FUS* and *C9ORF72*, directly or indirectly regulate protein trafficking or degradation via the ubiquitin-proteasome or autophagy pathways (Webster et al., 2017), which strongly implicates impaired protein homeostasis in ALS pathogenesis.

1.4.6. Non-cell autonomous toxicity and neuroinflammation

Various studies have implicated glial cells in the pathogenesis of ALS. Astrocytes derived from the direct reprogramming of SOD1-ALS, C9ORF72-ALS, and sALS patient fibroblasts are selectively toxic to wild-type (WT) neurons in co-culture (Meyer et al., 2014, Nagai et al., 2007, Di Giorgio et al., 2007). It has been demonstrated that astrocyte-derived extracellular vesicles and associated miRNA cargo are responsible for astrocyte-mediated toxicity in C9ORF72-ALS (Varcianna et al., 2019). In support of the non-cell autonomous nature of ALS, deletion of mutant-SOD1 exclusively from mouse astrocytes slowed late-stage disease progression

(Yamanaka et al., 2008). Moreover, astrocytes derived from fALS and sALS patient post-mortem neural progenitor cells (NPCs) induce motor neuron death *in vitro*, irrespective of the mutation they carry (Haidet-Phillips et al., 2011).

1.5. Animal models of ALS

1.5.1. Mouse models

The first animal model of ALS was the SOD1^{G93A} mouse (Gurney et al., 1994), which harbours mutant human SOD1 cDNA randomly inserted into its genome. This transgenic line remains the most widely used animal model of human ALS. SOD1^{G93A} mice present with hind limb weakness at ~90 days, concurrent with neurodegeneration that closely resembles human ALS pathology (Synofzik et al., 2010). Death occurs by ~135 days; however, this is dependent on the genetic background. Despite its widespread use, the SOD1^{G93A} mouse may display phenotypic traits that arise from overexpression of the SOD1 protein, as opposed to being an effect of the SOD1G93A mutation itself (Shibata, 2001). Indeed, overexpression of human WT SOD1 in mice causes an abnormal phenotype (Jaarsma et al., 2001).

The discovery of the C9ORF72 hexanucleotide (G4C2)_n repeat expansion (DeJesus-Hernandez et al., 2011, Renton et al., 2011) has led to the generation of various ALS/FTD animal models. Some of the first ALS/FTD transgenic mouse models were developed using a bacterial artificial chromosome (BAC) to express the G4C2 expansion. Whilst these models displayed molecular phenotypes similar to human C9ORF72-associated ALS/FTD, the mice were clinically unaffected with no evidence of neurodegeneration (O'Rourke et al., 2015, Peters et al., 2015). Conversely, other BAC transgenic mouse models expressing a similar number of repeats have since been shown to present with an age-dependent development of cognitive and behavioural dysfunction (Liu et al., 2016, Jiang et al., 2016). Notably, the Liu model included much more of the original human genomic context for the repeat expansion, suggesting that the surrounding regulatory genome is necessary to drive pathogenesis. Coincident with this was a much higher level of antisense transcription, which the authors linked to neuronal loss. However, there is some ongoing debate as to the validity of this model as it demonstrates inconsistent behavioural phenotypes and TDP-43 pathology (Alrafiah, 2018). Finally, when researchers utilised a viral-mediated delivery system to express the repeat expansion, mice not only displayed histopathological features, but also developed neurodegeneration and behavioural deficits comparable to those seen in patients (Chew et al., 2015).

Whilst these models show contrasting results, they do all provide evidence for gain-of-function toxicity associated with the G4C2 expansion. Observed pathological effects are generally all characteristic of ALS/FTD. In contrast, pathogenic mechanisms associated with C9ORF72 loss-of-function in transgenic mice appear to extend beyond the characteristic features of ALS/FTD. One of the earlier loss-of-function models generated by selective knockout of the C9ORF72 ortholog in mouse neurons and glia was shown to be insufficient to cause disease (Koppers et al., 2015). Conversely, mice harbouring loss-of-function mutations in the orthologue of *C9ORF72* were shown to develop an array of complications in the haematopoietic system including splenomegaly, neutrophilia, thrombocytopenia, increased expression of inflammatory cytokines, and severe autoimmunity, which ultimately led to a high mortality rate (Burberry et al., 2016). A similar result was observed by Jiang and colleagues, who reported that a chronic 50% reduction in C9ORF72 led to splenomegaly and enlarged lymph nodes (Jiang et al., 2016). Whilst ALS/FTD are not considered autoimmune disorders, it is evident that C9ORF72 is a multifactorial gene that operates in pathways extending beyond the CNS. This is evidence that the function of the actual C9ORF72 protein may not be important for the development of ALS-FTD, although this does not explain why ALS has not been linked to similar GC-rich expansions at other sites within the genome.

The identification of ALS-causing *TARDBP* mutations has led to the generation of a wide range of TDP-43 ALS/FTD mouse models. A limitation of these models is that observed phenotypes may be artefacts of TDP-43 overexpression. Indeed, overexpression of WT TDP-43 has been shown to cause an ALS phenotype (Xu et al., 2010). Recently, issues regarding overexpression were circumvented through the use of CRISPR/Cas9 genome editing; however, this model did not display a robust phenotype nor show signs of TDP-43 mislocalisation (White et al., 2018). Interestingly, TDP-43 was overexpressed in this model due to a circumventing of the normal autoregulation mechanism responsible for precise control of TDP-43 levels. The model developed by Wegorzewska and colleagues in 2009 accurately recapitulated clinical hallmarks of ALS/FTD, but lacked typical TDP-43-positive pathology (Wegorzewska et al., 2009).

1.5.2. Zebrafish models

Contrary to previous findings in mice (Koppers et al., 2015), haploinsufficiency of *C9orf72* orthologues in zebrafish cause motor axon and behaviour deficits (Ciura et al., 2013). Furthermore, expression of the G4C2 repeat expansion in zebrafish recapitulated key pathological hallmarks associated with ALS/FTD, commensurate with motor and cognitive

impairment as well as premature death (Shaw et al., 2018). Similar results were observed in a study of the same year, which showed that the expression of a comparable number of G4C2 repeats correlated with motor neuron toxicity; however, behavioural effects were not reported (Swinnen et al., 2018).

The zebrafish genome contains two orthologues of human *TDP-43*: *tardbp* and *tardbp1*. Transient knockdown of *tardbp* using morpholino oligonucleotides was shown to induce a motor phenotype concurrent with the shortening of motor neuron axons. In the same study, microinjection of human mRNA encoding known TDP-43 mutations (A315T, G348C and A382T) led to a similar phenotype (Kabashi et al., 2010). However, subsequent studies observed more profound effects associated with mutant TDP-43. Whilst *tardbp*-mutants showed no phenotype, Schmid et al. reported that double mutants for *tardbp* and its paralogue displayed muscle degeneration, strongly reduced blood circulation, mispatterning of vessels, impaired axon outgrowth, and premature death (Schmid et al., 2013). These results were reflected in a study of the same year; however, there was no report of circulatory defects (Hewamadduma et al., 2013). A more detailed discussion of zebrafish models of ALS is presented in chapter 4.

1.6. A literature review in the context of the present study: disrupted glycosyltransferase function is a cause of neurodegeneration

This following sections of this chapter are an extended version of work which I published during my PhD (Moll et al., 2020). It is evident that the pathophysiological mechanisms underpinning ALS are multifactorial, and there is complex interplay between genetic factors and molecular pathways. The main focus of my project was to experimentally evaluate a novel glycosyltransferase enzyme implicated in ALS. Therefore, the following sections of this introductory chapter will review dysregulated glycosyltransferase function as a cause of neurodegeneration in the context of Alzheimer's disease (AD), Parkinson's disease (PD), Huntington's disease (HD), and ALS.

Glycosyltransferases represent a large family of enzymes that catalyse biosynthesis of oligosaccharides, polysaccharides, and glycoconjugates. Sugar moieties are transferred from activated sugar donors to specific acceptor molecules via the formation of glycosidic bonds (Chuh et al., 2016). Acceptor molecules include other sugars, nucleic acids, lipids, and proteins. Glycosyltransferases reside predominantly within the Golgi apparatus of eukaryotes as type II transmembrane proteins. Over 90 glycosyltransferase families have been described (www.cazy.org/GlycosylTransferases.html). Sequence alignment tools have been useful for predicting glycosyltransferase function, including a metal-binding motif important for configuration of substrate within the active site (Lairson et al., 2008). However, even closely related sequences have been shown to exhibit different catalytic activity (Breton et al., 2006). Glycosyltransferases are classified as either 'retaining' or 'inverting' enzymes according to whether the anomeric bond within the donor substrate is retained or inverted during the sugar transfer.

1.6.1. Genetic mutations in glycosyltransferases are associated with neurodegeneration

Changes in expression levels of glycosyltransferases have been strongly linked with neurodegeneration (Ludemann et al., 2005, Desplats et al., 2007, Schneider, 2018), but determining whether these effects are upstream of neurotoxicity is difficult. Two distinct glycosyltransferase-associated mechanisms are prominent in the neurodegeneration literature: ganglioside synthesis and the addition of O-linked β -N-acetyl glucosamine to proteins (O-GlcNAcylation). Genetic mutations in the development of an age-associated

neurodegenerative disease are, by definition, upstream causes or risk factors rather than secondary to the disease process. Mutations discovered within glycosyltransferases and their implication in neurodegenerative diseases are summarised (**Table 1.1**).

Glycosyl-transferase	Functional consequence	Neurodegenerative disorder	Defect observed	Reference
ST6GAL1	Disrupted cell surface signalling	Alzheimer's disease	DNA mutations	(Lee et al., 2017)
B3GALT4	Reduced ganglioside biosynthesis (GD1b)	Parkinson's disease	Reduced gene expression	(Schneider, 2018)
ST3GAL2	Reduced ganglioside biosynthesis (GT1b)	Parkinson's disease Huntington's disease	Reduced gene expression	(Schneider, 2018) (Desplats et al., 2007)
B4GALNT1	Reduced ganglioside biosynthesis	Huntington's disease	Reduced gene expression	(Desplats et al., 2007)
ST8SIA3	Implicated in ganglioside biosynthesis but described role in N-glycosylation	Huntington's disease	Reduced gene expression	(Desplats et al., 2007)
ST3GAL5	Reduced ganglioside biosynthesis	Huntington's disease	Reduced gene expression	(Desplats et al., 2007)
GLT8D1	Reduced membrane expression of glycosphingolipids	ALS	DNA mutations	(Cooper-Knock et al., 2019)
UGT8	Disruption of myelin synthesis	ALS	DNA mutations	(Pamphlett et al., 2011)
EOGT	Disruption of O-GlcNAcylation	ALS	DNA mutations	(Moll et al., 2020)
OGT	Impaired O-GlcNAcylation	Alzheimer's disease ALS	Reduced concentration of O-GlcNAcylated proteins	(Liu et al., 2004) (Ludemann et al., 2005)
OGT	Excessive O-GlcNAcylation	Parkinson's disease	Increased concentration of O-GlcNAcylated proteins	(Wani et al., 2017)

Table 1.1. Defects affecting specific glycosyltransferase enzymes observed in neurodegenerative disease. Glycosyltransferase genes, functional consequences, associated neurodegenerative disorders, observed defects, and references are shown. Table taken from (Moll et al., 2020).

1.6.1.1. *UDP glycosyltransferase 8 (UGT8)*

UGT8 is a member of glycosyltransferase family 8. UGT8 functions in the biosynthesis of galactocerebroside, a sphingolipid that forms the myelin membrane in the central and peripheral nervous systems. Rare and potentially pathogenic copy number variants have been identified in the promotor region of UGT8 following an unbiased genome-wide screen for *de novo* DNA mutations in twelve trios, including sALS patients and unaffected parents (Pamphlett et al., 2011). Abnormal lipid biosynthesis and metabolism is a pathological hallmark of ALS (Dupuis et al., 2008, Dorst et al., 2011); therefore, it is possible that UGT8 plays a role in the hypolipidemia observed in ALS patients and the SOD1^{G93A} ALS mouse model (Kim et al., 2011, Yang et al., 2013). Mice lacking *ugt8a*, the ortholog of UGT8, exhibit impaired locomotor activity and disruption in nerve conduction, followed by degeneration of the myelin sheath (Bosio et al., 1996, Coetzee et al., 1996), which is rescued following transgenic expression of *ugt8a* (Zoller et al., 2005). Interestingly the rescue occurred with expression of *ugt8a* under a promoter exclusively expressed within oligodendrocytes, which is consistent with other evidence implicating these cells in ALS-associated neurodegeneration (Morrison et al., 2013).

1.6.1.2. *ST6 Beta-Galactoside Alpha-2,6-Sialyltransferase 1 (ST6GAL1)*

ST6GAL1 is an 'inverting' enzyme and a member of glycosyltransferase family 29. ST6GAL1 catalyses the transfer of sialic acid onto galactose-containing substrates including cell-surface signalling lipids and proteins (Garnham et al., 2019). A genome-wide association study implicated polymorphisms within ST6GAL1 in the conversion of mild cognitive impairment into clinical AD (Lee et al., 2017). Interestingly, ST6GAL1 is cleaved and occurs in a soluble form; this cleavage is mediated by BACE1 (Kitazume et al., 2001), which is also involved in the cleavage of APP to form β -amyloid. Indeed, overexpression of ST6GAL1 increases APP secretion (Nakagawa et al., 2006), suggesting that the activity of ST6GAL1 can directly modify the central pathway in the development of AD pathology.

1.6.2. Glycosyltransferases regulate ganglioside synthesis

Major gangliosides are sialic acid-containing glycosphingolipids. Within the mammalian brain they are synthesized in the endoplasmic reticulum from a lactosylceramide precursor before

remodelling during transit from the *cis*- to the *trans*-Golgi network by a series of glycosyltransferase enzymes (**Figure 1.1**). Mature gangliosides are expressed on the plasma membrane of most vertebrate cells and within bodily fluids. They are particularly abundant on neuronal and glial cells within the CNS where they are thought to function prominently in cell signalling (Vajn et al., 2013).

1.6.3. Gangliosides are differentially distributed in the mammalian CNS

Mapping ganglioside distribution patterns in the CNS may be crucial to understanding the functional properties of the various ganglioside sub-species. Ganglioside-monosialic acid 1 (GM1), ganglioside-di-sialic acid 1a (GD1a), ganglioside-di-sialic acid 1b (GD1b), and ganglioside-tri-sialic acid 1b (GT1b) are all derived from a common precursor (GM3) and constitute over 90% of total gangliosides within the typical mammalian brain. Their abundance is attributed to the high activity of the synthesising enzyme, β -1,4-N-acetylgalactosaminyl transferase 1 (B4GALNT1). Synthesis occurs via two primary pathways, designated a-series and b-series (**Figure 1.1**) (Ledeen, 1966, Yao et al., 2014).

Rodent-based studies have revealed cell type-specific expression of major CNS gangliosides during adulthood. By way of illustration, GD1b is specific to granule neurons throughout all layers of the cerebellar cortex, whilst GD1a is localised exclusively to the molecular layer (Kotani et al., 1993, Kawashima et al., 1996, Vajn et al., 2013). Immuno-labelling of GD1a, GD1b, and GT1b in the adult mouse CNS revealed high expression across all layers of the cerebral cortex. Conversely, GM1 was restricted to myelinated fibres within the lower layers (Vajn et al., 2013). The variability of ganglioside composition throughout nervous tissue is consistent with an important role in the formation and function of the CNS.

Region-specific alterations in ganglioside distribution within the mammalian brain are known to occur during development and ageing, with ganglioside composition changing from simple (e.g. GM3) to complex (e.g. GM1), compliant with the degree of neurogenesis, synaptogenesis, and axonal branching. Knowledge of how such alterations are regulated is limited, but it is thought to be modulated at the level of glycosyltransferase gene expression (Kracun et al., 1991, Ngamukote et al., 2007).

1.6.4. Gangliosides regulate neuroinflammation and neurotrophic action

Studies using genetically modified mice have shed light on the biological importance of gangliosides to nervous system function. A double knockout of genes encoding key glycosyltransferase enzymes involved in ganglioside biosynthesis, GM2- and GD3-synthase, displayed up-regulation of complement genes and their receptors in mouse cerebellum (Ohmi et al., 2009). This infers that gangliosides prevent the destruction of nervous tissue through complement-mediated neurodegeneration. The rise in complement activity coincided with impairments in the structure and function of lipid rafts, which anchor complement proteins to membrane bilayers. A follow-up study confirmed that maintenance of lipid rafts is key to the neuroprotective properties of gangliosides (Ohmi et al., 2011).

Gangliosides have also been shown to exhibit neurotrophic properties by enhancing neurite outgrowth and alleviating the deterioration of nervous tissue following injury (Kittaka et al., 2008, Ohmi et al., 2009). For example, GD3 synthase-deficient mice lacking b-series gangliosides showed a reduction in the regenerative capacity of axotomised hypoglossal nerves (Okada et al., 2002). A study of GM2 synthase-deficient mice has suggested that this is also true of a-series gangliosides, concurrent with a decrease in the expression of known neurotrophic factors compared to WT controls, supporting the notion that gangliosides regulate neuronal integrity (Kittaka et al., 2008).

Ganglioside function has been investigated in axon-glia junctions at the nodes of Ranvier in myelinated central and peripheral motor nerve fibres of GM2 synthase-deficient mice. Mutant mice presented with mislocalisation of ion channels and a reduction in motor nerve conduction, suggesting a role for gangliosides in stabilising the interactions between neurons and glia at paranodal junctions (Susuki et al., 2007). It has been suggested that gangliosides indirectly perpetuate nerve integrity by increasing the neuroprotective properties of astrocytes, the most abundant glial cell type within the CNS. In support of the knockout mouse models, a study found that ganglioside-depleted astrocytes were less able to augment the survival of hippocampal neurons *in vitro*. In the same study, neurotrophic activity was rescued following treatment with ganglioside GM3, suggesting it is involved in glial cell-mediated neuronal maintenance (Akasako et al., 2011). However, a more recent study argued that glial gangliosides are less significant to the age-related maintenance of neuronal integrity; a rescue experiment on GM2 synthase-deficient mice was performed by driving GalNAcT expression in a cell-restricted manner. Neuronal-specific expression of GalNAcT in these mice led to a lasting WT phenotype, whereas mice with glial-specific GalNAcT expression exhibited progressive tremor, weakness, and ataxia with ageing (Yao et al., 2014). Irrespective of this,

these studies form a compelling argument to support the various mechanisms through which gangliosides regulate neuroinflammation, neuronal plasticity, and synaptic function (**Figure 1.1**).

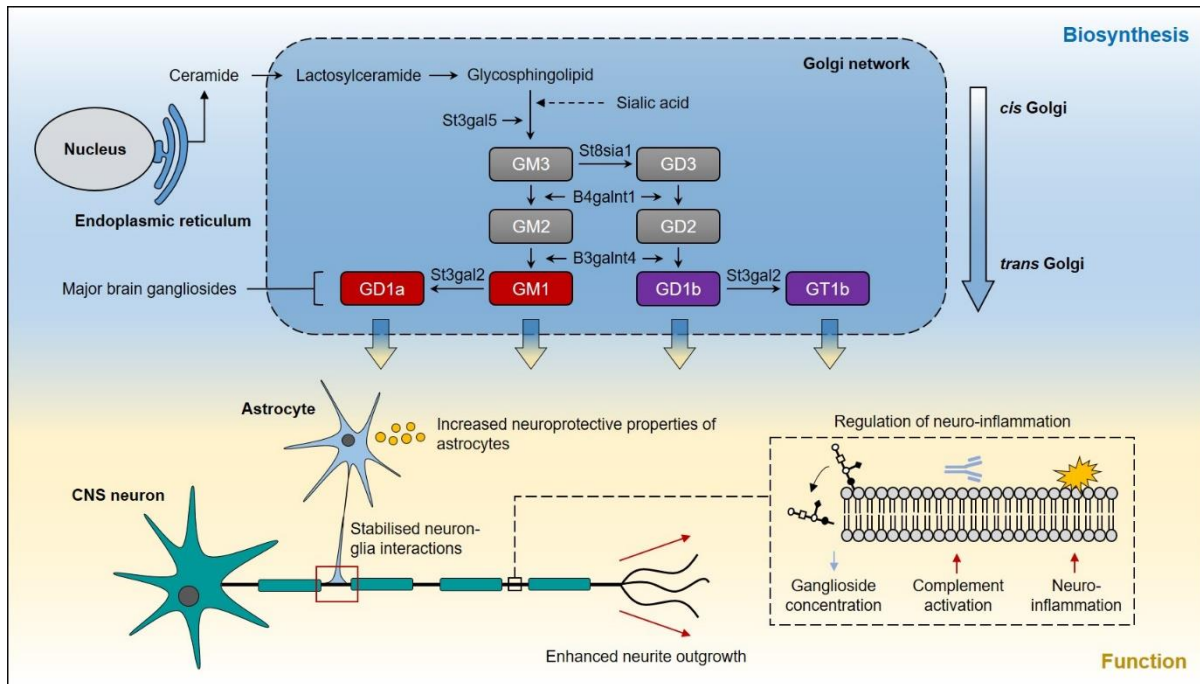


Figure 1.1. Schematic overview of the biosynthesis and function of major gangliosides within the mammalian brain. Lactosylceramide is synthesised at the cytoplasmic leaflet of the ER membrane from its ceramide precursor. De novo ceramide is transported to the Golgi apparatus and is converted to glycosphingolipids and sphingomyelin through the addition of saccharides and phosphocholine, respectively. Glycosphingolipids are transported in vesicles to the outer leaflet of the plasma membrane. Sialic acid-enriched glycosphingolipids form gangliosides, which are anchored to the membrane via their ceramide-lipid moiety. Four major gangliosides comprise >90% of total gangliosides within the brain. A-series gangliosides (red) are derived from GM3. B-series gangliosides (purple) are synthesised from GM3 by GD3 synthase (St8sia1). Nomenclature: the letter G denotes the “ganglioside” core; the second letter designates the quantity of sialic acid residues (M - mono; D - di; T - tri). Gangliosides are essential to maintaining neuronal integrity with functions including, but not limited to, increasing the neuroprotective properties of astrocytes, stabilising interactions between neurons and glia, enhancing neurite outgrowth, and negatively regulating neuroinflammation through activation of the complement pathway. Figure taken from (Moll et al., 2020).

1.6.5. Impaired ganglioside synthesis is linked to neurodegeneration

Altered levels of gangliosides have been reported in animal models of ALS and in post-mortem CNS tissue from ALS patients (Ariga, 2014, Dodge et al., 2015); similar findings have been reported in PD (Wu et al., 2012), HD (Desplats et al., 2007), and AD (Gyls et al., 2007).

1.6.5.1. *Parkinson's disease*

Reduced glycosyltransferase function with subsequent reduction in ganglioside synthesis has been implicated in the pathogenesis of PD. A recent report described a reduction in gene expression of the glycosyltransferases *B3GALT4* and *ST3GAL2* in neuromelanin-containing neurons in the substantia nigra pars compacta (SNpc) of PD patients, compared to controls (Schneider, 2018). These genes are key players in the ganglioside biosynthesis pathway (**Figure 1.1**). It is proposed that reduced *B3GALT4* and *ST3GAL2* expression leads to vulnerability of dopaminergic neurons via aberrant ganglioside synthesis. Consistent with this hypothesis, the number of GM1 ganglioside-expressing cells in the PD SNpc are reduced (Wu et al., 2012), and levels of the major brain gangliosides - GM1, GD1a, GD1b and GT1b - are decreased in whole SN homogenates from PD patients (Seyfried et al., 2018). Model systems provide evidence that dysfunction of ganglioside synthesis is a cause and not just an association of typical PD pathology. Genetically engineered mice lacking major brain gangliosides display overt motor impairment with increasing age, which is accompanied by loss of dopaminergic neurons from the SNpc and aggregation of α -synuclein (Wu et al., 2012).

1.6.5.2. *Huntington's disease*

In a similar manner to PD, reduced expression of glycosyltransferases involved in ganglioside synthesis has also been described in the R6/1 mouse model of HD and in human HD patients (Desplats et al., 2007). In this study >80% of gene expression changes observed in the striatum of R6/1 mice were also observed in the post-mortem caudate of human HD subjects. Overlapping genes were significantly enriched with glycosyltransferases involved in ganglioside synthesis including *ST3GAL5*, *ST8SIA3*, *B4GALNT1* and *ST3GAL2* (**Figure 1.1**). Consistent with impaired ganglioside synthesis, the same study reported reduced ganglioside concentrations within both the diseased human caudate and the mouse striatum.

1.6.5.3. *Alzheimer's disease*

There is good evidence for perturbed ganglioside metabolism in patients with AD, and in the development of β -amyloid pathology in particular (Barrier et al., 2007). In contrast to the findings in PD and HD, the key observation appears to be increased ganglioside synthesis. Elevated GM1, GM2 and GM3 levels have been reported in the cerebral cortices of AD brains (Kracun et al., 1992, Gylys et al., 2007). Development of β -amyloid deposition is the defining pathology of AD and within brains exhibiting early AD pathology, a significant proportion of β -amyloid is bound to ganglioside species (Yanagisawa and Ihara, 1998). It has even been suggested that insoluble GM1-bound β -amyloid is the key toxin leading to neuronal death (Hayashi et al., 2004), as a result of high affinity binding between GM1 and β -amyloid, which facilitates formation of insoluble β -pleated sheets (Yamamoto et al., 2007). With increasing age, GM1 is localised to pre-synaptic nerve terminals and this may have a role in directing β -amyloid deposition to the same locations (Yamamoto et al., 2008). Unlike evidence regarding gangliosides, reports of altered glycosyltransferase expression in AD are more limited. There is evidence that glycosyltransferase activity may modify AD pathology. Overexpression of the glycosyltransferase, B4GALNT1, leads to increased ganglioside expression but also increases APP cleavage to form β -amyloid pathology through suppression of lysosomal degradation of BACE1 (Yamaguchi et al., 2016). Currently, transgenic mouse models of AD do not mirror changes in ganglioside distribution seen in human post-mortem tissue (Barrier et al., 2007).

1.6.5.4. *Amyotrophic lateral sclerosis*

ALS has been linked to abnormal lipid metabolism (Desport et al., 2005) and in particular, gangliosides and their ceramide precursors are thought to be modulators of disease progression (Salazar-Grueso et al., 1990, Stevens et al., 1993). Whether ganglioside production is increased or decreased is controversial. As early as 1985, a 10% reduction in b-series gangliosides was identified within the motor cortex of ALS brains compared to non-ALS controls (Rapport et al., 1985). More recently, elevated levels of gangliosides GM1 and GM3 were reported within ALS post-mortem spinal cords compared to age-matched controls; findings were corroborated in the SOD1^{G93A} transgenic ALS mouse model (Dodge et al., 2015). Interestingly, autoantibodies against specific gangliosides produce an inflammatory disease of spinal motor neurons known as multifocal motor neuropathy with conduction block (Harschnitz et al., 2014), which is a frequent differential diagnosis of ALS. ALS specifically inflicts pathology on the upper and lower motor neurons within the corticospinal tract, the neuromuscular junction, and muscle. The accessibility of this system in disease models

facilitates the differentiation of up- and downstream disease associations. For example, increased expression of glycosphingolipids is observed in muscle tissue from end-stage mutant SOD1-ALS mice compared to controls, but similar changes were observed in response to surgically induced muscle denervation suggesting a downstream effect (Henriques et al., 2015). Moreover, neurotransmission at the neuromuscular junction is unchanged in aged GM2 and GD3-deficient mice, compared to controls (Zitman et al., 2011). The recent discovery that mutations in the glycosyltransferase GLT8D1 are associated with fALS is a step forward that places glycosyltransferase activity irrefutably upstream in the development of disease (Cooper-Knock et al., 2019).

1.6.6. Gangliosides as a therapeutic target

A growing body of evidence supports the role of gangliosides in the pathogenesis of neurodegenerative disease. With this came the realisation that gangliosides may offer a potential new class of therapeutic targets, although it is unclear whether they should be added or removed and in what context. The pharmacological use of gangliosides for targeting neurodegenerative disease processes is becoming increasingly well-documented (Schneider et al., 2015a, Schneider et al., 2015b, Knight et al., 2015, Henriques et al., 2015). The following sections of this introductory chapter will discuss the use of gangliosides for the treatment of AD, PD and ALS.

1.6.6.1. *Alzheimer's disease*

In 1994, a double-blind placebo-controlled trial of intramuscularly administered GM1 for the treatment of AD patients, found that GM1 did not significantly affect cognitive performance. This suggested it was not a viable approach for targeting cognitive deficits in AD (Flicker et al., 1994). However, a later study tested the effects of intracerebroventricular administration of GM1 to 5 early-onset AD patients, and identified improvements in the patients' ability to perform routine daily activities (Augustinsson et al., 1997). This was supported by a subsequent study of 5 early-onset AD patients, reporting that a continuous injection of GM1 into the frontal horns of the lateral ventricles for a twelve-month period improved motor function and neuropsychological ability (Svennerholm et al., 2002). All studies are limited by the low number of participants, but the positive effects observed in the latter two studies suggest that the route of administration affects the therapeutic potential of gangliosides.

The therapeutic value of gangliosides to AD is difficult to determine, due to conflicting reports coupled with reported studies having enrolled a relatively low number of participants. That said, a recent study reported symptomatic improvements in a Dutch APPE693Q mouse model of AD following targeted depletion of ganglioside GM2. Based on the hypothesis that GM2 accelerates the aggregation and accumulation of amyloid- β in AD (Yamamoto et al., 2005), Knight and colleagues increased the activity of a known GM2 catabolising enzyme, β -hexosaminidase. They observed a reduction in the level of ganglioside-bound amyloid- β , as well as improvements in learning behaviour and a reduction in anxiety (Knight et al., 2015).

1.6.6.2. Parkinson's disease

Having shown promise in preclinical animal models of PD through the rescue of SNpc neurons and an increase in dopamine synthesis (Schneider et al., 1995), the therapeutic potential of ganglioside GM1 has since been tested in human subjects. In 1995, Schneider and colleagues confirmed the safety and efficacy of GM1 treatment in PD patients (Schneider et al., 1995). This led to a randomised double-blind placebo-controlled study in 1998, during which significant improvements in the motor performance of PD patients were observed following GM1 treatment (Schneider et al., 1998). Since then, positron emission tomography scans of PD patients receiving GM1 treatment coincided with improvement in the efficacy of the PD drug, Ritalin, in striatal regions compared to controls. Correspondingly, the GM1-treated cohort displayed symptomatic improvement and a reduction in symptomatic progression over the course of the study. Although limited by the low number of participants (n=40), this pilot study provides additional data to support the therapeutic potential of GM1 in PD (Schneider et al., 2015a). However, the disease modifying potential of GM1 is limited by its lack of blood-brain barrier penetrability following systemic administration, indicating the need for membrane-permeable analogues. A previous study has addressed this issue, and the treatment of PD mice with a membrane-permeable analogue of GM1 was shown to attenuate prior manifestations of Parkinsonism (Wu et al., 2012).

Due to limits in bioavailability, methods of enhancing endogenous levels of GM1 in the brain have been explored. Sialidase enzymes were injected into the dorsal third ventricle in a mouse model of PD to catalyse the conversion of GD1a, GD1b and GT1b gangliosides into GM1. A significant increase in ganglioside expression levels was subsequently observed, marked with a reduction in the loss of dopaminergic neurons (Schneider et al., 2015b). With clinical trials still ongoing, research into the use of gangliosides to treat PD is showing more promise than in AD to date.

1.6.6.3. *Amyotrophic lateral sclerosis*

Studies on the therapeutic potential of gangliosides in ALS have been ongoing for decades, yet with inconsistent results. In 1984, a 6-month double-blind controlled trial of intramuscularly administered gangliosides was conducted in ALS patients. No differences were observed in the progression of muscle weakness between the group receiving ganglioside treatment compared to those receiving placebo, suggesting gangliosides are an ineffective treatment option (Harrington et al., 1984). These findings may have been limited by the route of administration, as observed in the AD studies. However, some years later, a patient that also underwent intramuscularly administered ganglioside therapy displayed a high anti-GM2 titre and developed ALS-like disorder. A subsequent decrease in anti-GM2 titre saw symptoms improve, suggesting the anti-GM2 was particularly reactive with motor neurons in the patient, potentially causing motor neuron-specific impairment (Yuki et al., 1991). However, this was an isolated case and it is not conclusive that ganglioside therapy caused ALS. In 1995, Matsumoto and colleagues identified GM2 as a major ganglioside in a neuroblastoma-spinal cord hybrid cell line, suggesting GM2 displays motor neuron specificity. Based on these reports, GM2 might serve as a potential target antigen in ALS (Matsumoto et al., 1995). An interesting follow-up study would be to analyse the presence of GM2 in the serum of a motor neuron disease patient cohort.

A potentially pathogenic role for anti-GM2 antibodies in ALS is inconsistent with reports on other anti-ganglioside antibodies. In 1988, a moderate increase in IgM anti-GM1 antibody titre was reported in the sera of ALS patients. These findings were replicated by the same research group a year later (Pestronk et al., 1988, Pestronk et al., 1989). However, when this concept was revisited in 2015, similar anti-GM1 antibody levels were identified between ALS patients and healthy controls (Kollewe et al., 2015), suggesting the expression of anti-ganglioside antibodies may not bear an impact on disease progression.

In recent years, gangliosides have shown promise as a therapeutic target in murine models of human ALS. rHIgM12 is a recombinant human immunoglobulin M, shown to bind with high affinity to gangliosides GD1a and GT1b. Administration of rHIgM12 in two SOD1 ALS mouse models (G93A and G86R) coincided with a 16-day delay in the onset of neurological deficits and a 5-day delay in weight loss compared to untreated controls (Xu et al., 2015). The therapeutic potential of gangliosides is supported by another study of the same SOD1 ALS mouse model (G93A). The disease course in this model was initially accelerated by inhibiting the synthesis of a complex ganglioside precursor, glucosylceramide. Subsequent infusion of exogenous ganglioside, GM3, delayed the onset of motor deficits and increased viability of

the mice (Dodge et al., 2015). Following on from these reports, a recent study sought to treat SOD1^{G86R} ALS mice with Conduritol B epoxide to increase the concentration of glucosylceramide, the precursor for all complex glycosphingolipids. Ganglioside distribution at neuromuscular junctions was maintained at a level that coincided with a reduction in motor neuron degeneration and a delay in disease onset. Whilst this study supports a role for complex glycosphingolipids in muscle innervation, it also suggests that the targeting of ganglioside precursors is a viable therapeutic approach for ALS (Henriques et al., 2017).

The efficacy of gangliosides as a treatment option has differed between neurodegenerative diseases and is likely influenced by factors such as the route of administration and bioavailability. However, attempts to overcome these limitations have proven successful and the recent targeting of a major ganglioside precursor in ALS is an exciting leap towards preventing the detrimental effects of perturbed ganglioside metabolism. Studies such as this highlight the considerable progress that has been made since the discovery of gangliosides 85 years ago (**Figure 1.2**). The future is likely to see more nuanced manipulation of ganglioside function to alter disease-associated changes in specific cell types at specific times.

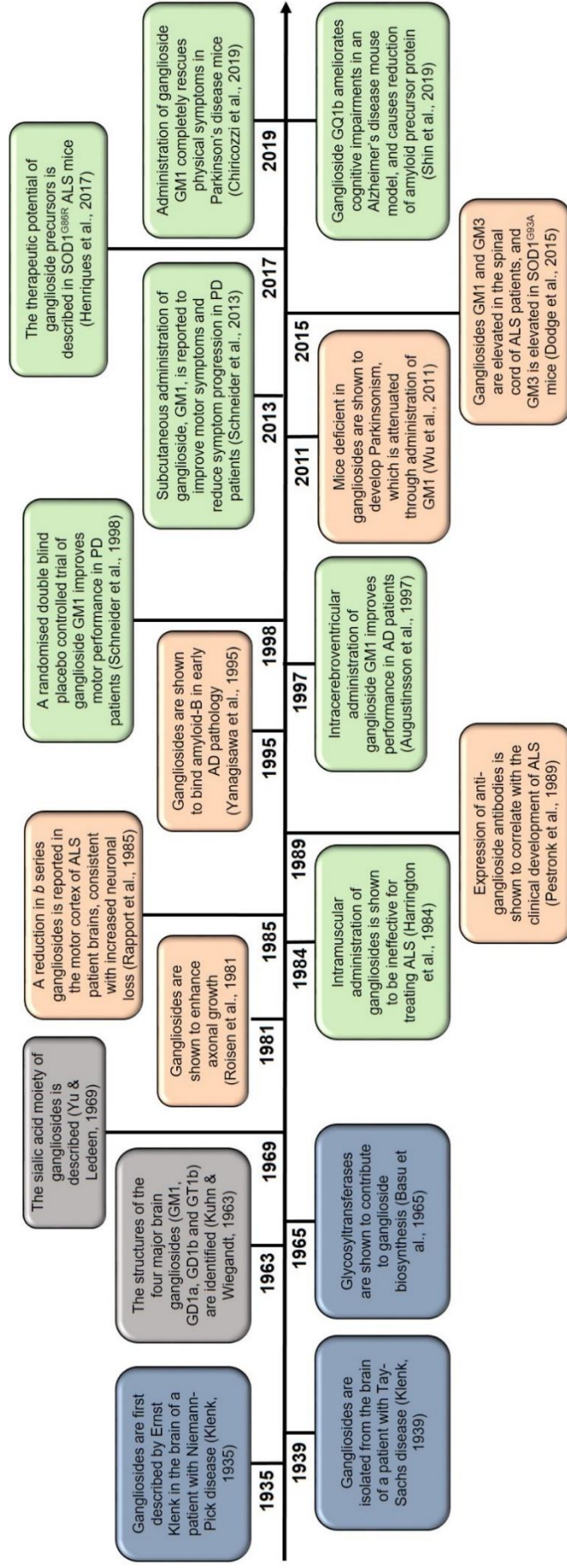


Figure 1.2. Timeline of the key events in the characterisation of gangliosides and their role in neurodegenerative disease .

Gangliosides were first described in 1935 by German scientist Ernst Klenk, who isolated them from the brain of a patient with Niemann-Pick disease, a lysosomal storage disorder characterised by the accumulation of lipids within the liver, spleen, lungs, bone marrow and brain (Klenk, 1935). Shortly afterwards, Klenk isolated a larger quantity of gangliosides from the brain of a patient with Tay-Sachs disease, a progressive neurodegenerative disorder characterised by the accumulation of gangliosides within CNS nerve cells (Klenk, 1939). Klenk coined the term 'gangliosides' to reflect their glycosidic nature and localisation to the ganglion cells within the brain. It was not until 1963 that the first ganglioside structure was described (Kuhn & Wiegand, 1963). Since then, studies have focused on understanding their structural complexity, biosynthesis, biological functions, pathological implications, and their potential as therapeutic targets.

Blue boxes – the discovery of gangliosides and their biosynthesis; grey boxes – studies on ganglioside structure; orange boxes – possible roles for gangliosides in the pathology of neurodegenerative disorders; green boxes – the therapeutic applications of gangliosides.

1.6.7. Glycosyltransferase O-GlcNAcylation: a key regulator of neurodegeneration?

1.6.7.1. O-GlcNAcylation is implicated in neurodegenerative disease

O-GlcNAcylation occurs predominantly in the brain and is regulated by the glycosyltransferases O-Linked N-Acetylglucosamine Transferase (OGT) and EGF Domain Specific O-Linked N-Acetylglucosamine Transferase (EOGT), which attach the GlcNAc moiety to acceptor proteins at specific serine/threonine residues via an O-linked glycosidic bond; the reverse reaction is catalysed by O-GlcNAcase (OGA). OGT acts intracellularly whereas EOGT acts extracellularly on secreted and membrane proteins. Together these reactions constitute a dynamic and reversible process (**Figure 1.3**).

Protein glycosylation, and more specifically the addition of O-GlcNAc groups to CNS proteins important for axonal and synaptic function, is significantly reduced in animal models of neurodegenerative diseases and in patient tissue from diseases including PD, HD, AD, and ALS (Liu et al., 2004, Ludemann et al., 2005, Kumar et al., 2014, Frenkel-Pinter et al., 2017, Wani et al., 2017) (**Table 1.1**). O-GlcNAcylation is reported to negatively regulate tau phosphorylation (Liu et al., 2004), which is key in the pathogenesis of a number of neurodegenerative diseases including AD. In contrast, an increase in O-GlcNAcylation is observed in the post-mortem temporal cortex of PD patients and is postulated to contribute to neurodegeneration through the inhibition of autophagy, leading to an increase in α -synuclein accumulation (Wani et al., 2017).

Neurofilaments are critical components of the neuronal cytoskeleton that can undergo O-GlcNAcylation (Yuan et al., 2012). Neurofilament levels are significantly higher in the serum and cerebrospinal fluid of ALS patients compared to controls (Benatar et al., 2018). This increase is thought to be a consequence of axonal damage. However, there is evidence that neurofilament damage may be upstream in the pathogenesis of ALS, including the observation that increased phosphorylation of neurofilaments is associated with neurotoxicity (Julien, 1997). It is thought that phosphorylation and O-GlcNAcylation are reciprocal, meaning that reduced O-GlcNAcylation could precipitate harmful phosphorylation; indeed, this has been observed in a transgenic rat model of SOD1-ALS (Ludemann et al., 2005).

OGT is an inverting enzyme and a member of glycosyltransferase family 41. OGT is highly enriched in the brain, where it is ten times more active than in peripheral tissue (Okuyama and

Marshall, 2003). OGT is localised to the nucleus, soma, dendrites, and pre-synaptic terminals of neurons (Akimoto et al., 2003). Removal of post-synaptic OGT from primary neurons inhibits both synapse formation and the development of dendritic spines (Lagerlof et al., 2017). This highlights the importance of OGT in maintaining synaptic stability, and notably loss of synaptic stability is a unifying feature of neurodegenerative disease. EOGT is an inverting enzyme and a member of glycosyltransferase family 61. Despite distinct sites of action, OGT and EOGT are both regulated via the hexosamine biosynthetic pathway (Ogawa et al., 2015). EOGT activity is involved in Notch signalling, which is important for neurodevelopment. Indeed, homozygous loss-of-function mutations in EOGT produce Adams-Oliver syndrome, a congenital developmental disorder associated with actin cytoskeleton defects (Schroder et al., 2019).

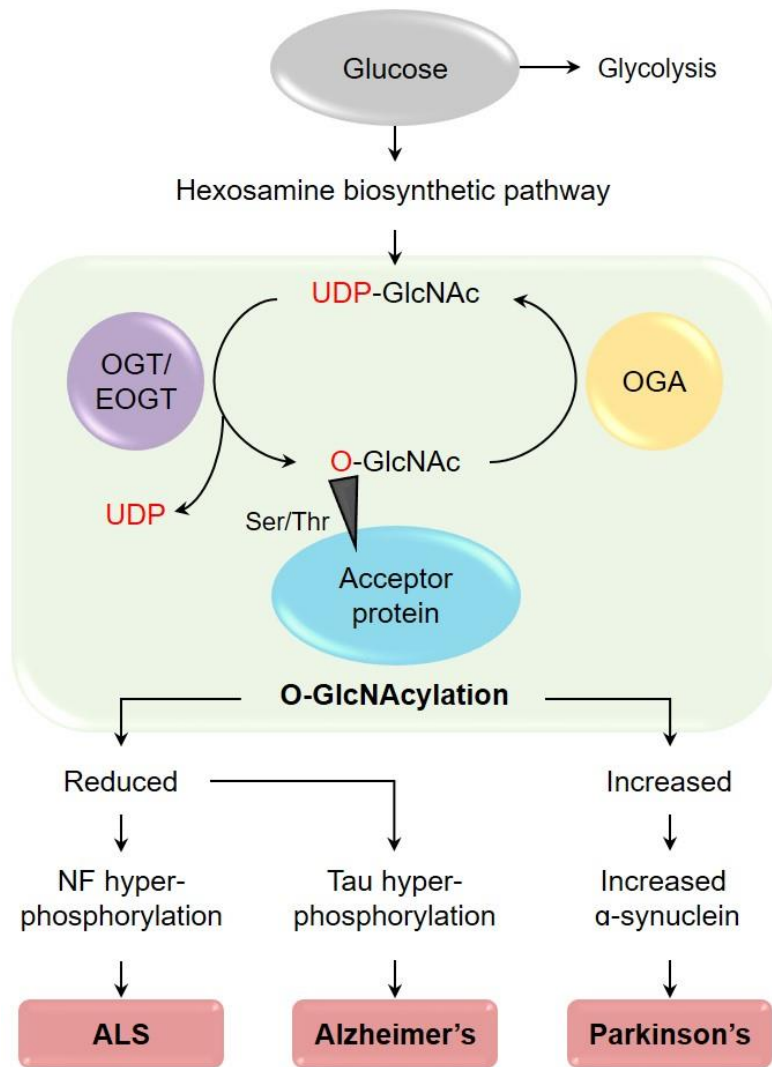


Figure 1.3. O-GlcNAcylation is implicated the pathophysiology of neurodegenerative disease. An overview of O-GlcNAcylation, a post-translational modification of O-GlcNAc, which has been implicated in neurodegenerative diseases: HD, AD, PD, and ALS. O-GlcNAcylation occurs predominantly in the brain and is regulated by the glycosyltransferases OGT and EOGT, which attach the O-GlcNAc moiety to acceptor proteins at specific serine / threonine residues via an O-linked glycosidic bond. OGT acts intracellularly whereas EOGT acts extracellularly on secreted and membrane proteins. Figure taken from (Moll et al., 2020).

1.6.7.2. ALS-associated genetic variants within O-GlcNAcylation pathway enzymes

As part of this literature review, we investigated EOGT mutations in the context of ALS. While homozygous EOGT mutations affect neurodevelopment, we hypothesised that heterozygous mutations within EOGT might negatively impact on the maintenance of axon integrity and increase the risk of developing ALS. To test this hypothesis, we performed rare-variant burden testing (Cirulli et al., 2015) within EOGT to check for a genetic association with ALS (Moll et al., 2020). We used whole genome sequencing data from 4493 sALS patients and 1924 control subjects (van der Spek et al., 2019), and identified 32 missense rare (MAF <1%) variants within EOGT that were exclusively or predominantly found in ALS cases (**see appendix 1**). When considering all rare missense variants found in cases and controls across all exons of EOGT, there was a significant enrichment of such mutations in ALS patients (Firth logistic regression, $p=0.007$). Similar testing did not identify an enrichment of ALS-associated mutations within OGT; indeed, we only identified two rare missense mutations within OGT in 4493 sALS patients. It should be noted that OGT is encoded on the X chromosome and therefore males are necessarily hemizygous, which may predispose to a neurodevelopmental phenotype rather than a late age-of-onset disease; for example, mutations within N terminal tetratricopeptide repeats of OGT are associated with X-linked intellectual disability (Gundogdu et al., 2018). There was no significant burden of ALS-associated mutations within OGA ($p=0.91$) (Moll et al., 2020).

1.6.8. Summary

Overall there is substantial evidence for dysfunction of glycosyltransferases in neurodegenerative diseases including ALS, AD, HD, and PD. There are diverse functions associated with glycosyltransferase activity and for many of the enzymes the biological pathway associated with their activity is not yet clear. However, in our analysis, dysfunction associated with neurodegenerative disease can be seen to converge on the ganglioside synthesis pathway and altered O-GlcNAcylation. The exact nature of the defect appears to be variable in different diseases; for example, ganglioside concentrations are reduced in PD and HD, increased in AD, and there is evidence for change in both directions in ALS. Similarly, increased O-GlcNAcylation is associated with the development of PD pathology but reduced O-GlcNAcylation is associated with the development of tau pathology. We suggest that consensus will arise via efforts to position glycosyltransferase dysfunction within the cascade of pathogenesis leading to neuronal death. It is not glycosyltransferase dysfunction *per se* that is interesting, but rather upstream changes in glycosyltransferase function that initiate toxicity.

With this in mind, we have highlighted genetic associations between mutations in glycosyltransferases and neurodegenerative disease, and we have revealed a new association between ALS and mutations in EOGT. Glycosyltransferases are likely to be an important therapeutic target in the effort to develop disease-modifying therapies for neurodegenerative disease.

1.7. Work leading up to this study: GLT8D1

1.7.1. Exome sequencing in an autosomal dominant ALS pedigree identifies candidate deleterious variants

The following sections are adapted from work published as part of my PhD (Cooper-Knock et al., 2019). Exome sequencing in two related individuals with autosomal dominant ALS (**Figure 1.4a**) identified five potential causal variants. Candidate monogenic causal variants were shared by both affected individuals, rare, and predicted deleterious. Variants were selected for further analysis if the Exome Aggregation Consortium (ExAC) frequency was <1/10,000 controls (Lek et al., 2016) and the Phred-scaled Combined Annotation Dependent Depletion (CADD) score was >25 (Kircher et al., 2014). Heterozygous variants in five genes met the filtering criteria: p.R92C (GenBank: NM_018446: c.274C>T) in *GLT8D1*, p.P529L (GenBank: NM_001267619: c.1586C>T) in *ARPP21*, p.A266T (GenBank: NM_003848: c.796G>A) in *SUCLG2*, p.R1252H (GenBank: NM_173689: c.3755G>A) in *CRB2*, and p.C116R (GenBank: NM_052837: c.346T>C) in *SCAMP3*. Subsequently, another family member developed unilateral weakness and upper motor neuron dysfunction suggestive of ALS. Detailed neurological investigation did not fulfil El-Escorial diagnostic criteria, but no alternative cause was identified. Screening this individual for the five candidate mutations revealed only p.R92C in *GLT8D1* and p.P529L in *ARPP21* (Cooper-Knock et al., 2019).

1.7.2. Targeted sequencing supports pathogenicity of variants within exon 4 of GLT8D1

Targeted DNA sequencing of the five candidate genes was performed in a cohort of 103 fALS and young sALS cases from the North of England. The cohort included 34 fALS patients in whom a genetic cause had not been identified, despite screening for ALS-associated mutations in *SOD1*, *C9ORF72*, *TARDBP*, and *FUS*; 61 young-onset sALS patients; and 13 *C9ORF72*-ALS patients. *SUCLG2*, *CRB2*, and *SCAMP3* were not mutated in any additional cases and were excluded from further analysis. In addition to the two individuals from the index pedigree, four of the screened patients also carried p.R92C (GenBank: NM_018446: c.274C>T) within *GLT8D1* exon 4 (**Tables 1.2, 1.3**). Another patient carried a rare deleterious p.G78W (GenBank: NM_018446: c.232C>A) change within the same exon of *GLT8D1*, suggesting a common pathogenic effect (**Figure 1.4b, Table 1.2**). Mutations were confirmed by Sanger sequencing by using independent DNA samples. In addition to an ExAC frequency

of <1/10,000 controls, similar mutations are absent from North of England controls (n = 220) and from unaffected family members within the index pedigree (**Figure 1.4a**). No patient with a mutation in *GLT8D1* carried an additional ALS-associated mutation, as determined from the ALS Online Genetics Database (Abel et al., 2012). No additional patients were identified with a mutation in *ARPP21* (Cooper-Knock et al., 2019).

GLT8D1 encodes a glycosyltransferase enzyme of unknown function, which is widely expressed (<http://www.gtexportal.org/home/>). Importantly, this class of proteins has not previously been associated with neurodegeneration, although *GLT8D1* has been identified as a schizophrenia risk gene (Sasayama et al., 2014, Yang et al., 2018). It is noteworthy that ALS and schizophrenia share common genetic risk (McLaughlin et al., 2017). Four of five identified *GLT8D1* mutations affect amino acids that show high evolutionary conservation, as determined by relative entropy using the NCBI “Conserved Domains Tool” (<https://www.ncbi.nlm.nih.gov/Structure/cdd/cddsrv.cgi>) (**Figure 1.4c**). All mutations are closely associated with the proposed *GLT8D1* ligand-binding site involving amino acid residues 71–76 (Bourne and Henrissat, 2001), suggesting that the discovered mutations may modify this activity (Cooper-Knock et al., 2019).

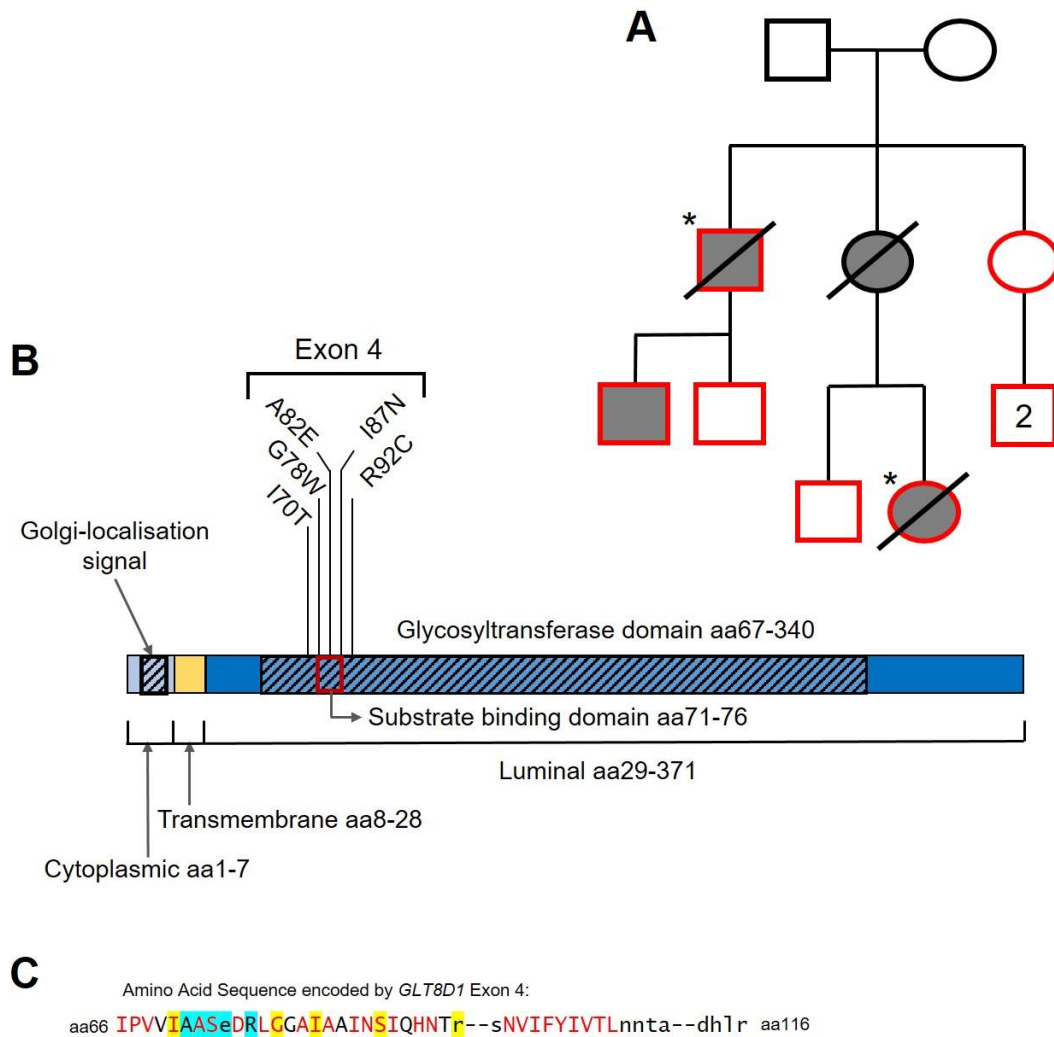


Figure 1.4. Discovery of ALS-Associated Mutations within Exon 4 of *GLT8D1* in Close Proximity to the Putative Substrate Binding Site. (A) Original pedigree in which p.R92C mutations were discovered. Exome sequencing was performed in two related individuals with ALS (*). Sanger sequencing (of red shapes) confirmed the p.R92C mutation is carried by ALS patients (shaded grey) and absent from unaffected individuals. (B) Identified structural and topological domains within *GLT8D1*, including the site of identified mutations within exon 4. (C) Sequence homology analysis within exon 4 localises ALS-associated mutations to close proximity with the substrate binding site of *GLT8D1*. ALS-associated amino acid changes (yellow highlight) affect evolutionary conserved bases (red text) with one exception. Amino acids which form the putative substrate binding site are indicated (blue highlight). Displayed sequence is glycosyltransferase domain encoded by exon 4 (amino acid [aa] 66–aa116). Figure adapted from (Cooper-Knock et al., 2019).

Of the six cases carrying the p.R92C mutation in *GLT8D1*, five cases including the two index cases also carried a p.P529L change (GenBank: NM_001267619: c.1586C>T) within cyclic AMP (cAMP)-regulated phosphoprotein 21 (*ARPP21*). In support of pathogenicity of the p.R92C *GLT8D1* mutation in the absence of the *ARPP21* variant, one patient carried only the *GLT8D1* mutation without an *ARPP21* change. Subsequent analysis of Project MinE whole-genome sequencing data from 4,493 ALS patients (Project MinE ALS Sequencing Consortium, 2018) identified two additional patients carrying the p.R92C mutation without a variant in *ARPP21*. Comparison between the 4,493 Project MinE patients and 60,706 controls sequenced by the ExAC (<http://exac.broadinstitute.org/>) revealed that the p.R92C change is significantly associated with ALS (Fisher exact test, odds ratio [OR] = 54.1, $p = 2.03E-08$), and this association remains significant when cases carrying a variant in *ARPP21* are excluded (Fisher exact test, OR = 20.3, $p = 0.0029$) (Cooper-Knock et al., 2019).

1.7.3. Exon 4 of GLT8D1 is significantly enriched with ALS-associated rare deleterious variants affecting conserved amino acids

Burden analysis was performed using Sequence Kernel Association Test-Optimal Unified Test (SKAT-O) (Lee et al., 2012) to compare rate of genetic variation within exon 4 of *GLT8D1* in a cohort of 1,138 fALS patients and 19,450 controls (as described in (Kenna et al., 2016)). Rare deleterious variants are significantly enriched in exon 4 in the fALS cohort (SKAT-O, $p=0.0025$); there is no significant ALS-association within *GLT8D1* when exon 4 is excluded (**see appendix 2**). Across all cohorts, five distinct rare deleterious mutations of *GLT8D1* exon 4 were identified in fourteen ALS patients (**Table 1.2**). Identification of additional fALS cases from an independent population with similar mutations in *GLT8D1* strongly suggests that *GLT8D1* is an ALS gene (Cooper-Knock et al., 2019).

DNA Change	Protein Change	Number of ALS Patients	ExAC Frequency	CADD Score	Mean disease duration (months)	Familial / Sporadic	Population
c.G274A	p.R92C	10	0.000025	31	21	Familial and Sporadic	UK, Belgium, Netherlands, USA
c.A361G	p.I70T	1	0	28.7	101	Sporadic	Netherlands
c.A412T	p.I87N	1	0	33	N/A	Familial	USA
c.G397T	p.A82E	1	0.000008	32	N/A	Familial	USA
c.C232A	p.G78W	1	0	32	58	Sporadic	UK

Table 1.2. Mutations identified with exon 4 of GLT8D1. DNA change, protein change, number of ALS patients, ExAC frequency, CADD score, average disease duration, disease characterisation, and population, are shown. Table adapted from (Cooper-Knock et al., 2019).

1.7.4. Clinical characteristics of patients with mutated GLT8D1

Clinical characteristics of cases carrying a mutation in *GLT8D1* are summarised in **Table 1.3**. Overall, disease characteristics are within the expected spectrum of ALS (Cooper-Knock et al., 2012). Phenotype data were not available from all cases; however, eight patients with p.R92C mutations suffered a particularly aggressive disease course with average survival of 21 months, but patients with p.G78W or p.I70T mutations lived >5 years. Average age of onset across all patients was 49.3 years, and three patients developed symptoms in their fourth decade; early onset is consistent with monogenic disease (Cooper-Knock et al., 2019).

Case Number	Familial/ Sporadic	Sex	Age of Onset (years)	Disease Duration (months)	Site of Onset	GLT8D1 Mutation	Cohort
1#	Familial	F	39	15	Limb	p.R92C	UK
2#	Familial	M	61	6	Limb	p.R92C	UK
3	Sporadic	F	43	13	Limb	p.R92C	UK
4	Familial	M	33	16	Limb	p.R92C	UK
5	Sporadic	M	44	11	Limb	p.R92C	UK
6	Sporadic	M	59	20	Limb	p.R92C	UK
7	Familial	F	54	>19	Limb	p.R92C	Netherlands
8	Sporadic	M	66	68	Limb	p.R92C	Belgium
9	Sporadic	M	56	101	Bulbar	p.I70T	Netherlands
10	Sporadic	F	38	58	Bulbar	p.G78W	UK

Table 1.3. Phenotype information for patients carrying ALS-associated mutations in GLT8D1. Case number, disease characterisation, sex, age of onset, average disease duration, site of disease onset, GLT8D1 mutation, and population cohort, are shown. # denotes patients that underwent exome sequencing. Table adapted from (Cooper-Knock et al., 2019).

1.8. Work leading up to this study: CAV1 and CAV2

1.8.1. Discovery of ALS-linked CAV1/CAV2 enhancer mutations

The following sections are adapted from work currently submitted for publication as part of my PhD (available at: https://papers.ssrn.com/sol3/papers.cfm?abstract_id=3606796). Non-coding regulatory sequence includes enhancers, which are cis-acting DNA sequences that modulate expression of target genes primarily through binding of transcription factors (TFs) (Koch et al., 2011). Physical interaction between an enhancer and the promoter of the target gene is mediated by DNA looping (Pennacchio et al., 2013). A novel pipeline was designed for the identification of disease-associated variation within enhancers (**Figure 1.5a**).

Sets of enhancers which regulate a common coding gene were aggregated. As previously described (Fishilevich et al., 2017), high quality manually curated links were identified between enhancers and coding genes based on corroboration between: correlated expression between genes, enhancer-RNAs (eRNAs), and TFs; expression quantitative trait loci (eQTL) within enhancers; capture Hi-C; and gene–enhancer genomic distances.

Following the aggregation of enhancers linked to individual coding genes, enhancer variants were filtered to remove those unlikely to be pathogenic prior to association testing. Enhancer variants were included if minor allele frequency (MAF) was <0.01 (Lek et al., 2016, van Rheenen et al., 2016), and LINSIGHT (Huang et al., 2017) score was >0.8 . A LINSIGHT score >0.8 is consistent with strong evolutionary selection (Huang et al., 2017). Following filtering, case and control variant frequencies for each set of enhancers were collapsed into a single SKAT burden test (Lee et al., 2012).

The pipeline was tested using whole genome sequencing (WGS) data from 4,495 ALS cases and 1,925 controls (*Project MinE, Data-Freeze-1*). Firstly, it was hypothesised correctly that aggregated enhancers linked to all genes within the ‘amyotrophic lateral sclerosis’ KEGG (Kyoto Encyclopaedia of Genes and Genomes) pathway (Kanehisa et al., 2017) would be enriched with ALS-associated genetic variation (SKAT-O, $p=0.02$, 377 variants, **see appendix 3**). Secondly, it was hypothesised that pathogenic enhancer variants are likely to cause reduced transcription of their target coding gene, which might be expected to mimic a haploinsufficiency mechanism. Therefore, variants were examined within enhancers linked to expression of *TBK1*, which is known to cause ALS via haploinsufficiency (Freischmidt et al.,

2015). Consistent with this hypothesis, genetic variation within *TBK1* enhancers is significantly associated with ALS ($p=0.003$, SKAT-O, 12 variants, **see appendix 4**).

The pipeline was applied to test for genetic association within enhancers linked to *CAV1* and *CAV2* expression. A significant enrichment of ALS-associated genetic variation was discovered within enhancers linked to *CAV1* ($p=3.88E-05$, SKAT-O, 40 variants) and *CAV2* ($p=1.52E-05$, 57 variants). In total, 56 (1.2%) sALS patients carry one or more ALS-associated variants within *CAV1/CAV2* enhancers compared to 2 (0.1%) of controls. There is significant overlap between enhancers and ALS-associated variants linked to *CAV1* and *CAV2* (**see appendix 5**), which reflects shared function between the two proteins.

1.8.2. Genetic variation within CAV1 coding sequence is associated with ALS

It is likely that genetic variation within linked enhancer and coding regions can produce similar phenotypes. ALS-associated genetic variation within *CAV1* and *CAV2* exons was assessed by rare-variant burden testing using WGS data from 4,495 ALS cases and 1,925 controls (*Project MinE Data-Freeze-1*). In addition to filtering by $MAF < 0.01$ (van Rheenen et al., 2016), a functional filter was introduced to identify variants which alter protein function (Cingolani et al., 2012). In *CAV1*, but not *CAV2*, coding sequence a significant enrichment of functional genetic variation in ALS patients was identified ($p=0.03$, 12 variants, Firth logistic regression, $\beta=1.47$, **Figure 1.5**). Coding and enhancer mutations occurred in independent individuals, which excludes the possibility that the observed convergence is a consequence of linkage disequilibrium.

1.8.3. CAV1/CAV2 function and association with ALS

Caveolin 1 (*CAV1*) and *caveolin 2* (*CAV2*) are scaffolding proteins and the main component of the *caveolae* plasma membranes. *CAV1* and *CAV2* are expressed in most cell types, except striated muscle cells, where *caveolin 3* is predominant. In motor neurons, *CAV1* and *CAV2* are expressed together in a hetero-oligomeric complex (de Almeida, 2017) within membrane lipid rafts (MLRs) on the cell surface and have a key role in organization of intercellular signalling (Sawada et al., 2019; Schmick and Bastiaens, 2014). *CAV1* activity promotes neurotrophic signalling, leading to enhanced neuronal survival (Head et al., 2011; Mandyam et al., 2017). In contrast, loss of *CAV1* accelerates neurodegeneration (Head et al., 2010, 2011). Abnormal neurotrophic signalling is well documented in ALS (Mutoh et al.,

2000; Turner et al., 2004), and in particular, deficient neurotrophic signalling is associated with an increased vulnerability to neuronal injury (Bemelmans et al., 2006; Ghavami et al., 2014; Kowiański et al., 2018; Tooze and Schiavo, 2008).

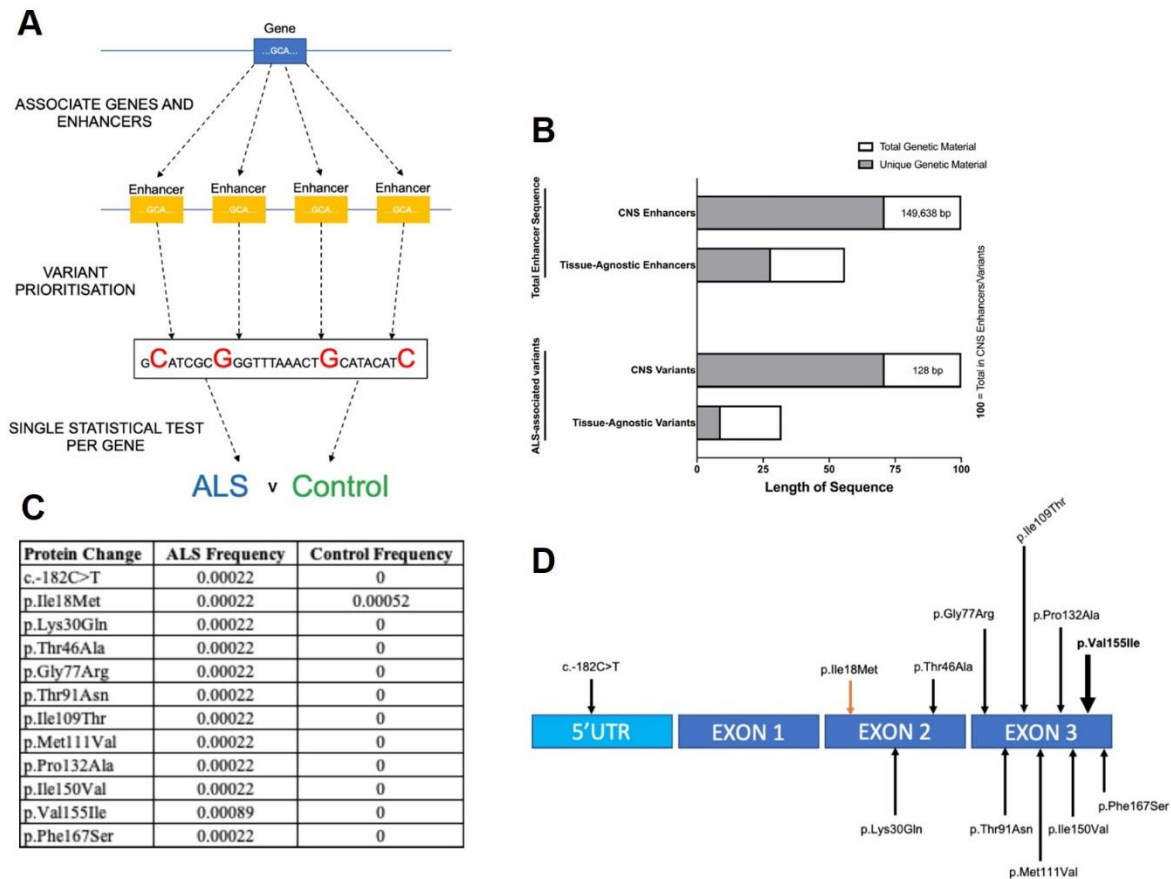


Figure 1.5. Significant enrichment of ALS genetic-risk within enhancers and coding regions linked to *CAV1* and *CAV2*. (A) Pipeline for variant filtering and burden testing; enhancers are first associated with genes based on epigenetic and transcriptome data (Fishilevich et al., 2017); enhancer variants are prioritised for further analysis if they are rare (MAF<0.01, (Lek et al., 2016) and evolutionary conserved (LINSIGHT score >0.8, (Huang et al., 2017)). (B) Quantity of genetic material (bp) relative to CNS enhancers derived from Hi-C data (Rhie et al., 2018); CNS enhancers = 100. Upper two bars denote total genetic material; lower two bars denote ALS-associated genetic variants only. Grey shading denotes material unique to CNS or tissue-agnostic enhancers versus material shared by both (white). (C, D) *CAV1*-coding variants passing filtering criteria are depicted in the table and figure. One variant is present at higher frequency in controls (orange arrow) and one variant is present in multiple ALS patients (bold arrow); all other variants were discovered in a single ALS patient and zero controls.

1.9. Overall objectives and hypotheses

1.9.1. Hypotheses:

1. Mutations in the glycosyltransferase domain of *GLT8D1* cause ALS via dysregulated ganglioside biosynthesis.
2. ALS-associated enhancer mutations linked to *CAV1* and *CAV2* cause downregulation of *CAV1* and *CAV2* expression and disrupt membrane lipid rafts.

1.9.2. Overall objectives:

1. Investigate the relative toxicity caused by overexpressing ALS-associated *GLT8D1* mutations in neuronal and non-neuronal cells.
2. Measure the effect of ALS-associated *GLT8D1* mutations on the glycosyltransferase activity of the enzyme.
3. Assess motor function in zebrafish larvae following targeted knockdown of the endogenous *glt8d1* orthologue using antisense morpholino oligonucleotides, and following overexpression of mutant human *GLT8D1* mRNA.
4. Evaluate the effect of an ALS-linked R92C mutation on membrane lipid raft integrity.
5. Investigate whether an ALS-linked R92C mutation causes fragmentation of the Golgi network.
6. Assess the relative expression of *CAV1/CAV2* mRNA and protein in patient-derived cells carrying an ALS-associated *CAV1/CAV2* enhancer variant.
7. Use CRISPR/Cas9 genome editing to disrupt the WT *CAV1/CAV2* enhancer sequence in a human neuronal cell model, and evaluate the effect on *CAV1/CAV2* mRNA expression.
8. Evaluate the effect of ALS-associated *CAV1/CAV2* enhancer variants on membrane lipid raft integrity.

Chapter 2. Materials and Methods

2.1. Materials

2.1.1. General materials

Bromophenol blue powder, glycerol, sodium chloride (NaCl) analytical grade, dimethylformamide (DMF), sodium dodecyl sulphate (SDS), Ethylenediaminetetraacetic acid (EDTA), Oxoid™ Phosphate Buffered Saline (PBS) Tablets (Dulbecco A), Hanks Balanced Salt Solution (HBSS) and nitrocellulose membranes were all purchased from ThermoFisher Scientific. SDS [Lauryl Sulphate] and HEPES free acid and Tris (molecular grade) were purchased from Melford. Acetic acid; Ammonium Persulphate (APS); β-Mercaptoethanol; Dithiothreitol (DTT); TEMED; Triton™ X-100; Trizma® base; and Tween® 20 were all purchased from Sigma-Aldrich.

2.1.2. General buffers and solutions

- PBS: 137mM NaCl, 3mM KCl, 8mM Na₂HPO₄, and 1.5mM KH₂PO₄, at pH 7.3. Oxoid™ PBS tablets were dissolved in 1L dH₂O, and the solution was autoclaved.
- 1x Tris Acetate EDTA (TAE) buffer: 40mM Tris, 40mM acetate, 1mM EDTA, at pH 8.0.
- 1x Tris-Buffered saline, 0.1% Tween® 20 Detergent (TBST): 20mM Tris, 137mM NaCl, 0.2% (v/v) Tween® 20, at pH 7.6.

Solutions for RNA work were pre-treated with (*Diethylpyrocarbonate*) DEPC to inhibit RNase activity. 0.001 volumes of DEPC was added to the appropriate solution and mixed for 1 hour. The solution was subsequently autoclaved to degrade the DEPC. For sterilisation, solutions were autoclaved in an MP25 autoclave (Rodwell) at 121°C, 15psi for 15 minutes.

2.1.3. Cell culture materials

Dulbecco's Modified Eagle Medium (DMEM), RPMI 1640, DMEM/F-12 GlutaMAX™, Penicillin/Streptomycin and 10x Trypsin were all purchased from Lonza. Neurobasal medium, foetal bovine serum (FBS), L-glutamine, sodium pyruvate, N-2 supplement, B-27 supplement, and Opti-MEM® Reduced Serum Medium were all purchased from ThermoFisher Scientific. Tetracycline-free FBS was purchased from Biosera. Flp-In™ T-REx™ Core Kit, Flp-In™ T-REx™ HEK293 cells, Blastidicin-S and Hygromycin-B, Zeocin™ and Tetracycline were all

purchased from Invitrogen. Plasma fibronectin was purchased from Merck. Gelatin powder was purchased from BDH Biochemical. Polyethylenimine (PEI) was purchased from Sigma-Aldrich. Epidermal growth factor (EGF), Heparin and fibroblast growth factor (FGF) were purchased from PeproTech. Smoothed agonist (SAG) was purchased from Millipore. All-trans retinoic acid (RA) and forskolin were purchased from Sigma-Aldrich.

2.1.4. Molecular biology materials

HyperLadder™ I, II, III, IV and V molecular weight markers, and accuzyme were purchased from Bioline. Pre-stained protein ladder (broad molecular weight) was purchased from Abcam. Agarose (molecular grade) was purchased from Melford. LB Broth, Miller (molecular genetics granular); and LB Agar, Miller (powder) were purchased from Fisher Scientific. DNA Polymerase I was purchased from Invitrogen. DH5- α Competent *E.coli* was purchased from New England BioLabs. T4 DNA Ligase and 10x Ligase Buffer were purchased from Promega. Ethidium bromide, phenol-chloroform and ampicillin were purchased from Sigma-Aldrich. *Bam*HI, *Xba*I, *Nhe*I, *Hind*III, *Bcl*I, and *Xho*I FastDigest restriction enzymes were purchased from ThermoFisher Scientific. 10x FastDigest green buffer, M-MLV reverse transcriptase, 5x first strand buffer, 0.1M dithiothreitol, random hexamer primer and DNTP mix were all purchased from ThermoFisher Scientific. Ethidium bromide was purchased from Sigma-Aldrich. 2x Brilliant III qPCR Master Mix; and 2x Brilliant III SYBR Green qPCR Master Mix were purchased from Agilent Technologies. Protein Assay Dye Reagent Concentrate (Bradford Reagent) was purchased from Bio-Rad. Bovine serum albumin (BSA) powder was purchased from Fisher Scientific. FLAG® Magnetic Beads were purchased from Sigma-Aldrich. Ultra-Pure ProtoGel® 30% (w/v) Acrylamide, 0.8% (w/v) Bis-Acrylamide Stock Solution (37.5:1) and EZ-ECL Kit were purchased from Geneflow. Original dried skimmed milk powder was purchased from Marvel. Paraformaldehyde (PFA), SIGMAFAST™ EDTA-free Protease Inhibitor Cocktail (PIC) tablets, Sodium Azide and ThiozolyI Blue Tetrazolium Bromide (MTT) powder were purchased from Sigma-Aldrich. PMSF protease inhibitor and TRIzol® LS Reagent were purchased from ThermoFisher Scientific. Fluorescent mounting medium (DAKO) was purchased from Aligent. Hoechst (33342) was purchased from ThermoFisher Scientific. Alt-R® S.p. Cas9 Nuclease V3, Alt-R® Cas9 Electroporation Enhancer and TracrRNA were purchased from Integrated DNA Technologies. VeriFi mix red was purchased from PCRBio. Normal horse serum was purchased from Vector.

Table 2.1. Molecular biology kit product details. Name, source and assay ID are shown.

Kit	Source	Identifier
mMESSAGE mMACHINE™ SP6 Transcription Kit	ThermoFisher Scientific	#AM1340
Pierce™ LDH Cytotoxicity Assay Kit	ThermoFisher Scientific	#88953
Plasmid Mini Kit	QIAGEN	#12125
Plasmid Midi Kit	QIAGEN	#12145
UDP-Glo™ Glycosyltransferase Assay Kit	Promega	#V6961
Pierce™ BCA Protein Assay Kit	ThermoFisher Scientific	#23225
Neon™ Transfection System Starter Pack Kit	Invitrogen	#MPK5000S
4D Nucleofector™ System	Lonza	#AAF-1002B #AAF-1002X
GenElute Mammalian Genomic DNA Miniprep Kit	Sigma-Aldrich	#G1N350
Direct-zol RNA Miniprep Kit	Zymo Research	#R2050
Alt-R CRISPR-Cas9 Control Kit, Human, 2 nmol	Integrated DNA technologies	#1072554

Table 2.2. Primary antibodies used for immunoblotting (WB) and immunocytochemistry (ICC). Antibody specificity, molecular weight (kDa), source, species, type, dilution (in 5% (w/v) BSA/PBS) and application are shown.

Antibody specificity	Molecular weight (kDa)	Source/product number	Species/type	Dilution used/application
GLT8D1	42	GeneTex/GTX123636	Rabbit/polyclonal	1:1000 for WB
GLT8D1	42	Sigma-Aldrich/HPA010588	Rabbit/polyclonal	1:200 for ICC
TGN-46	47	Abcam/ab50595	Mouse/monoclonal	1:500 for ICC
GM130	112	Abcam/ab52649	Rabbit/monoclonal	1:250 for ICC
α-Tubulin	50	Sigma-Aldrich/T9026	Mouse/monoclonal	1:5000 for WB/ICC

JL-8	32	Takara Bio/632380	Mouse/monoclonal	1:5000 for ICC/WB
FLAG M2	-	Sigma-Aldrich/F3165	Mouse/monoclonal	1:500 for WB
Caveolin1	22	GeneTex/GTX100205	Rabbit/polyclonal	1:1000 for WB
Caveolin1	22	Abcam/ab2910	Rabbit/polyclonal	1:500 for ICC
Caveolin2	21	Abcam/ab3417	Rabbit/polyclonal	1:500 for WB
Pax6	47	Abcam/ab5790	Rabbit/polyclonal	1:50 for ICC

Table 2.3. Secondary antibodies and molecular probes. Antibody specificity, source, dilution (in 5% (w/v) BSA/PBS) and application are shown.

Antibody	Source/product number	Dilution/application
Donkey anti-mouse (AlexaFluor™ 568)	Life Technologies	1:1000 for ICC
Donkey anti-rabbit (AlexaFluor™ 488)	Life Technologies	1:1000 for ICC
Goat anti-mouse (AlexaFluor™ 568)	Life Technologies	1:1000 for ICC
Goat anti-rabbit (AlexaFluor™ 488)	Life Technologies	1:1000 for ICC
Wheat Germ Agglutinin, AlexaFluor™ 488 Conjugate, fluorescent probe	Invitrogen/11261	2µg/mL for live imaging
Cholera Toxin Subunit B (Recombinant) AlexaFluor™ 555 Conjugate, fluorescent probe	Invitrogen/C22843	1µg/mL for live imaging
Anti-mouse-IgG HRP conjugate	Promega/W4021	1:5000 for WB
Anti-rabbit-IgG HRP conjugate	Promega/W4011	1:5000 for WB

Table 2.4. PCR primer sequences for molecular cloning and site-directed mutagenesis. Gene and reference ID, plasmid type, restriction endonuclease and primer sequences are shown. All oligonucleotides were purchased from Sigma-Aldrich.

Oligonucleotides for molecular cloning.

Gene / reference	Plasmid	Restriction endonuclease	Oligonucleotide sequence for amplification of DNA fragment (5'-3')
GLT8D1 IMAGE: 40116197	pEGFP-N1	GLT8D1-1-koz- NheI5	GGCGGGGCTAGCGCCACCATGTCATTC CGTAAAGTAAAC
	_GLT8D1-eGFP	GLT8D1-371- XhoI3	CCCGCCCTCGAGCTTTATGTTTGAGATC TCGGTATA
GLT8D1 IMAGE: 40116197	pcDNA5/FRT/TO_3x	GLT8D1-1-BclI5	GGCGGGTGATCAATGTCATTCCGTAAAGTAAAC
	FLAG-GLT8D1	GLT8D1-371stp- XhoI3	CCCGCCCTCGAGTCACTTTATGTTTGAG ATCTCGG

Oligonucleotides for site-directed mutagenesis.

Mutation	Forward / reverse	Sequence (5'-3')
GLT8D1 p.G78W	F	GCATCTGAAGACAGGCTTTGGGGGGCCATTGCAGCTA
	R	AGCTGCAATGGCCCCCAAAGCCTGTCTTCAGATGC
GLT8D1 p.R92C	F	AGCATTCAGCACAACTTGCTCCAATGTGATTTTCT
	R	AGAAAATCACATTGGAGCAAGTGTGCTGAATGCT

Table 2.5. Media compositions. Cell lines, media and supplements are shown.

Cell line	Media/source	Supplements
HEK293 / SH-SY5Y	DMEM, Lonza	10% (v/v) FBS and 50 U/mL Pen/Strep
N2A	DMEM, Lonza	10% (v/v) FBS, 50 U/mL Pen/Strep, 500mM sodium pyruvate
HEK293 stable	DMEM, Lonza	10% (v/v) tetracycline-free FBS, 50 U/mL Pen/Strep, 150ug/mL Hygromycin B, and 15ug/mL Blasticidin S
Fibroblast	DMEM, Lonza	10% (v/v) FBS and 50 U/mL Pen/Strep
Lymphoblast	RPMI 1640, Lonza	10% (v/v) FBS and 2mM L-glutamine
Pre-iNPC	DMEM/F-12	1% (v/v) B-27, 1% (v/v) N-2, 20ng/mL
	GlutaMAX™, Lonza	FGFb, 20ng/mL EGF, 5ng/mL Heparin

iNPC	DMEM/F-12 GlutaMAX™, Lonza	1% (v/v) B-27, 1% (v/v) N-2, and 40ng/mL FGFb
iNeuron	DMEM/F-12 GlutaMAX™, Lonza	2% (v/v) B-27, 1% (v/v) N-2)
iAstrocyte	DMEM, Lonza	10% (v/v) FBS, 0.3% (v/v) N-2, 50 U/mL Pen/Strep
Mouse primary	Neurobasal™, ThermoFisher Scientific	1X B27-supplement, 1X GlutaMax, 50 U/mL Pen/Strep

Table 2.6. Plasmid manipulations and origins. Plasmid ID, manipulations and the source are shown. The individuals who provided the plasmid or performed the manipulation are referred to by their initials: Dr Guillaume Hautbergue (GH); Dr Tennore Ramesh (TR); Tobias Moll (TM).

Plasmid	Manipulation	Company/origin
pcDNA5/FRT/TO_GFP	N/A	Addgene
pEGFP-N1	N/A	Clontech
PCS2+	N/A	Addgene
pEGFP-N1_GLT8D1	GLT8D1 (IMAGE: 40116197) inserted into NheI and XhoI restriction sites of pEGFP-N1.	Generated by GH/TM
pEGFP-N1_GLT8D1-G78W	G78W mutation inserted into pEGFP- N1_GLT8D1 via site- directed mutagenesis.	Generated by GH/TM
pEGFP-N1_GLT8D1-R92C	R92C mutation inserted into pEGFP- N1_GLT8D1 via site- directed mutagenesis.	Generated by GH/TM
pcDNA5/FRT/TO_3xFLAG	3xFLAG-M2 tag cloned into HindIII/BamHI sites of pcDNA5/FRT/TO_GFP.	Generated by GH/TM

pcDNA5/FRT/TO_3xFLAG-GLT8D1	GLT8D1 (IMAGE: 40116197) cloned into BamHI/XhoI restriction sites.	Generated by GH/TM
pcDNA5/FRT/TO_3xFLAG-GLT8D1-G78W	G78W mutation inserted into pcDNA5/FRT/TO_3xFLAG-GLT8D1 via site-directed mutagenesis.	Generated by GH/TM
pcDNA5/FRT/TO_3xFLAG-GLT8D1-R92C	R92C mutation inserted into pcDNA5/FRT/TO_3xFLAG-GLT8D1 via site-directed mutagenesis.	Generated by GH/TM
PCS2+_GLT8D1	GLT8D1 cloned into BclI/XbaI restriction sites of PCS2+.	Generated by TR/TM
PCS2+_GLT8D1-G78W	GLT8D1-G78W cloned into BclI/XbaI restriction sites of PCS2+.	Generated by TR/TM
PCS2+_GLT8D1-R92C	GLT8D1-R92C cloned into BclI/XbaI restriction sites of PCS2+.	Generated by TR/TM

Table 2.7. Oligonucleotide sequences for GLT8D1 cloning and knockdown in zebrafish. Label, relevant procedure and nucleotide sequence are shown.

Label	Relevant procedure	Sequence
GLT8D1-koz-NheI5	Generation of GFP-tagged GLT8D1	GGCGGGGCTAGCGCCACCA TGTCATTCCGTAAAGTAAAC
GLT8D1-371-XhoI3	Generation of GFP-tagged GLT8D1	CCCGCCCTCGAGCTTTATGT TTGAGATCTCGGTATA
FLAG HindIII Fwd	Generation of FLAG-tagged GLT8D1	AGCTTGCCACCATGGACTAC AAAGACCATGACGGTGATTA

		TAAAGATCATGACATCGATTA CAAGGATGACGATGACA AGG
FLAG BamHI Rvs	Generation of FLAG-tagged GLT8D1	GATCCCTTGTTCATCGTCATC CTTGTAATCGATGTCATGATC TTTATAATCACCGTCATGGTC TTTGTAGTCCATGGTGGC A
GLT8D1-1-BclI5	Generation of FLAG-tagged GLT8D1	GGCGGGTGATCAATGTCATT CCGTAAAGTAAAC
GLT8D1-371stp-XhoI3	Generation of FLAG-tagged GLT8D1	CCCGCCCTCGAGTCACTTTA TGTTTGAGATCTCGG
GLT8D1-G78W_QC_Fwd	GLT8D1 site-directed mutagenesis	GCATCTGAAGACAGGCTTTG GGGGGCCATTGCAGCTA
GLT8D1-G78W_QC_Rvs	GLT8D1 site-directed mutagenesis	AGCTGCAATGGCCCCCAA GCCTGTCTTCAGATGC
GLT8D1-R92C_QC_Fwd	GLT8D1 site-directed mutagenesis	AGCATTGAGCACAACACTTG CTCCAATGTGATTTTCT
GLT8D1-R92C_QC_Fwd	GLT8D1 site-directed mutagenesis	AGAAAATCACATTGGAGCAA GTGTTGTGCTGAATGCT
MO_GLT8D1	GLT8D1 splice blocking morpholino	CCTCTTACCTCAGTTACAATT TATA
GLT8D1_RT_Fwd	RT-PCR primers for GLT8D1	ACTGGGATTGTTGATGTTGA G
GLT8D1_RT_Rvs	RT-PCR primers for GLT8D1	TAACCACATTCACTCTGCGT
GLT8D1_Fwd	RT-PCR primers for assessing Glt8d1 knockdown in zebrafish	AGCCGGAGAGAGTCCAGTTT
GLT8D1_Rvs	RT-PCR primers for assessing Glt8d1 knockdown in zebrafish	TTGCATCGAAATCTGCTGAA
GLT8D1_miRNA1 top strand	miRNA against human GLT8D1	TGCTGTATAGGTTGAGGCC TACAATGTTTTGGCCACTGA CTGACATTGTAGGCTCAACC TATA

GLT8D1_miRNA1 bottom strand	miRNA against human GLT8D1	CCTGTATAGGTTGAGCCTAC AATGTCAGTCAGTGGCCAAA ACATTGTAGGGCCTCAACCT ATAC
GLT8D1_miRNA2 top strand	miRNA against human GLT8D1	TGCTGAATTGTACTGGTTTC CTGCTCGTTTTGGCCACTGA CTGACGAGCAGGACCAGTAC AATT
GLT8D1_miRNA2 bottom strand	miRNA against human GLT8D1	CCTGAATTGTACTGGTCCTG CTCGTCAGTCAGTGGCCAAA ACGAGCAGGAAACCAGTACA ATTC
GLT8D1_miRNA3 top strand	miRNA against human GLT8D1	TGCTGTAACCTTGGCAGCCTT TACAAAGTTTTGGCCACTGA CTGACTTTGTAAACTGCCAA GTTA
GLT8D1_miRNA3 bottom strand	miRNA against human GLT8D1	CCTGTAACCTTGGCAGTTTAC AAAGTCAGTCAGTGGCCAAA ACTTTGTAAAGGCTGCCAAG TTAC

2.2. Methods

2.2.1. Cell culture

2.2.1.1. HEK293, Neuro-2A and SH-SY5Y cell line maintenance

Human embryonic kidney 293 (HEK293) and human neuroblastoma SH-SY5Y cell lines used in this project were cultured in 10mL Dulbecco's Modified Eagle's Medium (DMEM) supplemented with 10% (v/v) foetal bovine serum (FBS) and 50 U/mL Penicillin/Streptomycin in T75 culture flasks. Neuro-2A (N2A) cell medium was supplemented with an additional 500mM sodium pyruvate. Cell lines were maintained at 37°C, 5% CO₂ and split every 3-4 days. For sub-culturing, media was removed and the cells were washed with sterile phosphate buffered saline (PBS). 2mL 1x trypsin was added to the adherent cells in a T75 and incubated for 3 minutes at 37°C. Flasks were tapped to dislodge trypsinized cells and 10mL of supplemented DMEM was added. Cells were centrifuged at 400xg for 4 minutes at room temperature (RT) and the supernatant was discarded. The cell pellet was re-suspended in fresh DMEM and ~1x10⁶ cells were transferred to a fresh T75 flask. Supplemented DMEM was added to create a final volume of 10mL. All adherent cell lines were seeded at ~20% confluency and sub-cultured when ~90% confluent. All experimental work was performed using HEK-293, N2A, and SH-SY5Y cells within the range of 7-32 passages.

2.2.1.2. HEK293 Sham and HEK293_GLT8D1-WT/R92C cell line generation

Stable HEK293 cells exhibiting tetracycline-inducible expression of wild type (WT) and mutant (p.R92C) GLT8D1 were generated using the Flp-InTM T-RExTM system. The pGKFLPobpA vector (Addgene) encoding a recombinase was co-transfected with either pcDNA5/FRT/TO, pcDNA5/FRT/TO_3xFLAG-GLT8D1, or pcDNA5/FRT/TO_3xFLAG-GLT8D1-R92C plasmids into the HEK293 Flp-InTM T-RExTM CVCL_U427 line in a ratio of 4:6 using polyethylenimine (PEI). Resulting clones were screened for ZeocinTM sensitivity, and Blasticidin-S/Hygromycin-B resistance, to ensure isogenic. Clones that were Blasticidin-S/Hygromycin-B-resistant but ZeocinTM-sensitive were expanded and cryopreserved (see section 2.2.1.9.). HEK293 Sham and HEK293_GLT8D1-WT/R92C stable cell lines were generated by Dr Adrian Higginbottom.

2.2.1.3. HEK293 Sham and HEK293_GLT8D1-WT/R92C stable cell line maintenance

HEK293 Sham and HEK293_GLT8D1-WT/R92C stable cell lines were cultured in 10mL DMEM supplemented with 10% (v/v) tetracycline-free FBS, 50 U/mL Penicillin/Streptomycin, 100µg/mL Hygromycin B and 15µg/mL Blasticidin S in 10cm plates at 37°C, 5% CO₂ and split every 3-4 days as previously described (see section 2.2.1.1).

2.2.1.4. Fibroblast cell maintenance

Human fibroblasts were initially cultured in 10mL Eagle's Minimum Essential Medium (EMEM) supplemented with 10% FBS, 1% MEM non-essential amino acids (Lonza), 1% MEM vitamins (Lonza), 1% Penicillin-Streptomycin, 1% Sodium Pyruvate and 1% Uridine (Sigma) in T75 culture flasks at 37°C, 5% CO₂, prior to cryopreservation (see section 2.2.1.11). Cells underwent a medium change every 2 days and were split when approaching confluence. Cells were split as previously described (see section 2.2.1.1) aside from centrifugation which was performed at 550xg for 4 minutes at RT. The cell pellet was re-suspended in fresh EMEM and 1/3 of the cell suspension was transferred to a fresh T75 flask. Supplemented EMEM was added to create a final volume of 10mL.

2.2.1.5. Lymphoblastoid cell maintenance

Human lymphoblastoid cell lines (LCLs) derived from Caucasian ALS patients (n=5) and neurologically normal controls (n=3), all of Northern European descent, were obtained from the UK Motor Neurone Disease Association (MNDA) DNA Bank. LCLs were cultured in suspension in 30mL RPMI 1640 medium (Lonza) supplemented with 2mM L-glutamine and 10% (v/v) FBS (Table 2.5) in T175 culture flasks at 37°C, 5% CO₂. Cells were seeded at a concentration of 2x10⁵ viable cells/mL and split every 3-4 days. For splitting, cells were centrifuged at 400xg for 4 minutes at RT and the supernatant was discarded. The cell pellet was re-suspended in fresh supplemented RPMI 1640 medium and ~6x10⁶ cells were transferred to a fresh T175 culture flask. Supplemented RPMI 1640 media was added to create a final volume of 30mL.

2.2.1.6. Generation of induced neural progenitor cells (iNPCs) from human fibroblasts

Prior to transduction, fibroblasts were cultured in 10mL DMEM supplemented with 10% (v/v) FBS and 50 U/mL Penicillin/Streptomycin in T75 culture flasks at 37°C, 5% CO₂ for a minimum of 1 week. Fibroblasts underwent a medium change every 2 days, and were split as previously

described (see section 2.2.1.4). 6-well culture plates were coated in plasma fibronectin (5µg/mL in PBS) for 5-30 minutes prior to seeding. Excess fibronectin was removed immediately before seeding $\sim 2 \times 10^5$ fibroblasts per well. Fibroblasts were incubated for 24 hours at 37°C, 5% CO₂. Fibroblasts were transduced using retroviral vectors (MOI 5-10) expressing Kruppel-like factor 4 (*Klf4*), POU transcription factor *Oct-3/4* (*Oct3/4*), SRY-related HMG-Box Gene 2 (*Sox2*), and a *c-Myc* substitute (Dr Laura Ferraiuolo personal communication). Culture media was changed 16 hours post-transduction to fibroblast media (see Table 2.5). After 24 hours, the media was changed to pre-iNPC media (see Table 2.5) containing epidermal growth factor (EGF, 20ng/mL), heparin (5ng/mL) and fibroblast growth factor (FGF, 20ng/mL). Media changes were performed every 2 days; EGF and heparin were removed 10 days post-transduction, and the concentration of FGF was increased to 40ng/mL. iNPCs were generated in collaboration with Dr Laura Ferraiuolo and Allan Shaw.

2.2.1.7. iNPC maintenance

iNPCs were cultured in DMEM/F-12 GlutaMAX™ supplemented with 1% (v/v) B-27, 1% (v/v) N-2, and FGF (20ng/mL) (see Table 2.5) at 37°C, 5% CO₂ in 10cm petri-dishes. 10cm dishes were pre-coated using plasma fibronectin (5µg/mL in PBS) for 30 minutes at RT prior to seeding. iNPCs underwent media changes every two days and were split when $\sim 90\%$ confluent. For splitting, media was removed and cells were incubated in 1mL accutase until they dislodged. Cells were re-suspended in iNPC-conditioned medium and centrifuged at 200xg for 4 minutes at RT. The supernatant was discarded and cells were re-suspended in fresh iNPC media. Excess fibronectin was removed from a fresh, pre-coated 10cm plate and iNPCs were re-plated at a suitable density to encourage contact-mediated recovery.

2.2.1.8. Differentiation of iNPCs into iNeurons

6-well culture plates were coated in fibronectin (5ug/mL in PBS) for 5-30 minutes prior to seeding. Excess fibronectin was removed and iNPCs were seeded into 6-well plates at a density of 2×10^5 cells per well. iNPCs were cultured in 2mL supplemented DMEM/F-12 GlutaMAX™ (see Table 2.5). Media was changed to a FGF-free iNeuron media (DMEM/F-12 GlutaMAX™, 1% (v/v) B-27, 1% (v/v) N-2) (see Table 2.5) 24 hours after seeding. After 48 hours, the media was changed to iNeuron media + γ -secretase inhibitor IX (DAPT, 2.5µM; Tocris). After 48 hours, media was changed to iNeuron media + smoothed agonist (SAG, 0.5µM) + all-trans retinoic acid (RA, 1µM) + forskolin (2.5µM) for 6 days with a media change every 2 days. At day 11, cells were cultured in iNeuron media + SAG (0.5µM) + RA (1µM) + forskolin (2.5µM) + growth factors: brain-derived neurotrophic factor (BDNF, 20ng/mL), ciliary

neurotrophic factor (CNTF, 20ng/mL) and glial cell-line derived neurotrophic factor (GDNF, 10ng/mL) for 4 days. iNeurons were fully differentiated at day 16.

2.2.1.9. Differentiation of iNPCs into iAstrocytes

For iAstrocyte differentiation, iNPCs were seeded as previously described (see section 2.2.1.7) but at a lower density of $\sim 1 \times 10^5$ cells per well in iNPC media (see **Table 2.5**). The following day, the media was changed to iAstrocyte media (DMEM supplemented with 10% (v/v) FBS, 0.3% (v/v) N-2) (see **Table 2.5**). iAstrocytes were allowed to mature for a minimum of 7 days until fully differentiated.

2.2.1.10. SH-SY5Y neuronal differentiation

Human SH-SY5Y neuroblastoma cells were seeded at densities of either 5×10^4 cells per well of a 6-well culture plate, or 2×10^3 cells per well of a 96-well culture plate in DMEM supplemented with 10% (v/v) FBS, 50 units/mL penicillin and 50 μ g/mL of streptomycin. 24 hours after seeding the media was changed to DMEM supplemented with 5% (v/v) FBS, 50 units/mL penicillin, 50 μ g/mL of streptomycin, 4mM L-glutamine, and 10 μ M retinoic acid. After 72 hours, the medium was switched to neurobasal media containing 1% (v/v) N-2 supplement 100x, 50 units/mL penicillin, 50 μ g/mL of streptomycin, 1% L-glutamine and 50ng/mL human BDNF. Cells were cultured for an additional 3 days until fully differentiated.

To confirm neuronal differentiation blinded, semi-automated analysis of neurite length was performed using the SimpleNeuriteTracer plugin for FIJI (Longair et al., 2011). 2D images were converted to 8-bit grayscale and successive points along the midline of a neural process were selected. The software automatically identified the path between the two points. Tracing accuracy was improved using Hessian-based analysis of image curvatures. The AnalyzeSkeleton plugin (Arganda-Carreras et al., 2010) was used to quantify the morphology of the traces.

2.2.1.11. Cryopreservation of Cell Lines

Unless stated otherwise, all cell lines were cryopreserved in freezing medium containing 90% (v/v) FBS + 10% (v/v) dimethyl sulfoxide (DMSO). Cells were pelleted as previously described (see section 2.2.1), and $\sim 5 \times 10^6$ cells were re-suspended in 1mL freezing medium. iNPCs were re-suspended in 1mL 90% (v/v) supplemented DMEM/F-12 GlutaMAXTM + 10% DMSO. Cells

were transferred to a cryogenic vial and were slowly frozen at -80°C in a CoolCell® SV2 (BioCision) overnight, then transferred to liquid nitrogen for long-term storage.

2.2.1.12. Tetracycline induction of stable HEK293 cell lines

To induce expression of the pcDNA5/FRT/TO_3xFLAG-GLT8D1-WT/R92C construct, cells were cultured in Blasticidin-S-free supplemented DMEM for 24 hours (refer to section 2.2.1.3), after which, tetracycline (stock concentration: 10µg/mL in 70% ETOH) was added to the culture media to create a final concentration of 10mg/mL. Induction pressure was stable for at least 48 hours.

2.2.1.13. Preparation and maintenance of dissociated primary mouse cortical neurons

The following protocol was performed under a Home Office project licence (I5BBF6E32) and in accordance with the Animals (Scientific Procedures) Act of 1986 (ASPA). Initially, culture plates were coated in an appropriate volume of poly-D-lysine (50µg/mL in dH₂O) overnight at 37°C, 5% CO₂. C57BL/6 mice were bred at the University of Sheffield Biological Services Unit and females were sacrificed by cervical dislocation. Cerebral cortices were isolated from embryonic day 14 embryos whilst submerged in cold HBSS^{-/-}. Meninges were manually removed using dissecting forceps and the tissue was washed 1x in 10mL HBSS^{-/-}, then resuspended in 5mL HBSS. Trypsin was added to a final concentration of 0.025% and incubated for 13 minutes at 37°C to encourage tissue dissociation. 5mL DNase (10µg/mL DNase in HBSS^{+/+}) was added for 2 minutes and the supernatant was aspirated. Tissue was resuspended in 1mL triturating solution (1% albumax, 25mg trypsin inhibitor, 10µg/mL DNase) and triturated through flame-polished glass Pasteur pipettes with progressively smaller openings to obtain a single cell suspension. Cells were re-suspended in supplemented neurobasal media (1x B27-supplement, 1x GlutaMax, 50 U/mL Penicillin/Streptomycin) and maintained at 37°C, 5% CO₂. A half media change was performed every 3-4 days until the day of experiment. Mouse primary cortical neurons were harvested by David Burrows and Dr Agnieszka Urbanek.

2.2.1.14. CRISPR editing of mammalian cell lines

Clustered Regularly Interspaced Short Palindromic Repeats (CRISPR)/Cas9 technology was utilised for genome editing in HEK293 and SH-SY5Y cell lines. gRNA duplexes were assembled from tracrRNA and crRNA in a thermocycler according to the manufacturer's instructions under RNase-free conditions. Cells were cultured to 70-90% confluent on the day

of transfection. 1mL antibiotic-free DMEM was prepared and incubated in 24-well plates at 37°C. CRISPR/Cas9 Ribonucleoproteins were formed by complexing 240ng gRNA duplex with 1250ng Alt-R V3 Cas9 Protein (IDT) in 10µL buffer R (from 10µL Neon transfection kit) - a 1:1 molar ratio - for 10 minutes. 1×10^5 viable cells were aliquoted per transfection and centrifuged at 400xg for 4 minutes. Cells were washed in Ca_2+ and Mg_2+ -free PBS (Sigma) and centrifuged at 400xg for 4 minutes. Cell pellets were resuspended in the 10µL buffer R containing Cas9 protein and gRNA duplexes. 2µL of 10.8µM electroporation enhancer (IDT) was added and the solution mixed thoroughly to ensure a suspension of single cells. 10µL of this mixture was loaded into a Neon transfection system and electroporated according to manufacturer's instructions (refer to section 2.2.3.2). Cells were then transferred to pre-warmed media in 24-well plates.

2.2.1.15. Determining CRISPR editing efficiency

Genomic DNA was isolated from CRISPR-edited and control cells using a GenElute Mammalian DNA Miniprep Kit (Sigma) according to manufacturer's instructions. A ~400bp region around the expected cas9 cut site was amplified by PCR using VeriFi mix (PCRbio). Expected amplification was confirmed using gel electrophoresis, and the products were Sanger-sequenced (Core Genomic Facility, University of Sheffield). Sequencing trace files were uploaded to TIDE (available at: <https://tide.deskgen.com/>) and an indel efficiency was calculated.

2.2.1.16. Liposome-mediated cell transfection

HEK293 and N2A cells were transfected 24 hours after seeding. Transfection conditions were adjusted according to the plate size, experiment, cell type, and cell density (**see Table 2.8**). Plasmid DNA was mixed with polyethylenimine (PEI) to promote endocytosis. The reaction mixture was diluted using Gibco™ Opti-MEM® I Reduced Serum Media and the samples were vortexed 14-16 times and incubated for 10 minutes at RT to allow DNA-liposome complexes to form. The reaction mixture was added to the culture media in a dropwise manner and cells were incubated at 37°C, 5% CO_2 .

Table 2.8. Transfection conditions according to plate size, experiment, cell type and cell density. (MTT = MTT cell viability assay; ICC = immunocytochemistry).

Plate/flask/cell line	Number of cells	Amount of DNA (μg)	Amount of PEI (μg)	Amount of Opti-MEM [®]
T75	1×10^6	10	35	333 μL
T175	5×10^6	30	105	1mL
10cm plate	2×10^6	15	52	500 μL
6-well plate (HEK)	2×10^5	2	7	200 μL
6-well plate (N2A)	3×10^5	2	6	200 μL
24-well plate (HEK) immunoblotting	5×10^4	0.7	1.75	50 μL
24-well plate (N2A) immunoblotting	7.5×10^4	0.7	2.1	50 μL
24-well plate (HEK) MTT / ICC	2.5×10^4	0.5	1.75	50 μL
24-well plate (N2A) MTT / ICC	3×10^4	0.5	1.75	50 μL

2.2.1.17. Electroporation-mediated cell transfection

2.2.1.17.1. Neon[®] Transfection System

Electroporation was performed using a Neon[®] Transfection System (Invitrogen) according to the manufacturers' guidelines. In brief, a Neon[®] Tube was filled with 3mL of Electrolytic Buffer and inserted into a Neon[®] Pipette Station. Cells were harvested as previously described (see section 2.2.1.1). Cells were centrifuged at 400xg for 4 minutes at RT and the media was removed. Cells were washed with Ca₂⁺ and Mg₂⁺-free PBS and re-centrifuged at 400xg for 4 minutes at RT. The PBS was aspirated and the cells were re-suspended in Resuspension Buffer R at a final density of 1×10^7 cells/mL. The amount of DNA used for transfection was dependent on cell concentration and the size of the culture plate used for subsequent seeding (see Table 2.9). DNA was gently mixed with the cell suspension and 10 μL was aspirated into a Neon[®] Tip using a Neon[®] Pipette, avoiding the formation of air bubbles. The Neon[®] Pipette containing the sample was inserted vertically into the Neon[®] Tube and electroporation was performed at 3 pulses of 1200V with a pulse width of 20ms. Following electroporation, cells were seeded into an appropriate culture plate and incubated at 37°C, 5% CO₂.

Table 2.9. Nucleofection conditions using the Neon® Transfection System (adapted from Invitrogen).

Plate	DNA (μg)	Volume of plating medium	Cell number
96-well	0.25 - 0.5	100 μL	1-2 x 10 ⁴
48-well	0.25 – 1.0	250 μL	2.5-5 x 10 ⁴
24-well	0.5 – 2.0	500 μL	0.5-1 x 10 ⁵
12-well	0.5 – 3.0	1mL	1-2 x 10 ⁵
6-well	0.5 – 3.0	2mL	2-4 x 10 ⁵
10cm	5.0 – 30.0	10mL	1-2 x 10 ⁶

2.2.1.17.2. 4D Nucleofector™ System

Nucleofection was performed following the dissociation of primary mouse cortical neurons (refer to section 2.2.1.13). Excess poly-D-lysine was removed from the culture plate, and the wells were washed 2x in dH₂O and 1x in sterile PBS. An appropriate volume of pre-warmed neurobasal media was added to the wells and the plates were incubated at 37°C, 5% CO₂. Fresh, dissociated cortical neurons were electroporated using a 4D Nucleofector™ System (Lonza) according to the manufacturer’s instructions. In brief, 100 μL reactions were assembled by mixing 82 μL Nucleofector™ Solution with 18 μL Supplement (sample contents confidential) to create the Nucleofector™ X Solution. 4-5x10⁶ cells were centrifuged at 80xg at RT, and the pellet was resuspended in 90 μL Nucleofector™ X Solution. 10 μL of plasmid DNA (2 μg) was added and the reaction was mixed gently. Samples were transferred to a single Nucleovette™ and electroporated using a randomly selected pre-programmed setting recommended by the manufacturer (voltage and pulse width were encrypted). The sample was incubated at RT for 10 minutes post-nucleofection, resuspended in pre-warmed neurobasal medium, and transferred to the culture plate which was pre-coated using poly-D-lysine (see section 2.2.1.13).

2.2.2. Molecular cloning

2.2.2.1. Plasmid cloning by polymerase chain reaction (PCR)

PCR reactions (50µL total) for the amplification of I.M.A.G.E. clones were assembled accordingly:

- 1µL DNA I.M.A.G.E. clone (100ng/µL)
- 34.5µL Milli-Q H₂O
- 5µL 10x Accuzyme™ reaction buffer
- 1µL Accuzyme™ DNA Polymerase
- 1µL DMSO
- 5µL 10x DNTP Mix (each at 10mM)
- 1.25µL forward primer (10µM)
- 1.25µL reverse primer (10µM)

PCR reactions were performed in a thermocycler according to the following parameters outlined in **Table 2.10**:

Table 2.10. PCR programme for I.M.A.G.E clone amplification.

Stage	Temperature	Time
Heated lid	110 °C	-
Pre-cycle step	95 °C	1 minute
Start cycle 30x		
Temperature step 1	95 °C	20 seconds
Temperature step 2	53 °C	20 seconds
Temperature step 3	72 °C	3 minutes
End cycle		
Post-cycle step	68 °C	4 minutes
Hold	10 °C	Infinite

2.2.2.2. Agarose gel electrophoresis

Agarose gel electrophoresis was used to separate linear DNA fragments produced by PCR or restriction digest. 1% agarose gels were prepared by dissolving 1g agarose powder in 100mL 1x Tris-acetate-EDTA (TAE) buffer (40mM Tris; 20mM NaOAc; 1mM EDTA; pH8.0) (w/v). The agarose solution was heated until fully dissolved, cooled, and 100ng/mL of ethidium bromide

was added to enable visualisation of the nucleic acid under ultraviolet (UV) light. The mixture was cooled slightly and poured onto a casting tray containing 30-well combs. The gel was left for 30 minutes to cool and set, then transferred to an electrophoresis tank and submerged in 1x TAE buffer. Combs were removed and samples were loaded consecutively alongside 5µL of a HyperLadder™ molecular weight marker. Electrophoresis was performed at 80V for 45-60 minutes, and gels were imaged using the GENI UV light imaging system (Syngene). For DNA extraction, bands were visualised on a UV-trans illuminator, excised using a scalpel and transferred to an Eppendorf tube.

2.2.2.3. DNA extraction from agarose gels

DNA was extracted from agarose gels using a QIAquick Gel Extraction Kit (QIAGEN), according to the manufacturers' instructions. In brief, 100µL Buffer QG (solubilisation and binding buffer) was added per 100mg gel and incubated at 50°C for 10 minutes with vortexing every 2-3 minutes until the gel completely dissolved. One gel volume of isopropanol was added to the sample and mixed. The sample was then transferred to a QIAquick spin column and drawn through via vacuum suction. 750µL Buffer PE (wash buffer) was applied to and drawn through the column. Excess Buffer PE was removed via centrifugation at 13,300xg for 1 minute at RT. 50µL Buffer EB (elution buffer) was added to the column and left to stand for 3 minutes at RT. DNA was eluted into an Eppendorf tube via centrifugation at 13,300xg for 1 minute at RT.

2.2.2.4. Restriction digests for PCR insert

Restriction digests were assembled accordingly:

- 50µL DNA (500ng/µL)
- 30µL Milli-Q H₂O
- 10µL 10x restriction buffer (NEB)
- 50 units of each restriction enzyme (**see Table 2.6**)

Reactions were incubated on a heat block overnight at 37°C.

2.2.2.5. Phenol-chloroform extraction for DNA purification

100µL of phenol-chloroform was added to the restriction digest reaction and vortexed for 1 minute at RT. Samples were centrifuged at 13,300xg for 3 minutes at RT and the supernatant was transferred to a fresh Eppendorf tube. 3M NaOAc was added (10% of total volume) and the sample was vortexed briefly. Twice the volume of 100% ETOH was added and the sample

was incubated at -20°C for 2-3 hours to precipitate the DNA. Samples were centrifuged at 13,300xg for 20 minutes at RT and the supernatant was discarded. The DNA pellet was washed in 70% ETOH to remove excess salts and left to air-dry for 1 hour at RT, then re-suspended in 16µL Milli-Q H₂O.

2.2.2.6. Plasmid ligation

Digestion reactions for the linearization of plasmids were assembled accordingly: 2µL plasmid DNA (500ng/µL); 2µL 10x restriction buffer; 1µL of each restriction enzyme (10 units / µg DNA) (**see Table 2.6**); 14µL Milli-Q H₂O. Reactions were incubated at 37°C for 2 hours. During the final 10 minutes of the digest, 1 unit of calf intestinal alkaline phosphatase (CIP) was added for every 1 pmol of DNA ends, to dephosphorylate DNA 5'-ends and ensure the vector did not re-circularise during ligation. A ligation reaction was then assembled accordingly:

- 16µL DNA (500ng/µL)
- 0.5µg pre-cut vector
- 5µL 5x ligation buffer
- 1µL T4 DNA ligase
- 2µL Milli-Q H₂O

Ligation reactions were incubated overnight at 16°C in a thermocycler.

2.2.2.7. Site-directed mutagenesis

50µL PCR reactions for site-directed mutagenesis were assembled accordingly:

- 0.5µL plasmid DNA (100ng/µL)
- 1.25µL forward oligonucleotide (125ng)
- 1.25µL reverse oligonucleotide (125ng)
- 5µL 10x dNTPs (each at 10mM)
- 5µL 10x PFU turbo buffer (2mM)
- 36µL Milli-Q H₂O
- 1µL PfuTurbo DNA polymerase

PCR reactions were run in a thermocycler according to the following parameters outlined in **Table 2.11**:

Table 2.11. PCR programme for site-directed mutagenesis.

Stage	Temperature	Time
Heated lid	110 °C	-

Pre-cycle step	95 °C	30 seconds
Start cycle 26x		
Temperature step 1	95 °C	10 seconds
Temperature step 2	53 °C	1 minute
Temperature step 3	72 °C	15 seconds
End cycle		
Post-cycle step	72 °C	10 minutes
Hold	10 °C	Infinite

Mutated inserts were subsequently validated by Sanger sequencing (Core Genomic Facility, University of Sheffield).

2.2.2.8. LB agar plates

Lysogeny broth (LB) agar (10g/L Tryptone, 5g/L Yeast extract, 10g/L NaCl, 15g/L Agar) was prepared by re-suspending 40g LB agar powder in 1L dH₂O, and autoclaving. The following steps were performed aseptically to avoid contamination. LB agar was heated until completely melted and left to cool for 15 minutes at RT. 50µg/mL ampicillin or 50µg/mL kanamycin selection antibiotic was added to the melted LB agar. The LB agar solution was then mixed, poured onto 10cm petri dishes, left to set at RT, and stored at 4°C.

2.2.2.9. Plasmid transformation into competent *E. coli*

The following steps were performed aseptically to avoid contamination: DH5-α competent *Escherichia coli* (*E. coli*) cells and plasmid DNA were thawed on ice. 1µL of plasmid DNA (500ng/µL) was added to 50µL of DH5- α cells and incubated on ice for 10 minutes. Samples were then heated for 5 minutes at 37°C before adding 1mL Lysogeny broth (LB) to stimulate bacterial growth. Samples were then incubated at 37°C for 1 hour, during which agar plates containing 50µg/mL of ampicillin were dried at 37°C. 100µL of each sample was transferred to an agar plate, streaked using a sterile cell spreader, and incubated overnight at 37°C. The following day, a single bacterial colony was selected and transferred to either 100mL (for Midiprep) or 2mL (for Miniprep) of liquid LB containing 50µg/mL of appropriate antibiotic (depending on the antibiotic resistance gene in the plasmid of interest) and incubated overnight at 37°C on a shaker.

2.2.2.10. DNA extraction and purification from bacterial cultures

2.2.2.10.1. Plasmid Miniprep

Minipreps were performed using a QIAGEN® Plasmid Mini Kit, according to the manufacturer's instructions. In brief, 1.5mL of bacterial cultures were harvested by centrifugation at 10,000xg for 1 minute at RT. The supernatant was discarded and the bacterial pellet was re-suspended in 200µL buffer P1. 200µL buffer P2 was added, the sample was gently inverted 5 times and incubated for 5 minutes at RT. 300µL Buffer S3 was added and inverted 10 times, then centrifuged at 10,000xg for 1 minute at RT. The supernatant was transferred to a fresh Eppendorf tube, mixed with 700µL isopropanol and incubated at RT for 10 minutes. Samples were centrifuged at 10,000xg for 10 minutes at RT and the supernatant was completely removed. The pellet was air dried for 10 minutes then re-suspended in 50µL buffer EB.

2.2.2.10.2. Plasmid Midiprep

Bacterial cultures were harvested by centrifugation at 6000xg for 15 minutes at 4°C. Plasmid purification was performed using the QIAGEN® Plasmid Plus Midi Kit, according to the manufacturer's instructions. For maximum DNA yield, pelleted bacteria was re-suspended in 4mL resuspension buffer (buffer P1) (50mM Tris-Cl, pH 8.0; 10mM EDTA; 100 µg/ml RNase A). 4mL lysis buffer (buffer P2) (200mM NaOH, 1% SDS) was added and mixed by inversion until a viscous lysate formed, and was incubated at RT for 3 minutes. 4mL neutralisation buffer (buffer P3) (3.0 M potassium acetate, pH 5.5) was added to the lysate, mixed 4-6 times by inversion and incubated at RT for 10 minutes. 2mL binding buffer (buffer BB) was added, mixed by inversion, and incubated at -20°C for 15 minutes to increase the yield of DNA further. The lysate was transferred to a QIAGEN Plasmid Plus spin column and drawn through via vacuum suction at ~300 mbar. 700µL endotoxin removal buffer (buffer ETR) was applied to the column and centrifuged at 10,000xg for 1 minute at RT. 700µL wash buffer (buffer PE) (10mM Tris-HCl pH 7.5, 80% ETOH) was subsequently applied to the column and centrifuged at 10,000xg for 1 minute at RT. Any residual wash buffer was removed by centrifugation at 10,000xg for 1 minute. To elute the DNA, 200µL elution buffer (buffer EB) (10mM Tris-Cl, pH 8.5) was applied to the columns, incubated at RT for 2 minutes, and centrifuged at 10,000xg for 1 minute. DNA was quantified using a NanoDrop™ 1000 Spectrophotometer (ThermoFisher Scientific) and sequence identity was confirmed via Sanger sequencing (Core Genomic Facility, University of Sheffield).

2.2.2.11. Restriction digests for plasmid characterisation

The following components were added to a clean Eppendorf tube in the order shown: 1µg digested DNA; 10 units of each restriction enzyme (**see Table 2.6**); 1µL 10x FastDigest Green Buffer. Volumes were adjusted to create a 10µL reaction by adding an appropriate volume of Milli-Q H₂O. The reaction mix was incubated at 37°C for 1 hour, after which the DNA fragments were separated via agarose gel electrophoresis (see section 2.2.2.2).

2.2.2.12. Quantitative Real-Time PCR (qRT-PCR)

Cells were cultured until at least 70% confluent, lysed on ice using an appropriate volume of Tri Reagent (Sigma) for 5 minutes and transferred to 1.5mL RNase-free tubes. Total RNA was extracted using a Direct-zol RNA Miniprep Kit (Zymo) according to manufacturer's instructions. During RNA purification, samples were treated with DNase (6 U/µL) to degrade genomic DNA prior to reverse transcription. RNA concentration was confirmed using a NanoDrop™ 1000 Spectrophotometer (ThermoFisher Scientific). 2µg of total RNA was then converted to cDNA by adding 1µL dNTPs (2mM each), 1µL 40µM random hexamer primer (ThermoFisher Scientific), and DNase/RNase-free water to a total volume of 14µL. This mixture was heated for 5 minutes at 70°C then incubated on ice for 5 minutes. 4µL of 5x FS buffer, 2µL 0.1M DTT, and 1µL M-MLV reverse transcriptase (ThermoFisher Scientific) were then added and the cDNA conversion was performed in a PCR thermocycler (37°C for 50 minutes, 70°C for 10 minutes). cDNA was amplified using RT-PCR with Brilliant III SYBR Green (Agilent) as per the manufacturer's instructions. CT analysis was performed using CFX Maestro software (BioRad).

2.2.3. Biochemical methods

2.2.3.1. Sodium dodecyl sulphate-polyacrylamide gel preparation

Spacer plates were assembled onto Mini-PROTEAN® Tetra Cell Casting Modules (BioRad). Resolving gels containing 12% polyacrylamide were prepared (w/v) (**see Table 2.12**) and transferred into the 1mm space separating the two spacer plates. Resolving gels were sealed with a layer of isopropanol for 15 minutes, which was subsequently removed before pouring a 5% stacking gel (**see table 2.12**) onto the surface. Mini-PROTEAN® Combs were inserted into the surface of the stacking gels and left to set for 15 minutes at RT.

Table 2.12. Composition of 12% resolving and 5% stacking polyacrylamide gels.

Reagent	5% stacking	12% resolving
dH ₂ O	5.8mL	3.5mL
30% (w/v) Acrylamide	1.7mL	4.0mL
Resolving buffer (1.5M Trizma®, 13.9mM sodium dodecyl sulphate (SDS), pH 8.8, filtered)	-	2.5mL
Stacking buffer (0.5 M Trizma®, 13.9mM SDS, pH6.8, filtered)	2.5mL	-
10% (w/v) APS	50uL	50uL
TEMED	20uL	20uL

2.2.3.2. Cell lysis for immunoblotting

2.2.3.2.1. IP lysis buffer

HEK293 and N2A cell lysis was performed on ice to minimise protein degradation. DMEM was removed from cultured cells, and cells were washed with ice-cold PBS. PBS was aspirated and replaced with ice-cold IP lysis buffer (150mM NaCl, 50mM HEPES, 1mM EDTA, 1mM DTT, 0.5% (v/v) Triton™ X-100, pH 8.0) containing an EDTA-free protease inhibitor cocktail (PIC) (SIGMAFAST™ Sigma-Aldrich) at 1% of the total volume (20µL/mL). 50µL IP lysis buffer was added per well of a 24-well plate, 200µL per well of a 6-well plate, and 500µL per 10cm plate. Cells were scraped into the IP lysis buffer and incubated on ice for 15 minutes. The lysate was transferred to pre-cooled micro-centrifuge tubes and centrifuged at 17,000xg for 5 minutes at 4°C. The supernatant was transferred to fresh pre-cooled Eppendorf tubes and the cell debris pellet was discarded.

2.2.3.2.2. Bradford protein assay

A Bradford assay was used to quantify total protein levels within cells lysed in IP lysis buffer. 1µL cell lysate was mixed with 1mL Bradford reagent (Bio-Rad) (pre-diluted 1:5 in dH₂O) and incubated at RT for 2 minutes. The sample was transferred to an optically clear polystyrene cuvette and the absorbance was read at 595nm, relative to a blank control, using a WPA S1200 Diode Array Spectrophotometer (Biochrom Ltd.). Protein concentrations were calculated using the Beer-Lambert law ($OD_{595nm} = \epsilon \times l \times c$; where $\epsilon = 1/15$, and $l = 1cm$) and

normalised to the least concentrated sample by adding the necessary volumes of complete IP lysis buffer.

2.2.3.2.3. Urea lysis buffer

Lymphoblastoid cell lysis was performed using urea lysis buffer [8M urea; 1% (w/v) DTT; 20% (w/v) SDS; 1.5M Tris pH 6.8; + dH₂O) (+ PIC [20µL/mL] + 1mM phenylmethylsulfonyl fluoride (PMSF) at RT to avoid precipitation of the urea out of solution. Media was removed from pelleted lymphoblastoid cells and the pellet was re-suspended in an appropriate volume of urea lysis buffer. Samples were syringed 10x using 25-gauge needles and incubated at RT for 15 minutes. Samples were further lysed by sonication (Soniprep 150, MSE) for 10 seconds at 50% amplitude followed by a 30-second incubation at RT; this process was repeated 3 times. Lysates were then centrifuged at 13,000xg for 5 minutes at RT, the supernatant was transferred to a fresh Eppendorf tube, and the pellet of debris was discarded.

2.2.3.2.4. Bicinchoninic acid (BCA) assay

BCA assays were used to quantify total protein levels within lymphoblastoid cell lysates. BCA assays were performed using a Pierce™ BCA Protein Assay Kit (ThermoFisher Scientific), according to the manufacturers' instructions. In short, a standard curve was created by diluting albumin standards in PBS at RT. A working reagent (WR) was then prepared by mixing BCA Reagent A with BCA Reagent B (50:1, Reagent A:B). Protein lysates were mixed thoroughly then diluted in PBS (1:10). 25µL of each standard or unknown sample was added per well of an optically clear 96-well plate, in triplicate. 200µL of the WR was added to each well and the plate was mixed thoroughly on a plate shaker for 30 seconds at RT. The plate was then incubated in the dark at 37°C for 30 minutes. The plate was cooled to RT and the absorbance was measured at 562nm on a PHERAstar® FS spectrophotometer (BMG Labtech). Absorbance data from the unknown samples were plotted against a standard curve and the concentrations were calculated.

2.2.3.3. SDS-polyacrylamide gel electrophoresis

Cell lysates were mixed with 4x Laemmli buffer (277.8mM Tris-HCl; 44.4% (v/v) glycerol; 4.4% SDS; 0.02% bromophenol blue; 355mM 2-mercaptoethanol; pH 6.8) and heated at 95°C for 5 minutes to denature the proteins. 12% SDS polyacrylamide gels were assembled into a Mini-PROTEAN® Tetra Vertical Electrophoresis Cell (Bio-Rad) and submerged in running buffer

(25mM Tris, 3.5mM SDS, 20mM glycine). 25µg of each denatured protein sample was loaded per well, alongside 2µL of a pre-stained protein ladder (ab116028, Abcam) to serve as a molecular weight marker. Gel electrophoresis was performed at 120V for approximately 1 hour, or until the dye front had reached the bottom of the gel. For immunoblotting of nitrocellulose membranes, gels were moved to a semi-dry transfer apparatus and assembled with nitrocellulose membranes (Bio-Rad) and transfer buffer (47.9mM Tris, 38.6mM glycine, 1.38mM SDS, 20% (v/v) methanol)-saturated Whatman® filter paper (Sigma-Aldrich). Protein within the gel was electrophoretically transferred to the nitrocellulose membranes at 0.15A per gel for 1 hour.

2.2.3.4. Immunoblotting

Nitrocellulose membranes were stained with Ponceau stain (0.1% (w/v) Ponceau S, 5% (v/v) acetic acid) for the rapid detection of protein bands. Membranes were blocked in 5% (w/v) milk (Marvel)/Tris Buffered Saline, with Tween® 20 (TBST) (20mM Tris, 137mM NaCl, 0.2% (v/v) Tween® 20, pH 7.6) overnight at 4°C. Membranes were then incubated with primary antibody (**see Table 2.2**) in 5% milk/TBST for 1 hour at RT. Membranes were washed 3x in TBST (10 minutes per wash) at RT, then incubated with a secondary antibody (**see Table 2.3**) conjugated to horseradish peroxidase (HRP) in 5% milk/TBST for 1 hour at RT. The membranes were washed 3x in TBST (10 minutes per wash) at RT and incubated with a chemiluminescent substrate and oxidising agent (1:1) (Pierce™ ECL, ThermoFisher Scientific) for 1 minute. The chemiluminescence signal was imaged using a G:BOX (Syngene).

2.2.3.5. Coomassie blue staining

12% polyacrylamide gels were prepared as previously described (see section 2.2.3.1). Following electrophoresis (see section 2.2.3.3), gels were submerged in 100mL Coomassie® Blue R-250 (ThermoFisher Scientific) staining solution (0.1% (v/v) Coomassie® R-250, 40% (v/v) ETOH, 10% (v/v) acetic acid) for 1 hour at RT on an orbital shaker. The staining solution was decanted and gels were rinsed 1x in dH₂O. Gels were submerged in 100mL destain solution (10% (v/v) ETOH, 7.5% (v/v) acetic acid) overnight at RT and imaged the following day using a white light illuminator.

2.2.3.6. Immunoprecipitation (IP) of FLAG-tagged GLT8D1

HEK293 cells were seeded at a density of 1x10⁶ cells per 10cm petri dish and cultured for 24 hours. Cells were subsequently transfected with pcDNA/FRT/TO_3xFLAG-GLT8D1 wild-type

and mutant vectors as previously described (see section 2.2.1.16). For the immunoprecipitation of GLT8D1 from stable HEK293 lines, cells were cultured in Blasticidin S-free supplemented DMEM for 24 hours prior to induction with 10mg/mL tetracycline for 48 hours (refer to section 2.2.1.12). 25x 10cm dishes were assembled for each condition to maximise protein yield. Prior to cell lysis, 300µL anti-FLAG® M2 magnetic beads (ThermoFisher) were blocked in BSA (1% in PBS) in 1.5mL Eppendorf tubes at 4°C on a rotating mixer. 48 hours post-transfection, media was removed, cells were washed in ice-cold PBS, and lysed in 500µL ice-cold IP lysis buffer (+ PIC [20µL/mL] + 1mM PMSF) for 3 minutes. Cells were removed using a cell scraper, transferred to pre-cooled Eppendorf tubes, and syringed 10x using 25-gauge needles. Lysates were centrifuged at 13,300xg for 5 minutes at 4°C. 50µL of the supernatant was retained as a reference for protein input. Total protein concentration within cell lysates was determined using a Bradford assay (see section 2.2.3.2.2). 1% BSA was separated from the anti-FLAG® M2 magnetic beads using a DynaMag™-2 Magnet (ThermoFisher) and replaced with the protein lysate. Samples were then incubated for 2-3 hours on a rotating mixer at 4°C. Protein lysate was separated from the magnetic beads using a DynaMag™-2 Magnet, and the supernatant was retained as a reference for flow-through. The magnetic beads were washed 3x in 1M NaCl (diluted in an appropriate volume of IP lysis buffer) followed by 2x washes in IP lysis buffer. Anti-FLAG® M2 magnetic beads were incubated with a FLAG® peptide (100µg/mL in lysis buffer) (Millipore) overnight at 4°C on a rotating mixer to purify FLAG-tagged products via competitive elution. Anti-FLAG® M2 magnetic beads were removed and the purified protein was fractionated on 12% polyacrylamide gels (see section 2.2.3.3) alongside the input and flow-through for either Coomassie blue staining (see section 2.2.3.5) or immunoblotting (see section 2.2.3.4). Purified protein was stored at -80°C.

2.2.3.7. Glycosyltransferase activity assay

Glycosyltransferase assays were performed in opaque, white 96-well plates using a UDP-Glo™ Glycosyltransferase Assay kit (Promega) according to the manufacturers' guidelines. In brief, a required volume of Nucleotide Detection Reagent was equilibrated to RT. 300µL UDP-Glo™ working solution was prepared by mixing 4µL UDP-Glo™ Enzyme with 296µL Enzyme Dilution Buffer. 10µL of UDP-Glo™ working solution was added per 1mL Nucleotide Detection Reagent and mixed to homogeneity immediately before use. A standard curve of 0-25µM UDP was generated to estimate the amount of UDP produced in the glycosyltransferase reaction. To create the standard curve, 25µM UDP solution was prepared in 1x glycosyltransferase reaction buffer (50mM Tris pH 7.5, 5mM MnCl₂) and serially diluted (1:2) with 25µL per well of a 96-well plate. A no-UDP served as a negative control. 25µL glycosyltransferase reactions

were assembled on ice accordingly:

- 1.5 μ L 0.1M MnCl₂
- 1.25 μ L 1M Tris
- 12.5 μ L UDP sugar substrate (serially diluted: 40mM-0.15625mM)
- Purified enzyme (serially diluted: 28mg/mL-0.109375mg/mL) in lysis buffer (see section 2.2.3.6)
- 8 μ L dH₂O.

To determine the kinetic parameters of the glycosyltransferase enzyme, multiple reactions with varying concentrations of either enzyme or substrate were carried out simultaneously in the presence of fixed volumes of all other components. Glycosyltransferase reactions were run at 37°C for 60 minutes and terminated through the addition 25 μ L nucleotide detection reagent to each well of the assay plate. Plates were mixed on a plate shaker for 30 seconds and incubated for 60 minutes in the dark at RT. Luminescence was recorded using a PHERAstar FS System (BMG Labtech). Statistical analysis was performed using GraphPad Prism (see section 2.2.6).

2.2.3.8. Immunocytochemistry

For Nikon Eclipse Ni-U fluorescence microscopy and SP5 confocal microscopy, cells were seeded at a density of 3×10^4 cells per well of a 24-well plate onto glass coverslips and cultured for 3 days prior to immunocytochemistry. For imaging using an Opera Phenix™ High Content Screening System (PerkinElmer), cells were seeded into black Greiner 96-well plates (ThermoFisher Scientific). The volumes of solutions used in this section were relative to the size of the well. Media was removed from cells in culture, and cells were washed 2x with PBS. Cells were fixed in 4% paraformaldehyde (PFA) at RT for 20 minutes, and then washed another 2x with PBS. Cells were blocked using 5% normal goat serum (NGS) (v/v) in PBS, and were incubated at RT for 45 minutes. Blocking buffer was removed and cells were incubated in 0.01% Triton™ X-100 (+ PBS) for 30 minutes at RT. Triton™ X-100 was removed and cells were incubated in primary antibody (**see Table 2.2**), diluted in 5% NGS (v/v), at RT for 1 hour or overnight at 4°C. Cells were washed 3x in PBS (5 minutes per wash), then incubated in an appropriate fluorescent secondary antibody (**see Table 2.3**), diluted in 5% NGS (v/v), in a dark environment at RT for 1 hour. The secondary antibody was removed and cells were incubated with a nuclear counterstain (Hoechst 33342) (1 μ g/mL in PBS) in the dark for 5 minutes at RT and washed 3x with PBS (5 minutes per wash). Cell-containing glass coverslips were mounted onto microscope slides using fluorescence mounting medium (DAKO) and stored in a dark environment at 4°C overnight to dry.

2.2.3.9. Multiphoton and confocal microscopy imaging and image analysis

Cells were imaged using either a Nikon Eclipse Ni-U microscope and Nikon DS-Ri1 camera with Nikon NIS-Elements Viewer software, or an SP5 confocal microscope system (Leica) with an X63/1.4 oil immersion objective lens. For confocal imaging, a z-stack was made up of images at 0.13µm intervals through the entire nuclear volume of the cell under consideration. Pixel intensity spatial correlation analysis was performed using ImageJ (NIH). The JACoP plugin was used for co-localisation analysis. Colour channels were split to create separate images, thresholds were automatically determined, and the M1/M2 and Pearson's coefficients were calculated (Manders et al., 1993).

2.2.3.10. Live-cell imaging using fluorescent molecular probes

Greiner 96-well culture plates were coated in sterile 0.5% (w/v) gelatin (100µL/well) overnight at 4°C prior to cell seeding. Cells were seeded at densities of 1×10^4 cells per well and cultured for 2 days prior to imaging. For live-cell imaging, fluorescent probe solutions of 1mg/mL (Molecular Probes®) were prepared by dissolving 5mg of lyophilized conjugate in 5mL of sterile PBS (**Table 2.3**). 1mg/mL conjugate stock solutions were diluted in Hanks Balanced Salt Solution (HBSS) to create a working concentration of 5µg/mL of labelling solution. Media was removed and 100µL of labelling solution was added to cell-containing wells and incubated for 45 minutes at 37°C, 5% CO₂. The labelling solution was removed, and cells were incubated with a nuclear counterstain (Hoechst 33342) (1µg/mL in HBSS) for 5 minutes at 37°C, 5% CO₂. Nuclear counterstain was removed and cells were washed 2x in PBS, then incubated in 200µL pre-warmed HBSS for confocal imaging. Live imaging was performed via confocal microscopy using an Opera Phenix™ High-Content Screening System (PerkinElmer) at 37°C, 5% CO₂. Cells were visualised within a high-resolution z-stack consisting of images at 0.5µm intervals through the entire nuclear volume of the cell. Images were analysed using Harmony High-Content Imaging and Analysis Software (PerkinElmer).

2.2.3.11. MTT cell viability assay

HEK293 and N2A cells were seeded at a density of 3×10^4 cells per well of a 24-well culture plate. Cell viability was assessed 2 and 3 days post transfection in N2A and HEK293 cells, respectively (see section 2.2.1.16). 55µL of 5mg/mL MTT [3-(4, 5-dimethylthiazol-2-yl)-2, 5-diphenyltetrazolium bromide] reagent was added per well of the 24-well culture plate and incubated at 37°C, 5% CO₂ for 1 hour. 550µL of un-precipitated SDS/DMF lysis buffer (20% (v/v) SDS [Melford]; 50% (v/v) di-methyl formamide (DMF); pH 4.7) was added per well and

mixed thoroughly to lyse the cells. Cells were incubated in a dark environment on an orbital shaker at RT for 1 hour. The colorimetric change was measured using a PHERAstar FS spectrophotometer (BMG Biotech), and absorbance readings taken at 590nm were normalised to media-only wells. Statistical analysis was performed using GraphPad Prism (GraphPad Software, Inc.) (see section 2.2.6).

2.2.3.12. *Lactate dehydrogenase assay*

A Pierce™ Lactate Dehydrogenase (LDH) Cytotoxicity Assay Kit (ThermoFisher Scientific) was used according to the manufacturers' instructions. Initially, HEK293 and N2A cells were seeded into white 96-well culture plates at a density of 2000 cells per well. Cytotoxicity was measured 2 and 3 days post transfection (see section 2.2.1.16) in N2A and HEK293 cells, respectively. Sterile, ultra-pure H₂O was added to one set of triplicate cell-containing wells (10% v/v) as a measure of spontaneous LDH activity. 10x lysis buffer was added to another set of triplicate cell-containing wells (10% v/v) to determine the maximum LDH activity. Cells were incubated at 37°C in 5% CO₂ for 45 minutes. 50µL of each sample medium was transferred to an optically clear 96-well plate in triplicate wells. 50µL of reaction mixture (lyophilizate, 11.4mL ultra-pure H₂O, 0.6mL assay buffer) was added to each sample well and plates were incubated in a dark environment for 30 minutes at RT. 50µL of stop solution was added to each sample well and the absorbance was measured at 490nm and 680nm on a PHERAstar FS spectrophotometer (BMG Biotech). The 680nm absorbance value was subtracted from the 490nm absorbance value to determine LDH activity. Statistical analysis was performed using GraphPad Prism (see section 2.2.6).

2.2.4. Modelling in zebrafish (*Danio rerio*)

All zebrafish work was performed in collaboration with Dr Tennore Ramesh. Dr Ramesh is a registered project licence holder (70/8058) under the Animals (Scientific Procedures) Act, 1986. I hold a Home Office approved personal licence (I5BBF6E32) to carry out regulated procedures on zebrafish, as specified on the project licence. However, all experimentation was performed using zebrafish larvae <5.2 days post-fertilisation, at a time when zebrafish are not protected by European law (EU Directive 2010/63/EU).

2.2.4.1. *RNA Synthesis for zebrafish embryo microinjection*

Capped RNA was synthesised using a mMMESSAGE mMACHINE® SP6 Transcription Kit

(ThermoFisher Scientific), according to the manufacturers' instructions, using DNA templates harbouring an SP6 promoter site downstream of the target sequence. Circular DNA fragments within PCS2+ vectors (**Table 2.6**) were linearized via a restriction digest (see section 2.2.2.11). 20µL of transcription reactions were assembled at RT accordingly: 10µL 2X NTP/CAP (10mM ATP; 10mM CTP; 10mM UTP; 2mM GTP; 8mM cap analog); 2µL 10X reaction buffer; 0.5µg linearized template DNA; 2µL enzyme mix (buffered 50% glycerol containing RNA polymerase, RNase Inhibitor, and other components). Nuclease-free water was added to create total reaction volume of 20µL. The reaction mixture was mixed thoroughly and incubated at 37°C for 2 hours to account for slower SP6 reactions and achieve maximum possible yield of RNA. RNA was recovered via Lithium Chloride (LiCl) precipitation by adding 30µL nuclease-free water and 30µL LiCl precipitation solution. Samples were mixed thoroughly, incubated at -20°C for 30 minutes and then centrifuged at 16,000xg for 15 minutes at 4°C. The supernatant was removed and the RNA pellet was washed with 1mL of 70% ETOH. Samples were re-centrifuged to maximise the removal of unincorporated nucleotides. The 70% ETOH was removed and the RNA pellet was air dried at RT for 10 minutes. RNA was diluted in 20µL of injection buffer (0.5% Fast Green, 200mM Tris–Cl pH 7.0, 20mM EDTA). RNA concentration was estimated using a NanoDrop™ 1000 Spectrophotometer (ThermoFisher Scientific® Inc.), and diluted in RNase-free water to achieve a final concentration of 200ng/µL. RNA stocks were stored in RNase-free Eppendorf tubes (3µL per tube to avoid repeated freeze-thaw cycles) at -80°C to prevent degradation. The quality of the transcription was assessed using a NanoDrop™ 1000 spectrophotometer and agarose gel electrophoresis (see section 2.2.2.2).

2.2.4.2. Generation of a morpholino for zebrafish embryo microinjection

Splice-blocking morpholino antisense oligonucleotides were designed and provided by Gene Tools, LLC, for the targeted knockdown of endogenous *glt8d1* in zebrafish embryos. The *glt8d1* start codon lies within exon 2, therefore skipping this exon was considered likely to alter expression of the gene. The morpholino sequence complementary to the splice junction target from 5' - 3' is shown below; brackets have been inserted either side of the pre-mRNA (sense strand) target to illustrate its position in the sequence:

5'-ACATCAGAGTCTGCATACCTGAAGT[ACGCAGAGgtaactatattttacac]gactttca-3'

Morpholino powder was reconstituted in sterile Milli-Q water and 1% phenol red to create a 1mM stock.

2.2.4.3. Zebrafish maintenance and breeding

Zebrafish of the AB strain were raised in recirculating systems (Tecniplast) at a density of 1 zebrafish per 0.25 litres of water. Water was maintained at pH 7.4, a temperature of 28°C, and electrolytic conductivity of 500 μ S/cm. Zebrafish were exposed to 14-hour light and 10-hour dark cycles. The night before breeding, adult male and female zebrafish were transferred to breeding tanks, separated by a clear plastic divider. At the start of the light cycle the following day, the dividers were removed and eggs were collected. Zebrafish embryos were transferred to petri dishes containing fresh E3 media (34.8g NaCl; 1.6g KCl; 5.8g CaCl₂·2H₂O; 9.78g MgCl₂·6H₂O) and incubated at 28°C.

2.2.4.4. Zebrafish embryo microinjection

Glass capillaries with an outside diameter of 1.0mm were pulled to form microinjection needles with an inner tip diameter of 10 μ m. Needles were back-loaded with 3 μ L of injection material using a micro loader pipette and inserted into the micro injector attached to a PV 820 Pneumatic PicoPump (World Precision Instruments). Needle tips were broken using forceps to allow ejection of the splice-blocking morpholino or RNA, leaving the needle narrow enough to pierce the chorion but deliver a consistent bead size. In order to calibrate the volume of each injection, a drop of oil was added to a graticule and the morpholino or RNA was injected into it, where 0.125mm contained approximately 1nL of injection material; the injection time was adjusted as required to obtain a 0.5nL, 1.0nL or 2.0nL volume of liquid. Embryos were lined up alongside a microscope slide, E3 media was removed, and oocytes were injected into the yolk at the one-cell stage with either 0.5nL, 1.0nL or 2.0nL of injection material. Embryos were transferred to petri dishes containing E3 media. Any unfertilised embryos, or embryos damaged during the injection process, were discarded into bleach. To increase the reliability of the data, zebrafish embryos from 3 separate clutch mates underwent the same injection process for each biological repeat where possible.

2.2.4.5. Behavioural analysis

The Zebrolab screening tool (ViewPoint) was used to record the activity of individual larva in an optically clear 96-well plate at 5 days post-fertilisation (dpf). Zebrafish embryos were washed in fresh E3 media (approximately 50 embryos per group) and transferred to a 96-well plate, one fish per well in 200 μ L E3 medium. 100 μ L of E3 media was removed from one column and replaced with 100 μ L of Tricaine (MS222) (400mg Tricaine powder; 97.9mL dH₂O; 2.1mL 1M Tris; pH 7) (Sigma-Aldrich) (164 mg/L) to create a non-motile control group. Fish

were left to acclimatise to the 96-well plate for 30 minutes. Zebrafish were then placed inside the Zebrabox observation chamber and were habituated at 10% light intensity for 30 minutes prior to behavioural testing. Zebrafish were exposed to a 10-minute light (10% intensity) cycle followed by a 10-minute dark (0% intensity) cycle. These cycles were then repeated to equal 40 minutes of tracking. Motor function was analysed according to the mean distance travelled and the average velocity of the zebrafish embryos. Statistical analysis was performed using GraphPad Prism (see section 2.2.6).

2.2.4.6. Zebrafish RT-PCR

Twenty zebrafish embryos (2dpf) were transferred to Eppendorf tubes containing 1mL E3 media, for each condition. Tricaine (164 mg/L) was added and the zebrafish were incubated at RT for 5 minutes. E3 media was removed and 500µL TRIzol reagent was added per tube. Samples were incubated at RT for 5 minutes. 100µL chloroform was added and the samples were mixed by inversion for 15 seconds. Samples were incubated for 10 minutes at RT, then centrifuged at 12,000xg for 15 minutes at 4°C. The top aqueous phase was transferred to a fresh Eppendorf tube and mixed with 250µL isopropanol to precipitate the RNA. Samples were incubated for 15 minutes at RT, then centrifuged at 12,000xg for 10 minutes at 4°C. The isopropanol was removed and the pellet was left to air dry for 10 minutes, then resuspended in 50µL RNase-free H₂O. RNA quality was assessed using a NanoDrop™ 1000 spectrophotometer (ThermoFisher Scientific). 2µg of total RNA was converted to cDNA as previously described (see section 2.2.2.12). PCR reactions were assembled accordingly:

- 4µL of 5x FIREPol® (Solis Biodyne)
- 1µM forward primer (see table 2.7)
- 1µM reverse primer (see table 2.7)
- 1µL template DNA
- Nuclease-free H₂O to create overall reaction volume of 20µL

The template was amplified using the following PCR programme outlined in **Table 2.13**:

Table 2.13. PCR programme for zebrafish RT-PCR.

Step	Temperature (°C)	Time	Cycles
Initial denaturation	94	3 minutes	-
Denaturation	94	30 seconds	
Primer annealing	60	45 seconds	35x
Elongation	72	2 minutes	
Final elongation	72	7 minutes	-
Hold	10	Infinite	-

PCR products were evaluated via agarose gel electrophoresis (see section 2.2.2.2).

2.2.4.7. Zebrafish immunoblotting

Dechorionated zebrafish embryos (2dpf) were transferred to Eppendorf tubes (20 embryos per tube) containing 1mL E3 media. Tricaine (164 mg/L) was added and the zebrafish were incubated at RT for 5 minutes. E3 media was removed and replaced with 3 μ L/embryo 2x Laemmli buffer (65.8mM Tris HCl; 26.3% (w/v) glycerol; 2.1% SDS; 0.01% bromophenol blue; 355mM 2-mercaptoethanol; pH 6.8). Zebrafish embryos were lysed by sonication (Soniprep 150, MSE) for 10 seconds at 25% amplitude followed by a 30-second incubation on ice; this process was repeated 3 times for each group. Embryos were subsequently boiled at 95°C for 10 minutes, then centrifuged at 10,000xg for 3 minutes at RT. 10 μ L of lysate was added per lane and fractionated on a 12% SDS-PAGE gel as previously described (see section 2.2.3.3).

2.2.6. Statistical analysis

Statistical analysis was conducted in GraphPad Prism 7 (La Jolla, CA). All bar graphs show the mean \pm SD. Data comparing two variables was transformed to identify outliers and analysed to identify statistical differences between the treatment groups. The statistical test used for datasets with greater than two conditions was a non-parametric analysis of variance (ANOVA). Non-parametric tests were chosen when data was not normally distributed, and to account for smaller sample sizes. Paired *t* tests were used for all *in vitro* datasets comparing two conditions. Zebrafish data were analysed using either a Mann-Whitney test or, in the case of survival data, a paired *t* test to account for continuity between time points.

Chapter 3. ALS-linked G78W and R92C variants in GLT8D1 are toxic to HEK293 and N2A cells and impair enzyme activity

3.1. Introduction

This chapter is an extended version of work published during my PhD (Cooper-Knock et al., 2019). I was responsible for conducting all experimental work presented within this chapter, and any collaborations are clearly stated. My focus was to generate cell models to characterise pathological mechanisms associated with ALS-linked GLT8D1-G78W and GLT8D1-R92C variants. The R92C mutation was chosen, as this was the most common and clinically aggressive mutation identified in ALS patients, affecting 10 individuals with a mean survival of 21 months. The GLT8D1-G78W mutation was also identified in our local patient population; GLT8D1-G78W was associated with a disease duration of 58 months, offering a slow disease progression compared to the aggressive GLT8D1-R92C (Cooper-Knock et al., 2019).

GLT8D1 is structurally and functionally uncharacterised; therefore, I began by identifying structural homologues to aid future crystallisation strategies for determining possible targets of interaction. In this chapter, I also describe the generation of GLT8D1 plasmid constructs with either a 3xFLAG- or eGFP-tag. The use of epitope tags was necessary given a lack of validated GLT8D1 antibodies, and generating an antibody of my own was not feasible due to time constraints. All overexpression experiments included an un-tagged control plasmid containing the same backbone, which was important, as GFP-tags have previously been shown to induce apoptosis *in vitro* (Liu et al., 1999, Coumans et al., 2014). eGFP-tags were useful for evaluating transfection efficiency under ultraviolet (UV) light. 3xFLAG-tags enabled the immunoprecipitation of recombinant GLT8D1 protein for the assessment of glycosyltransferase activity, using methods previously developed by our lab. In order to confirm the validity of the signal following the immunoprecipitation of GLT8D1, miRNA constructs targeting overexpressed and endogenous GLT8D1 were generated.

GLT8D1-3xFLAG constructs were also used to engineer stable isogenic Flp-In™ T-REx™ HEK293_GLT8D1^{WT/R92C}-3xFLAG cell models. Hereafter, these cell models will be referred to as isogenic HEK293-WT and isogenic HEK293-R92C. These cell lines utilise the Flp-In™ system which allows genomic site specific insertion of WT and mutant GLT8D1 into HEK293 cells; and the T-REx™ system, which allows for tetracycline-inducible expression of WT and mutant GLT8D1. The isogenic nature of HEK293-WT and HEK293-R92C cells was desirable to reduce variability not linked to the GLT8D1 mutation.

Given the difference in disease severity between patients with GLT8D1-G78W and GLT8D1-R92C mutations, I tested the relative toxicity of these two mutations *in vitro* via a combination of MTT and lactate dehydrogenase (LDH) assays. The MTT assay is a widely used measure of cell proliferation (Mosmann, 1983, van Tonder et al., 2015) and provides a useful indication of mitochondrial dysfunction. LDH assays (Chan et al., 2013) were subsequently performed to determine whether observed differences in the MTT signal were a result of growth inhibition or cytotoxicity.

3.2. Aims and objectives for characterising ALS-linked G78W and R92C mutations in GLT8D1

1. Generate pEGFP-N1-eGFP and pcDNA5/FRT/TO_3xFLAG plasmid constructs expressing GLT8D1-WT, GLT8D1-G78W and GLT8D1-R92C.
2. Integrate pcDNA5/FRT/TO_3xFLAG-GLT8D1-WT and pcDNA5/FRT/TO_3xFLAG-GLT8D1-R92C plasmids into the commercially available Flp-In™ HEK293 T-REx™ cell line and characterise cells for tetracycline-inducible expression of GLT8D1-WT and GLT8D1-R92C.
3. Generate microRNA plasmids for the targeted knockdown of endogenous and overexpressed GLT8D1 in HEK293 cells.
4. Identify structural homologues of GLT8D1 to aid future crystallisation strategies.
5. Assess the relative toxicity of GLT8D1-G78W and GLT8D1-R92C mutations in neuronal and non-neuronal cell lines via a combination of MTT and LDH assays.
6. Investigate the effect of GLT8D1-G78W and GLT8D1-R92C mutations on the enzymatic activity of GLT8D1.

3.3. Results

3.3.1. Generation and characterisation of pEGFP-N1_GLT8D1-eGFP and pcDNA5/FRT/TO_3xFLAG-GLT8D1 expression vectors

Plasmids utilised in this section were generated in collaboration with Dr Guillaume Hautbergue. For GFP-tagged fusions to the C-terminus of GLT8D1, pEGFP-N1 expression vectors (**Figure 3.1a**) were digested using NheI and XhoI restriction enzymes and purified via agarose gel electrophoresis and gel extraction. The GLT8D1 open reading frame (I.M.A.G.E.

40116197) was amplified using oligonucleotides GLT8D1-1-Kozak-NheI5 and GLT8D1-371-XhoI3 (**see Table 2.7**), and subsequently cloned as a PCR fragment into the NheI/XhoI restriction sites of pEGFP-N1 to create pEGFP-N1_GLT8D1-eGFP. The Kozak sequence in the forward primer was necessary due to the absence of an ATG codon for the initiation of translation (Kozak, 1990). GLT8D1-G78W and GLT8D1-R92C mutations were introduced via site-directed mutagenesis; PCR reactions were assembled using the following oligonucleotides: GLT8D1-G78W_QC_fwd and GLT8D1-G78W_QC_rev; or GLT8D1-R92C_QC_fwd and GLT8D1-R92C_QC_rev (**Table 2.7**). pEGFP-N1_GLT8D1-eGFP plasmids were validated via restriction digest (**Figure 3.1b**) and Sanger sequencing (**see appendix 6**).

For FLAG-tagged fusions, the GLT8D1 open reading frame (I.M.A.G.E. 40116197) was amplified using oligonucleotides GLT8D1-1-BclI5 and GLT8D1-371stp-XhoI3 (**Table 2.7**) and cloned as a BclI/XhoI PCR fragment into the BamHI/XhoI restriction sites of the pcDNA5/FRT/TO_3xFLAG vector to generate pcDNA5/FRT/TO_3xFLAG-GLT8D1 (**see appendix 7**). GLT8D1-G78W and GLT8D1-R92C mutations were introduced via site-directed mutagenesis; PCR reactions were assembled using the following oligonucleotides: GLT8D1-G78W_QC_fwd and GLT8D1-G78W_QC_rev; or GLT8D1-R92C_QC_fwd and GLT8D1-R92C_QC_rev (**Table 2.7**). pcDNA5/FRT/TO_3xFLAG-GLT8D1 plasmids were validated via restriction digest (**Figure 3.1b**) and Sanger sequencing (**see appendix 8**).

3.3.2. *Flp-InTM T-RExTM GLT8D1 isogenic HEK293 cell line generation*

Isogenic HEK293 cells stably expressing GLT8D1 were engineered for the production of recombinant enzyme for subsequent analysis of glycosyltransferase function. Therefore, it was important to generate a robust and highly proliferative cell model to achieve maximal biomass; hence, a neuronal line with stable expression of GLT8D1 was not deemed necessary at this stage of the project.

Isogenic HEK293-WT and HEK293-R92C cell lines utilised in this project were generated in collaboration with Dr Adrian Higginbottom. pcDNA5/FRT/TO_3xFLAG-GLT8D1 and pcDNA5/FRT/TO_3xFLAG-GLT8D1-R92C (see section 3.3.1) were stably transfected into the Flp-InTM T-RExTM (RRID: CVCL_U427) HEK293 cell line. pPGKFLPobpA (which expresses a codon optimised FLP DNA-recombinase) was co-transfected with each of the GLT8D1 plasmids separately. The FLP DNA recombinase catalysed recombination between the FRT site on the pcDNA5/FRT/TO_3xFLAG-GLT8D1 plasmids and the genomic FRT site in the Flp-InTM T-RExTM HEK293 cells, stably inserting the tetracycline-inducible GLT8D1 constructs

(**Figure 3.2**). Cells were screened for Zeocin™ sensitivity and Blastcidin-S/Hygromycin-B resistance to ensure isogenic, then expanded and cryopreserved. Zeocin™ resistance would suggest random integration of the pcDNA5/FRT/TO_GLT8D1 plasmid into the host cell genome, and not at the genomic FRT site. Blastcidin-S/Hygromycin-B selection antibiotics were added to the media to select for cells with pcDNA5/FRT/TO_3xFLAG-GLT8D1 stably integrated into the genomic FRT site. Tetracycline-inducible expression of GLT8D1-3xFLAG was confirmed via immunoblotting (**Figure 3.6**).

3.3.3. Generation of microRNA plasmids targeting human GLT8D1

MicroRNA (miRNA) knockdown of over-expressed and endogenous GLT8D1 was used to validate the specificity of GLT8D1 immunoblot bands. This was necessary because validated GLT8D1 antibodies were not available. miRNA sequences against human GLT8D1 (NCBI Reference Sequence: NM_152932.2, transcript variant 1) were designed using the 'miR RNAi' Block-IT RNAi designer tool (ThermoFisher). The target sequences are as follows:

- GLT8D1_miR1 target: **ATTGTAGGGCCTCAACCTATA** starts at 241nt
- GLT8D1_miR2 target: **GAGCAGGAAACCAGTACAATT** starts at 749nt
- GLT8D1_miR3 target: **TTTGTAAGGCTGCCAAGTTA** starts at 1075nt.

Synthesized oligonucleotides (**see Table 2.7**) were annealed and ligated into pcDNA6.2-GW/EmGFP vectors. HEK293 cells were co-transfected with pcDNA5/FRT/TO_3xFLAG vectors expressing GLT8D1-WT with and without pcDNA6.2-GW/EmGFP vectors expressing miRNA sequences (miR1-3 – see above). Knockdown was confirmed at two days post transfection via immunoblotting (**Figure 3.9**).

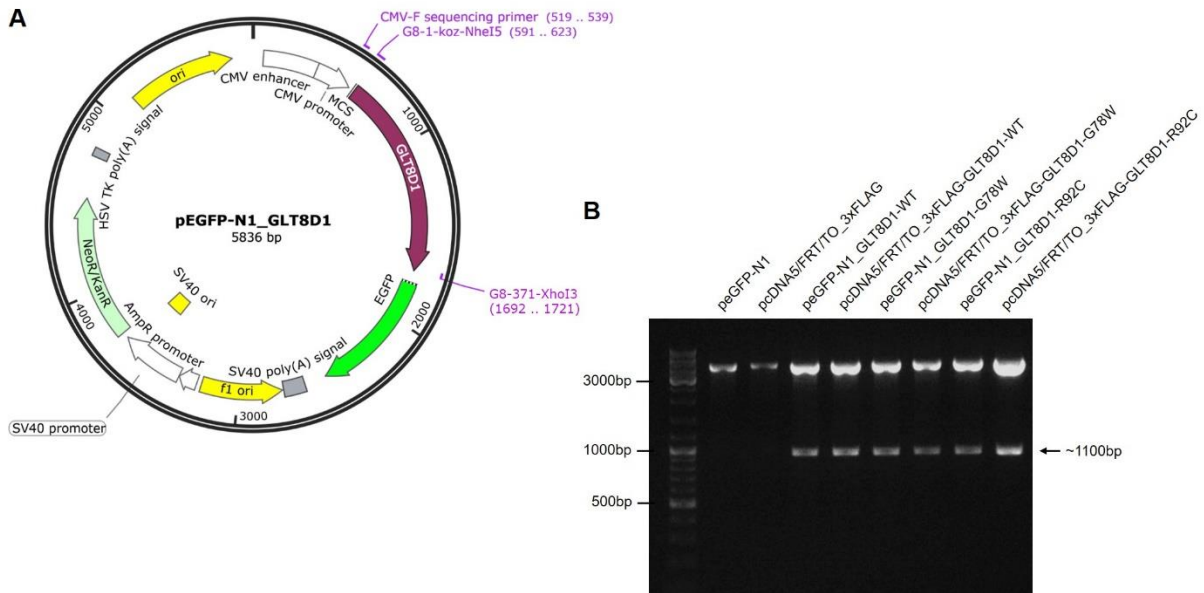


Figure 3.1. Construction and validation of pEGFP-N1_GLT8D1 and pcDNA5/FRT/TO_3xFLAG_GLT8D1 plasmids. (A) pEGFP-N1 plasmid map showing integration of WT GLT8D1 into the multiple cloning site under the control of a CMV promoter. GLT8D1 was cloned as a NheI / XhoI PCR fragment into the NheI and XhoI sites of pEGFP-N1. GLT8D1-G78W and GLT8D1-R92C mutations were subsequently introduced via site-directed mutagenesis and confirmed via Sanger sequencing (see appendix 6). See appendix 7 for pcDNA5/FRT/TO_3xFLAG_GLT8D1 plasmid maps, or refer to Figure 3.2 for a structural overview. (B) Restriction digest of pEGFP-N1 and pcDNA5/FRT/TO_3xFLAG plasmids to size the GLT8D1 inserts; pEGFP-N1_GLT8D1 plasmids were cut using NheI and XhoI restriction enzymes. pcDNA5/FRT/TO_3xFLAG plasmids were cut using BamHI and XhoI restriction enzymes. Agarose gel electrophoresis was performed to size the 1.1kb GLT8D1 inserts. The empty pEGFP-N1 and pcDNA5/FRT vectors show no insert present. Molecular weight markers are indicated (bp).

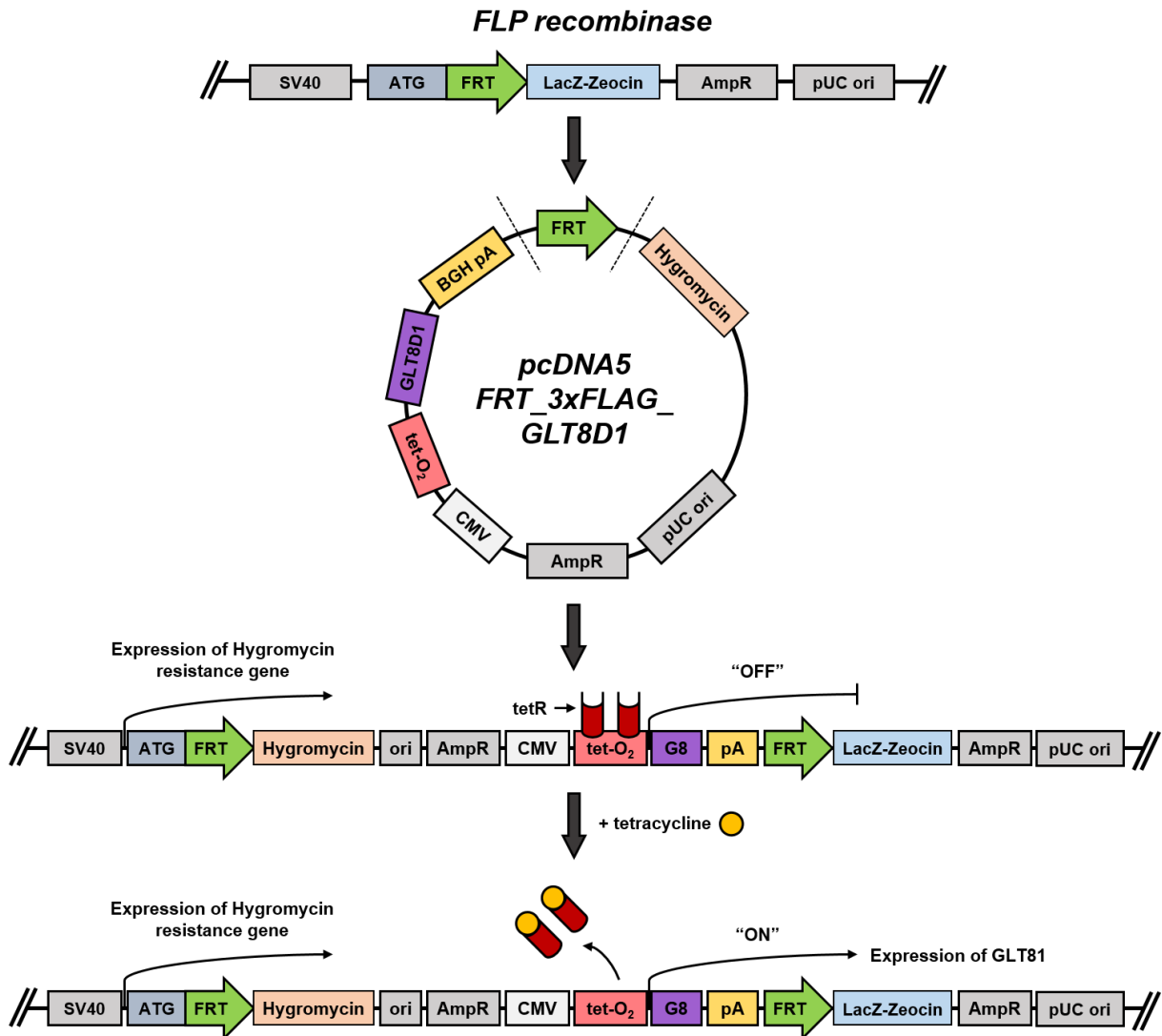


Figure 3.2. Flp-In™ and T-REx™ systems used to generate isogenic HEK293 cell lines with tetracycline-inducible expression of WT and mutated GLT8D1. pcDNA5/FRT/TO_3xFLAG vectors expressing WT GLT8D1 and GLT8D1-R92C were separately co-transfected with a FLP recombinase into the Flp-In™ T-REx™ mammalian cell line in a ratio of 6:4 using polyethylenimine. FLP recombinase catalyses homologous recombination between the genomic FRT site and the FRT site within the pcDNA5/FRT/TO vector. Successful integration of the pcDN5/FRT/TO_3XxFLAG-GLT8D1 plasmid is demonstrated through the Hygromycin-B resistant and Zeocin™ sensitive nature of the host cell line. GLT8D1 expression is repressed by the Tet repressor element (tetR). Expression of GLT8D1 is initiated through the addition of tetracycline, which de-represses the CMV/TetO2 promoter. (G8 – GLT8D1; FRT – flippase recognition target; AmpR – ampicillin resistant promoter; pA – polyadenylated tail). This figure was adapted from Invitrogen™.

3.3.4. Structural-based sequence alignment identifies 5GVV (*S. pneumonia glycosyltransferase glyE*) as a structural homologue of GLT8D1

Structural characterisation of GLT8D1 was performed in collaboration with Dr Sam Dix. The majority of proteins must fold to their active native state when they are released from ribosomes in order to perform their biological function. Proteins repeatedly unfold and refold during their lifetime (Englander and Mayne, 2014). The crystal structure for GLT8D1 is currently undefined. A well-established method of assigning protein fold, and therefore possibly function, is to identify a closely related homologue with a known structure. Sequence comparison tools such as BLAST (Altschul et al., 1990) are capable of assigning folds for up to 30% of genes in microbial genomes (Wang et al., 2000, Ginalski et al., 2005). To identify a structural homologue, the translated protein sequence of GLT8D1 was inputted into PDB-BLAST and aligned against all members of the Protein Data Bank (available at: <https://www.rcsb.org/>), which is comprised of all known protein structures to date. This identified 5GVV (*S. pneumoniae glycosyltransferase glyE*) as a potentially related homologue. Using Clustal Omega Multiple Sequence Alignment (available at: <https://www.ebi.ac.uk/Tools/msa/clustalo/>), the sequence identity between GLT8D1 and 5GVV was calculated to be only ~27% across the entire protein, which coincides with the N-terminal domain of 5GVV. The N-terminal domain contains core secondary structure features as well as the proposed GLT8D1 ligand-binding pocket (Bourne and Henrissat, 2001); therefore, the fold will likely be conserved (**Figure 3.3**). Of note, sequence similarity is not necessary for structural similarity. Therefore, seemingly unrelated proteins based on protein sequence alone are capable of adopting the same fold (Ginalski et al., 2005). Due to this predicted structural conservation, it is likely that GLT8D1 will adopt a similar fold to that of the N-terminal domain in 5GVV. The implication of the conserved fold for future experimentation is discussed in section 3.4.3.

The protein sequence encoding the C-terminal domain of 5GVV does not align closely with GLT8D1. Due to this breakdown in alignment, I propose truncation of the linker region connecting the two domains at protein position 266 leading to loss of the C-terminal domain. Finally, the lack of sequence complementarity at the beginning of the trace (**Figure 3.3a**) may represent a GLT8D1 Golgi-localisation signal, which is not present in prokaryotic cells; however, this is purely speculative and warrants functional characterisation. GLT8D1-Golgi localisation was subsequently investigated (see Chapter 5).

A

```

5GVV-A|PDBID|CHAIN|SEQUENCE|1-406 1 1-----M NTKRAVV 9
sp|Q68CQ7|GL8D1_HUMAN|1-371 1 MSFRKVNIIILVLAVALFLLVLHNFSLSSLLRNEVTDSGIVGPPIDFVFNALRHAVDGRQEEIPVV 69

5GVV-A|PDBID|CHAIN|SEQUENCE|1-406 10 F-----AGDYAYIRQIETAMKSLCRHNSHKIYLLN---QDIPQEWFSQ-----IRIYLQEMGGDL 62
sp|Q68CQ7|GL8D1_HUMAN|1-371 10 IAASEDRLLGGAIAAINSIQHNT-----RSNVIFYIVTLNNTADHLRSWLNSSDLSKSI RYKIVNFDPKL 132

5GVV-A|PDBID|CHAIN|SEQUENCE|1-406 63 IDCRLIGSQFQMNSNKLPHINHMFAFYFIPDFVTE-DKVLVLDSDLIVTGDITDLFELDLDGENYLAA 130
sp|Q68CQ7|GL8D1_HUMAN|1-371 63 LEGKLVKE-----DPDQGESMKPLTFAFYLPILVPSAKKAIYMDQDVIVQGDILALNNTALKPGHAAA 195

5GVV-A|PDBID|CHAIN|SEQUENCE|1-406 131 A-RSC-----FAGVGFNAGVLLINKKWGS ETRQKLIID 164
sp|Q68CQ7|GL8D1_HUMAN|1-371 131 FSEDCDSASTKVVIRGAGNQYNYIGYLDYKKERIRKLSMKASTCSFNPGVFVANLLEWKRNIITNQLEK 264

5GVV-A|PDBID|CHAIN|SEQUENCE|1-406 165 LTEKEHE NVEEGDQ-----SILNMLFKDQYSSLEDQYNFQIGDYGAATFKHQFIFDIPLLEPLP 223
sp|Q68CQ7|GL8D1_HUMAN|1-371 165 WMK---LNVEEGLYSRTLACGSIITPPLLIVFYQDHSITDPMWNRRLGSSAGKRYSPQF-----VKAA 324

5GVV-A|PDBID|CHAIN|SEQUENCE|1-406 224 LILHYISQDKPWNQFSVGRIRFVWWEYS LMDWSVILNEWFSKSVKYPKSKQIFKLCQCVNLTNSWCVEKI 292
sp|Q68CQ7|GL8D1_HUMAN|1-371 224 KLLHWNCHLKPWGRITAS--YTDVWE-----KWIIPD---PTGKFNLI-----VKAA 361

5GVV-A|PDBID|CHAIN|SEQUENCE|1-406 293 DYLAELQLEVFHFHIVAYTNMANELLALTRFPNVTVYFNSLMLLEQIVIASDLYLDLNHDRKLEDAYEF 361
sp|Q68CQ7|GL8D1_HUMAN|1-371 293 ---RRYTESLIK----- 371

5GVV-A|PDBID|CHAIN|SEQUENCE|1-406 362 VLKYYKMIAFDNTCSENLSIEYEGIYPSIIPKMMVAAIRSYMR 406
sp|Q68CQ7|GL8D1_HUMAN|1-371 -----

```

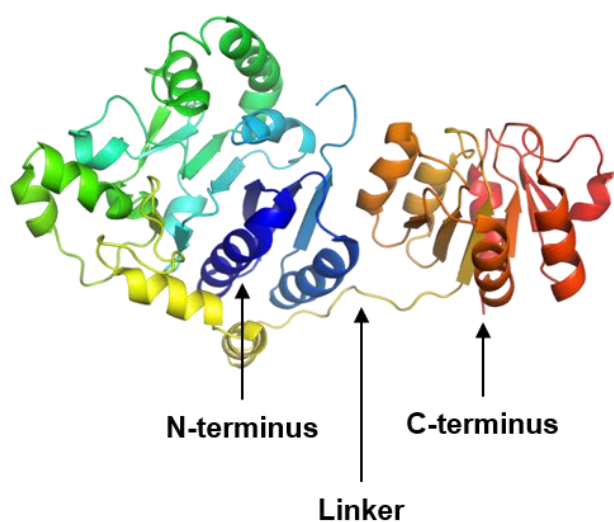
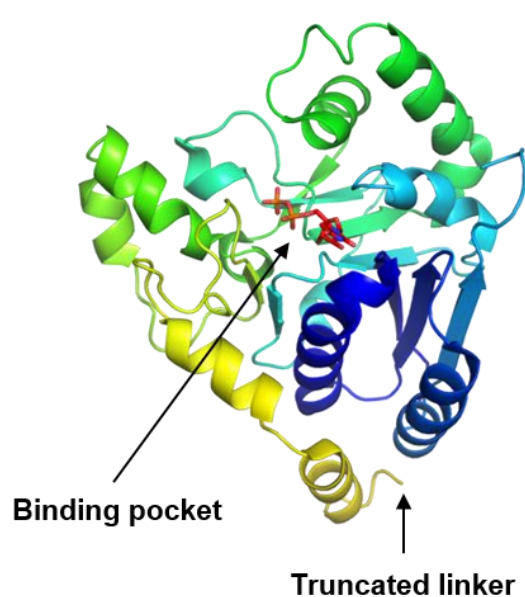
B**5GVV****C****GLT8D1**

Figure 3.3. Structural-based sequence alignment identifies 5GVV (*S. pneumoniae* glycosyltransferase glyE) as a related homologue of GLT8D1. (A) Protein sequence alignment showing degree of conservation between 5GVV and GLT8D1. The residue-enriched N-terminal domain is highly conserved between 5GVV and GLT8D1, suggesting GLT8D1 will adopt a similar fold to 5GVV. (B) Structural representation of aligned sequences showing two distinct protein domains separated by a linker sequence (yellow). The highly-conserved N-terminal domain contains the binding pocket and is enriched with amino acid residues that determine protein folding. The less conserved C-terminal domain is also shown. (C) Structure of the highly-conserved N-terminal domain with a truncated linker region to more closely resemble of the structure of GLT8D1. Structures were generated using PyMOL. (Figure kindly provided by Dr Sam Dix).

3.3.5. A *GLT8D1-R92C* mutation reduces viability and increases cytotoxicity of HEK293 and N2A cells

My next aim was to characterise the relative toxicity of *GLT8D1-G78W* and *GLT8D1-R92C* mutations via a combination of MTT proliferation and LDH cytotoxicity assays. MTT [3-(4,5-dimethylthiazol-2-yl)-2,5-diphenyltetrazolium bromide] is a yellow tetrazolium dye which is metabolised in the mitochondria by mitochondrial succinate dehydrogenase into an insoluble purple-coloured formazan product, measurable via spectrophotometry. Viable cells with an active metabolism exhibit high levels of MTT reduction to produce an absorbance maximum close to 570nm (Riss et al., 2004). WT and mutant *GLT8D1* were transiently overexpressed in HEK293 and N2A cells via liposome-mediated transfection with pEGFP-N1_*GLT8D1*-eGFP plasmids (see section 3.3.1). MTT assays were used to indirectly assess the viability of HEK293 and N2A cells at two and three days post transfection, respectively. Mutation-specific reductions in absorbance were observed across six biological repeats of the MTT assay in HEK293 cells, relative to over-expression of *GLT8D1*-WT (n=6, ANOVA $p=0.0281$) (**Figure 3.4a**). A similar reduction was seen in N2A cells, with *GLT8D1-R92C* producing a greater effect than *GLT8D1-G78W* (n=6, ANOVA $p=0.0281$) (**Figure 3.4b**).

To validate the observed MTT signal, LDH assays were performed to measure LDH in HEK293 and N2A extracellular growth medium, following transient overexpression of *GLT8D1*-WT-eGFP, *GLT8D1-G78W*-eGFP and *GLT8D1-R92C*-eGFP. This colorimetric assay quantitatively measures the release of the cytoplasmic enzyme, LDH, from necrotic cells with reduced plasma membrane integrity. LDH is a stable cytoplasmic enzyme present in all cells (Kumar et al., 2018) and is released into the extracellular space when the plasma membrane is damaged. The assay is based on the principle that LDH reduces nicotinamide adenine dinucleotide to its reduced form through the oxidation of lactate to pyruvate. The reaction products then interact with a tetrazolium salt to form a red formazan dye, which is quantifiable through measuring absorbance at 490nm and 680nm. The absorbance reading is proportional to the number of damaged cells (i.e. apoptotic or necrotic) within the culture. This assay was chosen based on its reliability, speed, and ease of evaluation (Chan et al., 2013, Fotakis and Timbrell, 2006). Expression of *GLT8D1-R92C* correlated with an increase in cytotoxicity across six biological repeats in HEK293 (n=6, ANOVA $p=0.0117$, **Figure 3.4c**) and N2A (n=6, ANOVA $p=0.0117$, **Figure 3.4d**) cells, compared to over-expression of *GLT8D1*-WT. *GLT8D1-G78W* produced a similar trend but this did not reach statistical significance (n=6, $p=0.4467$). R92C was the more cytotoxic of the two substitution mutations in both cell lines, which is in line with the observed clinical severity. Indeed, overexpressing any WT gene

in a model system can cause mutant phenotypes (Prelich, 2012), therefore it was important to include a WT transfection alongside a negative control in order to observe a defined mutation-specific effect.

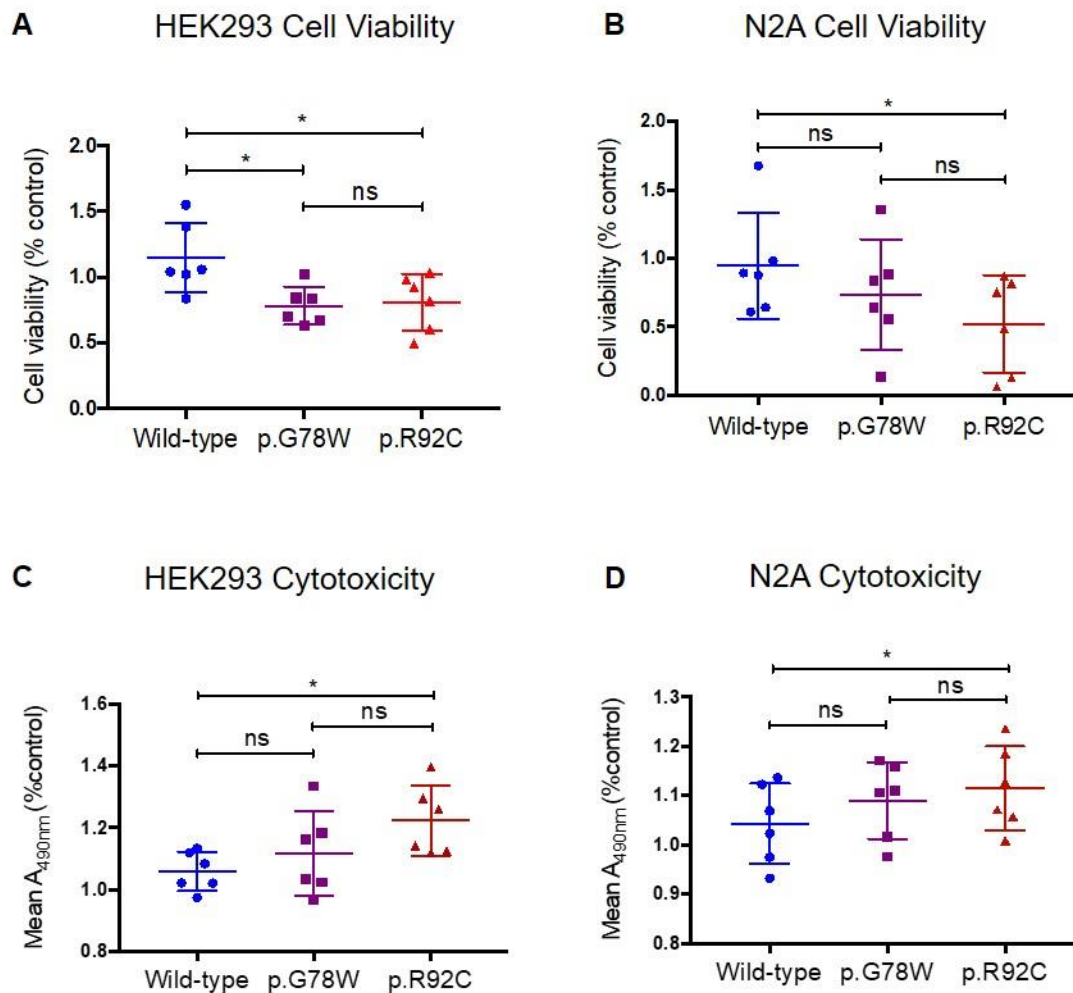


Figure 3.4. Overexpression of mutated GLT8D1 causes cytotoxicity and reduces viability in HEK293 and N2A cells compared to overexpression of the WT protein. Cell viability was indirectly measured using MTT assays (**A**, **B**) and cytotoxicity was measured using LDH assays (**C**, **D**). All experiments included six biological replicates and either two (MTT assays) or four (LDH assays) technical replicates were included per biological replicate. * $p < 0.05$; one-way ANOVA. Each data point is expressed as a percentage of a control transfection with an empty pGFP-N1 vector. Error bars represent mean and SD. Figure taken from (Cooper-Knock et al., 2019).

To confirm that observed differences in cell viability and cytotoxicity (**Figure 3.4**) were mutation-specific and not due to increased expression of the mutant protein, immunoblotting was used to quantify the relative expression level of GLT8D1-WT, GLT8D1-G78W and GLT8D1-R92C in HEK293 and N2A cells for each biological repeat of the MTT and LDH assays. No significant differences were observed in the level of protein expression in between the transfection groups in either cell line (n=6, ANOVA $p>0.05$, **Figure 3.5**). The band at ~70kDa is indicative of the GLT8D1-eGFP fusion protein (**Figure 3.5a, 3.5b**). Densitometry was performed on the bands representing the fusion product (**Figure 3.5c, 3.5d**).

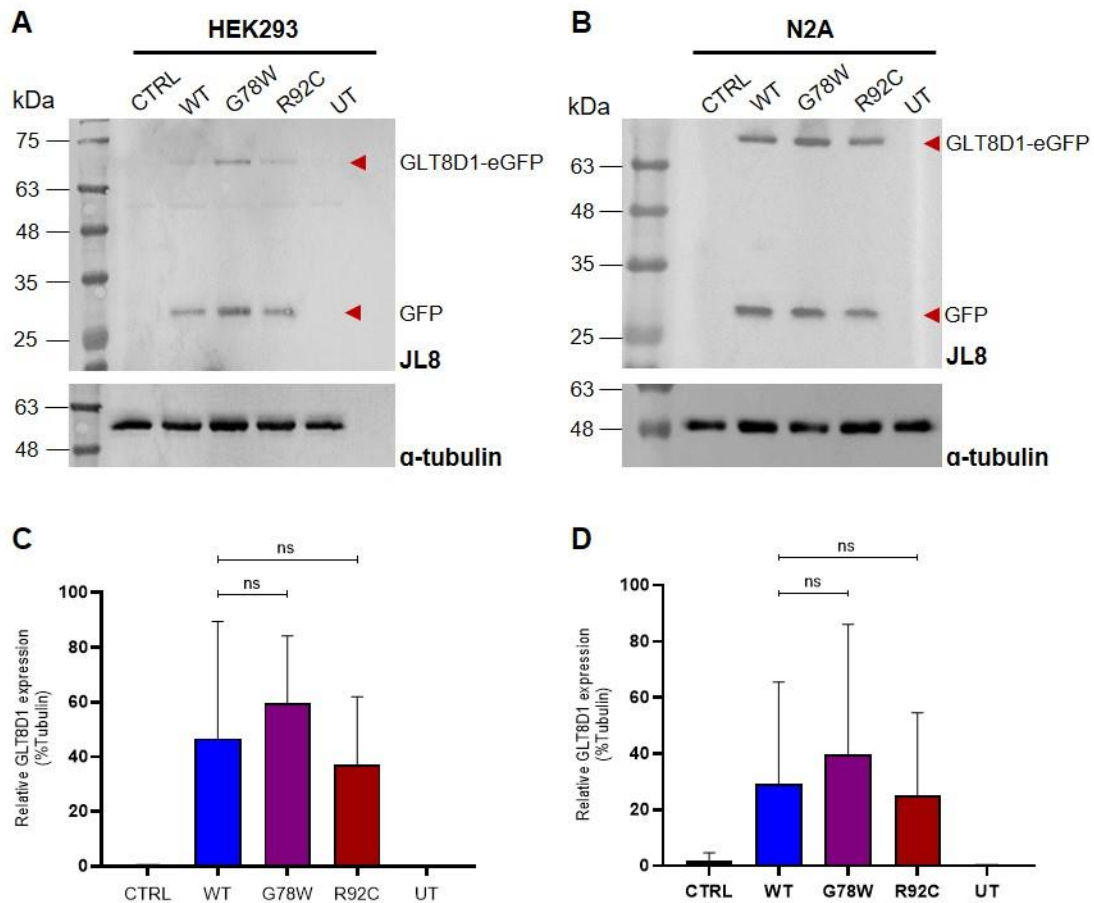


Figure 3.5. Immunoblotting shows similar expression levels of WT and mutant GLT8D1 in HEK293 and N2A cells. (A) Representative images showing overexpression of GFP-tagged WT and mutant GLT8D1 in HEK293 cells (left panel) and (B) N2A cells (right panel). Densitometry demonstrates non-significant differences between WT and mutant GLT8D1 expression in (C) HEK293 and (D) N2A cells ($n=6$, one-way ANOVA $p>0.05$). Error bars represent SD. Immunoblotting suggests that observed phenotypes were not a result of relative overexpression of mutated protein. Molecular weight markers are indicated (kDa). (CTRL - control; WT – wild-type; UT - un-transfected; G8 – GLT8D1). Figure adapted from (Cooper-Knock et al., 2019).

3.3.6. *An ALS-linked R92C mutation impairs the glycosyltransferase activity of GLT8D1*

Based on sequence homology, GLT8D1 is a member of glycosyltransferase family 8, and exon 4 contains ALS-associated mutations and encodes the substrate-binding site within the glycosyltransferase domain (**Figure 1.4**). To assess the impact of discovered mutations on glycosyltransferase activity, a uridine diphosphate (UDP)-Glo™ glycosyltransferase assay kit (Promega) with five commercially available UDP-sugar substrates was used.

GLT8D1-WT clone 2B1 and GLT8D1-R92C clone 2B1 were selected from my isogenic screen as they demonstrated a similar expression level after normalising for total protein concentration (**Figure 3.6**). 3xFLAG-tagged GLT8D1-WT and GLT8D1-R92C proteins were immunopurified from isogenic HEK293 cells in stringent conditions prior to competitive elution under a native form with a 3xFLAG peptide to preserve enzyme activity. Coomassie blue staining and immunoblotting were used to confirm that both proteins were purified in equivalent amounts (**Figure 3.7**).

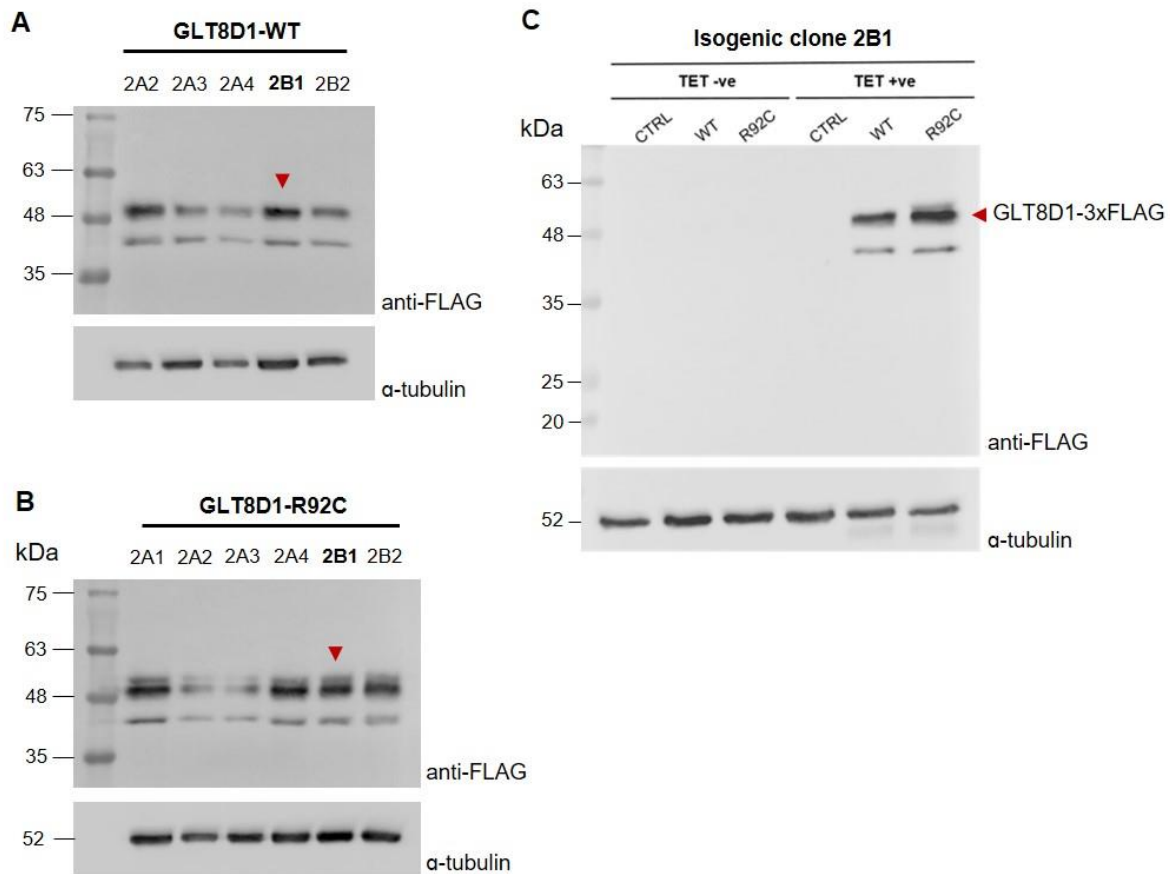


Figure 3.6. Immunoblotting confirms tetracycline-inducible expression of GLT8D1-WT and GLT8D1-R92C in isogenic HEK293 cells. Representative isogenic screen of selected (A) GLT8D1-WT and (B) GLT8D1-R92C clones showing tetracycline-induced expression of 3xFLAG-tagged GLT8D1. GLT8D1-WT clone 2B1 and GLT8D1-R92C clone 2B1 were selected for GLT8D1 immunoprecipitation (red arrows) as they demonstrated a similar level of expression between the WT and mutant form after normalising for total protein concentration. (C) Representative blot showing tetracycline-induced expression of GLT8D1-WT and GLT8D1-R92C in isogenic HEK293 cells. Relative GLT8D1 expression was detected using an anti-FLAG antibody; α -Tubulin served as a loading control. Molecular weight markers are indicated (kDa). (TET – tetracycline; CTRL – control (Sham)-transfected; WT – wild-type; -ve – negative; +ve – positive).

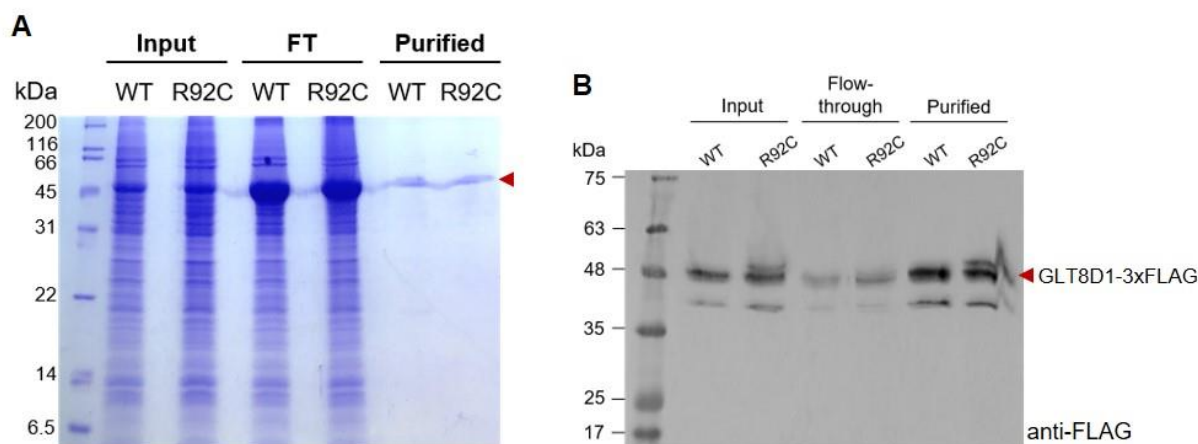


Figure 3.7. Immunopurification of GLT8D1-WT and GLT8D1-R92C from tetracycline-induced isogenic HEK293 cells. (A) Coomassie blue gel and **(B)** immunoblot showing purified GLT8D1-WT and GLT8D1-R92C in equivalent amounts (red arrows). Input represents ~0.1% of whole-cell protein extracts loaded onto anti-FLAG[®] M2 coated magnetic beads. FT indicates total remaining protein following incubation with a 3xFLAG peptide. Purified indicates 3xFLAG-GLT8D1 proteins. Molecular weight markers are indicated (kDa). (WT – wild-type; FT – flow-through).

The linear range for determination of accurate UDP concentration measurements was validated for the UDP-Glo[™] glycosyltransferase assay (**Figure 3.8**). Initial reaction velocity was measured at fixed enzyme concentration with increasing substrate concentrations. Initial reaction velocity is defined as the amount of product produced per unit time at the start of the reaction when the product concentration increases in a linear fashion. This is important for determining the rate of reaction before substrate levels are depleted (Choi et al., 2017). Data were fitted to a standard Michaelis-Menten equation by nonlinear regression to enable determination of maximal enzyme velocity (V_{max}) and the Michaelis constant (K_m). Purified GLT8D1 proteins behaved as expected for enzymes of this class (Sethi et al., 2010), and were purified in their active forms.

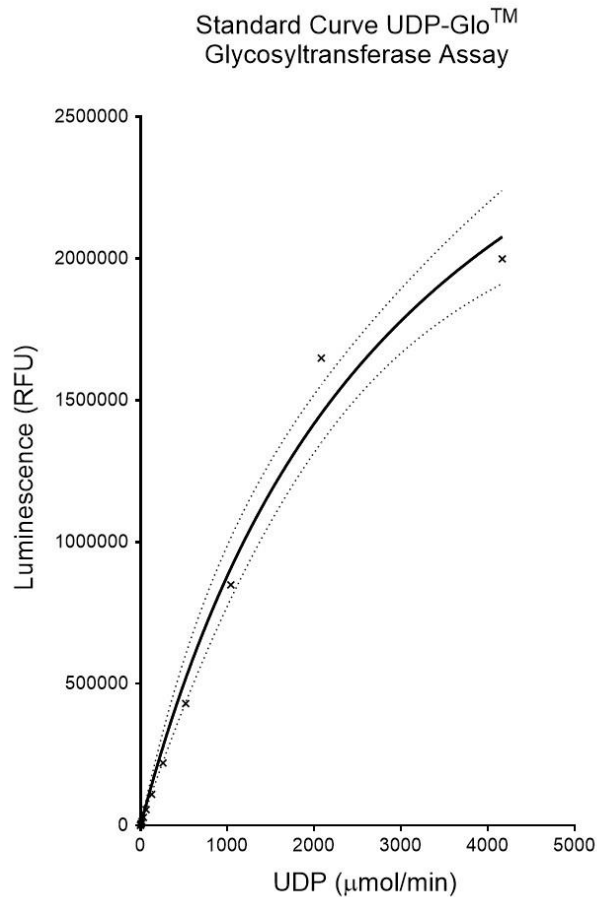


Figure 3.8. Validating the linear range for determination of accurate UDP concentration measurements for the UDP-Glo™ glycosyltransferase assay. Standard curve for the UDP-Glo assay illustrates linear correlation for <500 mmol/min UDP (RFU – relative fluorescence units; UDP – uridine diphosphate). Figure adapted from (Cooper-Knock et al., 2019).

Five commercially available UDP sugar substrates were tested: GalNAc, GlcNAc, Glucose, Galactose and Glucuronic acid. GLT8D1 only demonstrated sufficient affinity for UDP-Galactose. With UDP-Galactose as the target substrate, V_{max} was reduced ~25% (GLT8D1-WT: 37.79 mmol/min; GLT8D1-R92C: 30.65 mmol/min) and K_m was reduced ~40% (GLT8D1-WT: 1.226 mmol/l; GLT8D1-R92C: 0.7492 mmol/l) in the GLT8D1-R92C protein compared to GLT8D1-WT (**Figure 3.9a**). Next, I fixed substrate concentration to >10-fold higher than K_m in order to measure enzymatic activity at maximal enzyme velocity. I plotted the activities of enzymes as a function of enzyme concentration. At any enzyme concentration, the GLT8D1-R92C enzyme activity was reduced compared to GLT8D1-WT (**Figure 3.9b**). Enzyme activities measured in the linear range of the UDP-Glo™ glycosyltransferase assay indicated

an approximately 2-fold reduction for GLT8D1-R92C compared to GLT8D1-WT. These results suggest that ALS-linked mutations impair the normal function of the GLT8D1 protein.

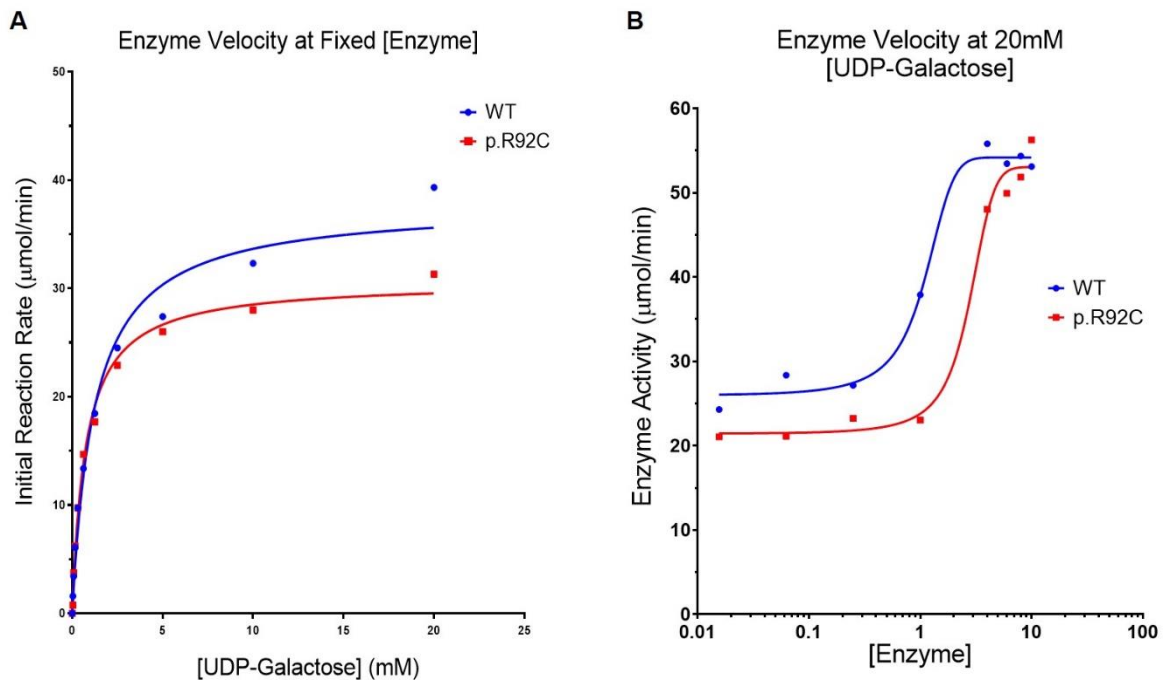


Figure 3.9. ALS-linked GLT8D1-R92C mutation impairs glycosyltransferase activity. (A) 3xFLAG-tagged GLT8D1-WT and GLT8D1-R92C proteins were immunopurified from tetracycline-induced isogenic HEK293 cells. Initial reaction velocity was measured at fixed enzyme concentration (3mg/25μL reaction) with variable substrate concentrations. Michaelis-Menten curves were fitted with nonlinear regression. (B) Enzyme concentration was varied in the presence of fixed substrate concentration (20mM) (15mol/l corresponding to >10xKm). The curve for GLT8D1-R92C enzyme velocity is right-shifted compared to GLT8D1-WT indicating lower enzyme activity at any given enzyme concentration. (WT – wild-type; UDP – uridine diphosphate).

3.3.7. ALS-linked G78W and R92C mutations impair the glycosyltransferase activity of GLT8D1

I validated my previous findings regarding glycosyltransferase function (see section 3.3.6) by transiently overexpressing GLT8D1 in HEK293 cells using pcDNA/FRT/TO-3xFLAG plasmids containing GLT8D1-WT, GLT8D1-G78W, and GLT8D1-R92C open reading frames. This also enabled me to investigate the effect of the GLT8D1-G78W variant on glycosyltransferase function, as a stable cell line expressing this mutation had not previously been engineered. 3xFLAG-tagged GLT8D1-WT, GLT8D1-G78W and GLT8D1-R92C proteins were transiently overexpressed in HEK293 cells via liposome-mediated transfection. Proteins were immunopurified as previously described (see section 3.3.6). Coomassie blue staining and immunoblotting were used to confirm that all three proteins were purified in equivalent amounts (**Figures 3.10c, 3.10d**). MicroRNA knockdown of GLT8D1 in HEK293 cells was used to validate the specificity of the signal following immunoprecipitation. For knockdown, HEK293 cells were co-transfected with pcDNA5/FRT/TO_3xFLAG vectors expressing GLT8D1-WT with and without pcDNA6.2-GW/EmGFP vectors expressing miRNA sequences targeting GLT8D1. All three miRNAs significantly reduced GLT8D1-3xFLAG levels (n=3, ANOVA $p=0.0398$) (**Figures 3.10a, 3.10b**). These results suggest that the purification signal observed following immunoprecipitation is representative of GLT8D1.

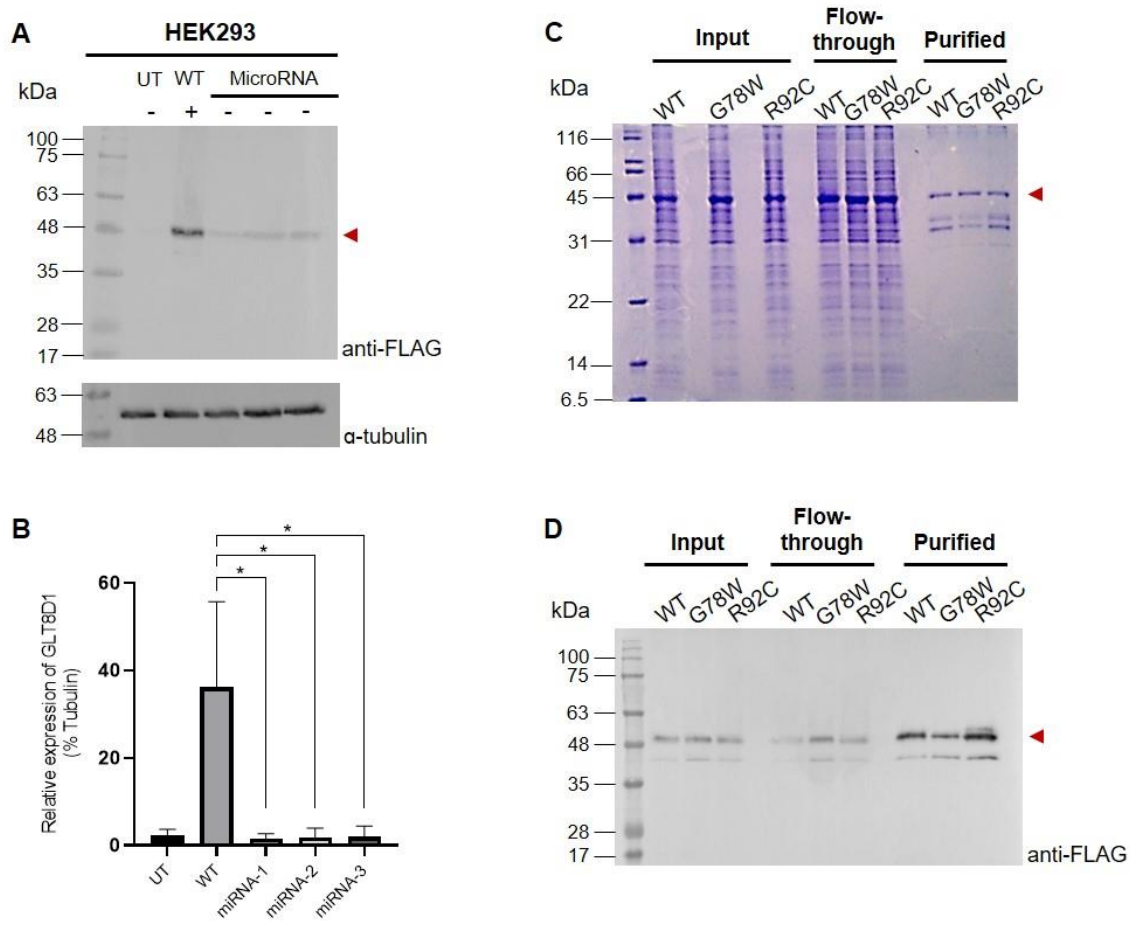


Figure 3.10. Immunopurification of GLT8D1-WT, GLT8D1-G78W and GLT8D1-R92C recombinant proteins from HEK293 cells. (A, B) Representative blot and densitometric analysis showing microRNA knockdown of GLT8D1 in HEK293 cells to validate the specificity of the signal following immunoprecipitation (n=3, ANOVA *p<0.05). (C, D) FLAG-tagged GLT8D1-WT, GLT8D1-G78W, and GLT8D1-R92C proteins were immunopurified in 1M NaCl-containing buffer to maximize dissociation of interacting partners, and were eluted in native conditions prior to analysis by SDS-PAGE, Coomassie staining and immunoblotting. Input represents ~0.1% of whole-cell protein extracts loaded onto anti-FLAG coated beads. FT indicates total remaining protein following incubation with a 3xFLAG peptide. Purified indicates FLAG-GLT8D1 proteins. Molecular weight markers are indicated (kDa). (UT – un-transfected; WT – wild type). Figures 3.9a and 3.9b were adapted from (Cooper-Knock et al., 2019).

In order to measure glycosyltransferase activity, the linear range was determined for the measurement of UDP concentration by the UDP-Glo™ assay (**refer to figure 3.8**). Initial reaction velocity was measured at a fixed enzyme concentration with increasing substrate concentrations. A similar reduction in glycosyltransferase activity was observed with UDP-Galactose as the target substrate. V_{max} was reduced ~30%–40% (GLT8D1-WT: 67.5 mmol/min; GLT8D1-G78W: 58.6 mmol/min; GLT8D1-R92C: 51.4 mmol/min), and K_m was reduced ~50% (GLT8D1-WT: 3.5 mmol/l; GLT8D1-G78W: 2.3 mmol/l; GLT8D1-R92C: 2.5 mmol/l) in GLT8D1-R92C and GLT8D1-G78W compared to GLT8D1-WT (**Figure 3.11a**). Consistent with the cell-based assays (see section 3.3.5), the relative effect of the two tested mutations mirrored the observed clinical severity, with GLT8D1-R92C producing a more severe phenotype. Next, UDP-Galactose substrate concentration was fixed to ~5-fold higher than K_m in order to measure near maximal enzymatic velocity. Enzyme activity was plotted as a function of enzyme concentration. At all enzyme concentrations, the activity of GLT8D1-R92C and GLT8D1-G78W proteins was reduced compared to the WT enzyme (**Figure 3.11b**).

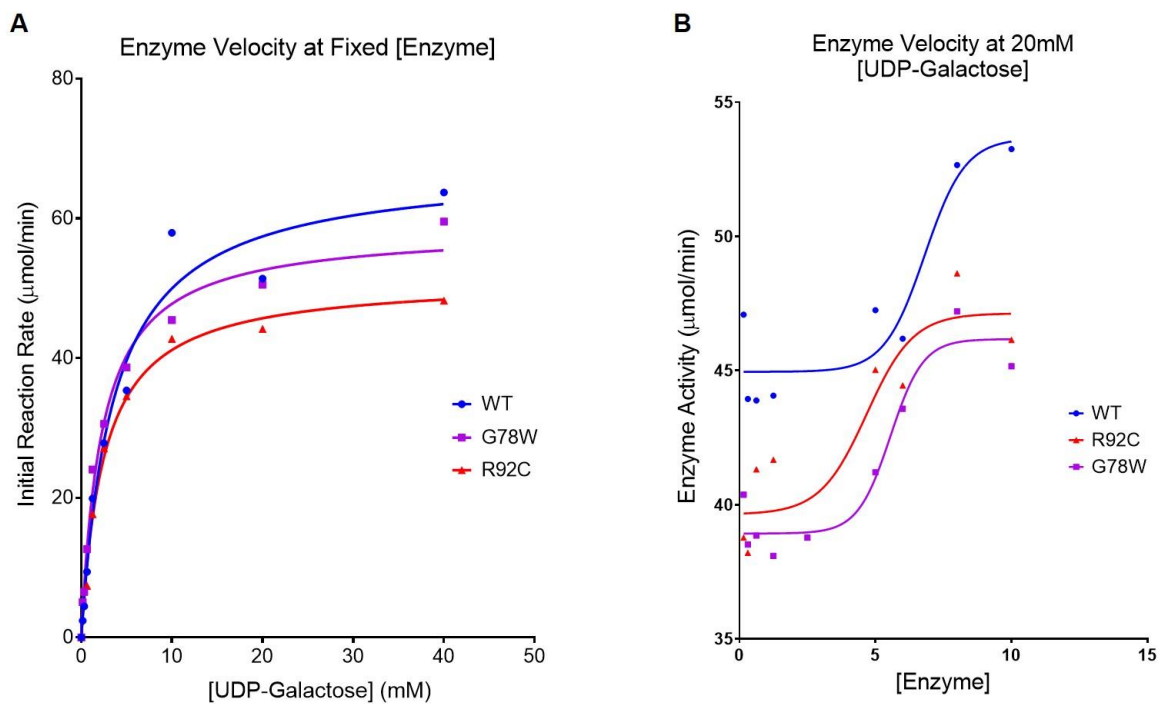


Figure 3.11. ALS-linked GLT8D1-G78W and GLT8D1-R92C mutations impair glycosyltransferase activity. (A) Initial reaction velocity at fixed enzyme concentration (3mg/25 μL reaction) with variable substrate concentration. (B) Enzyme activity at fixed substrate concentration (15mM) with variable enzyme concentration; Michaelis-Menten curves were fitted with nonlinear regression. The curves for GLT8D1-G78W and GLT8D1-R92C enzyme velocity are right-shifted compared to GLT8D1-WT indicating lower enzyme activity at any given enzyme concentration. (WT – wild-type; UDP – uridine diphosphate). Figure adapted from (Cooper-Knock et al., 2019).

3.4. Discussion

Within this chapter, I describe the generation of plasmid constructs expressing GLT8D1-WT, GLT8D1-G78W and GLT8D1-R92C. These plasmids were essential components for all subsequent experimentation linked to GLT8D1-ALS. In the current chapter, these plasmids were used to investigate the relative toxicity of ALS-linked GLT8D1 mutations in neuronal and non-neuronal cell lines. They were also used for the production of recombinant GLT8D1 protein to investigate the effect of ALS-linked mutations on glycosyltransferase function. Finally, these plasmids were used in the generation of an isogenic HEK293 cell model for studying the early biochemical effects of GLT8D1-ALS linked to an R92C mutation (see Chapter 5). In addition to the above, I briefly discuss the identification of a structural homologue for GLT8D1, which will aid future work on GLT8D1 crystallisation, which in turn will aid in identifying possible targets of interaction.

3.4.1. Generation of pEGFP-N1_GLT8D1-eGFP and pcDNA5/FRT/TO_3xFLAG-GLT8D1 plasmid constructs

GLT8D1 DNA exhibited stable growth in *E.coli*, and Sanger sequencing confirmed the sequence integrity of the cloned fragment (**see appendices 6 and 8**). The generation of tagged constructs expressing the gene of interest are useful tools for investigating the expression and localisation of the protein of interest. In addition, they provide specific means of purifying the recombinant protein (Jarvik and Telmer, 1998); however, there are caveats to their use (Liu et al., 1999, Coumans et al., 2014). For example, the epitope tag may interfere with protein structure or function (Jarvik and Telmer, 1998), and both N- and C-terminal GFP tagging have been demonstrated to adversely affect protein localisation (Palmer and Freeman, 2004, Hanson and Ziegler, 2004). In some instances, the C-terminus can fold inside the protein, which would prevent detection of a fluorescent signal. This is unlikely to be the case for GLT8D1-eGFP, as GFP-positive cells were clearly visible under UV light for all conditions. Despite these limitations, epitope tagging of GLT8D1 was necessary due to a lack of validated GLT8D1 antibodies. Indeed, I tested various anti-GLT8D1 antibodies, but their specificity was masked by the presence of multiple bands through immunoblotting (**see appendix 9**). I now have a system to test the specificity of commercially available anti-GLT8D1 antibodies through overexpression of GLT8D1-eGFP and GLT8D1-3xFLAG, followed by subsequent knockdown using miRNAs (**Figure 3.9a**). It is noteworthy that overexpression techniques may influence levels of the endogenous protein, which I was unable to measure. However, fluorescent tagging of endogenous protein is now possible using CRISPR/Cas9

genome editing (Ratz et al., 2015). Plasmid constructs are useful tools for studying short-term gene expression; however, transiently transfected cells do not integrate the plasmid into the genome and therefore express the gene of interest for a finite period of time, which can vary depending on the cell type. Gene expression is subsequently lost through factors such as cell division (Kim and Eberwine, 2010).

3.4.2. Generation of the *Flp-In T-RExTM GLT8D1* host cell lines

Isogenic HEK293 cells with tetracycline-inducible expression of GLT8D1-WT and GLT8D1-R92C (**Figure 3.2**) were initially engineered to produce recombinant protein for the assessment of enzymatic function. Compared to transient transfection, the amount of recombinant protein expressed via tetracycline induction is much lower. Therefore, in order to generate a sufficient yield for the assessment of enzymatic function, a larger cell biomass was required. The isogenic nature of these lines was desirable to reduce variability not linked to the GLT8D1-R92C mutation. Furthermore, overexpression of WT and mutant GLT8D1 upon induction would enable subsequent investigations into the early biochemical effects of an ALS-linked R92C mutation. The inducible nature of these cell lines prevents them adapting to the effects of the mutation, assuming selection pressure was maintained at a sufficient level to minimise unintended gene expression.

Isogenic HEK293 cells were characterised for tetracycline-inducible expression of GLT8D1-WT and GLT8D1-R92C at the protein level from the FRT site (**Figure 3.6**). A concentration of 10mg/mL tetracycline was sufficient to maintain induction for at least 48 hours without inducing cell toxicity. Basal levels of GLT8D1-WT and GLT8D1-R92C were undetectable through immunoblotting, even following overexposure of the image. This cell model is advantageous over transiently transfected models due to its isogenic nature and ability to switch on GLT8D1 expression.

The isogenic screen in HEK293-WT and HEK293-R92C cell lines suggests that an R92C mutation in GLT8D1 causes post-translational modification of the protein, represented by a double band in all blots targeting the mutant form. It is possible that the R92C mutation is causing GLT8D1 to misfold, which would suggest disruption of the ligand-binding pocket and explain why enzymatic activity in GLT8D1-R92C is reduced (**Figures 3.9 and 3.11**). Indeed, post-translational modifications such as phosphorylation are fundamental to proper enzymatic function. However, if these processes are not tightly regulated, they can lead to adverse effects such as hyper-phosphorylation, which is well described in many neurodegenerative

disorders. By example, hyper-phosphorylation of tau protein is implicated in Alzheimer's (Iqbal et al., 2010), Parkinson's (Zhang et al., 2018) and ALS (Strong et al., 2006).

3.4.3. Structural-based sequence alignment identifies 5GVV as a homologue of GLT8D1

The structure of a protein is fundamental to its function, and understanding protein fold is essential for curing disease (Pandey et al., 2016). Determining the crystal structure of proteins such as GLT8D1 is essential to understanding its enzymatic function. The Research Collaboratory for Structural Bioinformatics Protein Data Bank is an online resource for understanding the relationship between sequence, structure and function of biological macromolecules (available at: <https://www.rcsb.org/>). Using this resource, I identified glycosyltransferase glyE in *Streptococcus pneumonia* TIGR4 (Jiang et al., 2017) as a structural homologue of GLT8D1 (**Figure 3.3**). Further efforts to define the crystal structure of GLT8D1 were not pursued due to time constraints; however, I have identified a conserved fold that provides useful information for future crystallisation strategies. For example, the flexibility of the identified linker region can interfere with crystallization (Reddy Chichili et al., 2013, Pandey et al., 2016); therefore, it would be important to truncate this region prior to any structural work.

With more time, I would look to grow the GLT8D1 plasmids in *E. coli*, which is the most widely used expression system amongst structural biologists due to its rapid growth rate, high protein production, and relatively low cost (Pandey et al., 2016). The rationale for growth in *E. coli* is that mammalian cell systems do not typically yield sufficient protein for subsequent crystallisation, even under conditions of induced overexpression. Therefore, it is expensive to generate sufficient protein for structural studies (Andrell and Tate, 2013). I would then attempt to purify the recombinant GLT8D1 protein using techniques such as affinity chromatography (Vassilyeva et al., 2017), and then use macromolecular X-ray crystallography (Dessau and Modis, 2011) to determine its structure. Structural characterisation would aid future work in identifying possible targets of interaction.

3.4.4. ALS-linked GLT8D1 mutations are toxic to HEK293 and N2A cells

The next stage of this project was to examine the effects of GLT8D1-G78W and GLT8D1-R92C mutations on the viability of HEK293 and N2A cells. HEK293 cells were chosen based

on their high transfection efficiency (Thomas and Smart, 2005), suggesting observed effects would likely be representative of the entire cell population. N2A cells were necessary to investigate a neuronal phenotype, which is important when modelling neurodegenerative diseases such as ALS. Functional characterisation of ALS-linked GLT8D1 mutations was addressed through a combination of MTT and LDH assays. The MTT assay was used as an indirect measure of growth rate. This assay does not distinguish between growth inhibition and cytotoxicity; therefore, LDH assays were subsequently performed to determine whether the reduction observed in the MTT signal was due to cytotoxicity. A mutation-specific decrease in cell viability and an increase in cytotoxicity was observed across six biological repeats of the MTT and LDH assays, respectively (**Figure 3.4**). In accordance with the clinical phenotype, GLT8D1-R92C was notably the more toxic of the mutations in both assays, despite it demonstrating a lower expression level than the GLT8D1-G78W protein (**Figure 3.5**). This is consistent with the phenotypic data, as ALS patients with GLT8D1-R92C mutations experienced a more aggressive form of the disease, with a mean survival of 21 months, compared to the 58-month survival observed in the single patient with a GLT8D1-G78W mutation (**Table 1.3**) (Cooper-Knock et al., 2019). In contrast, the higher expression level of the GLT8D1-G78W protein may suggest that observed toxicity is due to level of expression rather than mutation-specific. However, GLT8D1-G78W toxicity is supported by its effect on glycosyltransferase function (**Figure 3.11**). To obtain a more defined mutation-specific effect, RNAi technology could be used to knockdown endogenous GLT8D1. In these circumstances, RNAi-resistant GLT8D1 plasmids would be required to maintain a high expression level of the transfected gene of interest. As such, the miRNA would be designed to target a section of the GLT8D1 sequence that is not present in the expression vector.

Two distinct protein bands were observed in all blots used to compare the relative expression of transiently expressed GLT8D1-eGFP protein (**Figure 3.5**). These bands are products of overexpression. The band at ~70kDa is representative of the GLT8D1-eGFP fusion product, but the lower band at ~27kDa may be present for various reasons. It is possible that there is a protease site proximal to the C-terminus that has been cleaved. Alternatively, it may be due to an unstable fusion. It may also suggest that the transfected plasmid contained traces of pEGFP-N1 minus the GLT8D1 sequence; however, this is unlikely given that single bacterial clones were carefully analysed via Miniprep prior to amplification using a Midiprep. Observed variability in the overexpression of GLT8D1 between biological repeats of the immunoblotting was unlikely due to inconsistent transfection efficiencies. Transfection efficiency, determined by the number of GFP-positive cells, was consistent at ~70-80% for HEK293 and ~30-40% for N2A across all three biological repeats. Rather, the variability is likely due to inconsistent signal intensities of the immunoblot bands between biological repeats. Indeed, it is important

to control for this variability to improve the accuracy and reliability of the data. However, in each biological repeat, the fluorescence intensity of the GLT8D1-R92C band was markedly lower, yet overexpression of this protein produced the more toxic phenotype in all subsequent experimentation, highlighting its relative pathogenicity.

When performing the MTT and LDH assays, it was important to control for cellular growth rate. For example, the growth rate of HEK293 cells is higher compared to N2A cells; therefore, it was important to seed the cells at different densities (**see Table 2.8**). When adherent cells reach confluence and growth becomes contact inhibited, the amount of MTT reduction per cell may decrease due to attenuated cellular metabolism. Furthermore, at ~30-40%, the transfection efficiency of N2A cells was significantly lower than HEK293 cells (~70-80%), suggesting that the effects of the GLT8D1-G78W and GLT8D1-R92C mutations were masked by a larger population of healthy N2A cells. Transfection efficiency was determined by the number of GFP-positive cells. Cell passage number is likely to influence transfection efficiency (de Los Milagros Bassani Molinas et al., 2014); therefore, all cell lines were maintained within the range of 7-32 passages to overcome this potential limitation.

It has been suggested that certain transfection reagents, including PEI, can cause fluorescence false positives, particularly when the GFP expression levels are low (Guo et al., 2001). Therefore, my experiments included a no-GFP control transfection as a comparison; I did not observe any false positive signals. Given the lower transfection efficiency of N2A cells, the correlation between GLT8D1-R92C and cytotoxicity is encouraging, particularly as it is in line with the observed clinical phenotype. PEI can be toxic to certain cell types if used in excess, but its use is warranted, as it demonstrates high transfection efficacy (Longo et al., 2013). The observed survival rate of N2A cells was markedly lower than HEK293 cells, possibly due to PEI; hence, the MTT and LDH assays were conducted in N2A cells 48 hours post transfection, compared to 72 hours in HEK293 cells. The shorter time scale in N2A cells enabled measurements of viability and toxicity to be performed before viable cells were reduced to a level that decreased the sensitivity of the assays. The generation of a stable neuronal cell line would overcome the limitation of PEI-mediated toxicity. Such lines have previously been generated using human neuroblastoma SH-SY5Y cells to model the neurodegenerative disorder, Niemann-Pick Disease Type C (Rodriguez-Pascau et al., 2012).

These results support my hypothesis, indicating that ALS-linked mutations in GLT8D1 lead to a dominant phenotype with neurotoxicity. Whilst my results provide novel insights into the transient effects of GLT8D1 mutations on cellular function, I may not recognise the longitudinal impact, which is important given that ALS is an age-related disorder (Hardiman et al., 2017).

The isogenic lines would be useful for longitudinal studies through maintaining induction over a defined period. The toxicity data presented here are consistent with an age-of-onset disorder. A sudden burst in the expression of ALS-linked GLT8D1 mutations is sufficient to cause a toxic phenotype. However, this does not mimic the physiological expression of the mutations in the patients, which are expressed at a lower level, hence the development of symptoms after many decades.

3.4.5. ALS-linked GLT8D1 mutations impair glycosyltransferase activity

Glycosyltransferase assays were performed using recombinant GLT8D1-WT and GLT8D1-R92C protein immunopurified from isogenic HEK293 cells, as well as following transient transfection with pcDNA5/FRT/TO_3xFLAG plasmids expressing GLT8D1-WT, GLT8D1-G78W and GLT8D1-R92C. Protein purification was assessed via Coomassie blue staining and immunoblotting (**Figures 3.7 and 3.10**); however, these techniques are not sensitive for the detection of low-level impurities (<100ng) (Raynal et al., 2014). Therefore, degradation products can easily go unnoticed, particularly in low concentration samples. More highly sensitive colorimetric staining methods can be used directly after agarose gel electrophoresis. Such techniques include zinc-reverse staining (Fernandez-Patron et al., 1998) and silver staining (Chevallet et al., 2006), both of which can detect protein bands as low as 10ng and 1ng, respectively.

Based on sequence homology, GLT8D1 is a member of glycosyltransferase family 8 and is expected to catalyse the transfer of a glycosyl group from a donor to an acceptor via a “retaining” mechanism involving a glycosyl-enzyme intermediate. Although the crystal structure of GLT8D1 is unknown, it contains a conserved “DXD” metal ion binding site that indicates that it is a Leloir glycosyltransferase where donor and acceptor binding sites are divided by a single “GT-A” fold (Bourne and Henrissat, 2001). Discovered ALS-associated mutations in GLT8D1 cluster together in a short sequence of ~20 amino acids in close proximity to the substrate-binding site, suggesting a common effect on this function. Consistent with this, I observed a significant reduction in enzyme activity in mutated GLT8D1-R92C and GLT8D1-G78W compared to the WT protein. Measured Km was reduced in the mutated proteins, commensurate with an increase in substrate affinity, which could impair cycling of substrate through the enzyme and, thus, reduce overall velocity (**Figure 3.11**). This could also resolve an apparent paradox between the observations that discovered GLT8D1 mutations are autosomal dominant but reduce enzyme activity suggesting a loss-of-function mechanism, which is often present in the case of autosomal recessive inheritance. I propose

that higher substrate affinity could result in a dominant-negative effect with a competitive antagonism of WT enzyme function. Classically, enzyme mutations are thought to be recessive but it is estimated that as many as 25% of enzyme mutations are autosomal dominant (Veitia, 2002), as in our patients. For example, dominant-negative mutations in the GTPase Ras increase its substrate affinity and, thus, allow it to act as a competitive antagonist of the WT protein (Nassar et al., 2010). I cautiously note the example of SOD1 mutations that were originally thought to cause ALS through loss-of-function, but were subsequently shown to cause gain-of-function toxicity (Boillee et al., 2006). My work awaits validation in a higher organism.

It is noteworthy that measured Km values were relatively high compared to reports of other members of the glycosyltransferase 8 family (Persson et al., 2001), suggesting low substrate affinity. It is possible that absolute substrate affinity would be higher under physiological conditions, particularly as the identities of the normal donor and acceptor for GLT8D1 are unknown, and glycosyltransferase enzymes with a GT-A fold structure have been observed to show cooperation between donor and acceptor binding (Shoemaker et al., 2008). My reaction conditions utilized UDP-galactose and occurred without an acceptor.

3.4.6. Clinicopathological characterisation of patients with ALS-linked GLT8D1 mutations

Clinically, patients carrying mutations in GLT8D1 are within the spectrum of sporadic ALS, suggesting that they may share a common disease mechanism. DNA samples (n=200, of which 21 have a positive family history of ALS) from the Sheffield Brain Tissue Bank were screened for mutations in GLT8D1 by Sanger sequencing. Unfortunately, pathological material was not available from any cases with identified GLT8D1 mutations and so I was not able to confirm the presence of TDP-43-positive neuronal inclusions, which are the hallmark of 97% of ALS cases (Neumann et al., 2006). GLT8D1-R92C patients all suffered limb onset disease which was unusually aggressive. In contrast the individual with a GLT8D1-G78W mutation suffered less aggressive bulbar onset disease. All patients suffered relatively young onset disease, which is consistent with a monogenic disorder, and all patients were within the spectrum of recognised ALS (Cooper-Knock et al., 2019) (**Tables 1.2, 1.3**). Clinical data were not available from patients carrying mutations other than GLT8D1-R92C and GLT8D1-G78W.

3.4.7. Ganglioside signalling as a GLT8D1-ALS pathological mechanism

Gangliosides are sialic acid-containing glycosphingolipids which are particularly abundant within the CNS (Vajn et al., 2013). Gangliosides within the CNS are typically synthesised in the endoplasmic reticulum (ER) from a lactosylceramide precursor, and are remodelled during transit from the cis-Golgi to the trans-Golgi network by a series of glycosyltransferase enzymes which incorporate galactose and GalNAc groups. Consistent with a role in this process, I have shown that GLT8D1 is able to accept UDP-galactose as a substrate. Mature gangliosides are carried to the cell surface where they function prominently in cell signalling (Yu et al., 2012). Interestingly, autoantibodies against specific gangliosides produce an inflammatory disease of spinal motor neurons known as multifocal motor neuropathy with conduction block (Harschnitz et al., 2014), which is an important differential diagnosis for ALS. Altered levels of gangliosides have been reported in animal models of ALS and in post-mortem CNS tissue from ALS patients (Dodge et al., 2015, Ariga, 2014). I have shown that ALS-linked mutations in GLT8D1 impair its glycosyltransferase activity, which I predict will negatively impact on ganglioside signalling. I subsequently investigated ganglioside signalling as a possible GLT8D1-ALS pathological mechanism in Chapter 5.

3.4.8. Summary

In summary, I have successfully generated plasmid constructs to investigate the functional implications of ALS-linked GLT8D1 mutations. These constructs were used to engineer isogenic HEK293-WT and HEK293-R92C cells, which will enable studies into the early biochemical effects of a GLT8D1-R92C mutation. I have shown that GLT8D1-G78W and GLT8D1-R92C mutations are toxic to neuronal and non-neuronal cells, and the relative toxicity of the mutations mirrors the clinical severity. Observed mutation-specific effects on cell toxicity are consistent with an age-of-onset disease, as overexpression in my model does not reflect the physiological expression of mutant GLT8D1 in the patients. It is difficult to rationalise this dramatic toxicity with a disease in which people do not present with symptoms for several decades. However, patients will express relatively lower levels of the mutant protein, and homeostatic mechanisms will likely curtail the effects of the mutations for a period of time.

I was the first to publish information regarding the substrate specificity of GLT8D1. I have shown that GLT8D1-G78W and GLT8D1-R92C mutations impair the glycosyltransferase activity of the enzyme with UDP-Galactose as the target substrate. The observed reduction in

reaction velocity is likely due to increased substrate affinity, which could impair cycling of the substrate through the enzyme. ALS-associated GLT8D1 mutations are autosomal dominant but the reduction in enzyme activity suggests a loss-of-function mechanism, which is often coincident with autosomal recessive inheritance. Indeed, misfolded SOD1 was initially proposed to cause ALS via a loss-of-function mechanism; however, a gain-of-function toxicity is now the accepted mechanism thought to arise from misfolding of the protein. It is possible that the R92C mutation is causing GLT8D1 to misfold. I propose that higher substrate affinity could result in a dominant-negative effect with a competitive antagonism of the WT enzyme function. The data presented here are consistent with the association of mutations in GLT8D1 with ALS. Confirmation of the pathogenic mechanism(s) will require validation in a higher organism but my discovery places this pathway upstream in the pathogenesis of ALS, making it an attractive therapeutic target.

Chapter 4. Knockdown of endogenous *glt8d1* and overexpression of mutant GLT8D1 produces motor impairment in zebrafish larvae

4.1. Introduction

This chapter is an extended version of work published during my PhD (Cooper-Knock et al., 2019). Unless stated otherwise, I was responsible for conducting all experimental work presented within this chapter, and any collaborations are acknowledged. Zebrafish (*Danio rerio*) have become increasingly popular as a model organism for the investigation of neurodegenerative disorders (Beattie et al., 2007) due to their ease of genetic manipulation, robust behavioural phenotypes, rapid development, and low maintenance cost (Grunwald and Eisen, 2002). The use of zebrafish embryos is particularly attractive, as their optical transparency enables the detection of morphological abnormalities and the visualisation of neuronal activity using non-invasive imaging techniques. This is useful when modelling neurodegeneration in a multicellular and complex system (Kalueff et al., 2014). In addition, a major advantage of zebrafish is the high homology in relation to human genes (Howe et al., 2013), which is important for modelling human genetic disorders such as ALS. Zebrafish have a fully sequenced genome, allowing for the straightforward comparison of zebrafish genes to human genes (Grunwald and Eisen, 2002). Zebrafish *glt8d1* shares 79% homology with its human *GLT8D1* orthologue, and the G78W and R92C mutation sites are highly conserved (Ensembl, 2020). These advantages influenced my decision to model GLT8D1-linked ALS in zebrafish.

My glycosyltransferase assay data suggest that ALS-linked GLT8D1 mutations cause a loss-of-function mechanism and a possible dominant negative effect (see sections 3.3.6 and 3.3.7). To investigate loss-of-function in the context of a whole organism, I assessed whether transient knockdown of endogenous *glt8d1* in zebrafish embryos via microinjection of antisense morpholino oligonucleotides (AMOs) led to the onset of a motor phenotype. I cautiously use the term “loss-of-function”, which more accurately describes genetic mutant models with verified loss-of-function mutations (Schmid and Haass, 2013). AMOs are a widely used tool in zebrafish research for the efficient and specific knockdown of gene function (Eisen and Smith, 2008, Bill et al., 2009); however, there are caveats to their use, which I will discuss in section 4.4.2. AMOs hybridise to mRNA target sequences to either block translation or pre-mRNA splicing. Translation blocking occurs when the AMO targets mRNA sequences proximal to the initiation codon. Splice blocking occurs when the AMO targets mRNA

sequences that span exon-intron boundaries, thus blocking the binding of splicing factors to the pre-mRNA (Xi et al., 2011). AMOs utilised in this project were designed to block pre-mRNA splicing of *glt8d1*, thus reducing expression of the protein.

In single cell-type culture models, GLT8D1-G78W and GLT8D1-R92C mutations are associated with gain-of-function toxicity (see section 3.3.5). Therefore, I decided to investigate the effects of transiently overexpressing mutant human GLT8D1 mRNA in zebrafish to place these mutations in the context of motor system function. Observed reductions in motor activity would be consistent with a gain-of-function mechanism. Importantly, characterising a toxic gain-of-function usually requires a heterozygous model that is generated using a genome editing method (Schmid and Haass, 2013). Human mRNA encoding GLT8D1-WT, GLT8D1-G78W, or GLT8D1-R92C was microinjected into zebrafish embryos at the one-cell stage and survival rates were recorded. A similar motor phenotype in both knockdown and overexpression models would be consistent with a proposed dominant negative effect.

4.2. Aims and objectives to investigate whether knockdown of endogenous *glt8d1*, or overexpression of mutant GLT8D1 mRNA, cause motor impairment in zebrafish larvae

1. Transiently knockdown endogenous *glt8d1* in zebrafish embryos using AMOs, and assess knockdown via RT-PCR.
2. Transiently overexpress synthesised GLT8D1-WT, GLT8D1-G78W and GLT8D1-R92C human mRNA in zebrafish embryos, and assess overexpression via immunoblotting.
3. Evaluate the effect of overexpressing mutant GLT8D1 on zebrafish embryo survival.
4. Assess the effect of endogenous *glt8d1* knockdown on motor function in zebrafish larvae.
5. Analyse the effect of overexpressing GLT8D1-G78W and GLT8D1-R92C human mRNA on motor function in zebrafish larvae, compared to overexpression of GLT8D1-WT human mRNA.
6. Validate the sensitivity of two automated tracking platforms (Viewpoint and EthoVision XT) for the behavioural analysis of zebrafish larvae.

4.3. Results

4.3.1. Knockdown of endogenous *glt8d1* impairs motor function in zebrafish larvae

All experimentation within this chapter was performed in collaboration with Dr Tennore Ramesh. Zebrafish embryos were microinjected at the one-cell stage with splice-blocking AMOs to transiently knockdown endogenous *glt8d1*. A commercially available anti-GLT8D1 antibody did not detect endogenous *glt8d1* in zebrafish embryos at 2dpf; therefore, I was unable to confirm knockdown via immunoblotting. However, knockdown of endogenous GLT8D1 RNA was confirmed at 2dpf via RT-PCR (n=1; no statistical analysis was performed) (**Figure 4.1**). Knockdown of GLT8D1 RNA was no longer present at the time of behavioural testing (5dpf), which is expected in transient models of this nature.

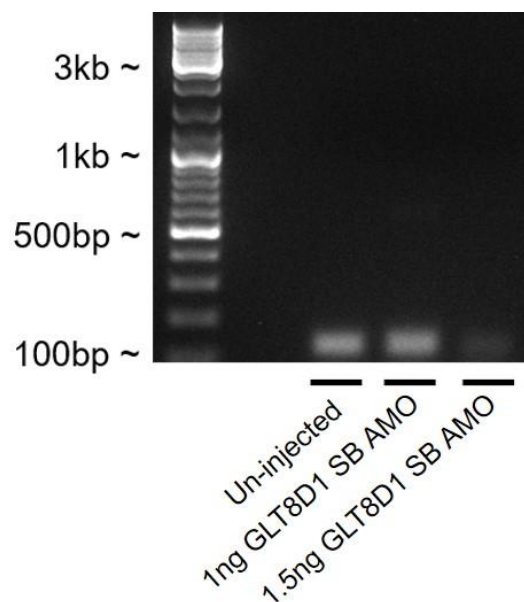


Figure 4.1. Agarose gel electrophoresis showing a reduction in the expression of zebrafish GLT8D1 RNA following microinjection of ~1.5ng splice blocking AMO. RNA was extracted from twenty zebrafish embryos at 2dpf per cohort, and knockdown was evaluated via RT-PCR following 1.0ng and 1.5ng doses of AMO. A 1.0ng dose of AMO did not lead to an observable reduction in GLT8D1 RNA levels compared to un-injected. A 1.5ng dose was sufficient to reduce GLT8D1 RNA, represented by the weaker band at the expected height of ~149bp. Molecular weight markers are indicated (bp/kb) (RT-PCR was performed by Dr Johnathan Cooper-Knock).

All zebrafish larvae appeared morphologically normal prior to behavioural testing. Zebrafish larvae behaviour was analysed at 5dpf to determine whether knockdown of endogenous *glt8d1* correlated with the onset of a motor phenotype. The distance moved by 96 zebrafish embryos for each condition from three separate clutch mates (~32 zebrafish per clutch) was evaluated via infrared tracking using a ZebraBox® apparatus with Zebralab software (ViewPoint) (Scott et al., 2016). This equipment is commonly used in the University of Sheffield CDBG aquarium. Knockdown of endogenous *glt8d1* correlated with a significant reduction in the distance moved by zebrafish larvae at 5dpf, compared to injection with a control AMO (n=96, *t* test, $p=0.0073$) (**Figure 4.2a**).

ViewPoint infrared tracking was compared to manual video observation. Observed inconsistencies in the automated tracking included automatically detected movements in the absence of observed movement, and failure to detect certain larvae. Due to these anomalies, I decided to validate the accuracy of the ViewPoint tracking software by trialling a commercially available alternative platform called EthoVision XT. EthoVision XT was chosen based on its precision in distinguishing between test subject and background (Noldus et al., 2001). I reanalysed the same videos and observed a similar reduction in the distance moved by zebrafish larvae injected with a GLT8D1 splice-blocking AMO compared to zebrafish injected with a control AMO (n=96, unpaired *t* test, $p=0.0017$) (**Figure 4.2b**). Using this software, I also measured the velocity of zebrafish larvae. Consistent with the distance moved, velocity was also reduced in zebrafish larvae injected with a GLT8D1 splice-blocking AMO, compared to larvae injected with a control AMO (n=96, unpaired *t* test, $p=0.0016$) (**Figure 4.2c**). This result gave me confidence in the accuracy of the ViewPoint software; therefore, subsequent behavioural analysis was performed using this platform to avoid additional costs.

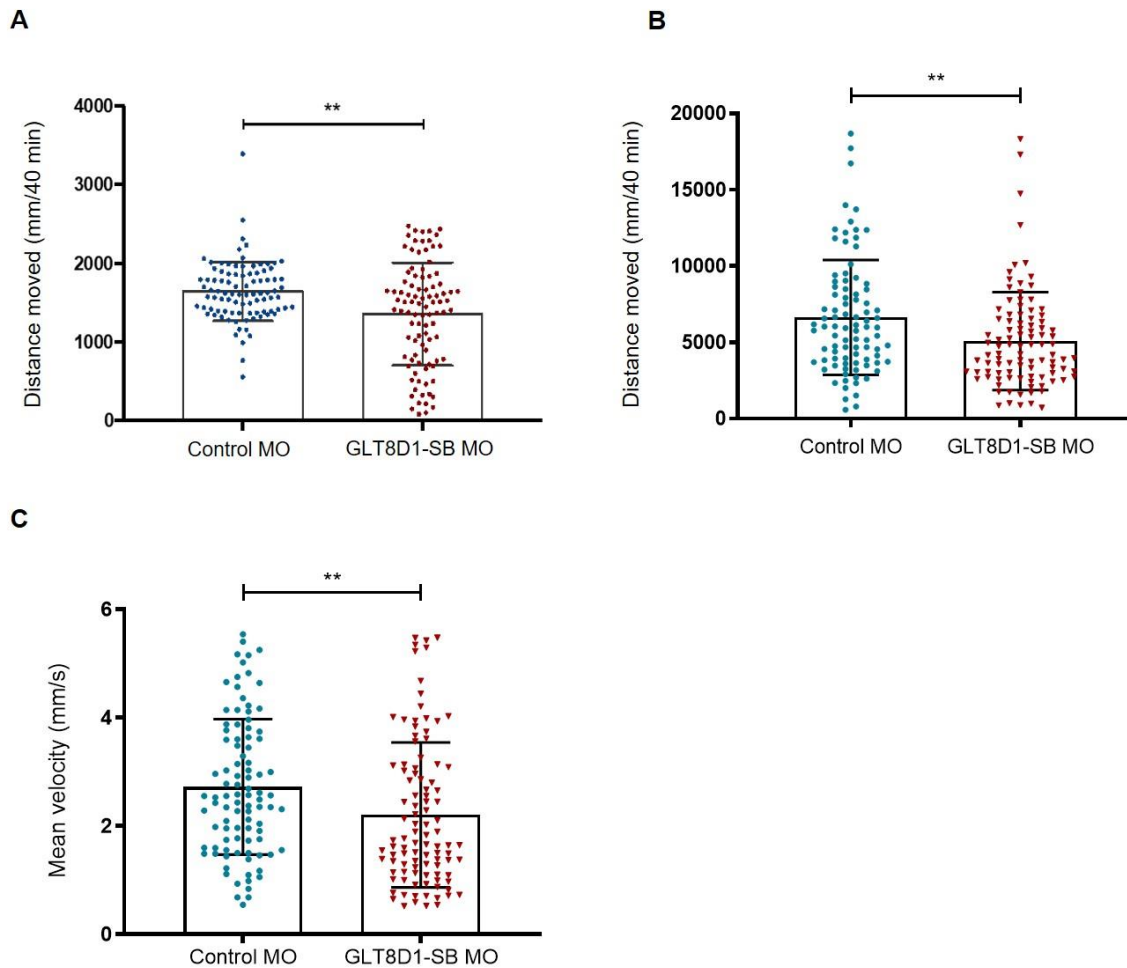


Figure 4.2. Knockdown of endogenous *glt8d1* correlates with a reduction in the velocity and distance moved by zebrafish larvae at 5dpf. Distance moved (mm) by 96 zebrafish larvae for each condition (5dpf) (~32 per clutch) during 40 minutes of automated tracking using **(A)** ViewPoint and **(B)** EthoVision XT. Injection with 1.5ng GLT8D1 splice blocking AMO correlates with a significant reduction in the distance moved by zebrafish larvae, compared to injection with 1.5ng control AMO (n=96, unpaired *t* test, ***p*<0.001). **(C)** EthoVision XT shows that the mean velocity (mm/s) is reduced in zebrafish larvae injected with a GLT8D1 splice-blocking AMO, compared to zebrafish injected with a control AMO (n=96, unpaired *t* test, ***p*<0.01). Each data point represents a single zebrafish larva (SB – splice blocking; MO - morpholino). Figure adapted from (Cooper-Knock et al., 2019).

4.3.2. Overexpression of *GLT8D1-G78W* and *GLT8D1-R92C* mRNA impairs motor function in zebrafish larvae, compared to overexpression of *GLT8D1-WT* mRNA

The observed behavioural phenotype following transient knockdown of endogenous *glt8d1* in zebrafish larvae is consistent with a role for *GLT8D1* in motor function. I then tested whether overexpression of *GLT8D1-G78W* and *GLT8D1-R92C* mRNA had a similar effect on motor activity, compared to overexpression of *GLT8D1-WT* mRNA. For RNA synthesis, full-length *GLT8D1* nucleotide sequences were linearised from pEGFP-N1_*GLT8D1*-eGFP vectors (see section 3.3.1) using *NheI* and *XhoI* restriction enzymes. Cleaved sequences were cloned into PCS2+ vectors. PCS2+ vectors contain an SP6 promoter required for the transcription of capped RNA *in vitro* (Wang et al., 2016). Restriction digests were used to confirm successful integration of *GLT8D1* nucleotide sequences into PCS2+ vectors (**Figure 4.3a**). PCS2+ vectors were also validated via Sanger sequencing (**see appendix 10**). mRNA encoding human *GLT8D1-WT*, *GLT8D1-G78W* and *GLT8D1-R92C* was synthesised from PCS2+ vectors using the mMESSAGE mMACHINE® SP6 Transcription Kit. The quality of the RNA was assessed via agarose gel electrophoresis (**Figure 4.3b**) and NanoDrop™ 1000 spectrophotometry.

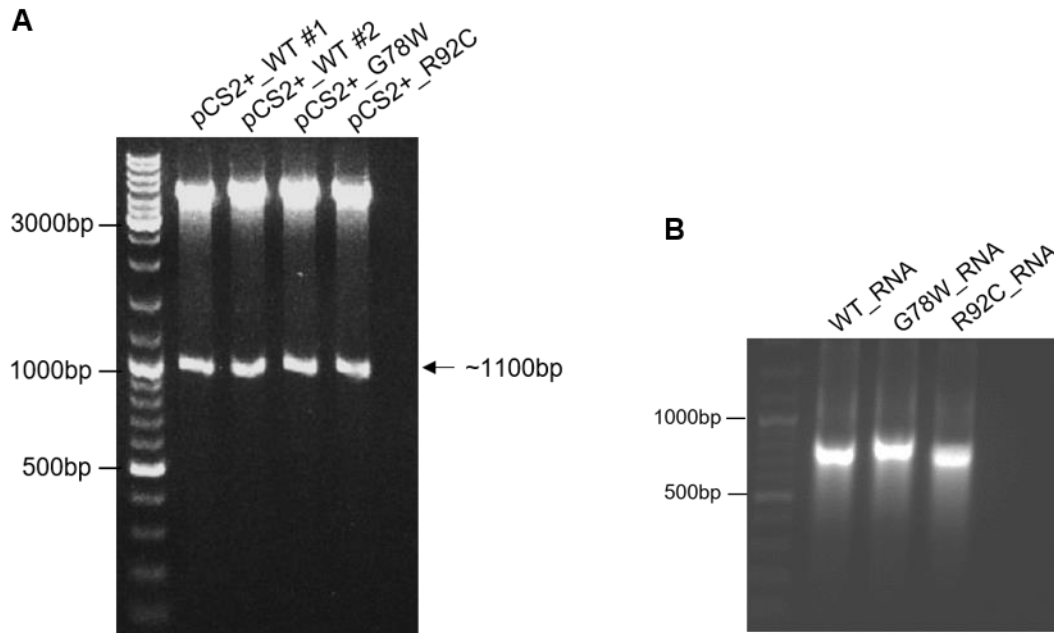


Figure 4.3. Generation of GLT8D1-WT, GLT8D1-G78W and GLT8D1-R92C mRNA for zebrafish embryo microinjection. (A) GLT8D1 sequences were cleaved from pEGFP-N1 expression vectors (see section 3.3.1) using NheI and XhoI restriction endonucleases and cloned into PCS2+ vectors. Restriction digests using BclI and XbaI restriction enzymes were performed to confirm the size of GLT8D1 inserts. PCS2+ plasmids were also validated via Sanger sequencing (see appendix 10). (B) PCS2+ vectors were linearized for SP6 RNA transcription *in vitro*. RNA quality was assessed using agarose gel electrophoresis and NanoDrop™ spectrophotometry. DNA ladder molecular weight markers are indicated (bp).

Synthesised mRNA did not contain an eGFP-tag; therefore, I aimed to confirm overexpression of GLT8D1 in zebrafish embryos using a commercially available anti-GLT8D1 antibody. To validate the anti-GLT8D1 antibody, I compared the relative expression level of GLT8D1 in embryos injected with 350pg and 700pg doses of mRNA encoding both GLT8D1-WT and GLT8D1-R92C. I observed stronger bands at the expected height of ~42kDa in zebrafish injected with 700pg mRNA, compared to those injected with 350pg mRNA, for both GLT8D1-WT and GLT8D1-R92C cohorts. I did not observe a protein band in the un-injected cohort (n=2, no statistical analysis was performed) (Figure 4.4). This suggests that endogenous levels of *glt8d1* are not detectable using this anti-GLT8D1 antibody. The molecular weight of the GLT8D1 bands were sized at 41.46kDa using GeneTools (Syngene).

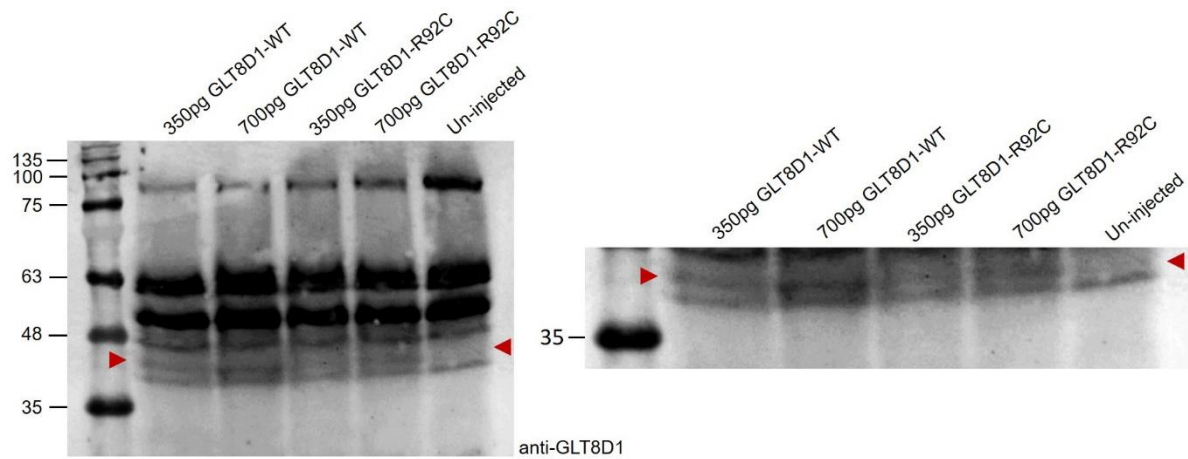


Figure 4.4. Overexpression of GLT8D1-WT and GLT8D1-R92C in zebrafish embryos is confirmed via immunoblotting at 2dpf. Representative blot used to validate the anti-GLT8D1 antibody, showing the relative expression level of GLT8D1 following injection with 350pg and 700pg doses of synthesised GLT8D1-WT and GLT8D1-R92C human mRNA (red arrows). Stronger bands are present at the high dose (700pg). The molecular weight of the GLT8D1 bands was sized at 41.46kDa using GeneTools (Syngene). The entire lysate of twenty zebrafish embryos was fractionated per lane (n=2, no statistical analysis was performed).

High quality human mRNA encoding GLT8D1-WT, GLT8D1-G78W or GLT8D1-R92C was microinjected into a fresh batch of zebrafish embryos at the one-cell stage to characterise the effect of overexpressing mutant GLT8D1 mRNA on survival. Two doses of mRNA were administered for each condition: 350pg and 700pg. Percentage embryo survival was recorded at 8-, 24-, and 48-hour time intervals post injection to compare the toxicity of GLT8D1-WT, GLT8D1-G78W and GLT8D1-R92C. Zebrafish from three separate clutch mates were injected for each condition.

I did not observe significant reductions in the survival rate between GLT8D1-WT and GLT8D1-G78W at doses of 350pg mRNA (24 hours: n=3, paired *t* test, $p= 0.501776$; 48 hours: n=3, paired *t* test, $p=0.694731$) or 700pg mRNA (24 hours: n=3; paired *t* test, $p=0.678639$; 48 hours: n=3, paired *t* test, $p= 0.850333$). Neither did I observe a significant reduction in the survival rate between GLT8D1-WT and GLT8D1-R92C at doses of 350pg mRNA (24 hours: n=3, paired *t* test, $p= 0.727215$; 48 hours: n=3, paired *t* test, $p= 0.292042$) or 700pg mRNA (24 hours: n=3, paired *t* test, $p= 0.146395$; 48 hours: n=3, paired *t* test, $p=0.0652$) (**Figure 4.5**). Data are also presented in the form of Kaplan-Meier survival curves (**see appendix 11**).

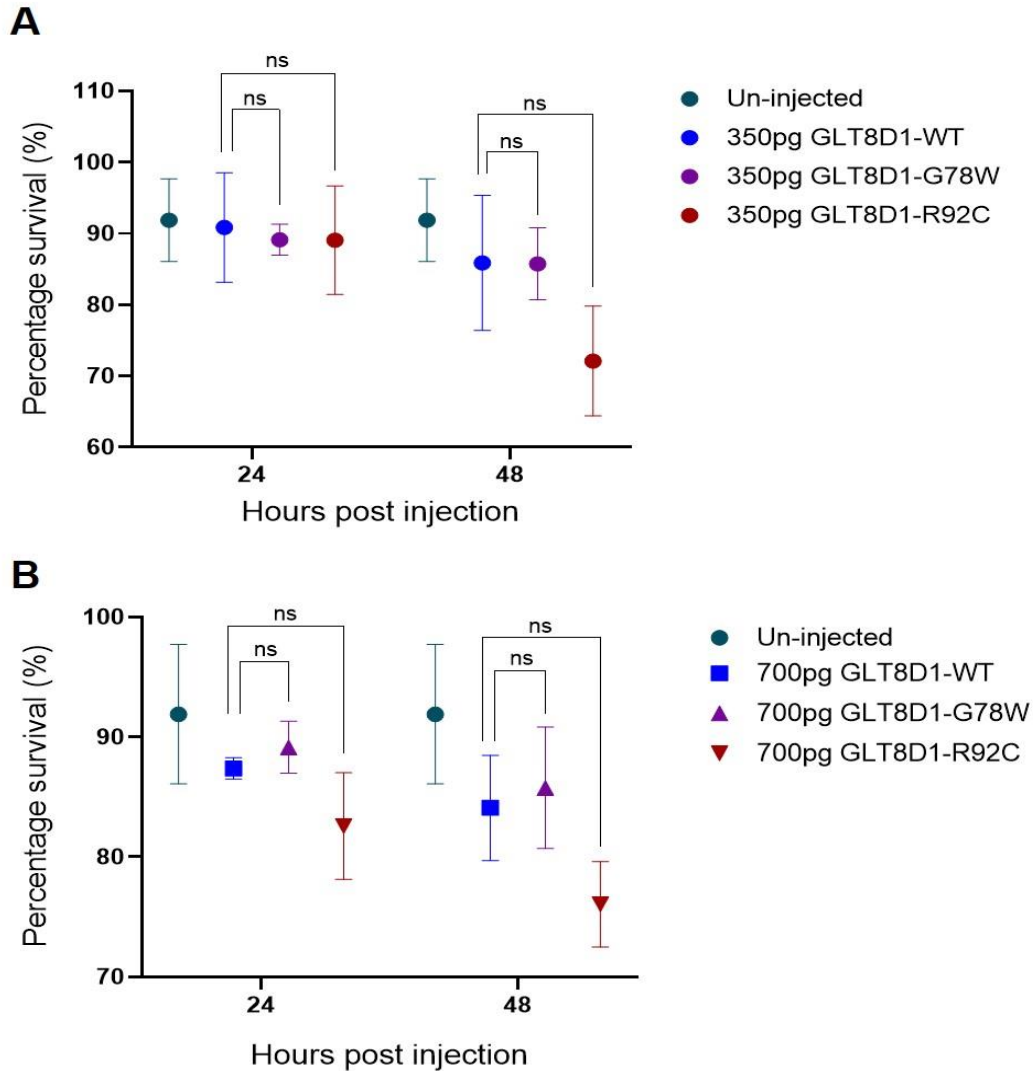


Figure 4.5. Survival of zebrafish embryos following microinjection of human mRNA encoding GLT8D1-WT, GLT8D1-G78W and GLT8D1-R92C. Injection of (A) ~350pg and (B) ~700pg mature mRNA encoding human GLT8D1-G78W or GLT8D1-R92C does not significantly reduce the survival of zebrafish embryos at 24- and 48-hours compared to mature mRNA encoding human GLT8D1-WT ($n=3$; paired t -test, $p>0.05$ for 350pg and 700pg doses). Turquoise line = un-injected; blue line = GLT8D1-WT mRNA; purple line = GLT8D1-G78W mRNA; red line = GLT8D1-R92C mRNA. Figure adapted from (Cooper-Knock et al., 2019).

Twenty zebrafish embryos from each cohort were selected at 2dpf to evaluate the overexpression of GLT8D1-WT, GLT8D1-G78W and GLT8D1-R92C via immunoblotting. All twenty selected embryos from each cohort were fractionated per lane. The molecular weight of the GLT8D1 bands were sized at 41.98kDa using GeneTools (Syngene). Protein bands appeared stronger in the GLT8D1-WT, GLT8D1-G78W and GLT8D1-R92C cohorts compared to the un-injected group, suggesting overexpression of GLT8D1 (n=2, no statistical analysis was performed) (**Figure 4.6a**). I performed only two biological repeats of the immunoblotting in order to maximise the number of zebrafish embryos for behavioural testing.

All zebrafish appeared morphologically normal prior to behavioural testing. Behavioural analysis was conducted in zebrafish larvae at 5dpf to assess the effects of overexpressing GLT8D1-WT, GLT8D1-G78W and GLT8D1-R92C human mRNA on zebrafish locomotion. I observed mutation-specific reductions in the distanced moved by zebrafish injected with GLT8D1-G78W (23 embryos from 1 clutch; *t* test, $p=0.0044$) and GLT8D1-R92C (49 embryos from 2 clutches; *t* test, $p=0.0315$) mRNA, following 40 minutes of behavioural tracking using ZebraBox® apparatus with Zebralab software (ViewPoint) (Scott et al., 2016) (**Figures 4.6b, 4.6c**).

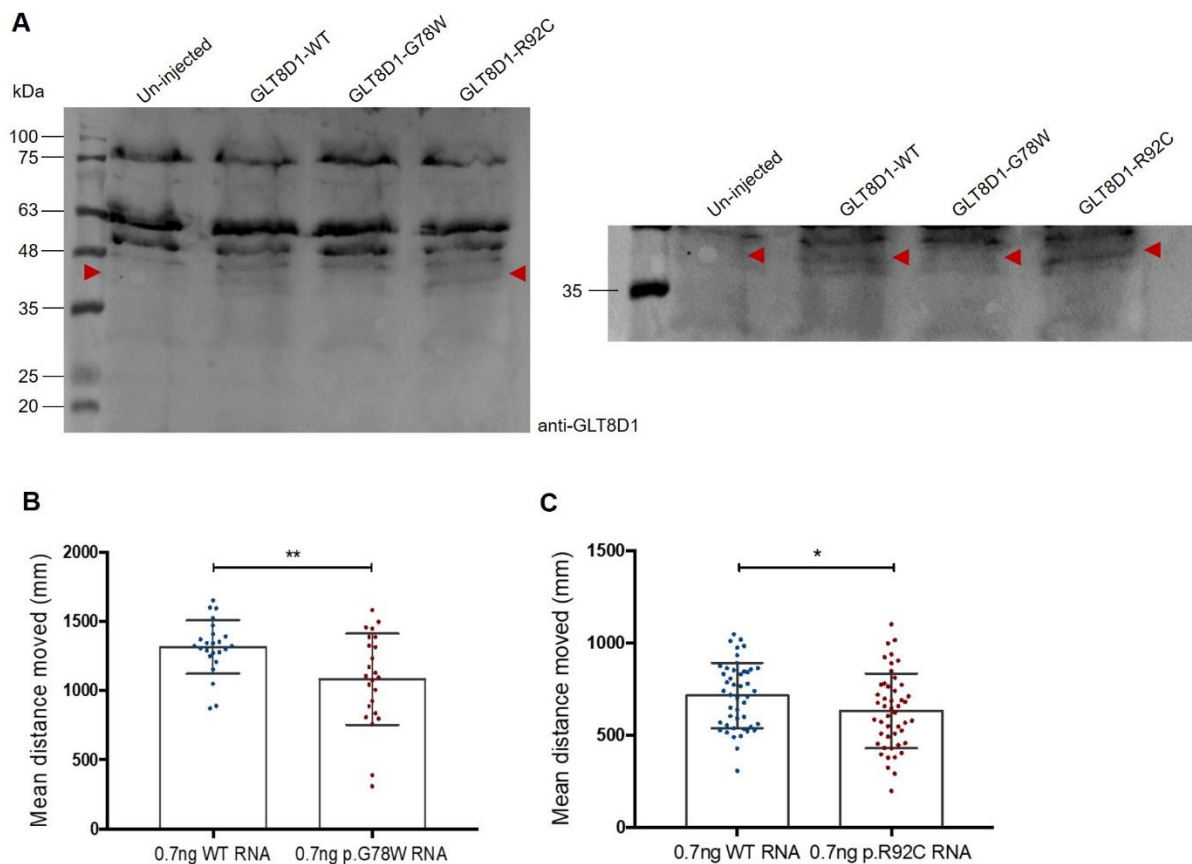


Figure 4.6. Overexpression of GLT8D1-G78W and GLT8D1-R92C mRNA produces motor impairment in zebrafish larvae, compared to overexpression of GLT8D1-WT. (A) Representative blot showing the relative expression of GLT8D1-WT, GLT8D1-G78W and GLT8D1-R92C protein (red arrows) in zebrafish larvae at 2dpf. Twenty embryos were fractionated per lane (n=2, no statistical analysis was performed). Molecular weight markers are indicated (kDa). Distance moved (mm/40 min) during two light-dark cycles (10 minutes per cycle) at 5dpf is reduced following injection with ~700pg mRNA encoding human (B) GLT8D1-G78W (23 embryos from 1 clutch) or (C) GLT8D1-R92C (49 embryos from 2 clutches) compared to ~700pg mRNA encoding human GLT8D1-WT. Each data point represents a single zebrafish larva. Un-paired *t*-test to compare the two injection groups * $p < 0.05$; ** $p < 0.01$. Figure adapted from (Cooper-Knock et al., 2019).

4.4. Discussion

4.4.1. Zebrafish as a neurodegenerative disease model

I chose zebrafish (*Danio rerio*) as the organism to initially model ALS-linked GLT8D1 mutations *in vivo* due to their fecundity, rapid development, and ease of genetic manipulation (Bradford et al., 2017). The zebrafish genome has been fully sequenced, and approximately 71% of the 20,479 human protein-coding genes have orthologues within the zebrafish genome. Moreover, 69% of the 26,206 protein-coding zebrafish genes have orthologues within the human genome (Howe et al., 2013). This makes zebrafish a useful model for the study of human genetic diseases. GLT8D1 shares 79% homology between zebrafish and humans, and the mutation sites are highly conserved (Ensembl, 2020). Zebrafish exhibit a wide range of complex behaviours such as social, anxiety, learning, and memory, which are useful for modelling neurological diseases (Basnet et al., 2019). Furthermore, high-throughput tracking of zebrafish embryos and larvae has greatly enhanced behavioural research in the zebrafish field (Kalueff et al., 2013). The development of software for tracking larval movements at high resolution enables experimenter-independent, high-throughput screening for motor activity deficits (Fontaine et al., 2008, Mirat et al., 2013). Finally, in contrast with mammals, the development of zebrafish larvae occurs externally, which makes them accessible for experimental manipulation (Schmidt et al., 2013).

There are limitations to the use of zebrafish as a model for ALS. ALS is characterised by the degeneration of upper and lower motor neurons; however, the relevance of zebrafish in modelling upper motor neuron disorders is limited due to the absence of corticospinal and rubrospinal tracts in their CNS (Babin et al., 2014). In contrast to mammals, zebrafish have a remarkable ability to regenerate damaged neurons leading to functional recovery. Indeed, most studies focus on axonal regeneration in adult zebrafish, which usually takes weeks to occur; however, there is also evidence of motor neuron regeneration in zebrafish at the larval stage, which is detectable within 48 hours (Ohnmacht et al., 2016). Whilst the regenerative capacity of adult and larval zebrafish neurons is apparent, it is usually studied in response to mechanical lesions or motor neuron ablation, which is inconsistent with my models. Furthermore, many studies take advantage of the optical transparency by analysing zebrafish at embryonic or early developmental stages, which is inconsistent with an age-related disorder such as ALS (Kabashi et al., 2010, Sukardi et al., 2011, Ciura et al., 2013, Schmid et al., 2013, Morrice et al., 2018, Svahn et al., 2018).

Reproducibility is a major concern with transient zebrafish models, or any transient model for that matter. Multiple studies in the ALS field have highlighted this. For example, AMO-mediated knockdown of zebrafish *C9orf72* resulted in behavioural deficits concurrent with reduced axonal length (Ciura et al., 2013). However, depletion of *C9orf72* transcripts in iPSC-derived neurons and the mouse CNS did not lead to any adverse effects (Donnelly et al., 2013, Sareen et al., 2013, Lagier-Tourenne et al., 2013). Therefore, stable mutants are critical to ensure that observed phenotypes in transient models are reliable. Stable, transgenic mutant zebrafish lines can be generated using CRISPR/Cas9 genome editing (Burket et al., 2008). However, when I was performing the zebrafish work, CRISPR/Cas9 genome editing was reported to cause numerous off-target mutations *in vivo* due to poor specificity of the single guide RNAs (Schaefer et al., 2017). The specificity of this technology has since improved dramatically (Anzalone et al., 2019, Kocak et al., 2019).

Various studies have used zebrafish as an *in vivo* model for investigating ALS pathogenesis; however, these models vary pathologically and phenotypically depending on the method of genetic manipulation (**Table 4.1**). Both of my models demonstrate an early-onset and dramatic effect compared to the human phenotype. This is similar to the early-onset phenotype seen in the SOD^{G93A} ALS mouse model (Gurney et al., 1994). Much like the SOD1^{G93A} model, this observed embryonic phenotype is not representative of the human disease. However, my models are transient, and do not reflect the physiological expression of GLT8D1 in the patients. Despite this, my models are useful as they provide evidence for motor system dysfunction linked to GLT8D1-ALS.

ALS gene	Genetic manipulation	Pathology	Phenotype	Reference
<i>C9ORF72</i>	Expression of 89 G ₄ C ₂ repeats	Accumulation of RNA foci and dipeptide repeat proteins; muscle atrophy; motor neuron loss	Motor deficits; cognitive impairment; premature death	(Shaw et al., 2018)
	Expression of ~70 G ₄ C ₂ repeats	Motor neuron toxicity	None recorded	(Swinnen et al., 2018)
	AMO-mediated knockdown	Axonal degeneration of motor neurons	Locomotion deficits	(Ciura et al., 2013)
<i>SOD1</i>	Expression of SOD1 ^{G93R} mutation	Neuromuscular junction defects; motor neuron loss; muscle atrophy	Decreased endurance in swim tunnel test; paralysis; premature death	(Ramesh et al., 2010)
	Expression of SOD1 ^{G93A} mutation	Defective motor neuron outgrowth and axonal branching; loss of neuromuscular junctions; alterations in motor neuron innervation patterns; motor neuron cell loss	Motor dysfunction; decreased activity	(Sakowski et al., 2012)
	Expression of SOD1 ^{T70I} mutation	Neuromuscular junction defects; susceptibility to oxidative stress	Adult-onset motor neuron disease phenotype	(Da Costa et al., 2014)
<i>TARDBP</i>	Knockout of both <i>tardbp</i> orthologues by genome editing with zinc finger nucleases	Muscle degeneration; reduced blood circulation; mispatterning of vessels; impaired spinal motor neuron axon outgrowth	Premature death	(Schmid et al., 2013)
	AMO-mediated knockdown; expression of TARDBP ^{A315T / G348C / A382T} mutations	Shorter motor neuronal axons, premature and excessive branching	Swimming deficits	(Kabashi et al., 2010)

	Knockout of both <i>tardbp</i> orthologues via targeted induced local lesions in genome	Shortened motor axons	Locomotion defects; premature death	(Hewamadduma et al., 2013)
	CRISPR-mediated knockout	No pathology	No abnormal phenotype	(Lebedeva et al., 2017)
<i>FUS</i>	AMO-mediated knockdown; expression of <i>FUS</i> ^{R521H} mutation	Reduced NMJ synaptic fidelity with reduced quantal transmission; enhanced motor neuron excitability	Impaired motor activity	(Armstrong and Drapeau, 2013)

Table 4.1. Zebrafish ALS models recapitulate pathological and phenotypic disease traits. Common ALS genes, genetic alterations, observed pathological and phenotypic traits, and references are shown.

4.4.2. Advantages and limitations concerning the use of AMOs

AMOs are useful tools for the functional characterisation of gene activity *in vivo*. The use of AMOs in zebrafish have been shown to be sequence specific and extremely potent in cells during the initial fifty hours of development; therefore, resulting phenotypes can be rapidly observed using a relatively inexpensive method (Corey and Abrams, 2001). Moreover, AMOs are water soluble and immune to nucleases (Summerton and Weller, 1997). Indeed, there are caveats to the use of AMOs, such as off-target effects not associated with loss-of-function of the target locus. Underlying off-target mechanisms are not fully understood, although p53-dependent neural toxicity is a well-described and consistent phenotype. Therefore, it may be justifiable to co-inject with an AMO targeting p53, although this approach should mask the effects of gene-specific p53-dependent phenotypes (Xi et al., 2011, Bedell et al., 2011).

Dose curves are often generated to overcome AMO-induced off-target toxicity. Increasing the AMO dosage will enhance phenotypic penetrance and subsequently increase phenotypic severity (Nasevicius and Ekker, 2000), but it may also increase the likelihood of off-target toxicity (Robu et al., 2007). A dose curve would provide information as to the upper limit for subsequent testing, as well as determine the lethal dose 50 (the dose at which $\geq 50\%$ of injected embryos die) for each tested AMO (Bedell et al., 2011). In the present study, I tested AMOs at doses of 1.0ng, 1.5ng and 2.0ng. 1.0ng and 1.5ng doses were well tolerated and larvae appeared morphologically normal; however, 2.0ng doses caused morphological

abnormalities and led to a higher rate of premature death. Therefore, in order to obtain maximal phenotypic penetrance without inducing high rates of morphological abnormality or fatality, 1.5ng AMO doses were administered to zebrafish embryos for subsequent behavioural testing. As a result, observed phenotypes were more likely to be knockdown specific.

Numerous other groups have performed AMO-mediated knockdown in zebrafish to model ALS-causing mutations. Knockdown of *C9orf72* (Ciura et al., 2013), *tardbp* (Kabashi et al., 2010) and *fus* (Armstrong and Drapeau, 2013) using AMOs have all been shown to correlate with the onset of a motor phenotype. However, it is noteworthy that the study by Kabashi and colleagues only reported knockdown of one *tardbp* orthologue, whereas a more recent study reported that two *tardbp* orthologues are present in zebrafish (Schmid et al., 2013). Much of the published work concerning transient knockdown of target genes in zebrafish using AMOs has been performed during the early developmental stages. Therefore, it is difficult to detect potential direct or indirect interactions between developmental and neurodegeneration processes, particularly in the context of late-onset diseases such as ALS (Schmid and Haass, 2013).

Due to controversies in the field pertaining to the non-specific effects of AMOs, future work should consider CRISPR/Cas9 genome editing to create a knockout zebrafish model to study GLT8D1 loss-of-function. This approach has already been applied in zebrafish to investigate other ALS-associated genes. For example, CRISPR-mediated knockout of FUS was not shown to cause an ALS-like phenotype (Lebedeva et al., 2017), contrary to previous reports using AMOs (Armstrong and Drapeau, 2013) (**Table 4.1**). Despite the aforementioned limitations, the use of AMOs *in vivo* is advantageous over knockdown using miRNAs, which may undergo nuclease-mediated degradation before obtaining modulation of the target gene (Rupaimoole et al., 2011). RNAi technology has been reported to work in zebrafish but with highly variable and controversial results (Wargelius et al., 1999, Li et al., 2000, Oates et al., 2000).

4.4.3. Transient knockdown of endogenous glt8d1 causes motor impairment in zebrafish larvae

Transient knockdown of endogenous *glt8d1* using splice-blocking AMOs was performed to test for a potential loss-of-function mechanism, and to indirectly assess whether GLT8D1 is

involved in motor system function. This is a transient model and therefore most resulting phenotypes are identified within the first 3 days of embryonic development, but sometimes persist to 5dpf. Observed effects rarely continue beyond 5dpf, possibly due to high rates of protein turnover (Bill et al., 2009). This is advantageous from an ethical standpoint as modelling can be performed at a stage in embryonic development when zebrafish are not protected by UK and EU legislation (ASPA, 1986).

Evaluation of *glT8d1* knockdown at 2dpf was not possible via immunoblotting because the anti-GLT8D1 antibody was only able to detect GLT8D1 when overexpressed (**Figure 4.4**). However, my AMO was designed to remove exon 2, which would lead to a frameshift allowing for easy assessment via RT-PCR (Bill et al., 2009). Therefore, knockdown was evaluated at the RNA level via RT-PCR at 2dpf, following 1.0ng and 1.5ng doses of AMO. I observed knockdown at the higher dose of 1.5ng, which was the same dose zebrafish received prior to behavioural testing. I performed behavioural analysis at 5dpf because zebrafish larvae are at a stage in their development when they exhibit robust locomotor activity. Moreover, they show responsiveness to light, and they are sufficiently developed to enable tracking technology to distinguish between zebrafish and background with higher precision (Colwill and Creton, 2011). Therefore, behavioural testing at an earlier time point may have reduced the accuracy of the tracking software. A recent study investigated the effects of C9ORF72-related dipeptide expression on zebrafish locomotion at 2dpf using a touch-evoked escape response. In this assay, the tail of the embryo is lightly touched with forceps. Healthy embryos responded by swimming away, whilst embryos with motor neuron impairment swam a shorter distance (Swaminathan et al., 2018). Whilst this technique can provide detailed measurements of force in the zebrafish embryos, I did not consider it to be suitable for higher throughput experiments such as my own.

The reduction in motor activity that I observed at 5dpf following knockdown of GLT8D1 RNA (**Figure 4.1**) may suggest a loss-of-function mechanism. Initially, behavioural analysis was performed using ViewPoint software (Scott et al., 2016). Observed anomalies during manual video observation led me to evaluate motor activity using an alternative tracking platform called EthoVision XT (Noldus et al., 2001). Both platforms showed similar trends and degrees of significance (ViewPoint: $p=0.0073$; EthoVision XT: $p=0.0017$) (**Figure 4.2**). This result gave me confidence in the ViewPoint software, which I subsequently used for the behavioural analysis of zebrafish larvae injected with human GLT8D1 mRNA.

4.4.4. Overexpression of mutant human GLT8D1 mRNA produces motor impairment in zebrafish larvae

ALS-linked GLT8D1 mutations are toxic to cells *in vitro* (see section 3.3.5); therefore, I decided to investigate the effects of mutant GLT8D1 in a zebrafish model to place these mutations in the context of motor system function. Microinjection of synthetic capped mRNA leads to global expression throughout the early zebrafish embryo, unlike injection of a zebrafish-compatible expression plasmid, which distributes in a mosaic manner. The use of such plasmids would suggest a limited number of cells in the multicellular embryo would express the protein of interest (Koster and Fraser, 2001).

Overexpression of GLT8D1-G78W and GLT8D1-R92C mRNA in zebrafish larvae did not significantly affect survival, compared to overexpression of GLT8D1-WT mRNA during the first 48 hours of embryogenesis (**Figure 4.5**). To determine overexpression, I evaluated the specificity of a commercially available anti-GLT8D1 antibody following injection with 350pg and 700pg doses of human mRNA encoding GLT8D1-WT and GLT8D1-R92C. I observed stronger protein bands at the expected height of ~42kDa following the higher dose of 700pg mRNA (**Figure 4.4**). Therefore, my immunoblotting is consistent with overexpression of GLT8D1-WT, GLT8D1-G78W, and GLT8D1-R92C at 2dpf (**Figure 4.6a**). The same antibody was unable to detect endogenous GLT8D1 in HEK293 and N2A cells; however, in the context of zebrafish, I have tentatively shown it is able to detect GLT8D1 when overexpressed.

Behavioural tests were conducted at 5dpf, a stage in development when zebrafish larvae use light to independently hunt for food (Clift et al., 2014). My data show that overexpression of GLT8D1-G78W and GLT8D1-R92C correlates with a reduction in the motor activity of zebrafish larvae, compared to overexpression of GLT8D1-WT (GLT8D1-G78W: 23 embryos from one clutch, *t* test, $p=0.0044$; GLT8D1-R92C: 49 embryos from two clutches, *t* test, $p=0.0315$) (**Figure 4.6b, 4.6c**). My focus was to utilise high-throughput behavioural testing to evaluate motor impairment in the zebrafish models; therefore, I did not perform neuropathological analysis. However, the optical transparency of zebrafish larvae makes it possible to visualize the soma and axons of the Mauthner cells, which are a large pair of easily identifiable neurons located in the brainstem of zebrafish. Mauthner cells are activated during escape behaviour (Korn and Faber, 2005), making them a useful tool for measuring neuronal activity during the aforementioned touch-evoked escape response (Swaminathan et al., 2018). These cells can be visualised through confocal imaging of calcium using fluorescent dyes (Feng et al., 2010) as a measure of neuronal activity.

4.4.5. Summary

To investigate whether GLT8D1 mutations are toxic within a whole organism, I overexpressed human mutated and WT GLT8D1 mRNA in zebrafish embryos. At the high dose (700pg), motor function was specifically impaired in zebrafish injected with either the GLT8D1-R92C or GLT8D1-G78W mRNA, compared to injection with GLT8D1-WT mRNA. This is consistent with a specific effect on the motor system. Further supporting a role for GLT8D1 in motor function, knockdown of endogenous *glt8d1* in zebrafish embryos produced a specific deficit of motor function without observable morphological abnormalities. Overlap between the effects of *glt8d1* knockdown and overexpression of mutated GLT8D1 is consistent with a dominant-negative mechanism.

Precedence exists for dominant-negative mutations in other ALS-associated genes, notably *TARDBP* and *OPTN*. Mutant cytoplasmic TDP-43 has been shown to reduce DNA repair through preventing the nuclear translocation of XRCC4-DNA ligase 4. This finding was concurrent with elevated levels of reactive oxygen species, suggesting both dominant-negative and loss-of-function effects of the mutation (Guerrero et al., 2019). Moreover, *OPTN* mutations are inherited in an autosomal recessive manner, and *OPTN* has been demonstrated to cause neurotoxicity through a loss-of-function mechanism. However, in heterozygous mutations with autosomal dominant inheritance, a dominant negative effect may play a role (Maruyama et al., 2010, Sakaguchi et al., 2011, Turner et al., 2013). *OPTN* has been shown to co-localise with inclusion bodies formed through the truncation of TDP-43. This co-localisation was dependent on the ubiquitin-binding domain of *OPTN*. Ubiquitin-binding domain mutants were shown to act as dominant-negative traps through the formation of WT-mutant hybrid complexes, which compromised the maturation of autophagosomes. This subsequently interfered with *OPTN*-mediated autophagy and the clearance of inclusion bodies (Shen et al., 2015).

In summary, my data suggest both GLT8D1 haploinsufficiency and gain-of-function toxicity may contribute to a behavioural phenotype in zebrafish larvae, which is consistent with previous reports on ALS genes *TARDBP*, *C9ORF72*, and *OPTN*. To fully characterise the effect of mutant GLT8D1 in the context of ALS, neuropathological analysis should be performed to assess hallmarks of the disease including degeneration of motor neurons, breakdown of neuromuscular junctions, and muscle atrophy. Finally, future work should aim to generate a stable transgenic zebrafish model using CRISPR/Cas9 genome editing to validate my observed phenotypes, but also to model GLT8D1 in the context of an age-related disorder.

Chapter 5. Membrane ganglioside concentration is dependent on GLT8D1 enzyme activity

5.1. Introduction

Glycosyltransferases function prominently in the biosynthesis of gangliosides, which are sialic acid-containing glycosphingolipids that are expressed ubiquitously, but most prominently on the surface of neuronal cells (Vajn et al., 2013). Therefore, the next stage of this project was to investigate whether an R92C mutation in GLT8D1 affects the expression of gangliosides. I imaged ganglioside expression in isogenic GLT8D1-WT and GLT8D1-R92C cell models using the same isogenic clones described previously (2B1) (see section 3.3.6). Ganglioside expression was assessed in two separate live imaging assays. Initial investigations utilised a Wheat Germ Agglutinin (WGA) Alexa-conjugated molecular probe, which selectively binds to sialic acid and N-Acetylglucosamine (GlcNAc) sugar residues. Gangliosides contain one or more sialic acids in their glyco-chain; therefore, I utilised WGA as an indirect indicator of membrane ganglioside expression. Secondly, a Cholera Toxin Subunit B (CTxB) Alexa-conjugated molecular probe was used to label the monosialoganglioside, GM1, both in the membrane and cytoplasmic regions. Ganglioside GM1 is highly abundant in the nervous system (Vajn et al., 2013) and localises to membrane lipid rafts (MLR). Disrupted MLR are associated with impaired neurotrophic signalling and consequent neurodegeneration (Sawada et al., 2019). Ganglioside expression was also evaluated in GLT8D1-ALS patient fibroblasts. I aimed to replicate my live imaging data in a neuronal model to place my findings in the context of the CNS, by re-programming GLT8D1-ALS patient and control fibroblasts into induced neurons (iNeurons) using a previously established method (Meyer et al., 2014).

GLT8D1 contains an arginine-lysine motif in its cytoplasmic domain, which likely represents a Golgi localisation signal (Uemura et al., 2015). To test for this, I utilised the previously engineered GLT8D1-eGFP constructs (see section 3.3.1) to investigate the intracellular localisation of GLT8D1 in HEK293 and N2A cells via immunocytochemistry, and assessed whether the localisation signal was affected by the presence of GLT8D1 mutations. Glycosyltransferase-mediated Golgi fragmentation has previously been described (Petrosyan and Cheng, 2013); therefore, I investigated whether the presence of an R92C mutation in GLT8D1 causes fragmentation of the network. Importantly, fragmentation of the Golgi is a well-described feature of ALS pathogenesis (Sundaramoorthy et al., 2015).

5.2. Aims and objectives for investigating the effects of an R92C variant in GLT8D1 on ganglioside expression and Golgi fragmentation

1. Confirm tetracycline-inducible expression of GLT8D1 in isogenic HEK293-GLT8D1 cells.
2. Examine the effect of an R92C variant in GLT8D1 on the expression of sialic acid residues and N-Acetylglucosamine in isogenic HEK293-GLT8D1 cell membranes.
3. Test whether the expression of sialic acid residues and N-Acetylglucosamine is reduced in GLT8D1-ALS patient fibroblasts compared to non-ALS controls.
4. Examine the effect of an R92C variant in GLT8D1 on the expression of ganglioside GM1 in membrane and cytoplasmic regions of isogenic HEK293-GLT8D1 cells.
5. Generate a neuronal cell model from GLT8D1-ALS patient and control fibroblasts for the live imaging of ganglioside dynamics.
6. Examine the intracellular localisation of GLT8D1 in neuronal and non-neuronal cell lines via transient transfection.
7. Investigate whether an R92C variant in GLT8D1 causes Golgi fragmentation in isogenic HEK293-GLT8D1 cells.

5.3. Results

5.3.1. An R92C variant in GLT8D1 reduces the expression of sialic acid and N-Acetylglucosamine (GlcNAc) residues in isogenic HEK293-GLT8D1 cell membranes

The following sections of this chapter utilised isogenic HEK293-GLT8D1 cells (see section 3.3.2) to test whether an R92C mutation affects membrane ganglioside expression. Isogenic HEK293-GLT8D1 cells were induced with tetracycline for 24 hours prior to live cell imaging with a WGA Alexa-conjugated molecular probe. The relative expression of WT and mutant GLT8D1 was assessed via immunoblotting for each biological repeat of the live imaging assay. Immunoblotting revealed a ~50% increase in the level of the mutant protein compared to the WT (n=3, *t*-test *p*=0.0197) (**Figure 5.1**). The selection pressure was sufficient to control gene transcription as basal levels of GLT8D1 were not within dynamic range of detectability in the un-induced (tetracycline-free) cells via immunoblotting. Protein bands in the un-induced cohort were only made visible following overexposure of the image (**see appendix 12**). Transcriptional control is important as leakiness (uncontrolled expression of the gene of interest) in the system may alter the cellular biochemistry. I observed a mutation-specific

reduction in the fluorescence intensity of WGA in isogenic HEK293-GLT8D1 plasma membranes across 3 biological repeats of the live imaging assay (n=3, unpaired *t*-test p=0.0145).

In addition, overexpression of WT GLT8D1 modestly enhanced the membrane fluorescence intensity of WGA compared to Sham-transfected control lines. All fluorescence intensity values were plotted as a percentage of cell area and normalised to Sham-transfected controls (**Figure 5.2**). Cells were co-labelled with a CellMask™ plasma membrane stain for accurate quantification of cell area (**see appendix 14**). WGA fluorescence intensity was also measured in the absence of tetracycline, showing a modest but non-significant decline in fluorescence intensity in the mutant line compared to WT (n=3, unpaired *t*-test p>0.05) (**see appendix 13**).

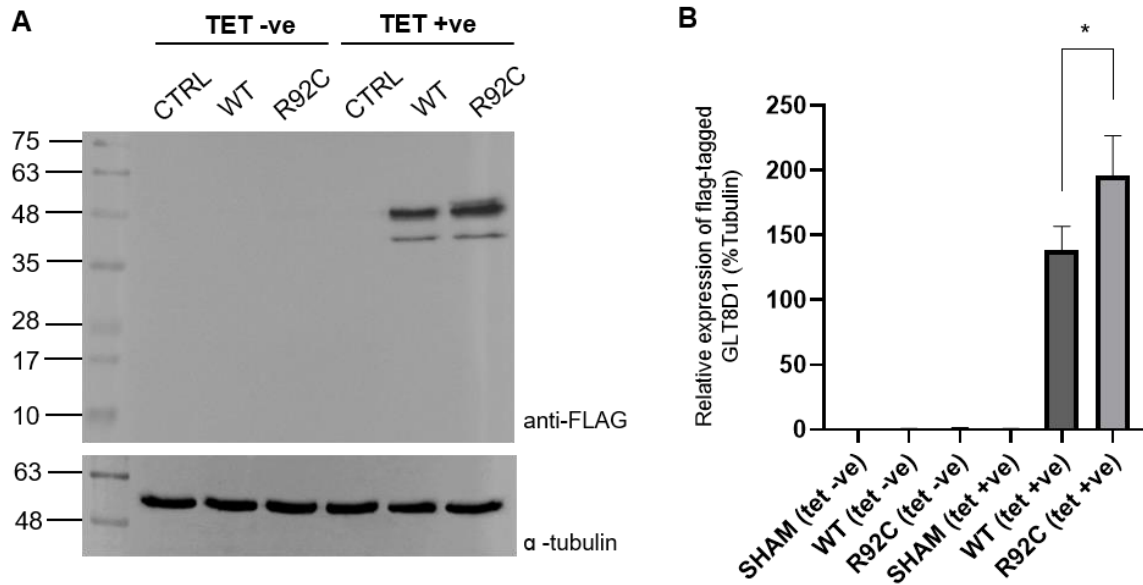


Figure 5.1. GLT8D1-R92C expression is enhanced in isogenic HEK293-GLT8D1 cell lines compared to WT. (A) Representative blot showing tetracycline-induced expression of WT and mutant GLT8D1 in isogenic HEK293-GLT8D1 cells. Relative GLT8D1 expression was detected using an anti-FLAG antibody; α -Tubulin was used as a loading control. Molecular weight markers are indicated (kDa). **(B)** Densitometric analysis shows enhanced levels of GLT8D1_R92C compared to GLT8D1-WT (unpaired *t*-test, $p < 0.05$; $n = 3$). Error bars represent mean \pm SD. (TET – tetracycline; SHAM – sham-transfected; WT – wild-type; -ve – negative; +ve – positive).

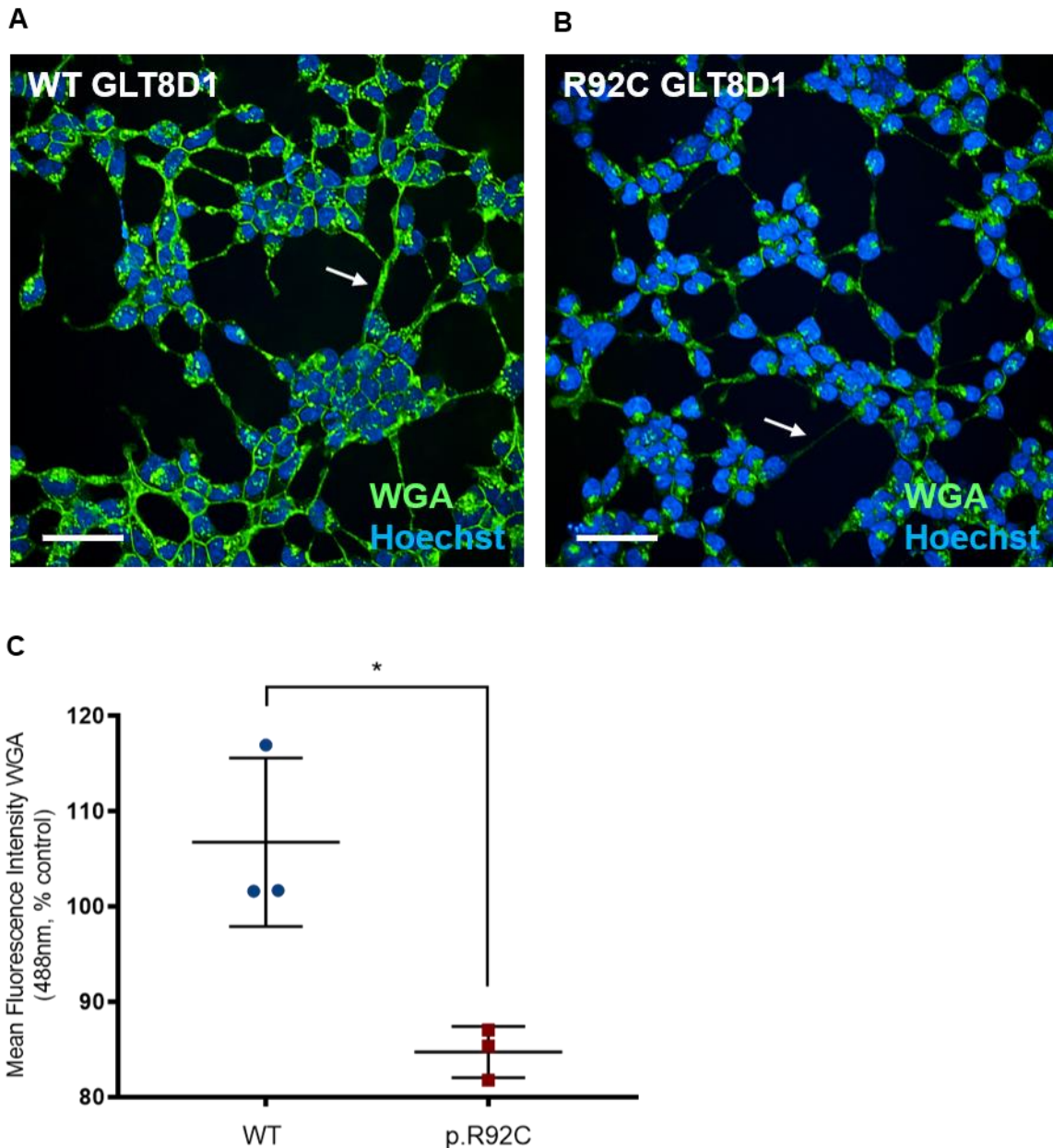


Figure 5.2. ALS-linked R92C mutation in GLT8D1 reduces membrane sialic acid and N-Acetylglucosamine (GlcNAc) expression in isogenic HEK293-GLT8D1 cells. Representative staining of sialic acid residues in isogenic HEK293-GLT8D1 cells overexpressing WT (**A**) and mutant (**B**) GLT8D1. Sialic acids were labelled using a WGA molecular probe (green). Nuclear counterstain (Hoechst 33342) is shown in blue. Scale bar = 50µm. (WT – wild type). (**C**) Fluorescence intensity of sialic acid residues at membrane of isogenic HEK293-GLT8D1 cells (white arrows) is reduced by ~20% when mutant (R92C) GLT8D1 is overexpressed compared to overexpression of WT GLT8D1. Each data point is expressed as a percentage of control (sham-transfected) (n=3, unpaired *t*-test, * *p*<0.05). Error bars represent mean ±SD.

5.3.2. Overexpression of mutant GLT8D1 reduces membrane and cytoplasmic GM1 expression in isogenic HEK293-GLT8D1 cells

Cholera Toxin Subunit B (CTxB) has been used as a neuroanatomical tracer for the retrograde labelling of ganglioside GM1. Specifically, the larger B-subunit of CTxB contains cholera toxin, which binds to the GM1 receptor with high affinity, facilitating entry into the cell via endocytosis (Singh et al., 2003, Iglesias-Bartolome et al., 2009). Isogenic HEK293-GLT8D1 cells were labelled with a CTxB Alexa-conjugated molecular probe for measuring membrane and cytoplasmic GM1 expression. The relative expression of WT and mutant GLT8D1 was assessed via immunoblotting for each biological repeat of the live imaging assay and again, mutant GLT8D1 expression was modestly enhanced compared to WT. I observed a mutation-specific reduction in the relative fluorescence intensity of membrane GM1 in the mutant (R92C) line compared to the WT line across 5 biological repeats of the assay (n=5, paired *t*-test $p=0.0477$). I observed a similar trend in cytoplasmic GM1 expression; however, these were data from 4 biological repeats and did not reach statistical significance (n=4, paired *t*-test $p=0.12$). All fluorescence intensity values were plotted as a percentage of cell area and normalised to Sham-transfected controls (**Figure 5.3**). As previously mentioned, cells were co-labelled with a CellMask™ plasma membrane stain to identify cell regions and for accurate quantification of cell area (**see appendix 14**). The additional biological repeats were performed in order to analyse a similar number of cells to those analysed in the WGA live imaging assay (~30,000 cells).

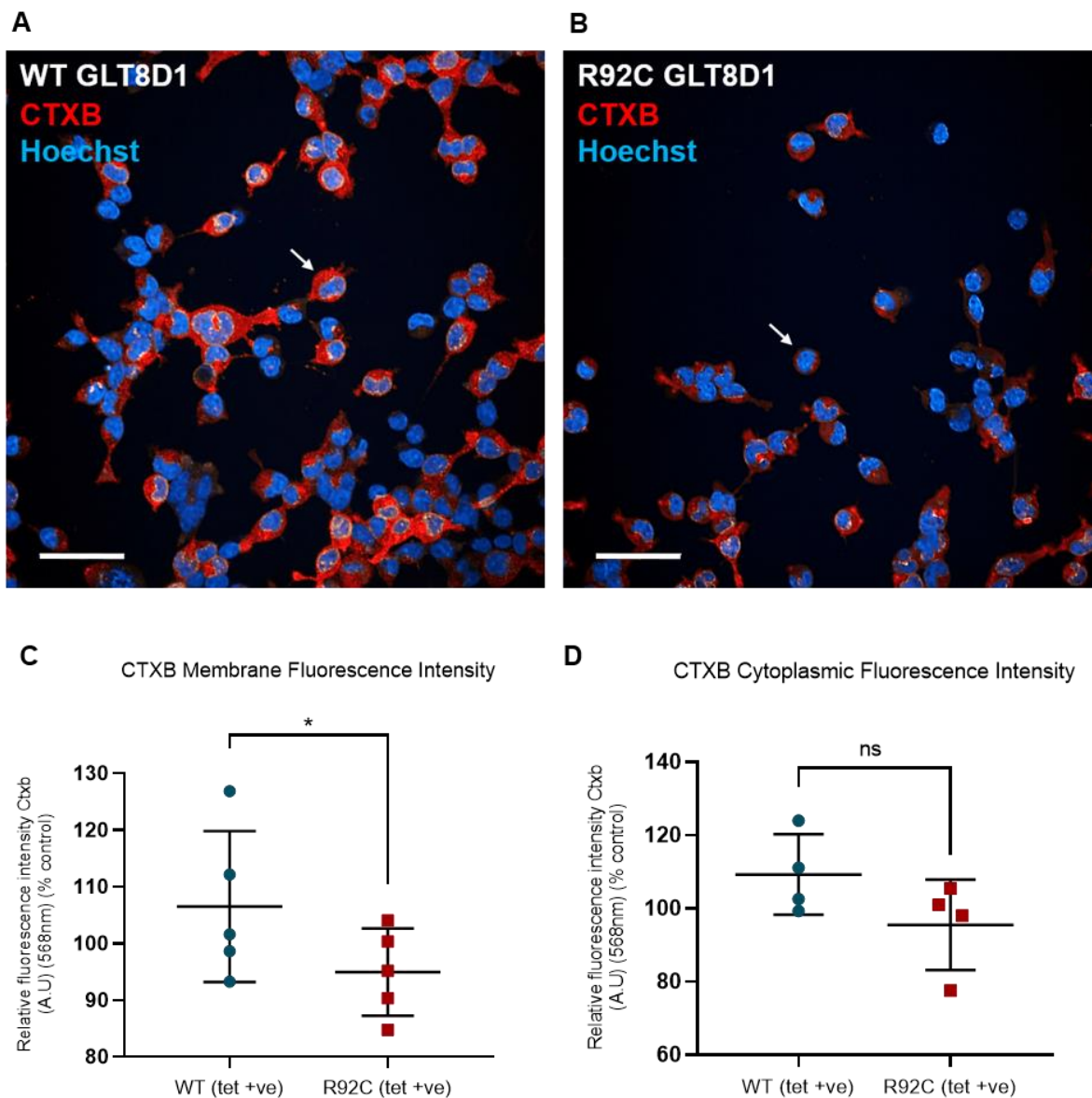


Figure 5.3. ALS-linked R92C mutation reduces membrane GM1 expression in isogenic HEK293-GLT8D1 cells. Representative staining of ganglioside GM1 (white arrows) in (A) WT and (B) mutant cells. GM1 was labelled using a CTxB molecular probe (red). Nuclear counterstain (Hoechst 33342) is shown in blue. Scale bar = 50 μ M. (WT – wild type). (C) Fluorescence intensity of membrane CTxB is reduced in mutant compared to WT (~10% reduction), (D) but unchanged in the cytoplasmic region. Each data point is expressed as a percentage of control (sham-transfected) (n=5, *t*-test, * *p*<0.05). Error bars represent mean \pm SD. (ns – not significant).

5.3.3. *GLT8D1-ALS patient fibroblasts did not successfully re-programme into induced neural progenitor cells*

My next aim was to replicate my live imaging data in a neuronal model to place my findings in the context of the CNS, which is relevant to ALS. This would be achieved by the re-programming of GLT8D1-ALS patient fibroblasts into induced neurons (iNeurons) using a previously established protocol (Meyer et al., 2014). I had only one GLT8D1 patient-derived fibroblast line available, which did not successfully re-programme. The retroviral transduction of fibroblasts did produce cells representative of a pre-iNPC state; however, they immediately reached senescence before fully differentiating into iNPCs. Slowly dividing fibroblasts do not usually re-programme well; therefore, I cultured the fibroblasts in EMEM as opposed to DMEM to test whether their growth rate improved, however this slowed the rate of division further (**Figure 5.4**). In summary, I was unable to generate iNPCs from GLT8D1-ALS patient fibroblasts.

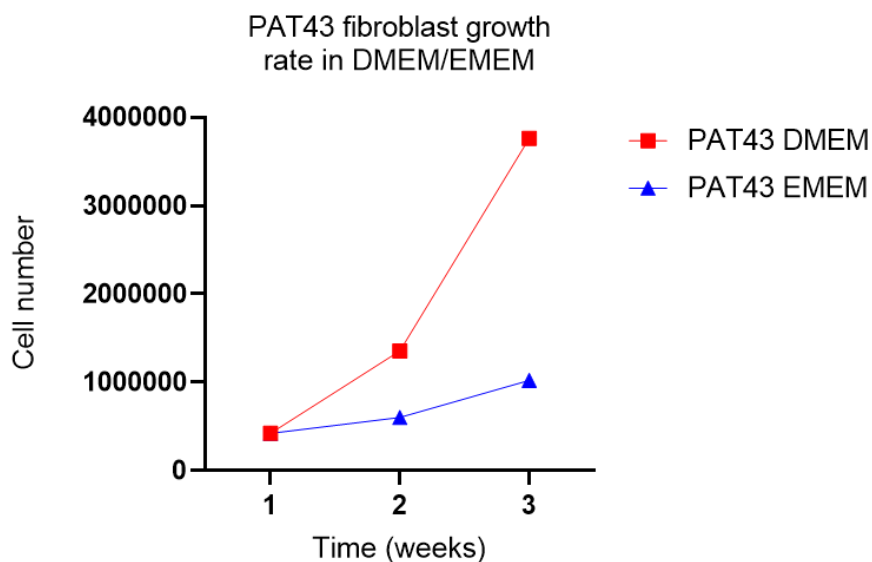


Figure 5.4. Poor growth rate was possibly a key factor preventing the direct conversion of GLT8D1-ALS patient fibroblasts into iNeurons. The growth rate of GLT8D1-ALS patient fibroblasts was evaluated in EMEM and DMEM. Cells were counted once per week over three consecutive weeks to compare the growth rate. Cells were split twice per week and re-seeded at the same density. Cells cultured in EMEM (blue line) displayed a reduction in growth rate compared to those cultured in DMEM (red line). Neither culture media improved the rate of cell division to a level required for successful re-programming. No statistical analysis was performed.

5.3.4. Membrane GlcNAc and sialic acid residue expression is unchanged in GLT8D1-ALS patient fibroblasts compared to an age- and sex-matched control

Due to the inability to generate a patient-derived neuronal model of GLT8D1, I designed tools for the CRISPR-mediated mutagenesis of a single age- and sex-matched control fibroblast line, which had been successfully re-programmed previously. Efforts to introduce the GLT8D1-R92C mutation in these cells were deferred due to the ongoing coronavirus pandemic. Instead, I performed live imaging of sialic acid and N-Acetylglucosamine (GlcNAc) sugar residues using the WGA Alexa-conjugate molecular probe, as previously described, in GLT8D1-ALS patient and control fibroblasts. I did not observe a significant difference in the fluorescence intensity between the two groups, although there was a possible trend towards reduced membrane sialic acid expression in the single patient line (n=3, paired *t*-test $p>0.05$) (**Figure 5.5**).

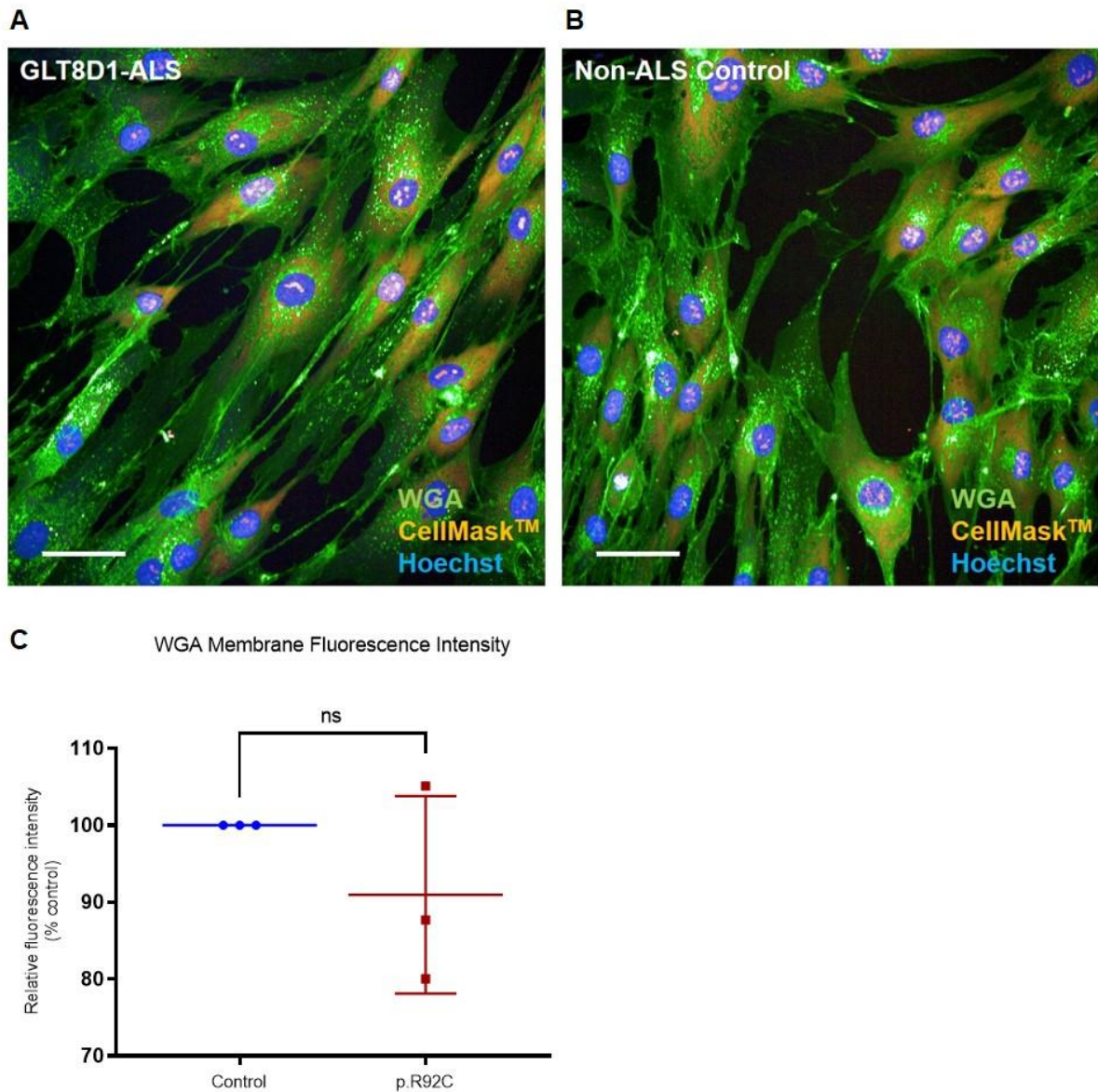


Figure 5.5. Membrane sialic acid and N-Acetylglucosamine (GlcNAc) expression is unchanged in GLT8D1-ALS patient fibroblasts compared to an age- and sex-matched control. Representative staining of sialic acid residues GLT8D1-ALS patient (**A**) and control (**B**) fibroblasts. Sialic acids were labelled using a WGA molecular probe (green). Nuclear counterstain (Hoechst) is shown in blue. Scale bar = 50 μ m. (**C**) Fluorescence intensity of membrane sialic acid residues is unchanged in patient cells compared to controls. Each data point in the patient group is expressed as a percentage of control (n=3, unpaired *t*-test, $p > 0.05$). Error bars represent mean \pm SD.

5.3.5. GLT8D1 is localised to the Golgi network when transiently overexpressed in HEK293 and N2A cells

GLT8D1 is reported to be a type II Golgi glycosyltransferase and contains an arginine-lysine motif in its cytoplasmic domain, which likely represents a Golgi localisation signal (Uemura et al., 2015). To investigate localisation to the Golgi apparatus, neuronal (N2A) and non-neuronal (HEK293) cells were transfected with pEGFP-N1_GLT8D1-eGFP expression vectors (see section 3.3.1). GLT8D1-Golgi localisation was investigated prior to the generation of isogenic HEK293-GLT8D1 cell lines. Cells were fixed and co-stained using JL-8 to label GFP-tagged proteins, and TGN-46 that usually localises to the trans-Golgi network membrane. These antibodies were chosen based on their previously reviewed applications in immunofluorescence microscopy (van Galen et al., 2014, Mukai et al., 2005). Initial imaging was performed using a Nikon Eclipse Ni-U microscope and this revealed possible localisation between GLT8D1 and the Golgi network in N2A cells (**Figure 5.6a, 5.6b**). This signal was subsequently confirmed in HEK293 and N2A cells using confocal microscopy (**Figure 5.6c, 5.6d**) to look at defined focal planes and eliminate out-of-focus signals to improve reliability (Nichols and Evans, 2011). The images shown (**Figure 5.6**) were acquired following transfection with a pEGFP-N1_GLT8D1-WT plasmid. The presence of an R92C mutation (as well as the G78W mutation presented in Chapter 3) in GLT8D1 did not affect the localisation signal (**see appendix 15**).

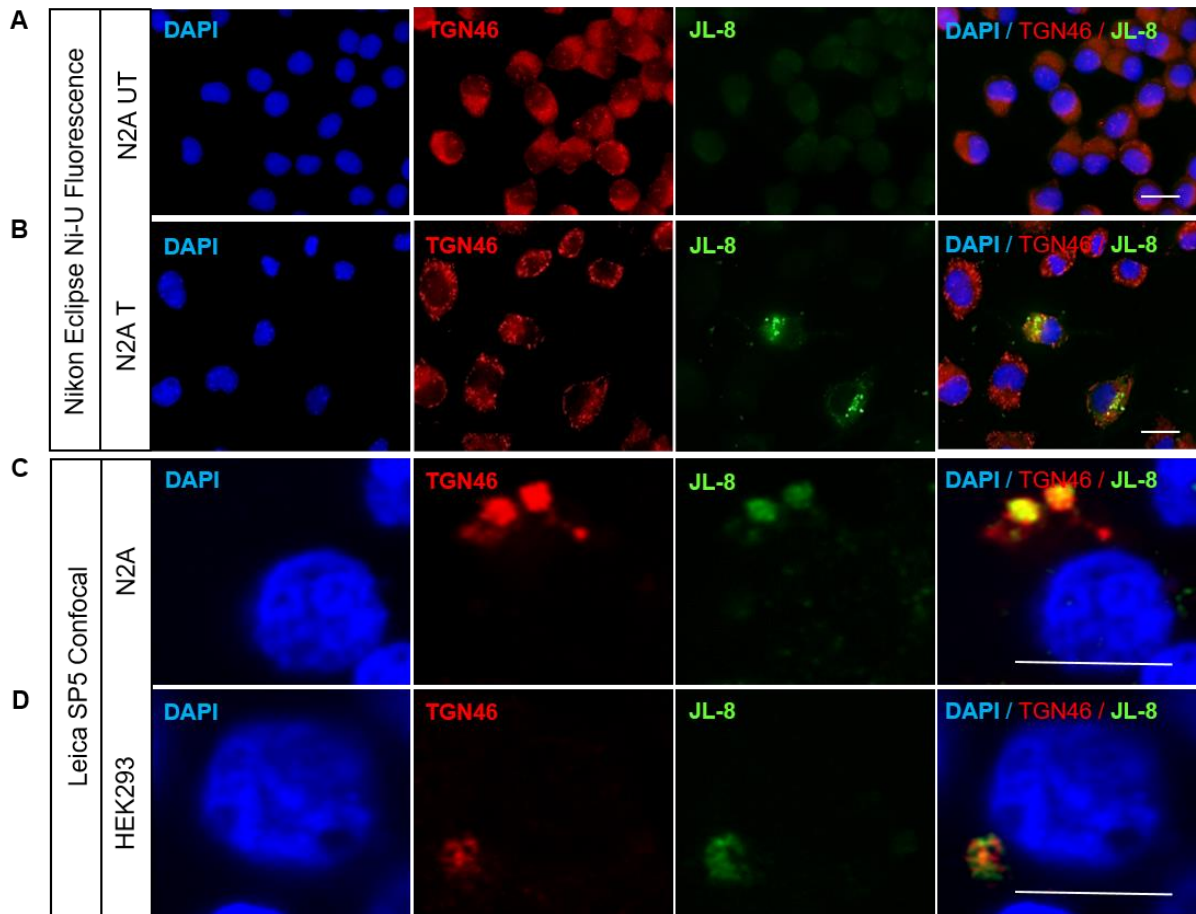


Figure 5.6. When transiently over-expressed in HEK293 and N2A cells, GLT8D1 is localised to the Golgi network. (A, B) The intracellular localisation of GLT8D1 was initially investigated in N2A cells via multiphoton fluorescence microscopy (top panel), and (C, D) subsequently confirmed in HEK293 and N2A cells using confocal microscopy (bottom panel). In both instances, the Golgi network was imaged using anti-TGN46 (red); GLT8D1-GFP fusion protein was imaged using JL8 (green). Nuclear counterstain (DAPI) is shown in blue. Scale bars are 50µM. (UT – un-transfected; T – transfected). Figure adapted from (Cooper-Knock et al., 2019).

5.3.6. Overexpression of an R92C variant in GLT8D1 causes fragmentation of the Golgi network in isogenic HEK293-GLT8D1 cells

Fragmentation of the Golgi network is a well-documented molecular consequence of ALS pathophysiology, yet the underlying mechanism remains unclear. Golgi fragmentation may result from inhibition of vesicular trafficking between the ER and Golgi, or from the Golgi to the plasma membrane (Sundaramoorthy et al., 2015). I have shown that GLT8D1 is localised to the Golgi network in neuronal and non-neuronal cell lines, and that the presence of either a G78W or an R92C mutation does not affect this localisation signal (see section 5.3.5). Glycosyltransferases are an essential component of the Golgi trafficking machinery (Martina et al., 2000); therefore, I hypothesise that mutant GLT8D1 may disrupt this trafficking, leading to fragmentation of the network.

I investigated Golgi fragmentation in isogenic HEK293-GLT8D1 cells using two antibodies that target different regions of the network: TGN46 that localises to the trans-Golgi, and GM130 that localises to the cis-Golgi. My preliminary data suggest enhanced fragmentation of both the trans- and cis-Golgi networks in isogenic HEK293-GLT8D1 cells overexpressing an R92C mutation compared to WT (**Figures 5.7, 5.8**). Overexpression of GLT8D1-WT caused a modest increase in Golgi fragmentation compared to sham-transfected control cells, but this was more profound following overexpression of GLT8D1-R92C. Overexpressing any WT gene can cause a mutant phenotype (Prelich, 2012) and my data are consistent with a mutation-specific effect. Due to the ongoing coronavirus pandemic, only two biological repeats of the Golgi fragmentation analysis were performed; therefore, the data presented here do not contain any statistical analysis. ~2000 cells were analysed for each condition per biological repeat.

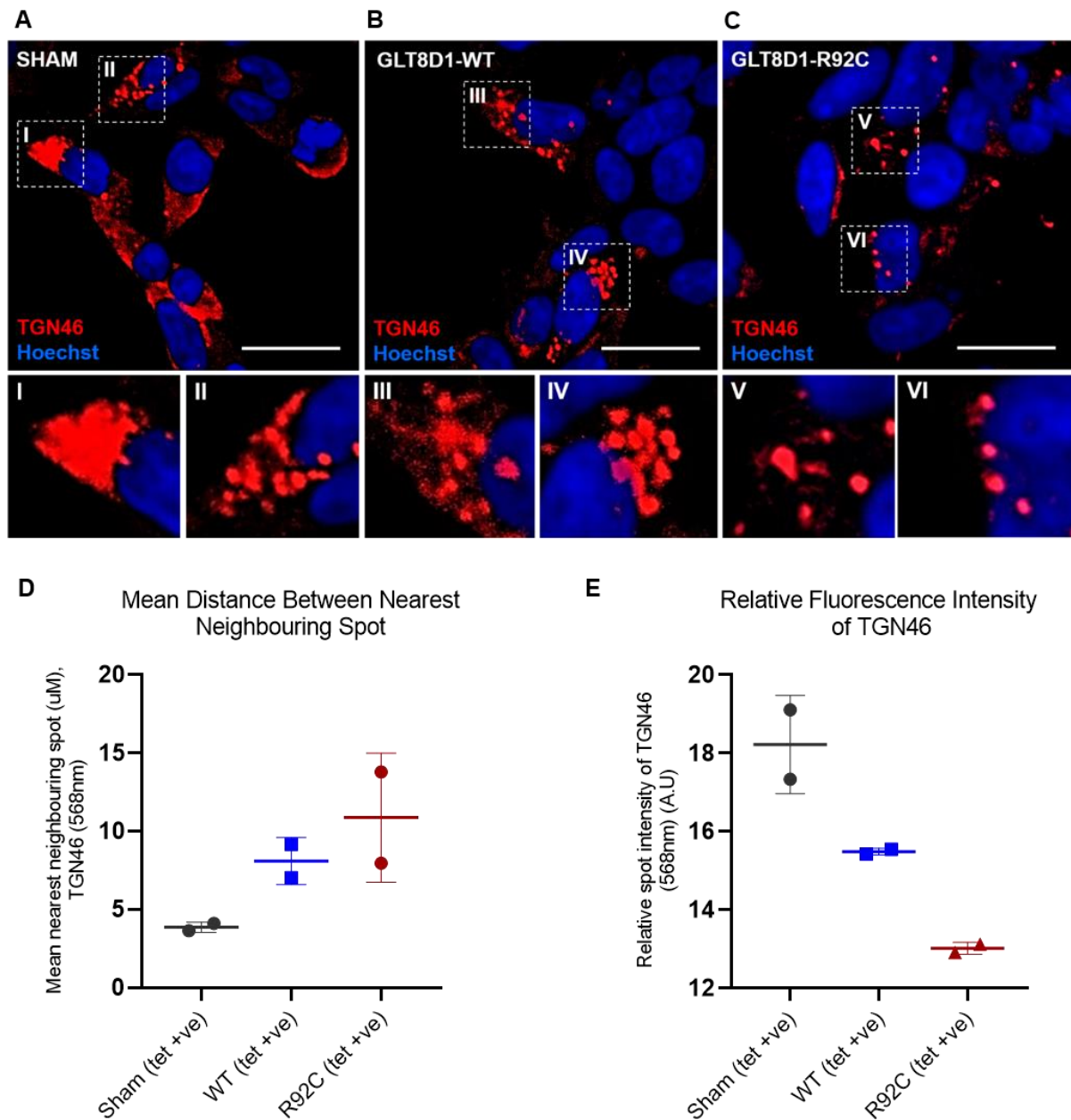


Figure 5.7. Preliminary data suggest that overexpression of GLT8D1-R92C causes fragmentation of the trans-Golgi network in isogenic HEK293 cells. Representative staining of the trans-Golgi network using a TGN46 antibody (red) in (A) HEK293-SHAM, (B) HEK293-GLT8D1-WT, and (C) HEK293-GLT8D1-R92C isogenic cell lines. The image segments outlined with a white box (upper) are magnified to delineate Golgi morphology (bottom). (D) The distance between the nearest neighbouring spot (μM) was measured for each condition. (E) Corrected spot intensity (568nm) was plotted for each condition. Each data point represents a technical repeat. Nuclear counterstain (Hoechst 33342) is shown in blue. Scale bar is $50\mu\text{M}$. (No statistical analysis was performed; $n=2$).

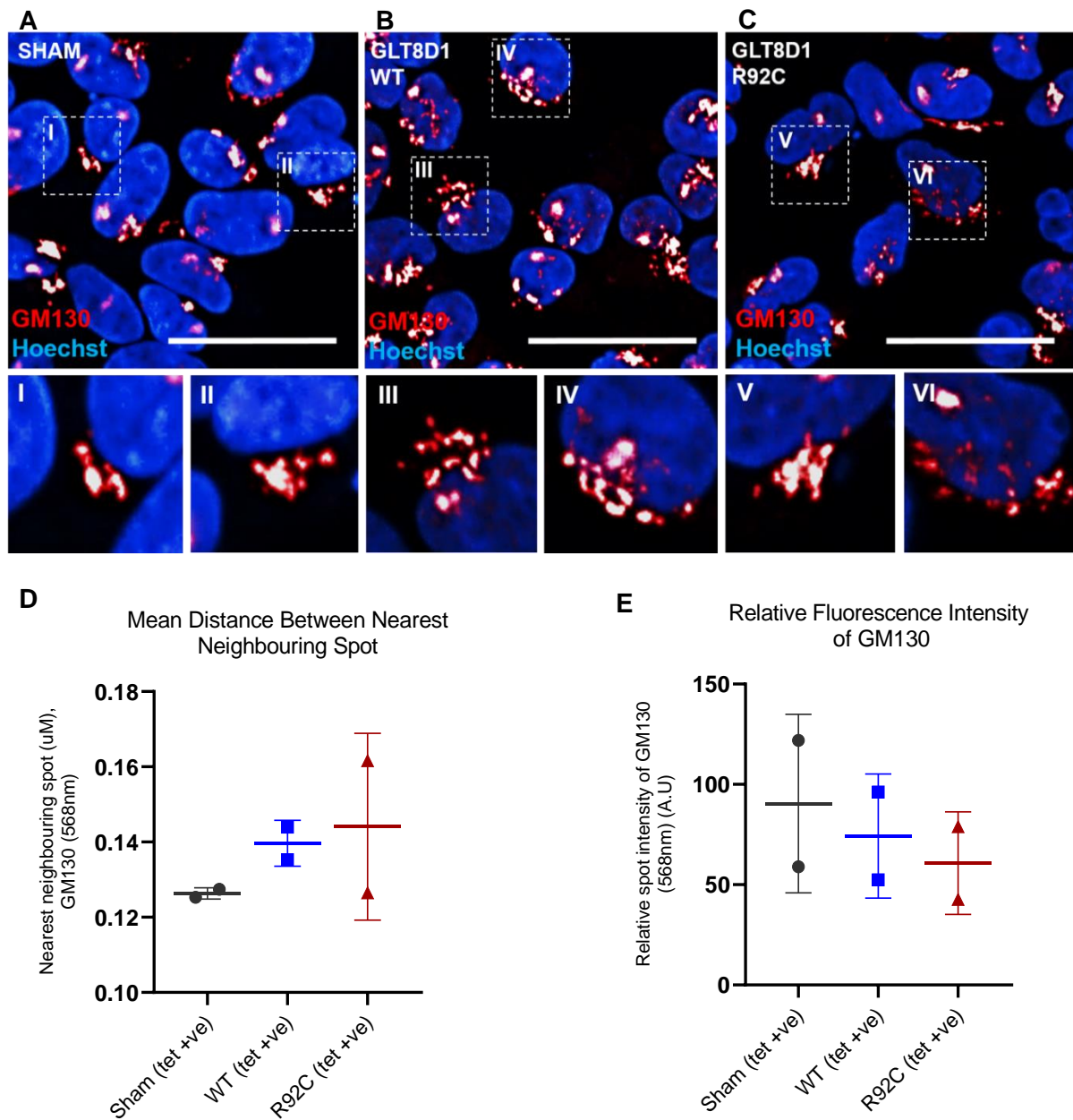


Figure 5.8. Preliminary data suggest that overexpression of GLT8D1-R92C causes fragmentation of the cis-Golgi network in isogenic HEK293 cells. Representative staining of the cis-Golgi network using a GM130 antibody (red) in (A) HEK293-SHAM, (B) HEK293-GLT8D1-WT, and (C) HEK293-GLT8D1-R92C isogenic cell lines. The image segments outlined with a white box (upper) are magnified to delineate Golgi morphology (bottom). (D) The distance between the nearest neighbouring spot (μM) was measured for each condition. (E) Corrected spot intensity (568nm) was plotted for each condition. Each data point represents a technical repeat. Nuclear counterstain (Hoechst 33342) is shown in blue. Scale bar is $50\mu\text{M}$. (No statistical analysis was performed; $n=2$).

5.4. Discussion

The overarching aim of the work described in this chapter was to place GLT8D1 mutations in the context of an ALS disease pathway. As discussed in the introductory chapter, two distinct glycosyltransferase-associated mechanisms are prominent in neurodegenerative disorders: ganglioside synthesis and O-GlcNAcylation (Moll et al., 2020). I focused on the dysregulation of ganglioside biosynthesis, as this pathway encompasses a broader range of glycosyltransferase enzymes compared to O-GlcNAcylation, which is a well-characterised post-translational modification mechanism involving glycosyltransferases OGT and EOGT (Yang and Qian, 2017). To place GLT8D1 mutations in the context of an ALS disease pathway, live imaging of gangliosides was performed in isogenic HEK293 cell lines overexpressing WT and mutant GLT8D1. To replicate my findings into a neuronal model, I attempted to re-programme GLT8D1-ALS patient fibroblasts into induced neurons (iNeurons) using a previously established method (Meyer et al., 2014). Ganglioside biosynthesis occurs predominantly in the Golgi network (Maccioni et al., 2011); therefore, I investigated whether GLT8D1 localises to the Golgi in HEK293 and N2A cells. I subsequently investigated glycosyltransferase-mediated Golgi fragmentation in isogenic HEK293-GLT8D1 lines as a potential mechanism for perturbed ganglioside biosynthesis.

5.4.1. An R92C variant in GLT8D1 reduces the expression of sialic acid and N-Acetylglucosamine (GlcNAc) residues in isogenic HEK293 cell membranes

Isogenic HEK293-GLT8D1 cells were used to characterise the early biochemical effects of the R92C variant in GLT8D1 through live cell imaging. In order to determine whether these early effects were mutation-specific and not due to enhanced levels of the mutant protein, immunoblotting was used to evaluate the relative expression of WT and mutant GLT8D1. Immunoblotting revealed that mutant GLT8D1 was expressed at a higher level than the WT, which may present a significant limitation. It might suggest that observed effects are due to enhanced expression of the mutant protein compared to WT (~50% increase). The double band in the mutant blot likely represents post-translational modification of GLT8D1 (**Figure 5.1**). Post-translational modifications are essential to the regulation of protein folding, their interaction with ligands and, in the case of enzymes, their catalytic activity. Common forms of post-translational modifications are phosphorylation and glycosylation (see Chapter 1), both of which are essential for regulating the activity of enzymes. I have previously shown that a GLT8D1-R92C mutation reduces enzymatic activity, which was expected given that the

mutation is proximal to the substrate binding site (Cooper-Knock et al., 2019) (see Chapter 3). Therefore, it is possible that the GLT8D1-R92C protein is not undergoing the necessary phosphorylation or glycosylation required for proper enzymatic function, which may also cause protein misfolding, hence the observed double band in the blot. In the future, I plan to test for post-translational modification by treating the GLT8D1-R92C cell lysates with enzymes prior to immunoblotting. Such enzymes include alkaline phosphatase to remove phosphates (Seo and Lee, 2004), or PNGase F to remove N-linked oligosaccharides (Suzuki et al., 1995). Furthermore, my immunoblotting shows that selection pressure was maintained to a high standard, suggesting a limited effect on the cellular biochemistry, which was consistent between all isogenic HEK293-GLT8D1 cell lines prior to performing the live imaging assays.

Lectins are carbohydrate- and glycoconjugate-binding proteins that are widely distributed throughout nature, whose primary function is to facilitate cell-to-cell contact. In vertebrates, there are two main classes of lectins: integral lectins of membranes, and soluble lectins present in intra and intercellular fluids. Lectins have a plethora of roles in animals including endocytosis, intracellular translocation of glycoproteins (Yamashita et al., 1999), glycoconjugate binding, apoptotic processes (Kilpatrick, 2002), defence mechanisms against microorganisms, as well as regulating the processes of cell adhesion and migration. In vertebrates, integral lectins facilitate the binding of glycoconjugates to cell membranes or vesicles, resulting in endocytosis or intracellular translocation (Sharon and Lis, 2004). WGA is a widely used lectin that binds specifically to *N*-acetyl-D-glucosamine and *N*-acetylneuraminic acid (sialic acid) residues, both of which are ubiquitously expressed in neuronal cell membranes. WGA has also been demonstrated to interact with sialic acid residues on glyconjugates and oligosaccharides (Iqbal et al., 2019). The neuronal specificity of WGA makes it a useful tracer for the tracking of neural connections in all regions of the brain (Yoshihara, 2002).

In the present study, WGA provided an indirect measure of plasma membrane integrity of isogenic HEK293 cells overexpressing WT and mutant GLT8D1. Membrane WGA expression was significantly reduced through overexpression of mutant GLT8D1 compared to WT, indicating a mutation-specific effect on the integrity of the plasma membrane (**Figure 5.2**). This was expected given that I previously observed enhanced levels of LDH in the culture media of cells transfected with GLT8D1-R92C plasmids compared to WT, which was indicative of reduced plasma membrane integrity (see section 3.3.6). It would be important to confirm this result via immunoblotting. These results suggest that an R92C mutation may alter the glycosylation profile of isogenic HEK293-GLT8D1 cells. However, to fully answer this question, lectin blotting could be used for the proteomic analysis of glycosylation patterns

within whole cell extracts (Cao et al., 2013) following overexpression of WT and mutant GLT8D1. Future work could utilise a panel of lectins including Maackia amurensis II and Sambucus nigra, both of which interact with N-Acetylneuraminic acid, the most prominently expressed sialic acid in mammalian cells (Wang and Brand-Miller, 2003).

WGA may also provide an indirect measure of membrane ganglioside expression, as gangliosides contain a variable number of negatively charged sialic acid residues (Frey and Lee, 2013). However, to my knowledge, WGA has not previously been used as a ganglioside marker. Assuming the role of WGA as an indirect marker for ganglioside expression, I subsequently tested whether expression levels of ganglioside GM1 were affected in a similar way. GM1 was chosen based on its association with membrane lipid rafts, which are key determinants of neurotrophic signalling (see section 5.4.2). Moreover, this ganglioside is essential to maintaining neuronal function to prevent neurodegeneration (Chiricozzi et al., 2020) and is strongly associated with neurodegenerative disorders (see Chapter 1).

5.4.2. Overexpression of mutant GLT8D1 reduces membrane and cytoplasmic GM1 expression in isogenic HEK293 cells

Whilst ALS is not considered an autoimmune disorder, immunological phenomena are suggested to be involved. Over the past few decades, numerous studies have described the detection of antibodies against a variety of gangliosides in ALS patients, but with widely differing frequencies and titres (Pestronk et al., 1989, Lamb and Patten, 1991, Yuki et al., 2014). As previously mentioned, it is noteworthy that autoantibodies against specific gangliosides produce an inflammatory disease of spinal motor neurons known as multifocal motor neuropathy with conduction block (Harschnitz et al., 2014), which is an important differential diagnosis for ALS (Cooper-Knock et al., 2019). However, a more recent study reported no statistically significant difference in the frequency of anti-ganglioside antibodies in ALS patients compared to controls (Kollewe et al., 2015). Although the role of anti-ganglioside antibodies in ALS is a controversial topic of debate, altered levels of gangliosides are widely reported in animal models of ALS and in post-mortem CNS tissue from ALS patients (Dodge et al., 2015, Ariga, 2014).

Ganglioside GM1 is highly abundant in the nervous system and is localised to MLR, which are membrane micro-domains enriched in cholesterol and sphingolipids, with important roles in

cell signalling (Vajn et al., 2013). GM1 is internalised via caveolae, which are a type of lipid raft domain in the plasma membrane (Crespo et al., 2008). Gangliosides, particularly GM1, are shown to be responsible for the trafficking and maintenance of these caveolae domains (Singh et al., 2010). The association of GM1 with MLR makes this ganglioside a useful target for measuring lipid raft integrity. Disrupted MLR are associated with impaired neurotrophic signalling and consequent neurodegeneration (Sawada et al., 2019). Cholera toxin is a protein enterotoxin that belongs to the family of AB5 toxins and is capable of binding up to five molecules of GM1 at a time via its B-subunits. The CTxB-GM1 complex undergoes retrograde trafficking from the plasma membrane to the trans-Golgi network. It is then transported through the Golgi and delivered to the ER (Fujinaga et al., 2003). Once in the ER, the A-subunit dissociates from the B-subunit, unfolding the toxin and enabling retro-translocation to the cytosol to induce disease (Chinnapen et al., 2007). The CTxB molecular probe utilised in my study was completely free of the toxic A-subunit.

In the present study, I observed a mutation-specific reduction in the fluorescence intensity of CTxB in the membrane of isogenic HEK293-GLT8D1 cells (**Figure 5.3**). Given the aforementioned role of ganglioside GM1 in the intracellular trafficking of cholera toxin, I also measured the relative expression of CTxB in cytoplasmic cell regions. Whilst a similar trend in fluorescence intensity was apparent, I did not observe a significant mutation-specific effect. I was unaware of the mechanisms regarding the internalisation of CTxB when performing the initial live imaging assay, hence the fewer biological repeats in cytoplasmic staining compared to membrane staining.

CTxB and WGA have previously been used as probes for gangliosides GM1 and GM3, respectively; however, they have been shown to form cross-links with gangliosides, thus modifying ganglioside distribution and behaviour in the plasma membrane (Hammond et al., 2005, Lingwood et al., 2008, Kaiser et al., 2009). Moreover, the specificity of these probes is under debate. A study using mouse embryonic neuroepithelial cells found that GM1 levels were barely detectable through thin-layer chromatography and immunoblotting. However, flow cytometry revealed that 80% of these cells were CTxB positive, indicating that the high affinity interaction between CTxB and GM1 in these cells may overestimate GM1 expression (Yanagisawa et al., 2006). Therefore, biochemical analysis such as immunoblotting should be performed in conjunction with CTxB cell staining to avoid mischaracterisation of the ganglioside species. This perhaps is not a limitation of my study, as I compared relative GM1 levels rather than attempting to quantify GM1 expression exactly. My data indicate that GM1 is expressed in HEK293 cells, which is inconsistent with a previous report that used high-performance thin layer chromatography and indirect immunofluorescence to conclude that

GM1 is not expressed in this cell line (Cho, 2010). However, more recent studies using similar CTxB molecular probes have shown GM1 to be expressed in HEK293 cells (Sano et al., 2014, Fernandez-Perez et al., 2017), supporting the validity of my data. Recently, fluorescent analogues of GM1 and GM3, which were shown to behave similarly to their native counterparts, were synthesised to measure the dynamic behaviour of these gangliosides in living cells (Komura et al., 2016). Future use of these fluorescent analogues may enable more sensitive studies into the effect of ALS-linked GLT8D1 mutations on ganglioside trafficking.

5.4.3. GLT8D1-ALS patient fibroblasts did not successfully re-programme into induced neural progenitor cells

The next aim of my project was to replicate live cell imaging data in a neuronal model to place my findings in the context of the CNS. Induced neurons (iNeurons) can be generated from the direct re-programming of human fibroblasts. Examples include the work of Deng and colleagues who transformed somatic fibroblasts into a chemically induced intermediate XEN-like state (a state that resembles extra-embryonic endoderm), bypassing the pluripotent stage (Li et al., 2017). This is a new and relatively untested re-programming method with narrow concentration windows and specific application durations required for small molecules to be effective. Therefore, I did not explore this method, but rather utilised methods previously developed by a member of our lab (Meyer et al., 2014).

iNeuron technology can provide a fast and simple method for the generation of specific neuronal subtypes. Moreover, this technology may circumvent problems such as uncontrolled cell differentiation and tumour formation, which are associated with human induced pluripotent stem cells (hiPSCs) (Li et al., 2017). I had fibroblasts available from a single ALS patient with an R92C mutation; however, attempts to generate a patient-derived neuronal model were unsuccessful. Following retroviral transduction, a small proportion of cells successfully converted to a pre-iNPC state, but their growth rate soon declined and they reached relatively premature senescence. I was therefore unable to generate a pure population of cells resembling an iNPC lineage. When cultured in DMEM, the GLT8D1-ALS patient fibroblasts demonstrated a relatively slow rate of cell division for cells of this type, which usually suggests that they will not re-programme well. Almost all fibroblasts grow more quickly in DMEM, as this media contains almost twice the concentration of amino acids and four times the amount of vitamins as EMEM. By example, the amino acid arginine has been shown to enhance fibroblast proliferation and reduce apoptosis *in vitro* (Fujiwara et al., 2014). However, some

fibroblasts do exhibit a higher growth rate in EMEM, possibly due to the metabolic signature of the cells. Therefore, I tested the growth rate of the fibroblasts in DMEM vs EMEM over a period of three consecutive weeks, hypothesising that if the growth rate improved, they may re-programme successfully. Unfortunately, the growth rate declined further in EMEM (**Figure 5.4**). It is possible that the R92C mutation is driving metabolic dysfunction; therefore, it would be interesting to investigate defective energy metabolism in this fibroblast line (Zhang et al., 2012).

Ageing is a leading risk factor for the development of neurodegenerative diseases such as ALS (Niccoli et al., 2017). It is important to recapitulate age-related characteristics by using motor neurons at relevant ages. Directly converted motor neurons have the advantage of preserving ageing-associated features from fibroblast donors, such as extensive DNA damage, loss of heterochromatin, and nuclear organization. An alternative method of generating motor neurons is via a pluripotent stem cell lineage, which resets the ageing phenotype (Tang et al., 2017). Therefore, directly reprogrammed motor neurons may be more suitable for modelling the late-onset pathogenesis of diseases such as ALS. Moreover, iAstrocytes derived from the direct conversion of ALS patient fibroblasts are selectively toxic to motor neurons (Haidet-Phillips et al., 2011, Meyer et al., 2014). This astrocyte-mediated motor neuron toxicity is lost when using the iPSC model. Due to these complications, I was unable to investigate whether iAstrocytes carrying a GLT8D1 mutation are selectively toxic to motor neurons. I do, however, have an age- and sex-matched control fibroblast line available, which has successfully been re-programmed into iNPCs previously. Fibroblasts were not available from additional patients with GLT8D1-ALS. I have additional fibroblasts from an individual with an R92C mutation; however, this patient has not been diagnosed with ALS, therefore was not included for experimentation. Future work will aim to utilise CRISPR/Cas9 genome editing to introduce the R92C mutation into the single age- and sex-matched control fibroblast line. I have designed gRNAs to target regions proximal to the R92C mutation, but experiments were postponed due to the ongoing coronavirus pandemic.

5.4.4. Membrane GlcNAc and sialic acid residue expression is unchanged in GLT8D1-ALS patient fibroblasts compared to an age- and sex-matched control

Due to the inability to directly convert GLT8D1-ALS patient fibroblasts into iNeurons, I decided to investigate sialic acid expression in the fibroblasts and compare with age- and sex-matched controls to place my findings in the context of the patients. Whilst I did observe a trend towards decreased sialic acid expression in the patient line, this experiment was limited by the lack of

available age- and sex-matched controls (**Figure 5.5**). Future experiments should include fibroblasts from at least three non-ALS controls, as well as from patients with mutations in other known ALS genes.

Following on from my unsuccessful attempts to generate an iNeuron model, I attempted overexpressing WT and mutant GLT8D1 in mouse primary cortical neurons via nucleofection using a Lonza 4D Nucleofector™ System. The aim of this experiment was to test whether ALS-linked GLT8D1 mutations impair neurotrophic signalling via the disruption of MLR in the context of the CNS. Unfortunately, the neurons did not survive the transfection process and subsequently failed to adhere or develop neurites. For future work, the manufacturer recommends a recovery step immediately after nucleofection, if the observed mortality rate is high. This requires adding pre-equilibrated recovery medium to the cuvette (as opposed to the standard culture media), followed by a 5-10-minute incubation at 37°C, 5% CO₂ prior to seeding (Amaxa™ 4D-Nucleofector™ Protocol for Primary Mammalian Neurons). I chose to use primary neurons because they are not tumour-derived, and therefore more accurately recapitulate the properties of neuronal cells *in vivo* (Gordon et al., 2013). I planned to confirm overexpression of mutant and WT GLT8D1 via immunoblotting, and assess the integrity of MLR using the live imaging techniques previously described in this chapter. I then planned to measure neurotrophic signalling by initially treating the neurons with neurotrophic factors such as BDNF, followed by an expression profile analysis of neurotrophin-mediated signalling targets including: P-TrkB, P-Akt, and P-ERK1/2 (Head et al., 2011). This would identify whether mutant GLT8D1 alters the expression of key receptors required for neurotrophic signalling, which may help to identify pathological mechanisms linking GLT8D1 mutations to the loss of motor neurons in ALS.

5.4.5. GLT8D1 is localised to the Golgi network when overexpressed in HEK293 and N2A cells

I observed localisation of GLT8D1 to the Golgi network in HEK293 and N2A cells (**Figure 5.6**); the presence of G78W and R92C mutations in GLT8D1 did not affect the observed localisation signal (**see appendix 15**). This suggests that the G78W and R92C mutation sites are not necessary for Golgi retention, which was expected given that the mutations are not localised to the cytoplasmic domain that contains the arginine-lysine motif representative of a Golgi localisation signal (Uemura et al., 2015) (**Figure 1.4**). Attempts to investigate GLT8D1-Golgi localisation via live-cell imaging were unsuccessful due to an undetectable eGFP signal. A

limitation of GFP is that it may lose its fluorescence during fixation (Swenson et al., 2007), hence the need for the JL-8 antibody. As previously discussed, GFP-tagging at either the N- or C-terminal domain can influence co-localisation (see section 3.4.1). Therefore, it is important to check the localisation of the endogenous protein with an antibody directed against the protein of interest. However, none of the available GLT8D1 antibodies demonstrated specificity *in vitro* (see appendix 16). Understanding protein subcellular localisation is essential to investigating protein function, cellular organisation, and identifying new disease pathways. For example, in the case of GLT8D1, the mutated forms of the protein may lead to dysfunction and/or fragmentation of the Golgi network, which is already proposed to be an early event in ALS (Sundaramoorthy et al., 2015, Gonatas et al., 1992). Golgi fragmentation was subsequently investigated as a potential GLT8D1-linked ALS pathogenic mechanism and is discussed in the following section.

5.4.6. Overexpression of an R92C variant in GLT8D1 may cause fragmentation of the Golgi network in HEK293 cells

The Golgi is an essential membrane-bound organelle that functions as a protein modification centre in the secretory pathway. It is comprised of three functional compartments: the cis-Golgi, which receives newly synthesised proteins and lipids from the ER; the medial-Golgi, which is the site of post-translational modification; and the trans-Golgi, which dispatches proteins and lipids to distinct subcellular destinations (Marsh and Howell, 2002, Brandizzi and Barlowe, 2013). Ganglioside biosynthesis is compartmentalised in the Golgi network, and is organised in distinct units formed by associations of particular glycosyltransferases, which concentrate in different Golgi sub-compartments (Petrosyan et al., 2012). The cytoplasmic tail of glycosyltransferases determines Golgi localisation (Uliana et al., 2006, Ali et al., 2012). These cytoplasmic tails also bind to the cytoskeleton to stabilise the Golgi (Yamaguchi and Fukuda, 1995, Wassler et al., 2001). Studies have shown that glycosyltransferases are involved in the maintenance of the Golgi architecture. For example, a mutation of the membrane-spanning domain of *N*-acetylglucosaminyltransferase was shown to cause a loss of Golgi structure in HeLa cells (Nilsson et al., 1996). More recently, a high abundance of glycosyltransferases in the Golgi was shown to positively correlate with fragmentation of this organelle (Petrosyan and Cheng, 2013). The evidence for glycosyltransferase-mediated Golgi fragmentation, concurrent with the pathogenic role of Golgi fragmentation in ALS, formed the basis of my investigation.

Golgi pathology is a feature of neurodegenerative disorders such as Alzheimer's (Sun et al., 2008), Parkinson's (Fujita et al., 2006), and ALS (Sundaramoorthy et al., 2015). Importantly, Golgi fragmentation has been shown to occur early in the disease stage prior to apoptosis (Gosavi et al., 2002, Liazoghli et al., 2005, Atkin et al., 2014, van Dis et al., 2014), suggesting that fragmentation of the network could be a trigger for neurodegeneration rather than a consequence of the disease. Golgi fragmentation was first identified in ALS-patient motor neurons in 1992, appearing as disconnected punctate structures (Gonatas et al., 1992). Since then, Golgi fragmentation has been identified in up to 70% of fALS patient motor neurons (Fujita et al., 2000, Ito et al., 2011) and 10-50% of sALS patient motor neurons (Gonatas et al., 2006, van Dis et al., 2014) bearing SOD1, FUS or OPTN mutations. Larger human motor neurons of the cerebral cortex and anterior horn appear to undergo more prominent Golgi fragmentation (Fujita et al., 1999, Fujita et al., 2000). Precedent exists for a link between the cytoplasmic mislocalisation of TDP-43 and Golgi fragmentation (Fujita et al., 2008). Indeed, Golgi fragmentation has been observed in the transgenic rats expressing mutant TDP-43^{M337V} (Tong et al., 2012), as well as in the SOD1^{G93A} ALS mouse model (Mourelatos et al., 1996). Moreover, in the SOD1^{G93A} model, Golgi fragmentation was shown to occur prior to the formation of SOD1 inclusions and neuromuscular denervation, suggesting it occurs upstream in the pathogenesis of ALS (van Dis et al., 2014). More recently, ALS-linked mutations in UBQLN2 were shown to inhibit protein transport from the ER to the Golgi in neuronal cells concurrent with fragmentation of both organelles (Halloran et al., 2019).

The causes and consequences of Golgi fragmentation in ALS are not well understood. A possible cause of Golgi fragmentation is the inhibition of bi-directional protein trafficking between the ER and the Golgi (Nassif et al., 2010). Similarly, if vesicular trafficking from the Golgi to the plasma membrane is inhibited, proteins accumulate within the Golgi which, if prolonged, can cause fragmentation (Persson et al., 1992, Zolov and Lupashin, 2005, Zhou et al., 2013). Vesicular trafficking has been shown to be inhibited in cells expressing the ALS-associated mutant proteins: SOD1, TDP-43, FUS and OPTN (Sundaramoorthy et al., 2015, Atkin et al., 2014, Soo et al., 2015). OPTN is involved in the maintenance of Golgi architecture, and functions specifically in membrane trafficking and exocytosis via interaction with myosin VI and Rab8 (Sahlender et al., 2005). It has also been shown to mediate post-Golgi trafficking to lysosomes, which is dependent on the Rab8-OPTN-htt complex (del Toro et al., 2009). Interestingly, FUS has been reported to interact with both myosin V1 (Takarada et al., 2009) and myosin V (Yoshimura et al., 2006). Therefore, impairment of intracellular trafficking of the complex including OPTN and/or FUS may cause pathological inclusions in ALS (Maruyama et al., 2010). Golgi fragmentation in ALS may also be linked to the disruption of autophagy. Autophagy is a natural regeneration process characterised by the proteolytic degradation of

cytosolic components at the lysosome (Glick et al., 2010). The roles of autophagy in ALS are unclear; however, multiple discovered ALS genes have been associated with dysregulated autophagy (Nguyen et al., 2019). That said, the association between glycosyltransferases and autophagy is not well founded.

Brefeldin A is a fungal metabolite, which inhibits protein transport from the ER to the Golgi, inducing fragmentation of the Golgi cisternae. This process is reversible, making Brefeldin A a useful tool for the study of Golgi biogenesis (Langhans et al., 2007). Pharmacological induction of Golgi fragmentation with Brefeldin A has been shown to increase autophagosome biogenesis and induce the accumulation of autophagosomes (Naydenov et al., 2012). Finally, Golgi fragmentation in ALS may be associated with dysregulated axonal homeostasis (Sundaramoorthy et al., 2015). Motor neurons contain long axons that require biosynthetic output from the ER and Golgi for the maintenance of essential features, such as synaptogenesis, synaptic plasticity, and neurite outgrowth (Horton and Ehlers, 2004, Tuck and Cavalli, 2010). Proteins and lipids must travel large distances along axons; however, they are also synthesised locally within neurites. Brefeldin A-induced Golgi fragmentation has been shown to reduce synaptic potentiation (Broutman and Baudry, 2001) and axonal outgrowth (Jareb and Banker, 1997), highlighting the importance of the secretory pathway in neuronal integrity.

My preliminary data indicate that an R92C mutation in GLT8D1 causes fragmentation of the cis- and trans-Golgi network in isogenic HEK293-GLT8D1 cell lines. These results are concurrent with a possible reduction in the relative fluorescence intensity of Golgi markers GM130 and TGN46 (**Figures 5.7, 5.8**). The most crucial aim moving forward is to obtain three biological repeats of these data, after which it would be interesting to investigate further the role of GLT8D1 in the stabilisation of the Golgi architecture. Golgi membranes are organised as stacks of multiple flat cisternae, which are further linked into a ribbon-like structure located in the perinuclear region (Klumperman, 2011). My images of the Golgi do not depict this ribbon-like structure because they were taken at 40x magnification. At a higher magnification, these structures would likely be more apparent. It would be interesting to test whether pharmacological induction of Golgi fragmentation using Brefeldin A is rescued following expression of WT GLT8D1 compared to its mutant form. This would help to determine whether GLT8D1 plays a role in the maintenance of the Golgi architecture.

To my knowledge, the degree of Golgi fragmentation as a predictor for the severity of neurotoxicity via MLR disruption has not previously been explored. Of note, it has been proposed that the association of microtubules with exposed MLR could mediate fragmentation

of the trans-Golgi cisternae (Rodriguez-Boulan and Musch, 2005). It would be interesting to investigate whether the severity of Golgi fragmentation correlates with dysregulated MLR-induced neurotoxicity. This could be tested via a dose-dependent treatment of primary neuron cultures with Brefeldin A to induce varying degrees of Golgi fragmentation. I would then test for a dose-dependent effect of Brefeldin A on the disruption of MLR using techniques previously described in this chapter. Neurotoxicity could be measured using techniques such as a multielectrode array (Bradley and Strock, 2019) or a neurite outgrowth assay (Filous and Silver, 2016).

5.4.7. Summary

In summary, I have shown that an ALS-linked R92C mutation correlates with a reduction in the MLR integrity of isogenic HEK293-GLT8D1 cell lines, evidenced by mutation-specific reductions in membrane WGA and GM1 expression. This discovery places ganglioside metabolism upstream in the pathogenesis of GLT8D1-ALS. Gangliosides are associated with MLR integrity, and are responsible for the maintenance of caveolae. I explore novel ALS-associated mutations in enhancers linked to the expression of caveolins 1 and 2 in Chapter 6. It is possible that GLT8D1 and caveolins 1 and 2 share a common pathophysiological pathway in ALS. Ganglioside biosynthesis occurs in the Golgi, and dysregulated trafficking of Golgi secretory proteins is associated with fragmentation of the network. I have shown that GLT8D1 localises to the Golgi when transiently overexpressed in neuronal and non-neuronal cell lines, and my preliminary data suggest that the GLT8D1-R92C mutation causes fragmentation of the cis- and trans-Golgi network in isogenic HEK293-GLT8D1 cell lines. Future work should focus on completing a third biological repeat of the Golgi fragmentation analysis, as well as comparing fragmentation with transiently transfected models to confirm the validity of my findings. Moreover, it would be interesting to test whether chemically induced Golgi fragmentation can be rescued following overexpression of WT GLT8D1.

Chapter 6. Characterisation of ALS-associated CAV1/CAV2 enhancer variants

6.1. Introduction

This chapter is an extended version of work currently under review (available at: https://papers.ssrn.com/sol3/papers.cfm?abstract_id=3606796). Experimental work presented within this chapter was performed in collaboration with Dr John Franklin, Helia Ghahremani Nezhad, and Samantha Allen. Genome-wide association studies suggest a significant proportion of missing heritability is distributed throughout non-coding chromosomal regions (van Rheenen et al., 2016). Indeed, 98% of all sequence (Elgar and Vavouri, 2008) and 85% of human DNA under evolutionary constraint (Ward and Kellis, 2012) is non-coding, suggesting an important role in all aspects of cellular function. To date, genetic discoveries within the non-coding genome have been limited by a shortage of appropriate methodology.

Non-coding regulatory sequence includes enhancers, which are cis-acting DNA sequences that modulate expression of target genes primarily through the binding of transcription factors (TFs) (Koch et al., 2011). Physical interaction between an enhancer and the promoter of the target gene is mediated by DNA looping (Pennacchio et al., 2013). Recently, a novel pipeline for the identification of disease-associated variation within enhancers was designed (see section 1.8). Variants were aggregated according to function, filtered based on evolutionary conservation (Hujoel et al., 2019), and collapsed into a single burden test (Cirulli and Goldstein, 2010). Application of this pipeline in an unbiased genetic screen identified significant ALS-associated variation within enhancers linked to the expression of caveolin 1 (CAV1) and caveolin 2 (CAV2) (see section 1.8).

CAV1 and CAV2 are expressed together in a hetero-oligomeric complex (de Almeida, 2017) within membrane lipid rafts (MLR), and have a key role in the organisation of cell signalling (Sawada et al., 2019, Schmick and Bastiaens, 2014). CAV1 activity promotes neurotrophic signalling, leading to enhanced neuronal survival (Head et al., 2011, Mandyam et al., 2017). In contrast, loss of CAV1 accelerates neurodegeneration (Head et al., 2011, Head et al., 2010). Finally, neuronal-targeted overexpression of CAV1 was shown to improve survival and reduce motor neuron death in the SOD1^{G93A} ALS mouse model (Sawada et al., 2019) and is being developed as a novel therapy for ALS (www.cavogene.com).

Burden testing derives power from aggregating mutations into a single statistical test; therefore, experimental evaluation is necessary to determine which individual mutations are

pathogenic. Indeed, it is likely that a significant proportion of variants are not pathogenic (Lee et al., 2012). To experimentally evaluate CAV1/CAV2-enhancer mutations, I acquired patient-derived lymphoblastoid cells (LCLs) from two patients carrying ALS-associated CAV1/CAV2-enhancer variants: CAV-ALS 1: chr7:116222625T>C; and CAV-ALS 2: chr7:115994269:C>T. LCLs are generated through infecting peripheral blood lymphocytes with Epstein Barr Virus. This process has been shown to immortalise human resting B cells *in vitro*, giving rise to an actively proliferating B cell population (Neitzel, 1986). Using these lines, I investigated CAV1/CAV2 expression at the mRNA and protein level. Reduced CAV1/CAV2 function is proposed to be toxic via disruption of MLR, leading to impaired cell signalling (Sawada et al., 2019). Therefore, I tested whether ALS associated enhancer variants impair MLR formation. MLR integrity was measured by expression of GM1 gangliosides, as labelled by CTxB (Aman et al., 2001) (refer to section 5.3.2).

Enhancers often act in a cell and tissue-specific manner (Andersson et al., 2014, Heinz et al., 2015) and therefore LCLs may not be representative of expression changes in the CNS. However, CAV1/CAV2-enhancers were derived in a tissue-agnostic manner; therefore, I hypothesised that expression changes may be replicated across multiple cell types. To validate my findings in a CNS relevant cell type, I subsequently investigated CAV1/CAV2 mRNA expression in differentiated SH-SY5Y cells, following CRISPR/Cas9 perturbation proximate to the chr7:116222625T>C patient-mutation.

CRISPR/Cas9 is a naturally occurring bacterial defence mechanism that has been repurposed as a powerful RNA-guided DNA targeting platform for genome editing (Jiang and Doudna, 2017). This technology can be used to precisely manipulate genomic sequences and relies on two main components: a Cas9 endonuclease, and an associated guide RNA (gRNA). gRNAs are duplexes constituting a crRNA, which is a nucleotide sequence complementary to the target DNA sequence, and a tracrRNA, which acts as a binding scaffold for the Cas9 nuclease (Cong et al., 2013, Mali et al., 2013). The gRNA recognises the target DNA sequence of interest, directing the associated Cas9 endonuclease to transiently bind and induce sequence-specific cleavage in the form of a double strand break (DSB). Cas9 will not bind to or cleave the target DNA sequence without the presence of a downstream protospacer adjacent motif (PAM) (Mojica et al., 2009). The most commonly used Cas9 from *Streptococcus pyogenes* (spCas9) recognizes PAM sites that contain a triplet NGG (where 'N' represents any nucleotide base). PAM sites are located immediately 3' of the target sequence, and Cas9 endonucleases can be changed depending on which PAM sites are available (Jinek et al., 2012). The binding of Cas9 promotes unwinding of the two DNA strands immediately upstream of the PAM site, and the spacer sequence of the crRNA then binds with

the unwound DNA to form an RNA-DNA heteroduplex to initiate a DSB (Sternberg et al., 2014). This DSB can subsequently be repaired by non-homologous DNA-end joining (NHEJ) or via homologous recombination (HR). The majority (up to 90%) of DSBs are repaired by NHEJ following cleavage by Cas9 (Liu et al., 2018). The NHEJ repair process is error prone, and thus random indels (insertion or deletion mutations) of unpredictable length may be introduced, disrupting gene function (Tuladhar et al., 2019). DSB repair via HR is less error prone and relies on a homologous donor template DNA to repair the break. Under physiological conditions, this usually comes from the sister chromatid. However, in CRISPR/Cas9 editing, this pathway can be leveraged to introduce specific desired sequence changes via the introduction of a pre-designed double- or single-stranded oligonucleotide template (Liu et al., 2018).

CRISPR/Cas9 editing efficiency is usually estimated by measuring the proportion of an edited population of cells in which an indel mutation has been introduced. There are numerous ways of evaluating CRISPR editing efficiency. In the current project, I utilised two similar platforms that rely on Sanger sequencing trace data: TIDE (Tracking of Indels by DEcomposition) and ICE (Inference of CRISPR Edits). Both provide a simple, rapid and cost-effective strategy that accurately quantifies the editing efficiency of indels in a targeted cohort of cells, and predicts similar editing efficiencies to that of next generation sequencing (the gold standard for measurement of indel efficiencies) (Sentmanat et al., 2018). Both platforms require two parallel PCR reactions to amplify an approximate 400bp region around the predicted Cas9 cut site, followed by Sanger sequencing. The two sequencing traces that are generated are analysed using specially designed software (TIDE: available at <http://tide.nki.nl/>; ICE: available at <https://ice.synthego.com/#/>) (Brinkman et al., 2014). TIDE is a well-established platform that has been shown to be superior to gel electrophoresis based assays such as the commonly used T7 endonuclease 1 mismatch-detection assay, however requires careful adjustment of specific parameters (e.g. alignment window, p-value, decomposition window) to obtain meaningful results. Furthermore, it can only accurately predict indels of a limited size of up to 10bp (Brinkman et al., 2014, Sentmanat et al., 2018). Therefore, it is important to compare against alternative platforms to validate CRISPR editing efficiencies. ICE is a more recently established online tool that does not require manual parameter adjustment.

6.2. Aims and objectives for experimentally evaluating ALS-associated CAV1/CAV2 enhancer variants

1. Investigate the relative expression of CAV1 and CAV2 in patient-derived LCLs carrying ALS-associated CAV1/CAV2 enhancer variants via qRT-PCR and immunoblotting.
2. Investigate the effect of identified enhancer mutations on MLR integrity in patient-derived LCLs via live cell imaging with CTxB.
3. Use CRISPR/Cas9 genome editing to introduce an indel mutation proximal to the discovered chr7:116222625T>C (CAV-ALS 1) patient mutation site in SH-SY5Y cells.
4. Evaluate CAV1/CAV2 expression in differentiated SH-SY5Y cells carrying a CAV1/CAV2 enhancer perturbation via qRT-PCR.

6.3. Results

6.3.1. *CAV1 and CAV2 expression is reduced in patient-derived cells carrying an ALS-associated enhancer variant*

Reduced CAV1 expression is toxic to neurons (Head et al., 2011, Head et al., 2010); therefore, I measured CAV1/CAV2 expression at the mRNA and protein level in LCLs derived from ALS patients carrying CAV1/CAV2 enhancer variants: chr7:116222625T>C (CAV-ALS 1) and chr7:115994269:C>T (CAV-ALS 2). Controls consisted of LCLs derived from three sALS patients without CAV1/CAV2 enhancer variants, and three neurologically normal controls (see **Table 6.1**).

LCL ID	Designated ID	Age when sample collected	Sex	Affectation status	CAV1/CAV2 enhancer variant	Diagnostic certainty	Age at onset
SC3504	Non-ALS Ctrl 1	48	F	Control	No	N/A	N/A
BC6333	Non-ALS Ctrl 2	68	M	Control	No	N/A	N/A
BC6086	Non-ALS Ctrl 3	56	M	Control	No	N/A	N/A
LPO0016	Non-CAV-ALS 1	78	M	Sporadic	No	ALS-Definite	75
LP0661	Non-CAV-ALS 2	49	F	Sporadic	No	PLS	45
SMA0064	Non-CAV-ALS 3	69	M	Sporadic	No	ALS-Definite	66
SP3363	CAV-ALS 1	72	M	Sporadic	chr7:116222625T>C	ALS-Definite	71
SP3388	CAV-ALS 2	53	F	Sporadic	chr7:115994269:C>T	ALS-Probable	52

Table 6.1. Summary of the LCLs used for characterising the relative expression of CAV1/CAV2 in patients carrying ALS-associated enhancer variants. Sample ID, age upon sample collection, sex, affectation status, enhancer variant, diagnosis, and age of disease onset, are shown.

A former member of our group had previously assessed the specificity of an anti-CAV1 antibody through overexpression of CAV1 using a commercially available pEGFP-N1-CAV1 construct (Addgene, plasmid #14433) in HEK293 cells. Targeted knockdown of CAV1 was performed via co-transfection with pcDNA6.2-EmGFP-miRNA vectors and pENTR/H1-TO-MCS-shRNA vectors targeting CAV1. CAV1 protein bands were sized at a molecular weight of ~20kDa using GeneTools (Syngene). (**Figure 6.1a**).

In cells carrying chr7:116222625T>C, CAV1 protein (n=3, 89% reduction, $p=0.05$, Mann-Whitney test) (**Figure 6.1b, 6.1c**) and mRNA (n=3, 89% reduction, $p=0.003$, Welch's *t*-test), (**Figure 6.2a**) was significantly reduced compared to mean expression in cells derived from neurologically normal controls. In addition, CAV2 mRNA (n=3, 93% reduction, $p=0.002$, Welch's *t*-test) (**Figure 6.2b**) expression was significantly reduced compared to mean expression in cells derived from neurologically normal controls. Unfortunately, immunoblotting for CAV2 was not possible due to lack of a sufficiently specific antibody (**see appendix 17**). Expression of CAV1 protein and CAV1/CAV2 mRNA was not significantly reduced compared to ALS patients without an enhancer mutation (n=3, $p>0.05$, Welch's *t*-test). Cells carrying chr7:115994269:C>T did not show significantly reduced expression of CAV1 protein or CAV1/CAV2 mRNA (n=3, $p>0.05$, Welch's *t*-test), compared to neurologically normal controls, or compared to ALS patients without an enhancer mutation. Expression of CAV1 and CAV2 mRNA was normalised to the housekeeping gene, *RPL13A*, which is stably expressed in LCLs (Hruz et al., 2011).

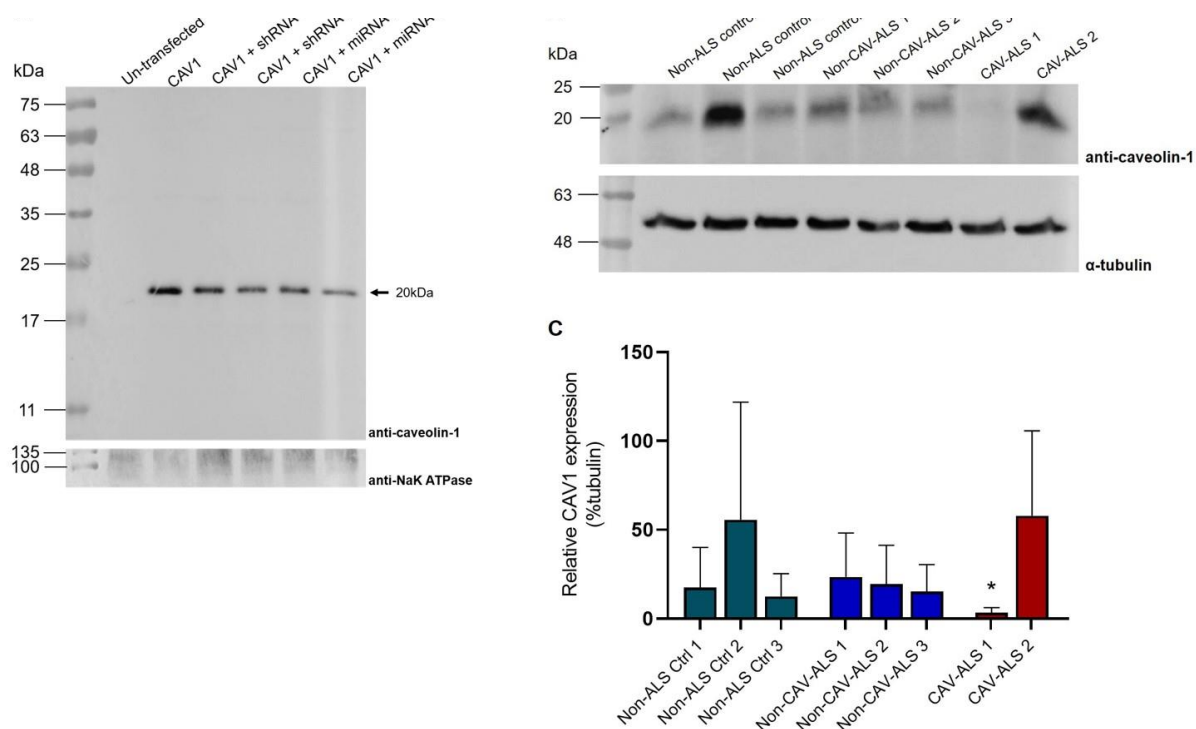


Figure 6.1. An ALS-associated CAV1/CAV2-enhancer variant reduces CAV1 protein expression in LCLs. (A) Representative immunoblot showing reduction of CAV1 protein in HEK293 cells co-transfected with pEGFP-N1-CAV1 vectors, with or without pcDNA6.2-EmGFP-miRNA and pENTR/H1-TO-MCS-shRNA vectors. The antibody used in this chapter detects CAV1 at a molecular weight of ~20kDa. Protein bands were sized using Gene Tools (Syngene). NaK ATPase served as a loading control (image kindly provided by Samantha Allen). (B) Representative immunoblot showing the relative expression level of CAV1 in non-ALS controls, non-CAV-ALS controls, and CAV-ALS patient LCLs; α -tubulin served as a loading control. Molecular weight markers are indicated (kDa). Protein bands were sized between ~19-22kDa using Gene Tools (Syngene). (C) Densitometric analysis suggests CAV1 expression is reduced in cells carrying a chr7:116222625T>C enhancer variant, compared to the mean CAV1 expression from neurologically normal controls (n=3, 89% reduction, $p=0.05$, Mann-Whitney test). CAV1 expression is not significantly reduced in cells carrying a chr7:115994269:C>T enhancer variant (n=3, $p>0.05$, Mann-Whitney test). Error bars represent mean \pm SD (* $p<0.05$).

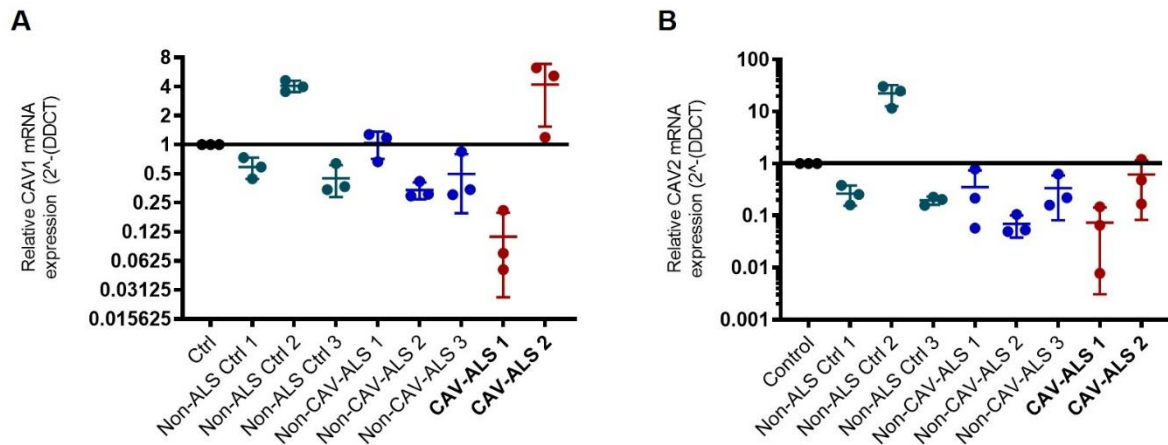


Figure 6.2. An ALS-associated CAV1/CAV2-enhancer variant reduces CAV1 and CAV2 mRNA expression in LCLs. qPCR measurement of (A) CAV1 and (B) CAV2 mRNA expression, relative to mean expression in neurologically normal controls; expression was normalised relative to the housekeeping gene, RPL13A (Hruz et al., 2011). Relative mRNA expression values were calculated using the $2^{-\Delta\Delta CT}$ method (Schmittgen and Livak, 2008). In cells carrying chr7:116222625T>C, CAV1 mRNA was reduced by 89% ($n=3$, $p=0.003$, Welch's t -test), compared to mean expression in cells derived from neurologically normal controls (black line). CAV2 mRNA was reduced by 93% ($n=3$, $p=0.002$, Welch's t -test), compared to mean expression in cells derived from neurologically normal controls. Data are presented on a logarithmic scale to account for wide-ranging numerical values. Error bars represent mean \pm SD.

6.3.4. An ALS-associated CAV1/CAV2 enhancer variant impairs MLR integrity in LCLs

Reduced CAV1/CAV2 function is proposed to be toxic via disruption of MLR, leading to impaired cell signalling (Sawada et al., 2019). Therefore, I tested whether an ALS-associated enhancer variant, which reduces CAV1/CAV2 expression, also impairs MLR formation. MLR integrity was measured by expression of GM1 gangliosides, as labelled by CTxB (Aman et al., 2001). I initially attempted co-labelling the cells with a CellMask™ plasma membrane stain in order to quantify CTxB fluorescence intensity relative to cell area. However, LCLs grow in clusters, making it difficult for automated software to distinguish individual cells accurately. Therefore, fluorescence intensity values presented in this chapter were not calculated relative to cell size. Representative images of CellMask™ and CTxB staining are shown (**Figure 6.3**).

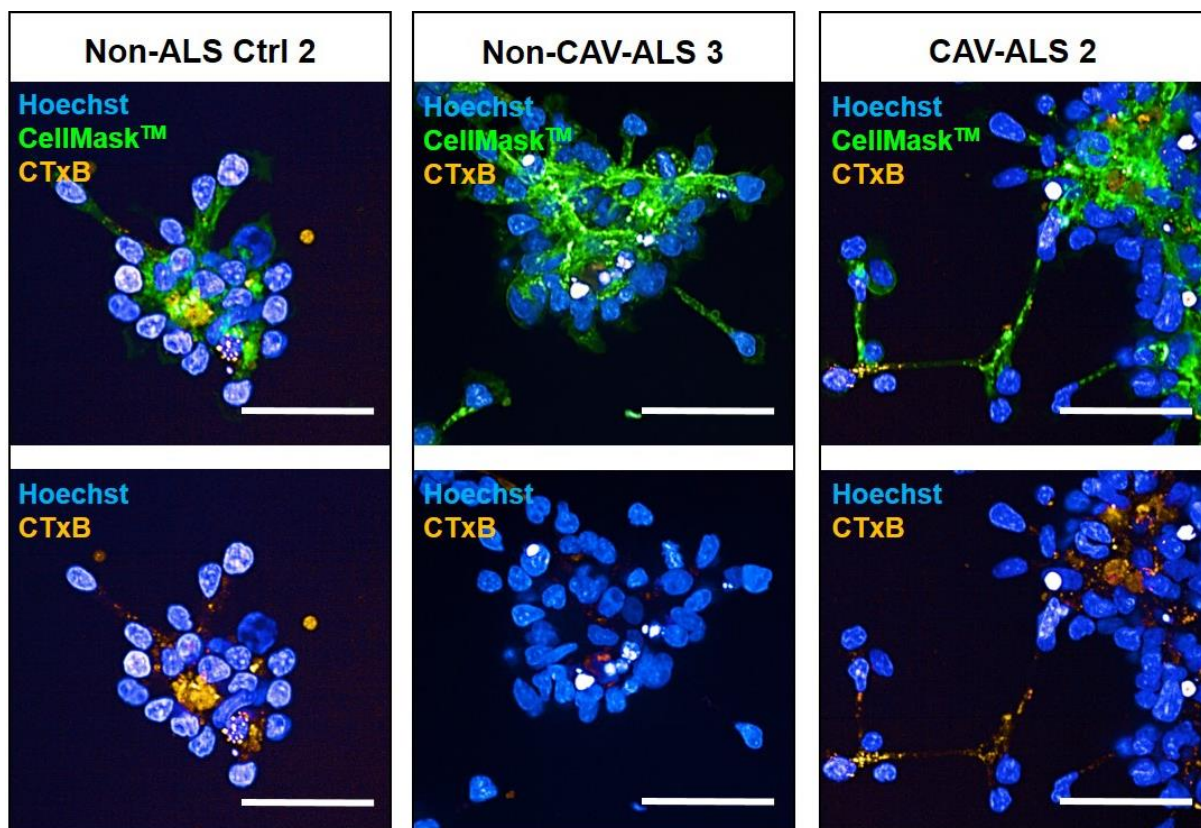


Figure 6.3. A CellMask™ plasma membrane stain was not suitable for determining cell area in LCLs. Healthy LCLs grow in clusters, which is problematic for the accurate quantification of cell size. Cells were co-labelled with CellMask™ plasma membrane stain (green) and CTxB (orange). Nuclear counterstain (Hoechst 33342) is shown in blue. Scale bars are 50µm.

Subsequent live imaging of CTxB in LCLs was performed in the absence of a plasma membrane marker. CTxB fluorescence was significantly reduced in LCLs carrying a chr7:116222625T>C (CAV-ALS 1) mutation, compared to cells derived from neurologically normal controls (n=6, Mann-Whitney test, $p=0.008$). Fluorescence intensity was not significantly reduced compared to ALS patients without a CAV1/CAV2 enhancer variant (n=6, Mann-Whitney test, $p>0.05$) (**Figure 6.4**). In all cell lines, GM1 expression and CAV1 protein expression are positively correlated ($r=0.6246$, $p=0.0196$, Pearson correlation) (**Figure 6.5**), which is consistent with direct dependence of MLR integrity on CAV1 function. Representative images of all LCLs probed with CTxB are provided (**see appendix 18**).

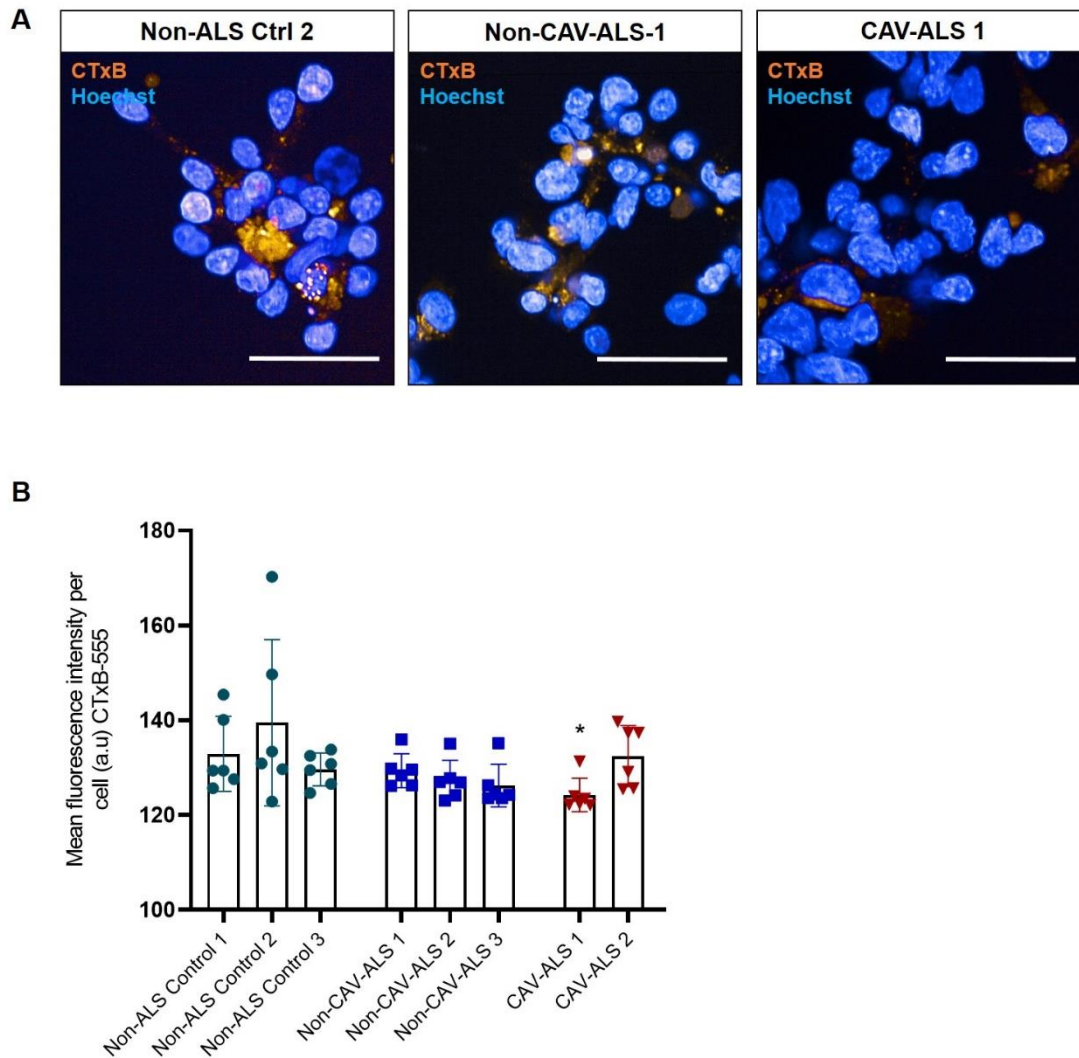


Figure 6.4. Patient-derived LCLs carrying an ALS-associated CAV1/CAV2 enhancer variant have disrupted MLR. (A) Representative images of ganglioside GM1 labelling with CTxB (orange) from a non-ALS control line, a non-CAV-ALS control line, and a CAV-ALS line. Nuclear counterstain (Hoechst 33342) is shown in blue. Scale bars are 50 μ m. **(B)** Fluorescence intensity of CTxB is reduced in cells carrying a chr7:116222625T>C variant (CAV-ALS 1), compared to cells derived from neurologically normal controls ($n=6$, $p=0.008$, Mann-Whitney test). Fluorescence intensity was not reduced compared to ALS patients without a CAV1/CAV2 enhancer variant ($n=3$, $p>0.05$, Mann-Whitney test). ~1000 cells were imaged per biological repeat from 15 fields of view, for each condition. Error bars represent mean \pm SD (* $p<0.05$).

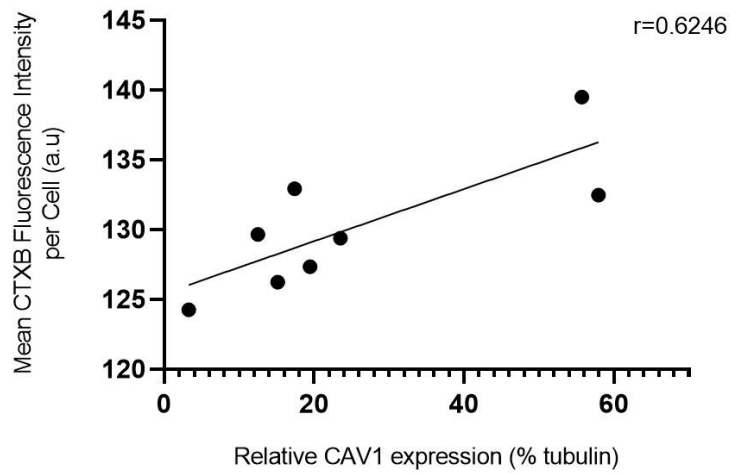


Figure 6.5. CTxB fluorescence intensity and CAV1 protein expression are positively correlated. Relative CAV1 protein expression (% α -tubulin) (x-axis) was plotted against the mean CTxB fluorescence intensity (a.u) (y-axis) in the same cell line. A linear regression line was fitted ($r=0.6246$, $p=0.0196$, Pearson correlation), which shows a moderate, positive correlation between CTxB fluorescence intensity and relative CAV1 protein expression.

6.3.5. CRISPR/Cas9 enhancer editing reduces CAV1/CAV2 expression in differentiated SH-SY5Y cells

Previous results suggest that patient-derived cells carrying an ALS-associated CAV1/CAV2 enhancer mutation display reduced CAV1/CAV2 expression and disrupted MLR, which is likely to lead to neurotoxicity (Sawada et al., 2019). To confirm whether the chr7:116222625T>C enhancer mutation is responsible for observed down-regulation of CAV1 at the mRNA and protein level, I planned initially to use CRISPR/Cas9 with homology-directed repair editing in an attempt to correct the mutant allele and restore genomic enhancer integrity and caveolin expression. Effective correction of the enhancer sequence would demonstrate whether discovered mutations are directly linked to observed changes in CAV1/CAV2 expression. This approach would be technically challenging for three reasons: i) patient-derived LCLs are difficult to transfect and grow from single cell clones, making them broadly unsuited to CRISPR experiments; ii) the targeted mutation is non-coding, which adds difficulties to using homology-directed repair, as the repair template cannot be edited to ablate the PAM site, thus permitting re-cleavage; iii) the lack of an appropriate PAM site in the immediate vicinity of chr7:116222625 would be likely to reduce homology-directed repair in these cells.

To assess the feasibility of correcting the mutation, I first used a CRISPR/Cas9 plasmid (PspCas9(BB)-2A-Puro PX459) (Ran et al., 2013), and subsequently a spCas9/gRNA ribonucleoprotein (RNP) complex to target the chr7:116222625T>C patient mutation in LCLs. gRNAs were designed using the CRISPOR web tool (Haeussler et al., 2016) (available at: <http://crispor.tefor.net>), and three guides were chosen based on proximity to mutation, predicted on- and off-target effect, and the availability of suitable PAM sites. Single stranded oligonucleotide donor templates for homology-directed repair were designed using the Benchling CRISPR web tool (available at: <https://www.benchling.com>).

Using the PX459 plasmid, I was unable to detect any editing as measured via TIDE or ICE using three different gRNA sequences (**see appendix 19**). One spCas9-gRNA RNP complex targeting the WT enhancer sequence 16bp downstream of the chr7:116222625T>C mutation site (gRNA sequence: 5-UUGUAAUCAGGAAUUUCCA-3) was electroporated into non-ALS control-1 LCLs. Sanger sequencing and analysis using ICE at 7-days post electroporation, demonstrated only 6% editing efficiency (**Figure 6.6**). Given the technical challenges and the lack of a suitable PAM site, I did not continue with my efforts to correct the chr7:116222625T>C enhancer mutation in LCLs. Instead, I focused on disrupting the WT

enhancer sequence close to the mutation site (chr7:116222625) in a neuronal cell model to link disrupted enhancer function to reduced caveolin expression in the context of the CNS.

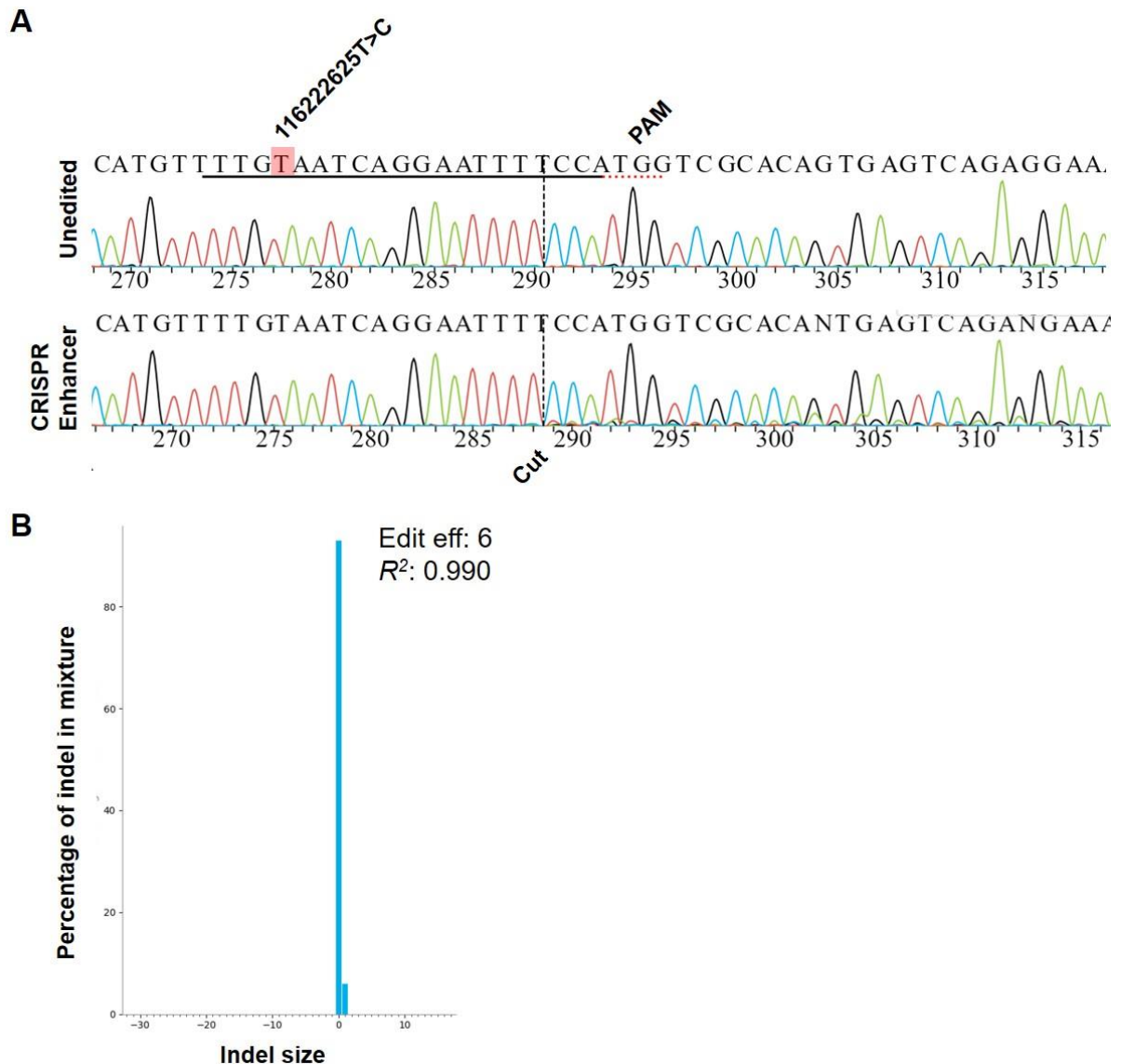


Figure 6.6. CRISPR-directed perturbation of a CAV-enhancer region proximate to a patient mutation in LCLs. (A) Sanger sequencing traces demonstrating spCas9 cut site adjacent to the PAM site, and subsequent waveform decomposition in enhancer-edited cells. The position of chr7:116222625T>C mutation is indicated. The black line indicates the gRNA sequence. **(B)** Indel distribution within the CAV-enhancer region in CRISPR-edited LCLs from non-ALS control-1. Editing efficiency was calculated to be 6% (ICE).

To disrupt enhancer function in a CNS-relevant human neuronal cell, I used the same CRISPR/spCas9 RNP editing strategy to introduce an indel mutation proximal to the site of the chr7:116222625T>C mutation in immature SH-SY5Y cells, as permitted by the availability of PAM sites. SH-SY5Y cells were subsequently differentiated into neurons using an established protocol (Forster et al., 2016). The same gRNA (5-UUGUAAUCAGGAAUUUCCA-3) targeting a PAM site 16bp downstream of the chr7:116222625T>C mutation site, was used. Sanger sequencing and analysis using TIDE and ICE at 7-days post electroporation revealed 72% editing efficiency (both modalities) in undifferentiated SH-SY5Y cells, and the majority of introduced changes were a single nucleotide insertion (chr7:116222638T>TT) (**Figure 6.7**). To investigate the relative effect on caveolin expression, a commercially available gRNA targeting *CAV1* exon 2 was chosen (to induce gene knockout via induction of a nonsense mutation) to serve as a positive control. In addition, a commercially available control gRNA targeting the hypoxanthine phosphoribosyltransferase (*HPRT*) locus served as a negative control (Liao et al., 2015).

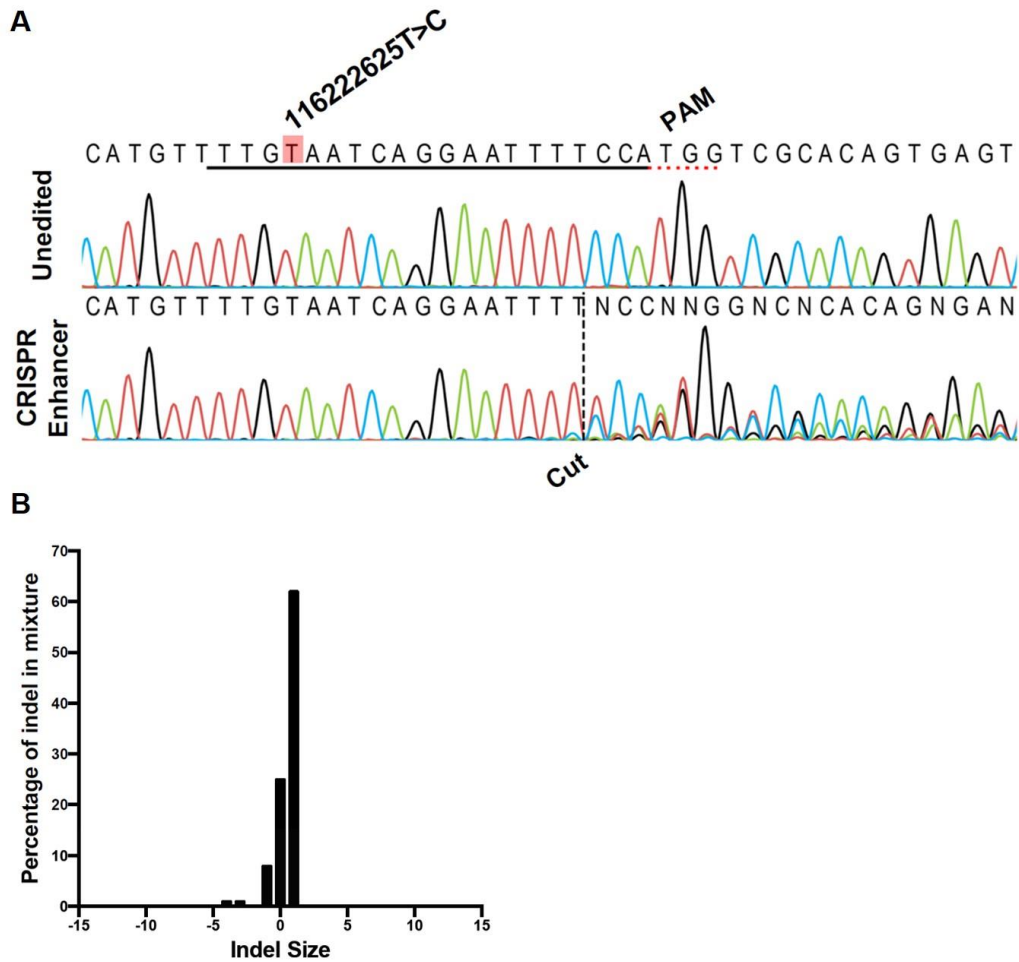


Figure 6.7. CRISPR-directed perturbation of a CAV-enhancer region proximate to a patient mutation in SH-SY5Y cells. (A) Sanger sequencing traces demonstrating spCas9 cut site adjacent to the PAM site, and subsequent waveform decomposition in enhancer-edited cells. The position of chr7:116222625T>C mutation is indicated. The black line indicates the gRNA sequence. **(B)** Indel distribution within the CAV-enhancer region in CRISPR-edited SH-SY5Y cells. Editing efficiency was calculated to be 72% (TIDE / ICE).

CRISPR/SpCas9-edited SH-SY5Y cells were differentiated into a neuronal phenotype (Forster et al., 2016). Differentiation was evaluated through expression of PAX6 and measurements of total neurite length. Preliminary immunocytochemistry data suggest that PAX6 expression is reduced in differentiated SH-SY5Y cells (n=2, no statistical analysis was performed) (**Figure 6.8a, 6.8b, 6.8e**). qRT-PCR data show variable PAX6 mRNA expression between differentiated and undifferentiated cells, with a significant reduction in the enhancer-edited line (n=3, $p=0.0001$, un-paired t -test). Reductions in PAX6 mRNA were not observed in differentiated *HPRT* control or *CAV1* exon 2-targeted cells, compared to undifferentiated cells (**Figure 6.8g**). Alterations in neurite length were assessed via immunostaining for α -tubulin, followed by semi-automated quantification using the Simple Neurite Tracer plugin for Fiji. Total neurite length was increased in differentiated cells, compared to undifferentiated (n=4, $p=0.01$, paired t -test) (**Figure 6.8c, 6.8d, 6.8f**). Differentiated cells were harvested, and RNA was extracted for qPCR. I confirmed reduced expression of *CAV1* (n=4, >99% reduction, $p<0.0001$, Welch's t -test) and *CAV2* (n=4, >99% reduction, $p<0.0001$, Welch's t -test) mRNA in enhancer edited cells. *CAV1/CAV2* mRNA expression was normalised relative to the housekeeping gene, *GAPDH*, which has previously been used as an internal reference in SH-SY5Y cells (Fan et al., 2016) (**Figure 6.9**). *CAV2* mRNA expression was reduced in the context of enhancer editing, but also by *CAV1*-coding editing, which likely reflects interdependence between the two genes (Drab et al., 2001).

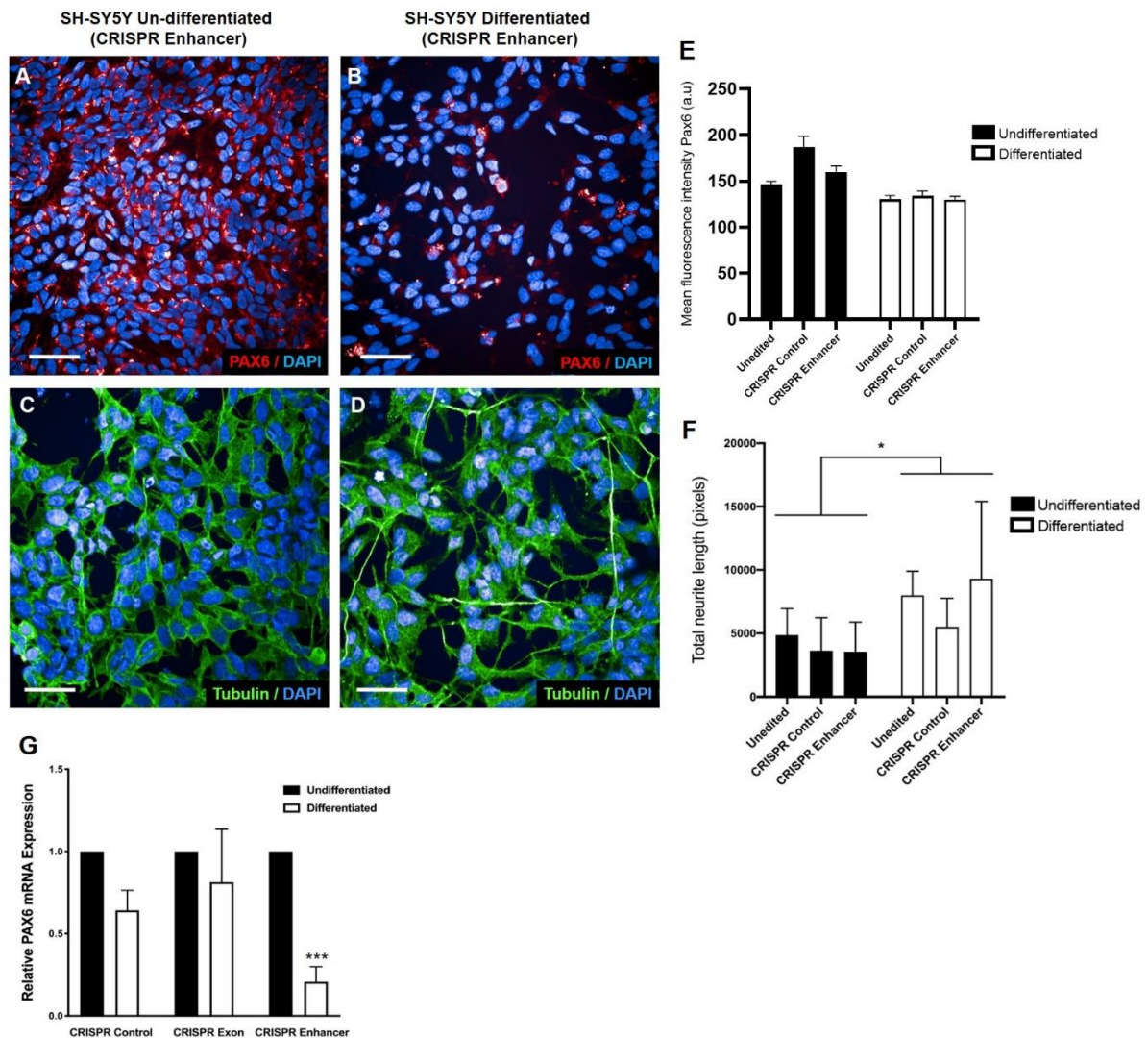


Figure 6.8. Increased dendrite length and altered PAX6 expression suggests successful neuronal differentiation of SH-SY5Y cells. Representative images of PAX6 staining in (A) un-differentiated and (B) differentiated SH-SY5Y cells with a CRISPR-induced enhancer perturbation. (C, D) Representative images of α -tubulin (green) staining in undifferentiated and differentiated SH-SY5Y cells carrying a CRISPR-induced enhancer perturbation. Nuclear counterstain (Hoechst 33342) is shown in blue. Scale bars are 50 μ m. (E) Quantification of PAX6 fluorescence intensity for the whole cell; no statistical analysis was performed (n=2). (F) Differentiated SH-SY5Y cells show increased total neurite length, based on α -tubulin staining (n=4, * p <0.05, paired t -test). (G) qRT-PCR data suggest PAX6 expression is reduced in differentiated enhancer-edited cells compared to undifferentiated enhancer-edited cells (n=3, p <0.001, un-paired t -test). Error bars represent mean \pm SD (* p <0.05; *** p <0.001). Representative images of PAX6 and α -tubulin staining from all experimental conditions are available (see appendices 20 and 21).

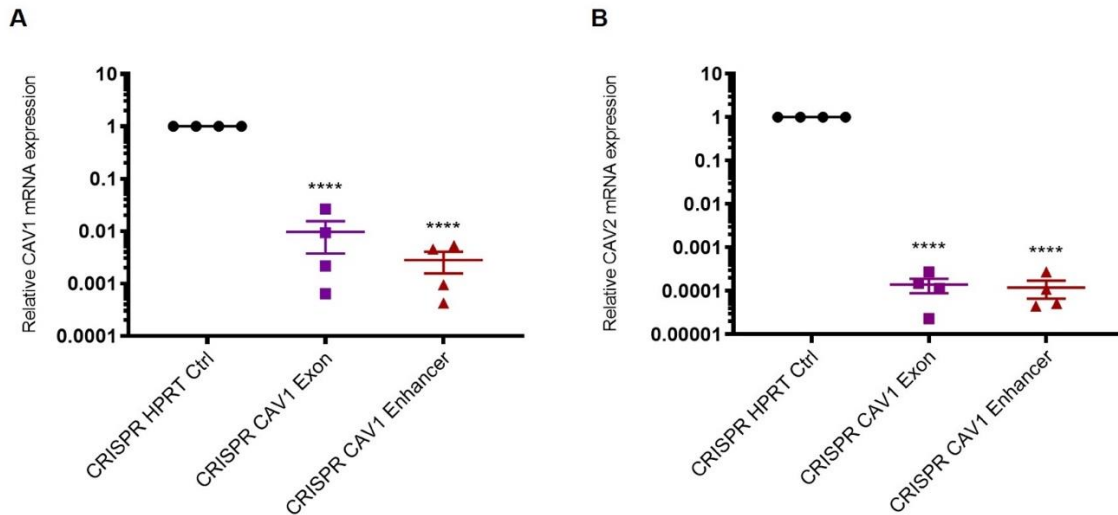


Figure 6.9. qPCR measurement of CAV1 mRNA and CAV2 mRNA reveals reduced expression in CAV-enhancer and CAV1-exon CRISPR-edited neurons, compared to CRISPR editing of HPRT. CRISPR-induced CAV-enhancer and CAV1-exon mutations correlated with reduced expression of **(A)** CAV1 ($n=4$, >99% reduction, $p<0.0001$, Welch's t -test) and **(B)** CAV2 ($n=4$, >99% reduction, $p<0.0001$, Welch's t -test) mRNA. Expression was normalised relative to the housekeeping gene, GAPDH (Fan et al., 2016). Relative mRNA expression values were calculated using the $2^{-\Delta\Delta CT}$ method (Schmittgen and Livak, 2008). Data are presented on a logarithmic scale to account for wide-ranging numerical values. Error bars represent mean \pm SD. (**** $p<0.0001$).

6.4. Discussion

CAV1 and CAV2 are integral membrane proteins located in caveolae in the outer cell membrane. They are also present intracellularly in the ER, Golgi apparatus, and transport vesicles (de Almeida, 2017). CAV1 and CAV2 form a stable hetero-oligomeric complex, which enables CAV2 to be trafficked to the plasma membrane. In the absence of CAV1, CAV2 forms monomers and dimers that localise to the Golgi network and become a target for degradation. Therefore, whilst CAV1 and CAV2 are often co-expressed, CAV2 expression in caveolae is largely dependent on the formation of the hetero-oligomeric complex with CAV1 (de Almeida, 2017).

CAV1 functions prominently in cell signalling and in the transport of cholesterol (Quest et al., 2008). Cell signalling mediated by CAV1 function includes neurotrophic signalling with important implications for neuronal cell death (Head et al., 2011, Mandyam et al., 2017). Indeed, premature apoptosis has been implicated in motor neuron loss in ALS (Guegan and Przedborski, 2003). In addition, dysregulated cholesterol metabolism is well described in ALS. High levels of cholesterol are toxic to neurons, and lower levels of cholesterol provide a neuroprotective phenotype (Abdel-Khalik et al., 2017). Interestingly, neuron-specific up-regulation of CAV1 in the SOD1^{G93A} ALS mouse model has been shown to extend survival and improve motor function (Sawada et al., 2019). Up-regulation of CAV1 is also demonstrated to improve cognition and hippocampal plasticity in aged mice, as well as promote axonal and dendritic growth in primary neurons, making it an area of interest for therapies targeting neurodegenerative disorders (Head et al., 2011, Mandyam et al., 2017).

6.4.1. CAV1 and CAV2 expression are reduced in patient-derived cells carrying an ALS-associated enhancer variant

In the present study, I hypothesised that discovered ALS-associated CAV1 enhancer mutations contribute to pathogenicity via downregulation of functional CAV1 protein. Therefore, immunoblotting was used to evaluate whether there was a difference in CAV1 protein expression between control and patient samples. Initially, the relative expression of CAV1 protein was explored using LCLs, as this was the only biological material available from patients with ALS-associated CAV1 enhancer mutations. LCLs are relatively simple to maintain, they exhibit a minimal somatic mutation rate during continuous culture, and they provide an unlimited source of biomolecules, which makes them useful for genetic screening, genotype-phenotype correlation studies, and functional assays (Mohyuddin et al., 2004,

Hussain and Mulherkar, 2012). An important caveat to their use is the fact that they are not neuronal, which limits their applicability for modelling diseases such as ALS.

LCL lysis for subsequent CAV1 immunoblotting was initially performed using IP lysis buffer; however, I did not detect a signal when probing with a validated anti-caveolin-1 antibody (**see appendix 22**). CAV1 is a membrane-bound protein; therefore, I hypothesised that the absence of the signal was due to CAV1 being expressed in an insoluble membrane fraction. I decided to trial urea buffer, which is capable of dramatically enhancing the solubility of membrane-bound proteins (Molloy et al., 1998, Harris et al., 2017). Use of this buffer meant it was not possible to quantify total protein within cell lysates accurately using a Bradford protein assay, which is incompatible with urea at a concentration higher than 3.0M (Gotham et al., 1988). However, I found the BCA assay to be compatible, as it provided an accurate quantification of total protein within lysates (Krieg et al., 2005). Had I still been unable to detect a signal following urea-based cell lysis, I would have considered subcellular fractionation (de Araujo and Huber, 2007) to isolate the membrane region of LCLs in order to provide a more accurate detection of potentially low abundant CAV1.

A previous member of our group had assessed the specificity of the anti-CAV1 antibody, following overexpression and targeted knockdown of CAV1 in HEK293 cells. The CAV1 protein signal was detectable when overexpressed in lysates that had been generated using IP lysis buffer. I speculate that the CAV1 signal is not within the dynamic range at endogenous levels in LCLs, where expression is low relative to kidney-derived cells (<https://www.proteinatlas.org>). This antibody detected CAV1 at the predicted molecular weight of ~20kDa (**Figure 6.1a**), which gave me confidence in the use of this antibody moving forward. In the present study, I observed a reduction in CAV1 expression at the protein level in cells with a chr7:116222625T>C enhancer mutation, compared to neurologically normal controls (n=3, 89% reduction, $p=0.05$, Mann-Whitney test), but not compared to ALS patients without a CAV1 enhancer mutation (n=3, $p>0.05$, Mann-Whitney test). In contrast, cells carrying an ALS-associated chr7:115994269:C>T mutation did not show reduced expression of CAV1 protein (n=3, $p>0.05$, Mann-Whitney test) (**Figure 6.1b, 6.1c**). I speculate that the latter mutation may influence transcription only in CNS cells, or alternatively this variant may be non-functional. Attempts to evaluate CAV2 expression at the protein level were not possible due to lack of a validated commercially available antibody (**see appendix 22**).

The observed reduction in CAV1 protein expression in the patient with a chr7:116222625T>C enhancer mutation does not confirm malfunction at the transcriptional level, which is a necessary prediction of the present model of enhancer dysfunction. Therefore, qRT-PCR was used to evaluate the relative expression of CAV1 and CAV2 at the mRNA level in LCLs. My

qRT-PCR data shows a similar trend in *CAV1* mRNA expression compared to immunoblotting, concurrent with a significant reduction in cells with the chr7:116222625T>C mutation (n=3, $p=0.003$, Welch's *t*-test) (**Figure 6.2a**). Moreover, I observed *CAV2* to follow a similar expression pattern across the various cohorts, with reduced expression level in the cells harbouring a chr7:116222625T>C mutation compared to neurologically normal controls (n=3, $p=0.002$, Welch's *t*-test) (**Figure 6.2b**). From these data, it can be inferred that *CAV1/CAV2* expression is affected at both the transcriptional and translational level, which led me to investigate this further using CRISPR/Cas9 genome editing.

6.4.2. Patient-derived LCLs carrying an ALS-associated CAV enhancer variant have disrupted MLR

Prior to genome editing, I investigated ganglioside metabolism (see Chapter 5) as a potential mechanism linked to ALS-associated *CAV1/CAV2* enhancer variants. As previously mentioned, ganglioside GM1 is highly expressed in the CNS and is localised to MLR, which are important for transmembrane signalling (Vajn et al., 2013). GM1 is internalised via caveolae (Crespo et al., 2008), and is shown to be responsible for the trafficking and maintenance of caveolae domains (Singh et al., 2010). The association of GM1 with MLR makes this ganglioside a useful target for measuring MLR integrity. My data indicate that CTxB expression may influence *CAV1* expression (**Figures 6.4, 6.5**) and, by extension, MLR integrity may be influenced by *CAV1* expression. This is consistent with previous work demonstrating that neuron-specific upregulation of *CAV1* increases CTxB expression in the spinal cord of the SOD^{G93A} ALS mouse model (Sawada et al., 2019).

The use of CTxB for the labelling of ganglioside GM1 and MLR has been discussed previously (see section 5.4.2). Live imaging of ganglioside GM1 using a CTxB molecular probe was challenging, as LCLs are non-adherent. To encourage cell adherence, I tested three different factors used for coating culture plates prior to seeding: fish gelatin (Huang et al., 2018), type I collagen (Heino, 2007), and plasma fibronectin (Hsiao et al., 2017). Of these factors, plasma fibronectin most effectively encouraged cell adherence following a 30-minute incubation at 5µg/mL, whereas cells were mobile when visualised under the microscope for plates pre-coated in fish gelatin or type 1 collagen. Plasma fibronectin is an extracellular matrix glycoprotein present in blood plasma and is a key modulator of cellular adhesion (Hsiao et al., 2017). When measuring the fluorescence intensity of cells, it is ideal to display the data as a percentage of cell area to account for variability in cell sizes between groups. Therefore, I attempted co-labelling the LCLs with CellMaskTM, a fluorescent lipophilic membrane dye

(Takov et al., 2017), to calculate cell size. However, LCLs grow in clusters, making it difficult for automated software to detect individual cells (**Figure 6.3**). This perhaps limits the reliability of my data, as it suggests that the mean fluorescence intensity is not representative of individual cells. However, my results were consistent across all biological repeats of this assay, despite variations between the sizes of the cell clusters. I have previously linked an ALS-associated GLT8D1 mutation to disrupted MLR (Chapter 5), and the results in the present chapter may suggest a convergence between GLT8D1- and CAV1-ALS disease pathways.

6.4.3. CRISPR/Cas9 genome editing of human cells

To determine whether the chr7:116222625T>C enhancer mutation is responsible for observed down-regulation of CAV1 at the mRNA and protein level, I planned to use CRISPR/Cas9 genome editing to correct the mutation and restore genomic enhancer integrity. Effective correction of the enhancer sequence would demonstrate whether discovered mutations are directly linked to observed changes in CAV1/CAV2 expression.

LCLs have a relatively low transfection efficiency, and to my knowledge, the highest reported editing efficiency in this cell line using the CRISPR system to induce homology-directed recombination, was ~20% (Johnston et al., 2019). This study utilised a Cas9-GFP-gRNA plasmid, but there are key limitations to plasmid-based approaches for CRISPR-induced editing. For example, cells must be amenable to transfection, plasmids may randomly integrate into the host genome, off-target effects can occur due to prolonged Cas9 expression, and plasmids demonstrate variable CRISPR editing efficiencies (Kim et al., 2014). The authors recommended delivering Cas9-RNP-gRNA complexes (Johnston et al., 2019), which was previously shown to be feasible in LCLs (Jiang et al., 2018). Delivery of Cas9-RNP complexes has been shown to provide more efficient on-target cleavage and reduce off-target cleavage, compared to plasmid transfection (Kim et al., 2014, Liang et al., 2015). Moreover, the Cas9-gRNA-RNP complex can be electroporated into the cell and is degraded over time, which limits the potential for off-target effects (Schumann et al., 2015). Overall, studies that have used the RNP delivery system have consistently reported high editing efficiencies across a variety of cell lines (Hendel et al., 2015, Lin et al., 2014).

Initially, I planned to correct the chr7:116222625T>C enhancer mutation in LCLs via CRISPR/Cas9-based editing. To assess the feasibility of this, I used the RNP delivery system to target the WT enhancer sequence, by introducing an indel mutation in LCLs from a neurologically normal patient. Analysis using TIDE (Brinkman et al., 2014) demonstrated only

achieved 6% editing efficiency (**Figure 6.6**). In order to generate a pure population of CRISPR-edited cells, the LCLs would need to be serially diluted into single cell colonies, and subsequently expanded over several months. Unfortunately, LCLs do not readily expand from single cell colonies, rather they aggregate into clusters to remain healthy, and at lower concentrations, their death rate increases (Hussain and Mulherkar, 2012). However, a recent study described an efficient method of generating of a pure population of CRISPR-edited LCLs via fluorescent activated cell sorting, allowing for the expansion of transfected groups of cells in a matter of weeks (Johnston et al., 2019). This is a new approach that I may have considered pursuing with more time.

Given the technical challenges and the lack of a suitable PAM site, I did not continue with my efforts to correct the chr7:116222625T>C enhancer mutation in LCLs. Instead, I focused on targeting the WT enhancer sequence 16bp downstream of the chr7:116222625T>C mutation site in a neuronal model to place this mutation in the context of the CNS. I chose SH-SY5Y cells, a human neuroblastoma line that has been extensively used in Parkinson's and Alzheimer's research (Xicoy et al., 2017, Agholme et al., 2010). There are several advantages to the use of SH-SY5Y cells; for example, their continuous proliferation at the undifferentiated stage enables the user to generate a large biomass of post-mitotic neurons with relative ease and minimal cost. Moreover, SH-SY5Y cells are human-derived; therefore, they express many human-specific proteins and protein isoforms, which are not inherently present in primary rodent cultures (Kovalevich and Langford, 2013).

I used the RNP complex delivery system to introduce an indel mutation proximal (16bp downstream) to the patient enhancer mutation site in SH-SY5Y cells. My experiments did not include a DNA repair template, as I was aiming to disrupt the WT enhancer. CRISPR edits were evaluated through a combination of Sanger sequencing and waveform decomposition analysis (Brinkman et al., 2014). Both TIDE and ICE analysis platforms demonstrated similarly high levels of editing efficiency (~72%) in my SH-SY5Y model (**Figure 6.7**). Efficiently edited cell pools are acceptable alternatives to clonally isolated cells with specific knockouts and are more easily attainable (Ran et al., 2013). However, edited pools have some limitations: DNA double strand breaks are often associated with undesired off-target effects such as translocations (Kosicki et al., 2018), or the activation of p53 (Haapaniemi et al., 2018), which may differentially affect the properties of individual cells.

6.4.4. Generation of a CRISPR-edited neuronal model

My next aim was to differentiate the CRISPR-edited SH-SY5Y cells into neurons, in order to model CAV1-ALS in the context of the CNS. Differentiated SH-SY5Y cells are morphologically similar to primary neurons, displaying extended processes, decreased proliferation rate, and increased expression of neuron-specific markers (Gordon et al., 2013). There are numerous methods of inducing SH-SY5Y neuronal differentiation, and the best characterised is through the addition of 10 μ M retinoic acid to the culture media. Retinoic acid is a vitamin A derivative with known growth-inhibiting and cellular differentiation-promoting properties (Melino et al., 1997).

In order to generate a neuronal model, CRISPR-edited human SH-SY5Y neuroblastoma cells were differentiated into neurons over a one-week period, as previously described (Forster et al., 2016). Neuronal differentiation was initiated one-week post nucleofection. Successful differentiation was initially evaluated via PAX6 expression. Fully differentiated neurons are post-mitotic, and PAX6 expression is usually discontinued in the precursor progeny following cell cycle exit. Therefore, post-mitotic neurons do not normally express detectable levels of the protein (Hsieh and Yang, 2009, Sebastian-Serrano et al., 2012). Preliminary staining for PAX6 suggests reduced expression in differentiated cells, compared to undifferentiated (n=2, no statistical analysis was performed) (**Figure 6.8**). However, PAX6 reduction was confirmed at the mRNA level in enhancer-edited cells (n=3, $p < 0.001$, un-paired t -test) (**Figure 6.9**). Co-staining for other neuronal markers such as NeuN (Gusel'nikova and Korzhevskiy, 2015) would have strengthened the characterisation of this model; however, additional readouts were investigated. Differentiated cells presented with extended neuritic processes (n=4, $p = 0.01$, paired t -test) (**Figure 6.8**). I also observed reductions in growth rate and cell clustering, which is consistent with previous studies (Forster et al., 2016). An overview of the experimental procedure used to generate a CRISPR-edited neuronal model is shown (**Figure 6.10**).

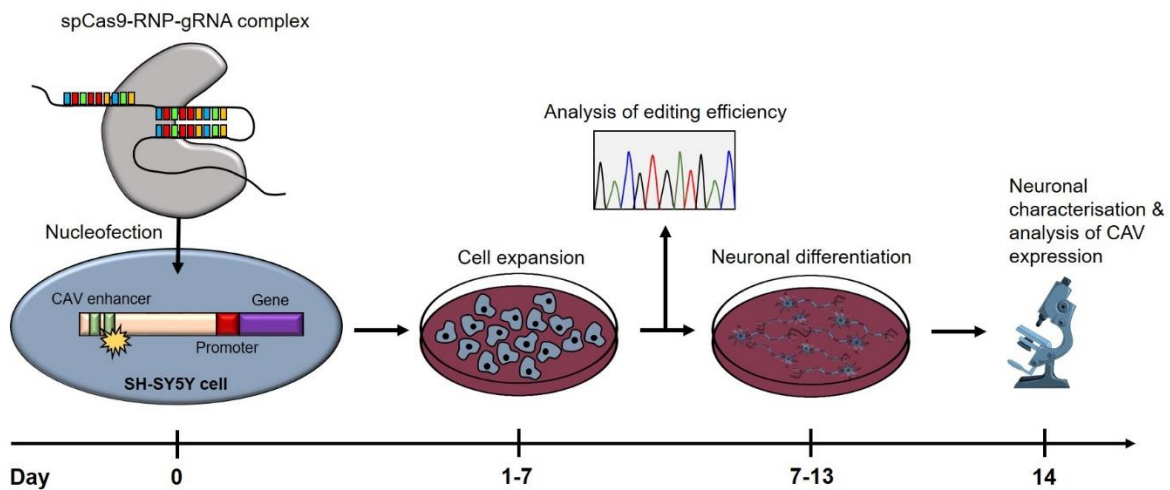


Figure 6.10. Schematic representation of the generation of a neuronal model of CAV-associated ALS. Cas9-gRNA complexes targeting the CAV-WT enhancer sequence were electroporated into SH-SY5Y cells at day 0 and cells were subsequently expanded over a period of one week. At day 7, editing efficiency was evaluated via Sanger sequencing, TIDE, and ICE, and cells were differentiated into a neuronal phenotype as previously described (Forster et al., 2016). At day 14, differentiated neurons were characterised via immunocytochemistry and measurements of total neurite length; and CAV1/CAV2 expression was assessed via qRT-PCR.

CAV1 has been shown to inhibit neuronal differentiation by decreasing neurite outgrowth and branching in PC12 cells (Gaudreault et al., 2005). In addition, CAV1 is shown to block the formation of neurites and phosphorylation of ERK in bFGF-treated N2A cells (Kang et al., 2006). However, PC12 and N2A cells are derived from rat and mouse, respectively (Hu et al., 2018, Namsi et al., 2018); therefore, to be consistent with my previous work, I chose to model the CAV1-enhancer variant in a human-derived neuronal cell line. CAV1 has been demonstrated to inhibit neuronal differentiation of neural progenitor cells via the downregulation of VEGF signalling and the inhibition of p-p44/42MAPK, p-Akt and p-Stat3 (Li et al., 2011). In the current study, CAV1 enhancer-edited SH-SY5Y cells did not display enhanced neurite development, compared to HPRT controls and unedited cells ($n=3$, $p>0.05$, paired t -test) (**Figure 6.8**). However, PAX6 expression was significantly reduced in the differentiated cells carrying a CAV1 enhancer perturbation, compared to CRISPR control cells with edited *HPRT* ($n=3$, $p=0.0294$, un-paired t -test) (**Figure 6.8**). This result suggests that a reduction in CAV1 expression improves neuronal differentiation, which is consistent with

previously published work (Kang et al., 2006, Li et al., 2011). It would be expected, therefore, that disruption of the CAV1 exon would have a similar effect on PAX6 expression; however, this was not the case in the present study. This may be because of unmeasured effects on additional genes under control of the same enhancer.

In my neuronal model, I observed reductions in *CAV1* (n=4, $p < 0.0001$, Welch's *t*-test) and *CAV2* (n=4, >99%, $p < 0.0001$, Welch's *t*-test) mRNA, consistent with a functional effect of the enhancer on expression (**Figure 6.7**). Reductions in *CAV1/CAV2* expression greater than the editing efficiency are notable; however, phenotypic change in excess of editing efficiency is well described and may be a consequence of CRISPR interference (Gaj et al., 2017). Importantly, this mutation does not mimic exactly the one seen in the patient, and it is possible that observed effects on expression are a result of an artefact. However, it is unlikely that an unpredictable off-target effect produced the exact changes predicted by our other lines of evidence. It is very difficult to determine whether there were any off-target effects resulting from my experiment, although use of the RNP delivery system will have helped to mitigate this (Lin et al., 2014). One consideration would be to utilise bulk RNA-sequencing; however, this usually reflects the average gene expression across thousands of cells by combining genomic readouts from individual cells to generate an overall representation. As such, single-cell RNA (scRNA) sequencing has become more favourable for studying the key biological questions of cell heterogeneity, although this technology is still in its developmental stage. Compared to bulk RNA sequencing, scRNA sequencing produces noisier and more variable data. Both methodologies introduce amplification errors, which often leads to imbalanced proportions or complete lack of variant alleles (Chen et al., 2019).

Until recently, it was challenging to introduce or correct disease-causing genetic variants efficiently without causing excess by-products (Jinek et al., 2012, Cong et al., 2013, Mali et al., 2013, Kosicki et al., 2018). However, prime editing has since been described, which is a 'search-and-replace' genome editing technology that mediates targeted indels as well as all 12 possible base-to-base conversions in human cells without requiring double-strand breaks or donor DNA templates (Anzalone et al., 2019). This CRISPR technology could be applied to efficiently correct the chr7:116222625T>C enhancer mutation and determine whether it is responsible for the downregulation of *CAV1*. I am planning to pursue this strategy in the future.

6.4.5. Summary

Genetic discoveries in ALS have focused on high effect variants within coding genes in patients with autosomal dominant inheritance. The non-coding genome is thought to contain

missing heritability (Pallares, 2019). A new approach was developed to discover genetic association within gene enhancer-elements. This new methodology successfully identified and validated ALS-associated genetic variation within enhancer and coding regions associated with CAV1, suggesting CAV1 is a new ALS gene.

This work builds upon previous observations that CAV1 function is neuroprotective in neurodegenerative disease (Head et al., 2010, Head et al., 2011) and in ALS in particular (Sawada et al., 2019). Until now, it was not clear whether CAV1 dysfunction was a cause or effect of neuronal toxicity. However, discovery of genetic risk associated with CAV1/CAV2 expression places this pathway upstream in the development of disease. Using patient-derived cells, I have shown that ALS-associated genetic variation within CAV1/CAV2 enhancers reduces the expression of CAV1 and CAV2 and disrupts MLR, which is consistent with impaired neurotrophic signalling and consequently neurodegeneration (Sawada et al., 2019). Moreover, CRISPR/SpCas9 perturbation proximate to this mutation reduced CAV1 and CAV2 expression in human neuronal cells, suggesting that this enhancer-region is functional within the CNS. Future work should investigate CTxB expression in my CRISPR-edited neuronal model to validate the findings in LCLs regarding the role of CAV1/CAV2 on MLR integrity. Data presented in this chapter provide links with my previous work, as both CAV1 and GLT8D1 appear to function prominently in the maintenance of MLR. Together, these results place perturbed ganglioside metabolism upstream in the pathogenesis of ALS (see Chapter 5).

Enhancer function is thought to depend on the binding of TFs (Koch et al., 2011). Current understanding of function within enhancer regions is limited (Levo et al., 2015), in part because of a paucity of variants with validated biological impact. This incomplete understanding is reflected in our failure to link a TF to observed changes in CAV1/CAV2 expression (data not shown). The discovery of ALS-associated CAV1/CAV2 enhancer variations forms a platform for improved understanding of molecular function within these regions. Moreover, the discovery of disease-associated genetic variation is a means of overcoming a reliance on unphysiological *in vitro* assays to understand enhancer biology (Gasperini et al., 2020).

The premise of personalised medicine for complex disease is that gene-environment interactions leading to disease are likely to be heterogeneous (Li et al., 2019). It is possible that in a significant number of ALS patients, genetic mutations leading to reduced CAV1/CAV2 function are a cause of neuronal toxicity. Upregulation of CAV1 is in development as a therapeutic tool (Head et al., 2011) (www.cavogene.com), and data presented here suggest that this could be applied to genetically selected ALS patients in a personalised medicine approach.

Chapter 7. Conclusions and future directions

7.1. Conclusions

ALS is a universally fatal and relatively common neurodegenerative disease. Neurodegenerative diseases exhibit late age of onset and it is therefore reasonable to assume that genetic mutations are upstream in disease pathogenesis. Discovery of genetic variants of ALS have been instrumental in elucidating pathological mechanisms that cause motor neuron loss (Renton et al., 2014). Here I describe the discovery and characterisation of novel ALS-associated genes: *GLT8D1*, *CAV1*, and *CAV2*. This project has focused primarily on the generation of cell and animal models to experimentally evaluate the pathogenicity of discovered variants. *GLT8D1* is part of a large family of proteins called glycosyltransferases, and members of this protein group have been previously implicated in neurodegenerative diseases, including ALS (Ariga, 2014, Dodge et al., 2015). Moreover, I have provided new evidence that genetic mutations within the glycosyltransferase, EOGT, are significantly associated with sALS (Moll et al., 2020). *CAV1* function is already implicated in the pathogenesis of ALS (Sawada et al., 2019), and is currently being developed as a novel ALS therapy (www.cavogene.com).

7.1.1. ALS-associated GLT8D1 mutations act via a dominant-negative mechanism

The majority of this project focused on understanding how newly discovered ALS-associated G78W and R92C variants in *GLT8D1* cause loss of motor neurons, and identifying potential therapeutic targets for neuroprotection. Initially, I engineered plasmid constructs expressing WT and mutant forms of *GLT8D1* for transient overexpression in neuronal and non-neuronal cells. Overexpression of *GLT8D1*-R92C produced the more toxic phenotype in MTT and LDH assays, which is in line with the observed clinical severity. Observed *in vitro* cellular toxicity is still consistent with an age-of-onset disease because my overexpression model does not reflect the physiological expression of mutant *GLT8D1* in the patients. Rather, *GLT8D1*-ALS patients are likely to present with lower levels of the mutant protein, which may be counteracted by homeostatic mechanisms for decades prior to disease onset.

The plasmid constructs expressing FLAG-tagged WT and mutant *GLT8D1* were used to engineer stable isogenic HEK293 cells with tetracycline-inducible expression of *GLT8D1*-WT and *GLT8D1*-R92C. These lines were initially generated for the production of purified

recombinant protein for the assessment of glycosyltransferase function. I hypothesised that the presence of either mutation would impact enzymatic activity, as ALS-linked GLT8D1 mutations cluster proximal to the proposed ligand-binding site (Cooper-Knock et al., 2019). I was the first to publish information regarding the substrate specificity of GLT8D1, and in doing so, I observed a mutation-specific reduction in enzymatic activity with UDP-galactose as the target substrate. I validated my findings following immunoprecipitation of recombinant protein from HEK293 cells transiently transfected with FLAG-tagged GLT8D1-WT, GLT8D1-G78W, and GLT8D1-R92C constructs. Similarly, I observed reductions in enzyme activity for both mutations compared to WT with UDP-galactose as the target substrate, with R92C producing the greater effect. In both instances, reduced enzyme velocity was commensurate with increased substrate affinity, which could impair cycling of the substrate through the enzyme. I propose that higher substrate affinity could cause competitive antagonism of WT function and a dominant negative effect, which would explain why ALS-associated GLT8D1 mutations are autosomal dominant.

Precedence exists for dominant-negative mutations in other ALS-associated genes, notably *TARDBP* and *OPTN* (Shen et al., 2015, Guerrero et al., 2019). I cautiously note the example of *SOD1* mutations that were originally thought to cause ALS through loss-of-function but were subsequently shown to cause a gain-of-function toxicity arising from misfolding of the *SOD1* protein (Boillee et al., 2006). It is possible that G78W and R92C mutations in GLT8D1 increase the proteins' propensity to misfold. My discovery implicates dysregulated glycosyltransferase function in the pathogenesis of ALS, making it an attractive new therapeutic target.

The next stage of the project was to investigate whether GLT8D1 mutations are toxic within a whole organism. Using zebrafish as the model organism, I overexpressed human mutated and WT GLT8D1 mRNA. Whilst embryo survival was unaffected, motor function was specifically impaired in zebrafish larvae expressing either the GLT8D1-R92C or GLT8D1-G78W mutated mRNA at 5dpf. This is consistent with a specific effect on the motor system. Further supporting a role for GLT8D1 in motor function, knockdown of the endogenous *glt8d1* orthologue in zebrafish embryos produced a specific deficit of motor function without observed morphological abnormalities at 5dpf. Overlap between the effects of *glt8d1* knockdown and overexpression of mutated GLT8D1 mRNA is consistent with my proposed dominant-negative mechanism.

7.1.2. *GLT8D1 mutations fragment the Golgi and disrupt ganglioside-containing membrane lipid rafts*

The final stages of my work on GLT8D1 focused on linking discovered mutations to a disease pathway. The most likely candidate was ganglioside metabolism, as various glycosyltransferases are shown to be key modulators of this pathway (Moll et al., 2020). Gangliosides are sialic acid-containing glycosphingolipids that are particularly abundant within the CNS (Vajn et al., 2013). Gangliosides within the CNS are typically synthesized in the ER from a lactosylceramide precursor and are remodelled during transit from the *cis*- to the *trans*-Golgi network by a series of glycosyltransferase enzymes that incorporate galactose and GalNAc groups (Moll et al., 2020). Consistent with a role in this process, GLT8D1 shows prominent CNS expression; moreover, GLT8D1 carries a Golgi localisation signal and is able to accept galactose as a substrate. Mature gangliosides are carried to the cell surface where they function prominently in cell signalling (Yu et al., 2012) as well as enhance neurite outgrowth and survival (Kittaka et al., 2008). Interestingly, autoantibodies against specific gangliosides produce an inflammatory disease of spinal motor neurons known as multifocal motor neuropathy with conduction block (Harschnitz et al., 2014), which is a common differential diagnosis of ALS. Altered levels of gangliosides have been reported in animal models of ALS and in post-mortem CNS tissue from ALS patients (Dodge et al., 2015, Ariga, 2014). The role of gangliosides in maintaining CNS integrity, coupled with various lines of evidence implicating their role in neurodegenerative disease, suggests that dysregulation of this pathway would likely explain the loss of motor neurons in our patient cohort.

I investigated ganglioside expression in stable isogenic HEK293 cells expressing GLT8D1-WT and GLT8D1-R92C, and showed that an R92C mutation reduced the fluorescence intensity of sialic acid marker, WGA, and ganglioside GM1 marker, CTxB, at the plasma membrane. I propose that the reduction in glycosyltransferase activity caused by the GLT8D1 mutations negatively impacts on ganglioside signalling. Gangliosides are important constituents of membrane lipid rafts (MLR), which have a key role in the organisation of cell signalling and neuronal survival. Disrupted MLR are associated with impaired neurotrophic signalling and consequent neurodegeneration (Sawada et al., 2019, Schmick and Bastiaens, 2014). My findings place dysregulated ganglioside metabolism upstream in the pathogenesis of GLT8D1-ALS, and provide justifiable cause to investigate gangliosides, and GM1 in particular, as a potential therapeutic target in patients with ALS-linked GLT8D1 mutations. Indeed, gangliosides have previously been explored as potential therapeutic targets in a variety of neurodegenerative disorders, including ALS (Knight et al., 2015, Schneider et al.,

2015a, Henriques et al., 2017). Future work will focus on confirming whether discovered ALS-associated GLT8D1 mutations do indeed impair neurotrophic signalling and whether this is key to the development of neurodegeneration.

GLT8D1 contains an arginine-lysine motif in its cytoplasmic domain, which likely represents a Golgi localisation signal (Uemura et al., 2015). To test for this, I transiently overexpressed GFP-tagged constructs expressing WT GLT8D1 sequences in HEK293 and N2A cells, and observed localisation to the Golgi network. The presence of G78W or R92C mutations in GLT8D1 did not affect the localisation signal. Glycosyltransferases have previously been shown to influence Golgi architecture (Nilsson et al., 1996, Petrosyan and Cheng, 2013). Moreover, Golgi fragmentation is a well-described feature of neurodegenerative diseases, including ALS, and is associated with the dysregulated trafficking of Golgi secretory proteins (Sundaramoorthy et al., 2015). Based on these lines of evidence, I hypothesised that mutations within GLT8D1 would cause fragmentation of the Golgi network. To investigate this, I stably overexpressed GLT8D1-WT and GLT8D1-R92C in isogenic HEK293 cells and performed immunocytochemistry using *cis*- and *trans*-Golgi markers GM130 and TGN46, respectively. My preliminary data indicate that an R92C mutation causes fragmentation of both the *cis*- and *trans*-Golgi compartments. This result may explain the aforementioned mutation-specific impairment of ganglioside metabolism, as ganglioside biosynthesis is compartmentalised in the Golgi and is organised in distinct units formed by associations of particular glycosyltransferases (Giraud and Maccioni, 2003). Therefore, I propose that fragmentation of the Golgi network may cause dysregulated ganglioside metabolism, both of which may be an upstream cause of impaired glycosyltransferase function. I have summarised my key findings from the experimental evaluation of ALS-associated GLT8D1 mutations in **Figure 7.1**.

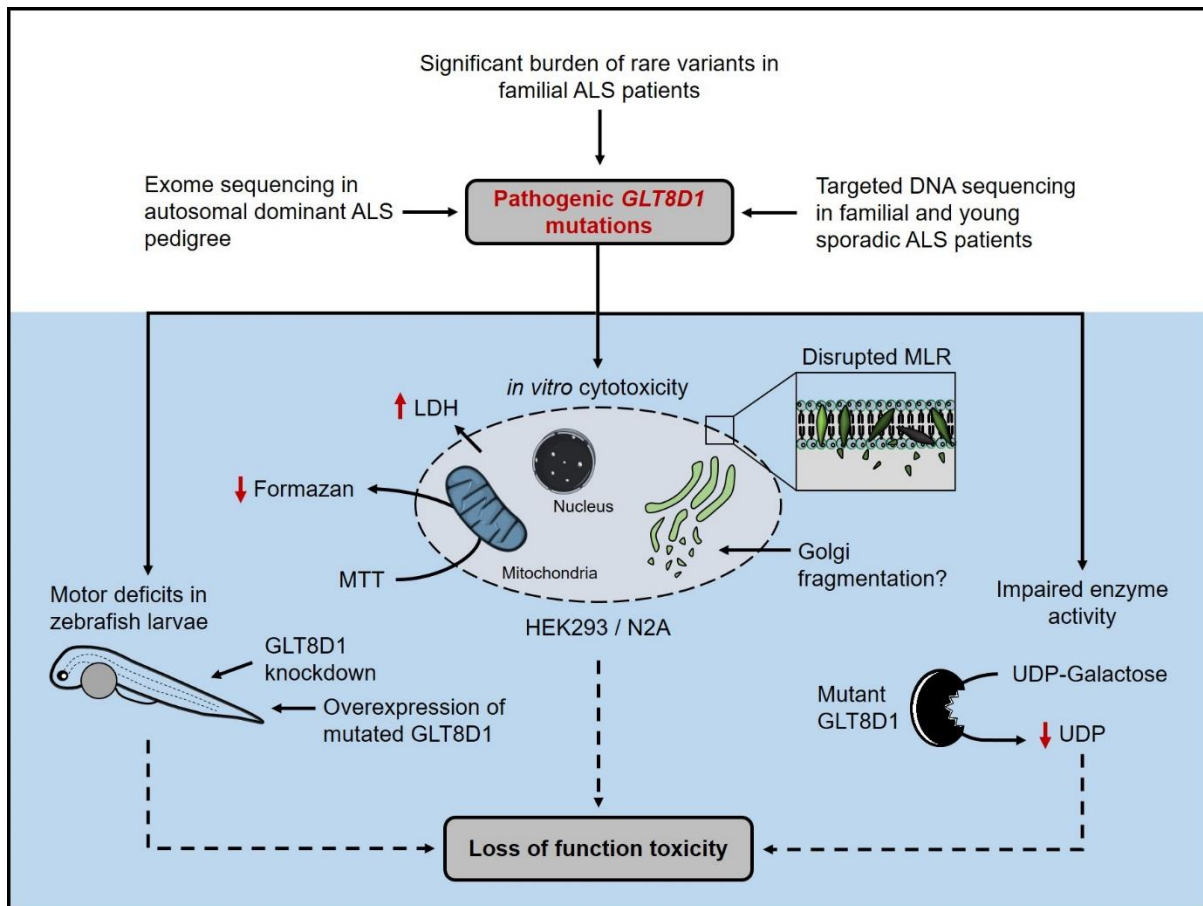


Figure 7.1. Graphical summary of key findings from the characterisation of pathogenic variants in GLT8D1. Exosome sequencing in an autosomal dominant ALS pedigree identified heterozygous p.R92C mutations in GLT8D1 that co-segregate with disease. Targeted sequencing in 103 familial and young sporadic ALS patients from the North of England identified five additional patients with two missense mutations in GLT8D1: p.R92C and p.G78W. Sequencing of an ALS international cohort confirmed significant ALS-association with genetic variation in exon 4 of GLT8D1 in familial ALS patients, including three additional rare deleterious missense mutations. G78W and R92C variants are toxic to HEK293 and N2A cells when overexpressed, and an R92C change disrupts MLR integrity. Preliminary data suggest an R92C mutation causes fragmentation of the Golgi network. Both G78W and R92C mutations in GLT8D1 impair the glycosyltransferase activity of the enzyme. Knockdown of endogenous *glt8d1*, and overexpression of mutant human GLT8D1 mRNA, produces motor deficits in zebrafish larvae 5dpf. These data indicate a loss of function mechanism and a possible dominant negative effect. Figure adapted from (Cooper-Knock et al., 2019).

7.1.3. *CAV1/CAV2 enhancer mutations also disrupt membrane lipid rafts*

The final stage of my project was to investigate novel ALS-associated enhancer variants in *CAV1/CAV2*. *CAV1* and *CAV2* are integral membrane-bound proteins located in the caveolae of the plasma membrane. Together they form a stable hetero-oligomeric complex, suggesting that they are often co-expressed (de Almeida, 2017). *CAV1* functions prominently in neurotrophic signalling, and dysregulated cell signalling has important implications for neuronal cell death (Head et al., 2011, Head et al., 2010, Mandyam et al., 2017). The role of *CAV2* is far less studied than *CAV1* (de Almeida, 2017). Enhancers are non-coding regulatory sequences that modulate expression of target genes through the binding of transcription factors (Koch et al., 2011). Physical interaction between an enhancer and the promoter of the target gene is mediated by DNA looping (Pennacchio et al., 2013).

I investigated two *CAV1/CAV2* enhancer variants in patient-derived LCLs by evaluating the expression of *CAV1* and *CAV2* at the mRNA and protein levels. One of the enhancer mutations (chr7:116222625T>C) correlated with a reduction in the expression of *CAV1* mRNA and protein, as well as a reduction in *CAV2* mRNA. A second enhancer mutation (chr7:115994269:C>T) did not affect the expression of *CAV1* or *CAV2* at either the mRNA or protein level. I speculate that this variant may influence transcription only in CNS cells, or alternatively this variant may be non-functional.

To validate whether the chr7:116222625T>C mutation causes a reduction in *CAV1/CAV2* expression, I utilised CRISPR/Cas9 genome editing to disrupt the WT enhancer in a human neuronal model to place my findings in the context of the CNS. Guide RNAs were designed to specifically target a region proximal to the patient mutation site (~16bp downstream) in SH-SY5Y cells. I demonstrated 72% editing efficiency in immature SH-SY5Y cells via analysis using two similar platforms: TIDE and ICE. CRISPR-edited SH-SY5Y cells were subsequently differentiated into neurons using a previously established method (Forster et al., 2016), and successful differentiation was confirmed through alterations in Pax6 expression and total neurite length, which was quantified through staining with α -tubulin. Fully differentiated neurons showed reductions in *CAV1* and *CAV2* expression at the mRNA level, supporting the above correlation as possible cause that the enhancer is important for *CAV1/CAV2* expression.

The discovery that an enhancer mutation within *CAV1/CAV2* causes downregulation of *CAV1/CAV2* mRNA and protein builds on previous lines of work highlighting *CAV1* as potential therapeutic target for neurodegenerative disease. For example, neuron-specific up-regulation

of CAV1 in the SOD1^{G93A} ALS mouse model has shown to extend survival and improve motor function (Sawada et al., 2019). Up-regulation of CAV1 is also demonstrated to improve cognition and hippocampal plasticity in aged mice, as well as promote axonal and dendritic growth in primary neurons (Head et al., 2011, Head et al., 2010, Mandyam et al., 2017).

As previously mentioned, CAV1 and CAV2 are structural components of caveolae, which are small vesicular invaginations of MLR that are important for signal transduction (Sowa et al., 2001). Therefore, I hypothesised that the observed mutation-specific reduction in CAV1 and CAV2 expression would negatively impact MLR integrity. To test for this, I performed live imaging of ganglioside GM1 using CTxB in patient-derived LCLs as a measure of MLR integrity. I observed a reduction in CTxB expression in the chr7:116222625T>C patient line compared to neurologically normal control patients without a CAV1/CAV2 enhancer variant. Strikingly, CAV1 protein expression was shown to positively correlate with the fluorescence intensity of CTxB, suggesting a direct dependence of CAV1 expression on MLR integrity. Indeed, gangliosides, particularly GM1, are shown to be responsible for the trafficking and maintenance of these caveolae domains (Singh et al., 2010). I propose a convergence between GLT8D1- and CAV-ALS disease pathways via disrupted MLR integrity and subsequently dysregulated neurotrophic signalling.

7.1.4. Identified genetic risk factors converge on disruption of neurotrophic signalling

Neurotrophic factors are endogenous signalling proteins that promote the survival and integrity of specific neuronal populations, as well as stimulating neuronal differentiation (Ekester, 2004). Impaired neurotrophic signalling pathways, and the brain-derived neurotrophic factor (BDNF) signalling pathway in particular, is a well described feature in ALS pathophysiology (Bronfman et al., 2007, Sleight et al., 2019, Pradhan et al., 2019). Various neurotrophic growth factors are shown to promote neuronal survival and stimulate regeneration in the CNS. For example, co-administration of ciliary neurotrophic factor (CNTF) and BDNF in the ALS wobbler mouse was shown to arrest disease progression (Mitsumoto et al., 1994). Moreover, the BDNF agonist, 7,8-dihydroxyflavone, improved motor neuron deficits in SOD1^{G93A} ALS mice (Korkmaz et al., 2014). ALS patient motor neurons express high levels of the BDNF receptor's truncated isoform, TrkB.T1. Targeted deletion of TrkB.T1 has been demonstrated to slow the onset of motor neuron degeneration, as well as delay the development of muscle weakness by 33 days in SOD1^{G93A} ALS mice (Yanpallewar et al., 2012).

Despite these encouraging pre-clinical studies, no neurotrophins have yet succeeded in a clinical phase III trial, possibly due to low blood-brain-barrier penetrance or limited biological half-life (Henriques et al., 2010). Interestingly, the most effective ALS treatment, Riluzole, is an anti-excitotoxic substance that has been demonstrated to stimulate the synthesis of neurotrophins BDNF and GDNF in cultured mouse astrocytes (Mizuta et al., 2001). Indeed, early synaptic hyper-excitability of MNs is thought to enhance BDNF-mediated signalling, thus causing glutamate excitotoxicity, and motor neuron death. Therefore, manipulation of BDNF may provide a viable therapeutic option in the future (Pradhan et al., 2019). My work suggests that this therapy may need to be applied in a personalised fashion to patients with relevant genetic risk.

My work builds upon previous observations that CAV1 function is neuroprotective in neurodegenerative disease (Head et al., 2010) and in ALS in particular (Sawada et al., 2019). Until now, it was not clear whether CAV1 dysfunction was a cause or effect of neuronal toxicity. However, discovery of genetic risk associated with CAV1/CAV2 expression places this pathway upstream in the development of disease. My proposed mechanism of neurodegeneration resulting from ALS-associated CAV1/CAV2 enhancer variants is summarised in **Figure 7.2**.

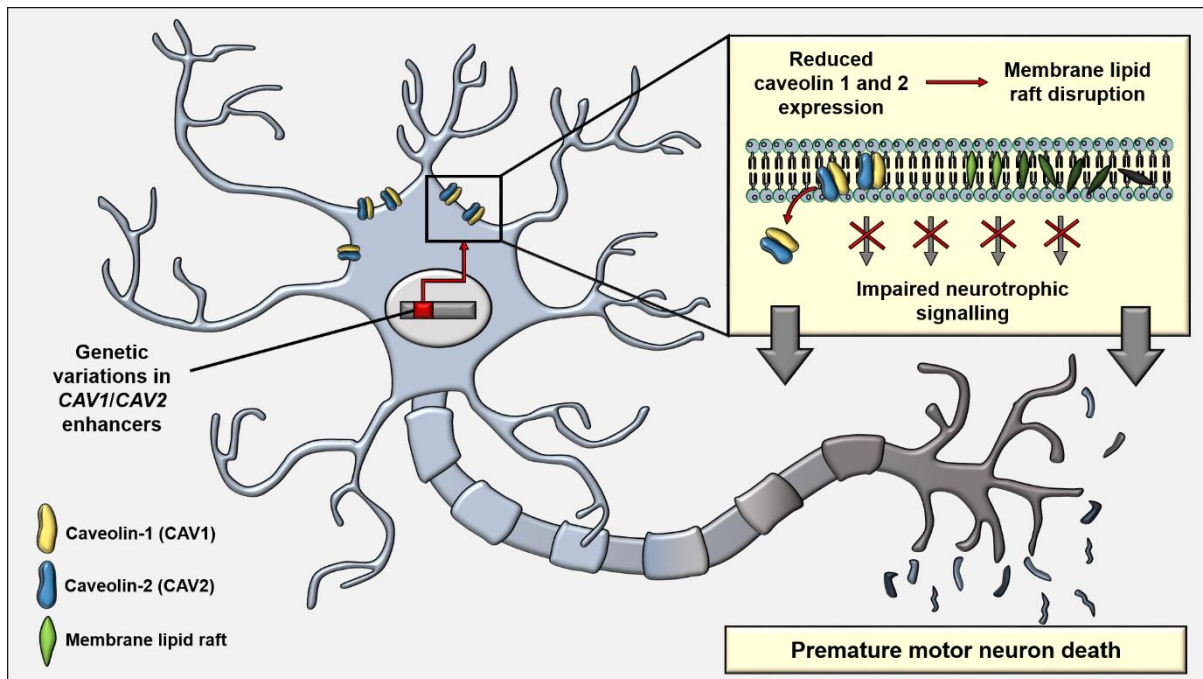


Figure 7.2. Graphical summary of key findings from the characterisation of pathogenic enhancer variants in CAV1 and CAV2, and a proposed ALS disease pathway. A reduction in CAV1/CAV2 expression within neurons may cause disruption of MLR, which leads to impaired neurotrophic signalling and premature motor neuron death.

7.2. Future directions

At present, it is still not fully understood how mutations in the glycosyltransferase domain of GLT8D1 cause ALS. I have suggested that ALS-associated GLT8D1 variants may increase the propensity of the protein to misfold, thus reducing enzymatic activity. Therefore, future work should consider defining the crystal structure of the WT and mutant GLT8D1 protein in order to identify potential mutation-specific structural alterations. With more time, my main focus would be to complete a third biological repeat of the Golgi fragmentation analysis. Indeed, my GLT8D1 *in vitro* data was generated primarily through the use of HEK293 cells, which are useful tools for providing insights into potential pathogenic mechanisms; however, this work requires validation in a neuronal model to place these findings in the context of the CNS. Therefore, I would re-attempt the nucleofection of primary neurons with mutant GLT8D1 constructs for the subsequent assessment of MLR integrity and measurements of neurotrophic signalling.

My zebrafish data suggest that *GLT8D1* is involved in motor system function. However, to fully characterise the effect of mutant *GLT8D1* within a whole organism, future work should aim to create a transgenic zebrafish line using CRISPR/Cas9 genome editing; this technology has developed considerably in the past few years alone. The generation of a transgenic line is important for modelling an age-related disorder such as ALS. Moreover, neuropathological analysis should be performed in this line in order to fully characterise *GLT8D1* as a new ALS gene. Routine neuropathological investigations should include measurements of motor neuron loss, TDP-43 pathology, neuromuscular junction defects, and oxidative stress.

As with any disease-associated genetic discovery, it is extremely important to scan larger patient cohorts to identify additional ALS-linked *GLT8D1* and *CAV1/CAV2* variants, as this would determine the true frequency of the mutations within the population. This search may lead to the discovery of additional patient material such as fibroblasts, which would aid in my previously unsuccessful attempts to generate a co-culture model to address the potential for astrocyte-mediated motor neuron toxicity. If additional fibroblast samples were not obtainable, my focus would be to genetically manipulate control fibroblast lines using CRISPR/Cas9 prior to direct conversion into iNPCs. Recent advancements in this technology such as the CRISPR-prime editing method (Anzalone et al., 2019) would suggest that mutations can be introduced with high precision, and may also be applicable to my proposed *GLT8D1* zebrafish model (Liu et al., 2020a).

In conclusion, ALS is a complex multifactorial disease with several known dysregulated biological pathways. Understanding the various mechanisms involved in the pathogenesis is key to the development of effective treatments. Therefore, effective treatment of the disease will likely require modulation of more than one target, and possibly a personalised medicine approach. Finally, the rapid degeneration of motor neurons in ALS patients suggests that successful early diagnosis is critical in treating the disease effectively, and therefore the development of better biomarkers will be necessary. My work on two new genetic variants discovered using two different methodologies is remarkable in that it converges on a single therapeutic target: neurotrophic signalling via MLR, as summarised in **Figure 7.3**.

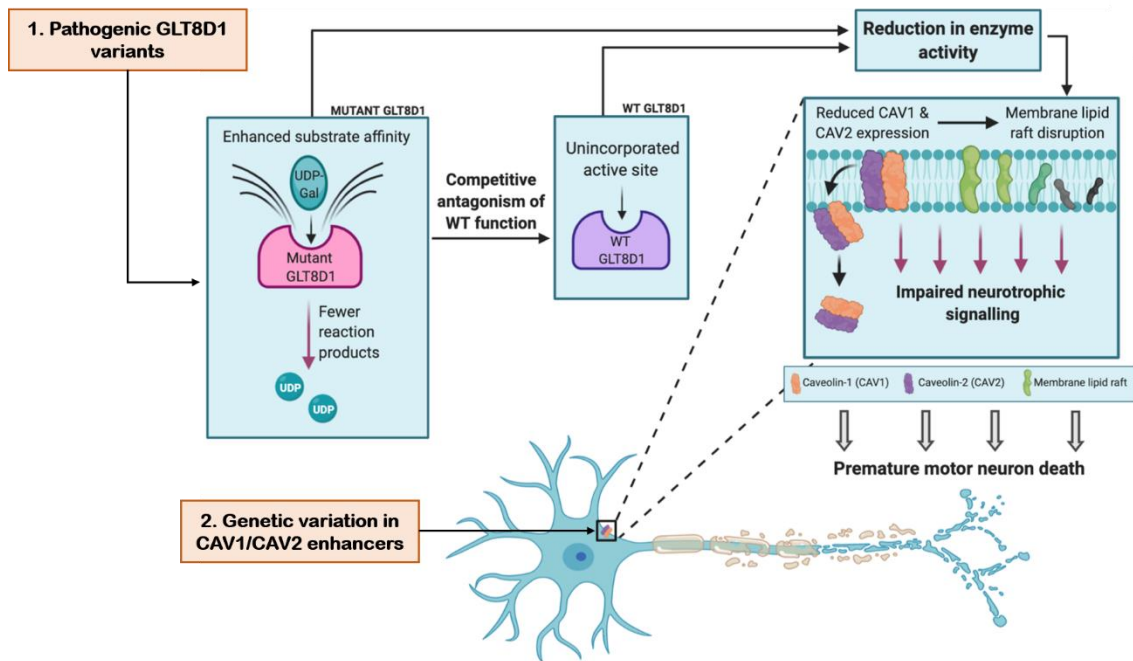


Figure 7.3. ALS-associated GLT8D1 and CAV1/CAV2 enhancer variants likely converge on the same pathological mechanism of disrupted neurotrophic signalling. A reduction in CAV1/CAV2 expression within neurons causes disruption of MLR. Impaired enzyme activity of GLT8D1 is also linked to disruption of MLR. This proposed mechanism would lead to impaired neurotrophic signalling and premature motor neuron death.

References

- ABDEL-KHALIK, J., YUTUC, E., CRICK, P. J., GUSTAFSSON, J. A., WARNER, M., ROMAN, G., TALBOT, K., GRAY, E., GRIFFITHS, W. J., TURNER, M. R. & WANG, Y. 2017. Defective cholesterol metabolism in amyotrophic lateral sclerosis. *J Lipid Res*, 58, 267-278.
- ABE, K., ITOYAMA, Y., SOBUE, G., TSUJI, S., AOKI, M., DOYU, M., HAMADA, C., KONDO, K., YONEOKA, T., AKIMOTO, M., YOSHINO, H. & EDARAVONE, A. L. S. S. G. 2014. Confirmatory double-blind, parallel-group, placebo-controlled study of efficacy and safety of edaravone (MCI-186) in amyotrophic lateral sclerosis patients. *Amyotroph Lateral Scler Frontotemporal Degener*, 15, 610-7.
- ABEL, O., POWELL, J. F., ANDERSEN, P. M. & AL-CHALABI, A. 2012. ALSod: A user-friendly online bioinformatics tool for amyotrophic lateral sclerosis genetics. *Hum Mutat*, 33, 1345-51.
- AGHOLME, L., LINDSTROM, T., KAGEDAL, K., MARCUSSON, J. & HALLBECK, M. 2010. An in vitro model for neuroscience: differentiation of SH-SY5Y cells into cells with morphological and biochemical characteristics of mature neurons. *J Alzheimers Dis*, 20, 1069-82.
- AKASAKO, Y., NARA, K., NAGAI, Y. & HASHIMOTO, Y. 2011. Inhibition of ganglioside synthesis reduces the neuronal survival activity of astrocytes. *Neurosci Lett*, 488, 199-203.
- AKIMOTO, Y., COMER, F. I., COLE, R. N., KUDO, A., KAWAKAMI, H., HIRANO, H. & HART, G. W. 2003. Localization of the O-GlcNAc transferase and O-GlcNAc-modified proteins in rat cerebellar cortex. *Brain Res*, 966, 194-205.
- AL-CHALABI, A., FANG, F., HANBY, M. F., LEIGH, P. N., SHAW, C. E., YE, W. & RIJSDIJK, F. 2010. An estimate of amyotrophic lateral sclerosis heritability using twin data. *J Neurol Neurosurg Psychiatry*, 81, 1324-6.
- AL-CHALABI, A. & HARDIMAN, O. 2013. The epidemiology of ALS: a conspiracy of genes, environment and time. *Nat Rev Neurol*, 9, 617-28.
- AL-CHALABI, A., JONES, A., TROAKES, C., KING, A., AL-SARRAJ, S. & VAN DEN BERG, L. H. 2012. The genetics and neuropathology of amyotrophic lateral sclerosis. *Acta Neuropathol*, 124, 339-52.
- ALAMI, N. H., SMITH, R. B., CARRASCO, M. A., WILLIAMS, L. A., WINBORN, C. S., HAN, S. S. W., KISKINIS, E., WINBORN, B., FREIBAUM, B. D., KANAGARAJ, A., CLARE, A. J., BADDERS, N. M., BILICAN, B., CHAUM, E., CHANDRAN, S., SHAW, C. E., EGGAN, K. C., MANIATIS, T. & TAYLOR, J. P. 2014. Axonal transport of TDP-43 mRNA granules is impaired by ALS-causing mutations. *Neuron*, 81, 536-543.
- ALI, M. F., CHACHADI, V. B., PETROSYAN, A. & CHENG, P. W. 2012. Golgi phosphoprotein 3 determines cell binding properties under dynamic flow by controlling Golgi localization of core 2 N-acetylglucosaminyltransferase 1. *J Biol Chem*, 287, 39564-77.
- ALONSO, A., LOGROSCINO, G., JICK, S. S. & HERNAN, M. A. 2009. Incidence and lifetime risk of motor neuron disease in the United Kingdom: a population-based study. *Eur J Neurol*, 16, 745-51.
- ALRAFIAH, A. R. 2018. From Mouse Models to Human Disease: An Approach for Amyotrophic Lateral Sclerosis. *In Vivo*, 32, 983-998.
- ALTSCHUL, S. F., GISH, W., MILLER, W., MYERS, E. W. & LIPMAN, D. J. 1990. Basic local alignment search tool. *J Mol Biol*, 215, 403-10.
- AMAN, A. T., FRASER, S., MERRITT, E. A., RODIGHERIO, C., KENNY, M., AHN, M., HOL, W. G., WILLIAMS, N. A., LENCER, W. I. & HIRST, T. R. 2001. A mutant cholera toxin B subunit

- that binds GM1- ganglioside but lacks immunomodulatory or toxic activity. *Proc Natl Acad Sci U S A*, 98, 8536-41.
- ANDERSSON, R., GEBHARD, C., MIGUEL-ESCALADA, I., HOOF, I., BORNHOLDT, J., BOYD, M., CHEN, Y., ZHAO, X., SCHMIDL, C., SUZUKI, T., NTINI, E., ARNER, E., VALEN, E., LI, K., SCHWARZFISCHER, L., GLATZ, D., RAITHEL, J., LILJE, B., RAPIN, N., BAGGER, F. O., JORGENSEN, M., ANDERSEN, P. R., BERTIN, N., RACKHAM, O., BURROUGHS, A. M., BAILLIE, J. K., ISHIZU, Y., SHIMIZU, Y., FURUHATA, E., MAEDA, S., NEGISHI, Y., MUNGALL, C. J., MEEHAN, T. F., LASSMANN, T., ITOH, M., KAWAJI, H., KONDO, N., KAWAI, J., LENNARTSSON, A., DAUB, C. O., HEUTINK, P., HUME, D. A., JENSEN, T. H., SUZUKI, H., HAYASHIZAKI, Y., MULLER, F., FORREST, A. R. R., CARNINCI, P., REHLI, M. & SANDELIN, A. 2014. An atlas of active enhancers across human cell types and tissues. *Nature*, 507, 455-461.
- ANDRELL, J. & TATE, C. G. 2013. Overexpression of membrane proteins in mammalian cells for structural studies. *Mol Membr Biol*, 30, 52-63.
- ANZALONE, A. V., RANDOLPH, P. B., DAVIS, J. R., SOUSA, A. A., KOBLAN, L. W., LEVY, J. M., CHEN, P. J., WILSON, C., NEWBY, G. A., RAGURAM, A. & LIU, D. R. 2019. Search-and-replace genome editing without double-strand breaks or donor DNA. *Nature*, 576, 149-157.
- ARGANDA-CARRERAS, I., FERNANDEZ-GONZALEZ, R., MUNOZ-BARRUTIA, A. & ORTIZ-DESOLORZANO, C. 2010. 3D reconstruction of histological sections: Application to mammary gland tissue. *Microsc Res Tech*, 73, 1019-29.
- ARIGA, T. 2014. Pathogenic role of ganglioside metabolism in neurodegenerative diseases. *J Neurosci Res*, 92, 1227-42.
- ARMSTRONG, G. A. & DRAPEAU, P. 2013. Loss and gain of FUS function impair neuromuscular synaptic transmission in a genetic model of ALS. *Hum Mol Genet*, 22, 4282-92.
- ATKIN, J. D., FARG, M. A., SOO, K. Y., WALKER, A. K., HALLORAN, M., TURNER, B. J., NAGLEY, P. & HORNE, M. K. 2014. Mutant SOD1 inhibits ER-Golgi transport in amyotrophic lateral sclerosis. *J Neurochem*, 129, 190-204.
- AUGUSTINSSON, L. E., BLENNOW, K., BLOMSTRAND, C., BRANE, G., EKMAN, R., FREDMAN, P., KARLSSON, I., KIHLGREN, M., LEHMANN, W., LEKMAN, A., MANSSON, J. E., RAMSTROM, I., WALLIN, A., WIKKELSO, C., GOTTFRIES, C. G. & SVENNERHOLM, L. 1997. Intracerebroventricular administration of GM1 ganglioside to presenile Alzheimer patients. *Dement Geriatr Cogn Disord*, 8, 26-33.
- BABIN, P. J., GOIZET, C. & RALDUA, D. 2014. Zebrafish models of human motor neuron diseases: advantages and limitations. *Prog Neurobiol*, 118, 36-58.
- BARBER, S. C., MEAD, R. J. & SHAW, P. J. 2006. Oxidative stress in ALS: a mechanism of neurodegeneration and a therapeutic target. *Biochim Biophys Acta*, 1762, 1051-67.
- BARRIER, L., INGRAND, S., DAMJANAC, M., RIOUX BILAN, A., HUGON, J. & PAGE, G. 2007. Genotype-related changes of ganglioside composition in brain regions of transgenic mouse models of Alzheimer's disease. *Neurobiol Aging*, 28, 1863-72.
- BASNET, R. M., ZIZIOLI, D., TAWEEDET, S., FINAZZI, D. & MEMO, M. 2019. Zebrafish Larvae as a Behavioral Model in Neuropharmacology. *Biomedicines*, 7.
- BEATTIE, C. E., CARREL, T. L. & MCWHORTER, M. L. 2007. Fishing for a mechanism: using zebrafish to understand spinal muscular atrophy. *J Child Neurol*, 22, 995-1003.
- BEDELL, V. M., WESTCOT, S. E. & EKKER, S. C. 2011. Lessons from morpholino-based screening in zebrafish. *Brief Funct Genomics*, 10, 181-8.

- BEER, A. M., COOPER-KNOCK, J., HIGGINBOTTOM, A., HIGHLEY, J. R., WHARTON, S. B., INCE, P. G., MILANO, A., JONES, A. A., AL-CHALABI, A., KIRBY, J. & SHAW, P. J. 2015. Intermediate length C9orf72 expansion in an ALS patient without classical C9orf72 neuropathology. *Amyotroph Lateral Scler Frontotemporal Degener*, 16, 249-51.
- BENATAR, M., WUU, J., ANDERSEN, P. M., LOMBARDI, V. & MALASPINA, A. 2018. Neurofilament light: A candidate biomarker of presymptomatic amyotrophic lateral sclerosis and phenoconversion. *Ann Neurol*, 84, 130-139.
- BILL, B. R., PETZOLD, A. M., CLARK, K. J., SCHIMMENTI, L. A. & EKKER, S. C. 2009. A primer for morpholino use in zebrafish. *Zebrafish*, 6, 69-77.
- BILSLAND, L. G., SAHAI, E., KELLY, G., GOLDING, M., GREENSMITH, L. & SCHIAVO, G. 2010. Deficits in axonal transport precede ALS symptoms in vivo. *Proc Natl Acad Sci U S A*, 107, 20523-8.
- BLOKHUIS, A. M., GROEN, E. J., KOPPERS, M., VAN DEN BERG, L. H. & PASTERKAMP, R. J. 2013. Protein aggregation in amyotrophic lateral sclerosis. *Acta Neuropathol*, 125, 777-94.
- BOILLEE, S., VANDE VELDE, C. & CLEVELAND, D. W. 2006. ALS: a disease of motor neurons and their nonneuronal neighbors. *Neuron*, 52, 39-59.
- BOSIO, A., BINCZEK, E., LE BEAU, M. M., FERNALD, A. A. & STOFFEL, W. 1996. The human gene CGT encoding the UDP-galactose ceramide galactosyl transferase (cerebroside synthase): cloning, characterization, and assignment to human chromosome 4, band q26. *Genomics*, 34, 69-75.
- BOURNE, Y. & HENRISSAT, B. 2001. Glycoside hydrolases and glycosyltransferases: families and functional modules. *Curr Opin Struct Biol*, 11, 593-600.
- BOWLING, A. C., SCHULZ, J. B., BROWN, R. H., JR. & BEAL, M. F. 1993. Superoxide dismutase activity, oxidative damage, and mitochondrial energy metabolism in familial and sporadic amyotrophic lateral sclerosis. *J Neurochem*, 61, 2322-5.
- BOYLAN, K. 2015. Familial Amyotrophic Lateral Sclerosis. *Neurol Clin*, 33, 807-30.
- BRADFORD, Y. M., TORO, S., RAMACHANDRAN, S., RUZICKA, L., HOWE, D. G., EAGLE, A., KALITA, P., MARTIN, R., TAYLOR MOXON, S. A., SCHAPER, K. & WESTERFIELD, M. 2017. Zebrafish Models of Human Disease: Gaining Insight into Human Disease at ZFIN. *ILAR J*, 58, 4-16.
- BRADLEY, J. A. & STROCK, C. J. 2019. Screening for Neurotoxicity with Microelectrode Array. *Curr Protoc Toxicol*, 79, e67.
- BRANDIZZI, F. & BARLOWE, C. 2013. Organization of the ER-Golgi interface for membrane traffic control. *Nat Rev Mol Cell Biol*, 14, 382-92.
- BRETON, C., SNAJDROVA, L., JEANNEAU, C., KOCA, J. & IMBERTY, A. 2006. Structures and mechanisms of glycosyltransferases. *Glycobiology*, 16, 29R-37R.
- BRINKMAN, E. K., CHEN, T., AMENDOLA, M. & VAN STEENSEL, B. 2014. Easy quantitative assessment of genome editing by sequence trace decomposition. *Nucleic Acids Res*, 42, e168.
- BRONFMAN, F. C., ESCUDERO, C. A., WEIS, J. & KRUTTGEN, A. 2007. Endosomal transport of neurotrophins: roles in signaling and neurodegenerative diseases. *Dev Neurobiol*, 67, 1183-203.
- BROUTMAN, G. & BAUDRY, M. 2001. Involvement of the secretory pathway for AMPA receptors in NMDA-induced potentiation in hippocampus. *J Neurosci*, 21, 27-34.
- BURATTI, E. 2015. Functional Significance of TDP-43 Mutations in Disease. *Adv Genet*, 91, 1-53.

- BURATTI, E. & BARALLE, F. E. 2012. TDP-43: gumming up neurons through protein-protein and protein-RNA interactions. *Trends Biochem Sci*, 37, 237-47.
- BURBERRY, A., SUZUKI, N., WANG, J. Y., MOCCIA, R., MORDES, D. A., STEWART, M. H., SUZUKI-UEMATSU, S., GHOSH, S., SINGH, A., MERKLE, F. T., KOSZKA, K., LI, Q. Z., ZON, L., ROSSI, D. J., TROWBRIDGE, J. J., NOTARANGELO, L. D. & EGGAN, K. 2016. Loss-of-function mutations in the C9ORF72 mouse ortholog cause fatal autoimmune disease. *Sci Transl Med*, 8, 347ra93.
- BURKET, C. T., MONTGOMERY, J. E., THUMMEL, R., KASSEN, S. C., LAFAVE, M. C., LANGENAU, D. M., ZON, L. I. & HYDE, D. R. 2008. Generation and characterization of transgenic zebrafish lines using different ubiquitous promoters. *Transgenic Res*, 17, 265-79.
- BUTTI, Z. & PATTEN, S. A. 2018. RNA Dysregulation in Amyotrophic Lateral Sclerosis. *Front Genet*, 9, 712.
- BYRNE, S., HEVERIN, M., ELAMIN, M., WALSH, C. & HARDIMAN, O. 2014. Intermediate repeat expansion length in C9orf72 may be pathological in amyotrophic lateral sclerosis. *Amyotroph Lateral Scler Frontotemporal Degener*, 15, 148-50.
- CAO, J., GUO, S., ARAI, K., LO, E. H. & NING, M. 2013. Studying extracellular signaling utilizing a glycoproteomic approach: lectin blot surveys, a first and important step. *Methods Mol Biol*, 1013, 227-33.
- CHAN, F. K., MORIWAKI, K. & DE ROSA, M. J. 2013. Detection of necrosis by release of lactate dehydrogenase activity. *Methods Mol Biol*, 979, 65-70.
- CHANG, Y., KONG, Q., SHAN, X., TIAN, G., ILIEVA, H., CLEVELAND, D. W., ROTHSTEIN, J. D., BORCHELT, D. R., WONG, P. C. & LIN, C. L. 2008. Messenger RNA oxidation occurs early in disease pathogenesis and promotes motor neuron degeneration in ALS. *PLoS One*, 3, e2849.
- CHEN, G., NING, B. & SHI, T. 2019. Single-Cell RNA-Seq Technologies and Related Computational Data Analysis. *Front Genet*, 10, 317.
- CHEVALLET, M., LUCHE, S. & RABILLOUD, T. 2006. Silver staining of proteins in polyacrylamide gels. *Nat Protoc*, 1, 1852-8.
- CHEW, J., GENDRON, T. F., PRUDENCIO, M., SASAGURI, H., ZHANG, Y. J., CASTANEDES-CASEY, M., LEE, C. W., JANSEN-WEST, K., KURTI, A., MURRAY, M. E., BIENIEK, K. F., BAUER, P. O., WHITELAW, E. C., ROUSSEAU, L., STANKOWSKI, J. N., STETLER, C., DAUGHRITY, L. M., PERKERSON, E. A., DESARO, P., JOHNSTON, A., OVERSTREET, K., EDBAUER, D., RADEMAKERS, R., BOYLAN, K. B., DICKSON, D. W., FRYER, J. D. & PETRUCCELLI, L. 2015. Neurodegeneration. C9ORF72 repeat expansions in mice cause TDP-43 pathology, neuronal loss, and behavioral deficits. *Science*, 348, 1151-4.
- CHINNAPEN, D. J., CHINNAPEN, H., SASLOWSKY, D. & LENCER, W. I. 2007. Rafting with cholera toxin: endocytosis and trafficking from plasma membrane to ER. *FEMS Microbiol Lett*, 266, 129-37.
- CHIO, A., LOGROSCINO, G., TRAYNOR, B. J., COLLINS, J., SIMEONE, J. C., GOLDSTEIN, L. A. & WHITE, L. A. 2013. Global epidemiology of amyotrophic lateral sclerosis: a systematic review of the published literature. *Neuroepidemiology*, 41, 118-30.
- CHIRICOZZI, E., LUNGHI, G., DI BIASE, E., FAZZARI, M., SONNINO, S. & MAURI, L. 2020. GM1 Ganglioside Is A Key Factor in Maintaining the Mammalian Neuronal Functions Avoiding Neurodegeneration. *Int J Mol Sci*, 21.
- CHO, J. H., KIM, J. S., LEE, Y. C., OH, K. B., KWAK, D. H., KIM, W. S., HWANG, S. S., KO, K., CHANG, K. T. AND CHOO, Y. K. 2010. Differential expression patterns of gangliosides in the tissues and cells of NIH-mini pig kidneys. *Animal Cells and Systems*, 14, 7.

- CHOI, B., REMPALA, G. A. & KIM, J. K. 2017. Beyond the Michaelis-Menten equation: Accurate and efficient estimation of enzyme kinetic parameters. *Sci Rep*, 7, 17018.
- CHUH, K. N., BATT, A. R. & PRATT, M. R. 2016. Chemical Methods for Encoding and Decoding of Posttranslational Modifications. *Cell Chem Biol*, 23, 86-107.
- CINGOLANI, P., PLATTS, A., WANG LE, L., COON, M., NGUYEN, T., WANG, L., LAND, S. J., LU, X. & RUDEN, D. M. 2012. A program for annotating and predicting the effects of single nucleotide polymorphisms, SnpEff: SNPs in the genome of *Drosophila melanogaster* strain w1118; iso-2; iso-3. *Fly (Austin)*, 6, 80-92.
- CIRULLI, E. T. & GOLDSTEIN, D. B. 2010. Uncovering the roles of rare variants in common disease through whole-genome sequencing. *Nat Rev Genet*, 11, 415-25.
- CIRULLI, E. T., LASSEIGNE, B. N., PETROVSKI, S., SAPP, P. C., DION, P. A., LEBLOND, C. S., COUTHOUIS, J., LU, Y. F., WANG, Q., KRUEGER, B. J., REN, Z., KEEBLER, J., HAN, Y., LEVY, S. E., BOONE, B. E., WIMBISH, J. R., WAITE, L. L., JONES, A. L., CARULLI, J. P., DAY-WILLIAMS, A. G., STAROPOLI, J. F., XIN, W. W., CHESI, A., RAPHAEL, A. R., MCKENNA-YASEK, D., CADY, J., VIANNEY DE JONG, J. M., KENNA, K. P., SMITH, B. N., TOPP, S., MILLER, J., GKAZI, A., CONSORTIUM, F. S., AL-CHALABI, A., VAN DEN BERG, L. H., VELDINK, J., SILANI, V., TICOZZI, N., SHAW, C. E., BALOH, R. H., APPEL, S., SIMPSON, E., LAGIER-TOURENNE, C., PULST, S. M., GIBSON, S., TROJANOWSKI, J. Q., ELMAN, L., MCCLUSKEY, L., GROSSMAN, M., SHNEIDER, N. A., CHUNG, W. K., RAVITS, J. M., GLASS, J. D., SIMS, K. B., VAN DEERLIN, V. M., MANIATIS, T., HAYES, S. D., ORDUREAU, A., SWARUP, S., LANDERS, J., BAAS, F., ALLEN, A. S., BEDLACK, R. S., HARPER, J. W., GITLER, A. D., ROULEAU, G. A., BROWN, R., HARMS, M. B., COOPER, G. M., HARRIS, T., MYERS, R. M. & GOLDSTEIN, D. B. 2015. Exome sequencing in amyotrophic lateral sclerosis identifies risk genes and pathways. *Science*, 347, 1436-41.
- CIURA, S., LATTANTE, S., LE BER, I., LATOUCHE, M., TOSTIVINT, H., BRICE, A. & KABASHI, E. 2013. Loss of function of C9orf72 causes motor deficits in a zebrafish model of amyotrophic lateral sclerosis. *Ann Neurol*, 74, 180-7.
- CLIFT, D., RICHENDRER, H., THORN, R. J., COLWILL, R. M. & CRETON, R. 2014. High-throughput analysis of behavior in zebrafish larvae: effects of feeding. *Zebrafish*, 11, 455-61.
- COETZEE, T., FUJITA, N., DUPREE, J., SHI, R., BLIGHT, A., SUZUKI, K., SUZUKI, K. & POPKO, B. 1996. Myelination in the absence of galactocerebroside and sulfatide: normal structure with abnormal function and regional instability. *Cell*, 86, 209-19.
- COLWILL, R. M. & CRETON, R. 2011. Locomotor behaviors in zebrafish (*Danio rerio*) larvae. *Behav Processes*, 86, 222-9.
- CONG, L., RAN, F. A., COX, D., LIN, S., BARRETTO, R., HABIB, N., HSU, P. D., WU, X., JIANG, W., MARRAFFINI, L. A. & ZHANG, F. 2013. Multiplex genome engineering using CRISPR/Cas systems. *Science*, 339, 819-23.
- COOPER-KNOCK, J., HEWITT, C., HIGHLEY, J. R., BROCKINGTON, A., MILANO, A., MAN, S., MARTINDALE, J., HARTLEY, J., WALSH, T., GELSTHORPE, C., BAXTER, L., FORSTER, G., FOX, M., BURY, J., MOK, K., MCDERMOTT, C. J., TRAYNOR, B. J., KIRBY, J., WHARTON, S. B., INCE, P. G., HARDY, J. & SHAW, P. J. 2012. Clinico-pathological features in amyotrophic lateral sclerosis with expansions in C9ORF72. *Brain*, 135, 751-64.
- COOPER-KNOCK, J., MOLL, T., RAMESH, T., CASTELLI, L., BEER, A., ROBINS, H., FOX, I., NIEDERMOSER, I., VAN DAMME, P., MOISSE, M., ROBBERECHT, W., HARDIMAN, O., PANADES, M. P., ASSIALIOUI, A., MORA, J. S., BASAK, A. N., MORRISON, K. E., SHAW, C. E., AL-CHALABI, A., LANDERS, J. E., WYLES, M., HEATH, P. R., HIGGINBOTTOM, A.,

- WALSH, T., KAZOKA, M., MCDERMOTT, C. J., HAUTBERGUE, G. M., KIRBY, J. & SHAW, P. J. 2019. Mutations in the Glycosyltransferase Domain of GLT8D1 Are Associated with Familial Amyotrophic Lateral Sclerosis. *Cell Rep*, 26, 2298-2306 e5.
- COOPER-KNOCK, J., SHAW, P. J. & KIRBY, J. 2014. The widening spectrum of C9ORF72-related disease; genotype/phenotype correlations and potential modifiers of clinical phenotype. *Acta Neuropathol*, 127, 333-45.
- COREY, D. R. & ABRAMS, J. M. 2001. Morpholino antisense oligonucleotides: tools for investigating vertebrate development. *Genome Biol*, 2, REVIEWS1015.
- COUMANS, J. V., GAU, D., POLJAK, A., WASINGER, V., ROY, P. & MOENS, P. 2014. Green fluorescent protein expression triggers proteome changes in breast cancer cells. *Exp Cell Res*, 320, 33-45.
- COZZOLINO, M. & CARRI, M. T. 2012. Mitochondrial dysfunction in ALS. *Prog Neurobiol*, 97, 54-66.
- CRESPO, P. M., VON MUHLINEN, N., IGLESIAS-BARTOLOME, R. & DANIOTTI, J. L. 2008. Complex gangliosides are apically sorted in polarized MDCK cells and internalized by clathrin-independent endocytosis. *FEBS J*, 275, 6043-56.
- CROW, J. P., YE, Y. Z., STRONG, M., KIRK, M., BARNES, S. & BECKMAN, J. S. 1997. Superoxide dismutase catalyzes nitration of tyrosines by peroxynitrite in the rod and head domains of neurofilament-L. *J Neurochem*, 69, 1945-53.
- DA COSTA, M. M., ALLEN, C. E., HIGGINBOTTOM, A., RAMESH, T., SHAW, P. J. & MCDERMOTT, C. J. 2014. A new zebrafish model produced by TILLING of SOD1-related amyotrophic lateral sclerosis replicates key features of the disease and represents a tool for in vivo therapeutic screening. *Dis Model Mech*, 7, 73-81.
- DA CRUZ, S., BUI, A., SABERI, S., LEE, S. K., STAUFFER, J., MCALONIS-DOWNES, M., SCHULTE, D., PIZZO, D. P., PARONE, P. A., CLEVELAND, D. W. & RAVITS, J. 2017. Misfolded SOD1 is not a primary component of sporadic ALS. *Acta Neuropathol*, 134, 97-111.
- DAL CANTO, M. C. & GURNEY, M. E. 1994. Development of central nervous system pathology in a murine transgenic model of human amyotrophic lateral sclerosis. *Am J Pathol*, 145, 1271-9.
- DE ALMEIDA, C. J. G. 2017. Caveolin-1 and Caveolin-2 Can Be Antagonistic Partners in Inflammation and Beyond. *Front Immunol*, 8, 1530.
- DE ARAUJO, M. E. & HUBER, L. A. 2007. Subcellular fractionation. *Methods Mol Biol*, 357, 73-85.
- DE CONTI, L., AKINYI, M. V., MENDOZA-MALDONADO, R., ROMANO, M., BARALLE, M. & BURATTI, E. 2015. TDP-43 affects splicing profiles and isoform production of genes involved in the apoptotic and mitotic cellular pathways. *Nucleic Acids Res*, 43, 8990-9005.
- DE LOS MILAGROS BASSANI MOLINAS, M., BEER, C., HESSE, F., WIRTH, M. & WAGNER, R. 2014. Optimizing the transient transfection process of HEK-293 suspension cells for protein production by nucleotide ratio monitoring. *Cytotechnology*, 66, 493-514.
- DE VOS, K. J., CHAPMAN, A. L., TENNANT, M. E., MANSER, C., TUDOR, E. L., LAU, K. F., BROWNLEES, J., ACKERLEY, S., SHAW, P. J., MCLOUGHLIN, D. M., SHAW, C. E., LEIGH, P. N., MILLER, C. C. J. & GRIERSON, A. J. 2007. Familial amyotrophic lateral sclerosis-linked SOD1 mutants perturb fast axonal transport to reduce axonal mitochondria content. *Hum Mol Genet*, 16, 2720-2728.
- DE VOS, K. J., GRIERSON, A. J., ACKERLEY, S. & MILLER, C. C. 2008. Role of axonal transport in neurodegenerative diseases. *Annu Rev Neurosci*, 31, 151-73.

- DEJESUS-HERNANDEZ, M., MACKENZIE, I. R., BOEVE, B. F., BOXER, A. L., BAKER, M., RUTHERFORD, N. J., NICHOLSON, A. M., FINCH, N. A., FLYNN, H., ADAMSON, J., KOURI, N., WOJTAS, A., SENGDY, P., HSIUNG, G. Y., KARYDAS, A., SEELEY, W. W., JOSEPHS, K. A., COPPOLA, G., GESCHWIND, D. H., WSZOLEK, Z. K., FELDMAN, H., KNOPMAN, D. S., PETERSEN, R. C., MILLER, B. L., DICKSON, D. W., BOYLAN, K. B., GRAFF-RADFORD, N. R. & RADEMAKERS, R. 2011. Expanded GGGGCC hexanucleotide repeat in noncoding region of C9ORF72 causes chromosome 9p-linked FTD and ALS. *Neuron*, 72, 245-56.
- DEL TORO, D., ALBERCH, J., LAZARO-DIEGUEZ, F., MARTIN-IBANEZ, R., XIFRO, X., EGEEA, G. & CANALS, J. M. 2009. Mutant huntingtin impairs post-Golgi trafficking to lysosomes by delocalizing optineurin/Rab8 complex from the Golgi apparatus. *Mol Biol Cell*, 20, 1478-92.
- DENG, H., GAO, K. & JANKOVIC, J. 2014a. The role of FUS gene variants in neurodegenerative diseases. *Nat Rev Neurol*, 10, 337-48.
- DENG, Q., HOLLER, C. J., TAYLOR, G., HUDSON, K. F., WATKINS, W., GEARING, M., ITO, D., MURRAY, M. E., DICKSON, D. W., SEYFRIED, N. T. & KUKAR, T. 2014b. FUS is phosphorylated by DNA-PK and accumulates in the cytoplasm after DNA damage. *J Neurosci*, 34, 7802-13.
- DESPLATS, P. A., DENNY, C. A., KASS, K. E., GILMARTIN, T., HEAD, S. R., SUTCLIFFE, J. G., SEYFRIED, T. N. & THOMAS, E. A. 2007. Glycolipid and ganglioside metabolism imbalances in Huntington's disease. *Neurobiol Dis*, 27, 265-77.
- DESPOINT, J. C., TORNAY, F., LACOSTE, M., PREUX, P. M. & COURATIER, P. 2005. Hypermetabolism in ALS: correlations with clinical and paraclinical parameters. *Neurodegener Dis*, 2, 202-7.
- DESSAU, M. A. & MODIS, Y. 2011. Protein crystallization for X-ray crystallography. *J Vis Exp*.
- DI GIORGIO, F. P., CARRASCO, M. A., SIAO, M. C., MANIATIS, T. & EGGAN, K. 2007. Non-cell autonomous effect of glia on motor neurons in an embryonic stem cell-based ALS model. *Nat Neurosci*, 10, 608-14.
- DODGE, J. C., TRELEAVEN, C. M., PACHECO, J., COOPER, S., BAO, C., ABRAHAM, M., CROMWELL, M., SARDI, S. P., CHUANG, W. L., SIDMAN, R. L., CHENG, S. H. & SHIHABUDDIN, L. S. 2015. Glycosphingolipids are modulators of disease pathogenesis in amyotrophic lateral sclerosis. *Proc Natl Acad Sci U S A*, 112, 8100-5.
- DONNELLY, C. J., ZHANG, P. W., PHAM, J. T., HAEUSLER, A. R., MISTRY, N. A., VIDENSKY, S., DALEY, E. L., POTH, E. M., HOOVER, B., FINES, D. M., MARAGAKIS, N., TIENARI, P. J., PETRUCCELLI, L., TRAYNOR, B. J., WANG, J., RIGO, F., BENNETT, C. F., BLACKSHAW, S., SATTLER, R. & ROTHSTEIN, J. D. 2013. RNA toxicity from the ALS/FTD C9ORF72 expansion is mitigated by antisense intervention. *Neuron*, 80, 415-28.
- DORST, J., KUHNLEIN, P., HENDRICH, C., KASSUBEK, J., SPERFELD, A. D. & LUDOLPH, A. C. 2011. Patients with elevated triglyceride and cholesterol serum levels have a prolonged survival in amyotrophic lateral sclerosis. *J Neurol*, 258, 613-7.
- DRAB, M., VERKADE, P., ELGER, M., KASPER, M., LOHN, M., LAUTERBACH, B., MENNE, J., LINDSCHAU, C., MENDE, F., LUFT, F. C., SCHEDL, A., HALLER, H. & KURZCHALIA, T. V. 2001. Loss of caveolae, vascular dysfunction, and pulmonary defects in caveolin-1 gene-disrupted mice. *Science*, 293, 2449-52.
- DUAN, W., LI, X., SHI, J., GUO, Y., LI, Z. & LI, C. 2010. Mutant TAR DNA-binding protein-43 induces oxidative injury in motor neuron-like cell. *Neuroscience*, 169, 1621-9.
- DUPUIS, L., CORCIA, P., FERGANI, A., GONZALEZ DE AGUILAR, J. L., BONNEFONT-ROUSSELOT, D., BITTAR, R., SEILHEAN, D., HAUW, J. J., LACOMBLEZ, L., LOEFFLER, J. P. &

- MEININGER, V. 2008. Dyslipidemia is a protective factor in amyotrophic lateral sclerosis. *Neurology*, 70, 1004-9.
- EISEN, J. S. & SMITH, J. C. 2008. Controlling morpholino experiments: don't stop making antisense. *Development*, 135, 1735-43.
- EKESTERN, E. 2004. Neurotrophic factors and amyotrophic lateral sclerosis. *Neurodegener Dis*, 1, 88-100.
- ELGAR, G. & VAVOURI, T. 2008. Tuning in to the signals: noncoding sequence conservation in vertebrate genomes. *Trends Genet*, 24, 344-52.
- ENGLANDER, S. W. & MAYNE, L. 2014. The nature of protein folding pathways. *Proc Natl Acad Sci U S A*, 111, 15873-80.
- FALLINI, C., BASSELL, G. J. & ROSSOLL, W. 2012. The ALS disease protein TDP-43 is actively transported in motor neuron axons and regulates axon outgrowth. *Hum Mol Genet*, 21, 3703-18.
- FAN, W., CHANG, S., SHAN, X., GAO, D., ZHANG, S. Q., ZHANG, J., JIANG, N., MA, D. & MAO, Z. 2016. Transcriptional profile of SH-SY5Y human neuroblastoma cells transfected by Toxoplasma rhoptry protein 16. *Mol Med Rep*, 14, 4099-4108.
- FENG, Y., YAN, T., ZHENG, J., GE, X., MU, Y., ZHANG, Y., WU, D., DU, J. L. & ZHAI, Q. 2010. Overexpression of Wld(S) or Nmnat2 in mauthner cells by single-cell electroporation delays axon degeneration in live zebrafish. *J Neurosci Res*, 88, 3319-27.
- FERNANDEZ-PATRON, C., CASTELLANOS-SERRA, L., HARDY, E., GUERRA, M., ESTEVEZ, E., MEHL, E. & FRANK, R. W. 1998. Understanding the mechanism of the zinc-ion stains of biomacromolecules in electrophoresis gels: generalization of the reverse-staining technique. *Electrophoresis*, 19, 2398-406.
- FERNANDEZ-PEREZ, E. J., SEPULVEDA, F. J., PEOPLES, R. & AGUAYO, L. G. 2017. Role of membrane GM1 on early neuronal membrane actions of Abeta during onset of Alzheimer's disease. *Biochim Biophys Acta Mol Basis Dis*, 1863, 3105-3116.
- FERRANTE, R. J., BROWNE, S. E., SHINOBU, L. A., BOWLING, A. C., BAIK, M. J., MACGARVEY, U., KOWALL, N. W., BROWN, R. H., JR. & BEAL, M. F. 1997. Evidence of increased oxidative damage in both sporadic and familial amyotrophic lateral sclerosis. *J Neurochem*, 69, 2064-74.
- FERRARI, R., KAPOGIANNIS, D., HUEY, E. D. & MOMENI, P. 2011. FTD and ALS: a tale of two diseases. *Curr Alzheimer Res*, 8, 273-94.
- FERRI, A., COZZOLINO, M., CROSIO, C., NENCINI, M., CASCIATI, A., GRALLA, E. B., ROTILIO, G., VALENTINE, J. S. & CARRI, M. T. 2006. Familial ALS-superoxide dismutases associate with mitochondria and shift their redox potentials. *Proc Natl Acad Sci U S A*, 103, 13860-5.
- FILOUS, A. R. & SILVER, J. 2016. Neurite Outgrowth Assay. *Bio Protoc*, 6.
- FISHILEVICH, S., NUDEL, R., RAPPAPORT, N., HADAR, R., PLASCHKES, I., INY STEIN, T., ROSEN, N., KOHN, A., TWIK, M., SAFRAN, M., LANCET, D. & COHEN, D. 2017. GeneHancer: genome-wide integration of enhancers and target genes in GeneCards. *Database (Oxford)*, 2017.
- FLICKER, C., FERRIS, S. H., KALKSTEIN, D. & SERBY, M. 1994. A double-blind, placebo-controlled crossover study of ganglioside GM1 treatment for Alzheimer's disease. *Am J Psychiatry*, 151, 126-9.
- FONTAINE, E., LENTINK, D., KRANENBARG, S., MULLER, U. K., VAN LEEUWEN, J. L., BARR, A. H. & BURDICK, J. W. 2008. Automated visual tracking for studying the ontogeny of zebrafish swimming. *J Exp Biol*, 211, 1305-16.

- FORSTER, J. I., KOGLSBERGER, S., TREFOIS, C., BOYD, O., BAUMURATOV, A. S., BUCK, L., BALLING, R. & ANTONY, P. M. 2016. Characterization of Differentiated SH-SY5Y as Neuronal Screening Model Reveals Increased Oxidative Vulnerability. *J Biomol Screen*, 21, 496-509.
- FOTAKIS, G. & TIMBRELL, J. A. 2006. In vitro cytotoxicity assays: comparison of LDH, neutral red, MTT and protein assay in hepatoma cell lines following exposure to cadmium chloride. *Toxicol Lett*, 160, 171-7.
- FREISCHMIDT, A., WIELAND, T., RICHTER, B., RUF, W., SCHAEFFER, V., MULLER, K., MARROQUIN, N., NORDIN, F., HUBERS, A., WEYDT, P., PINTO, S., PRESS, R., MILLECAMPS, S., MOLKO, N., BERNARD, E., DESNUELLE, C., SORIANI, M. H., DORST, J., GRAF, E., NORDSTROM, U., FEILER, M. S., PUTZ, S., BOECKERS, T. M., MEYER, T., WINKLER, A. S., WINKELMAN, J., DE CARVALHO, M., THAL, D. R., OTTO, M., BRANNSTROM, T., VOLK, A. E., KURSULA, P., DANZER, K. M., LICHTNER, P., DIKIC, I., MEITINGER, T., LUDOLPH, A. C., STROM, T. M., ANDERSEN, P. M. & WEISHAUPT, J. H. 2015. Haploinsufficiency of TBK1 causes familial ALS and fronto-temporal dementia. *Nat Neurosci*, 18, 631-6.
- FRENKEL-PINTER, M., SHMUELI, M. D., RAZ, C., YANKU, M., ZILBERZWIGE, S., GAZIT, E. & SEGAL, D. 2017. Interplay between protein glycosylation pathways in Alzheimer's disease. *Sci Adv*, 3, e1601576.
- FREY, S. L. & LEE, K. Y. 2013. Number of sialic acid residues in ganglioside headgroup affects interactions with neighboring lipids. *Biophys J*, 105, 1421-31.
- FUJINAGA, Y., WOLF, A. A., RODIGHIERO, C., WHEELER, H., TSAI, B., ALLEN, L., JOBLING, M. G., RAPOPORT, T., HOLMES, R. K. & LENCER, W. I. 2003. Gangliosides that associate with lipid rafts mediate transport of cholera and related toxins from the plasma membrane to endoplasmic reticulum. *Mol Biol Cell*, 14, 4783-93.
- FUJITA, K., YAMAUCHI, M., SHIBAYAMA, K., ANDO, M., HONDA, M. & NAGATA, Y. 1996. Decreased cytochrome c oxidase activity but unchanged superoxide dismutase and glutathione peroxidase activities in the spinal cords of patients with amyotrophic lateral sclerosis. *J Neurosci Res*, 45, 276-81.
- FUJITA, Y., MIZUNO, Y., TAKATAMA, M. & OKAMOTO, K. 2008. Anterior horn cells with abnormal TDP-43 immunoreactivities show fragmentation of the Golgi apparatus in ALS. *J Neurol Sci*, 269, 30-4.
- FUJITA, Y., OHAMA, E., TAKATAMA, M., AL-SARRAJ, S. & OKAMOTO, K. 2006. Fragmentation of Golgi apparatus of nigral neurons with alpha-synuclein-positive inclusions in patients with Parkinson's disease. *Acta Neuropathol*, 112, 261-5.
- FUJITA, Y., OKAMOTO, K., SAKURAI, A., AMARI, M., NAKAZATO, Y. & GONATAS, N. K. 1999. Fragmentation of the Golgi apparatus of Betz cells in patients with amyotrophic lateral sclerosis. *J Neurol Sci*, 163, 81-5.
- FUJITA, Y., OKAMOTO, K., SAKURAI, A., GONATAS, N. K. & HIRANO, A. 2000. Fragmentation of the Golgi apparatus of the anterior horn cells in patients with familial amyotrophic lateral sclerosis with SOD1 mutations and posterior column involvement. *J Neurol Sci*, 174, 137-40.
- FUJIWARA, T., KANAZAWA, S., ICHIBORI, R., TANIGAWA, T., MAGOME, T., SHINGAKI, K., MIYATA, S., TOHYAMA, M. & HOSOKAWA, K. 2014. L-arginine stimulates fibroblast proliferation through the GPRC6A-ERK1/2 and PI3K/Akt pathway. *PLoS One*, 9, e92168.

- GAJ, T., OJALA, D. S., EKMAN, F. K., BYRNE, L. C., LIMSIRICHAJ, P. & SCHAFFER, D. V. 2017. In vivo genome editing improves motor function and extends survival in a mouse model of ALS. *Sci Adv*, 3, eaar3952.
- GARNHAM, R., SCOTT, E., LIVERMORE, K. E. & MUNKLEY, J. 2019. ST6GAL1: A key player in cancer. *Oncol Lett*, 18, 983-989.
- GASPERINI, M., TOME, J. M. & SHENDURE, J. 2020. Towards a comprehensive catalogue of validated and target-linked human enhancers. *Nat Rev Genet*, 21, 292-310.
- GAUDREAU, S. B., BLAIN, J. F., GRATTON, J. P. & POIRIER, J. 2005. A role for caveolin-1 in post-injury reactive neuronal plasticity. *J Neurochem*, 92, 831-9.
- GENDRON, T. F., BIENIEK, K. F., ZHANG, Y. J., JANSEN-WEST, K., ASH, P. E., CAULFIELD, T., DAUGHRITY, L., DUNMORE, J. H., CASTANEDAS-CASEY, M., CHEW, J., COSIO, D. M., VAN BLITTERSWIJK, M., LEE, W. C., RADEMAKERS, R., BOYLAN, K. B., DICKSON, D. W. & PETRUCELLI, L. 2013. Antisense transcripts of the expanded C9ORF72 hexanucleotide repeat form nuclear RNA foci and undergo repeat-associated non-ATG translation in c9FTD/ALS. *Acta Neuropathol*, 126, 829-44.
- GINALSKI, K., GRISHIN, N. V., GODZIK, A. & RYCHLEWSKI, L. 2005. Practical lessons from protein structure prediction. *Nucleic Acids Res*, 33, 1874-91.
- GIRAUDO, C. G. & MACCIONI, H. J. 2003. Endoplasmic reticulum export of glycosyltransferases depends on interaction of a cytoplasmic dibasic motif with Sar1. *Mol Biol Cell*, 14, 3753-66.
- GLICK, D., BARTH, S. & MACLEOD, K. F. 2010. Autophagy: cellular and molecular mechanisms. *J Pathol*, 221, 3-12.
- GONATAS, N. K., STIEBER, A. & GONATAS, J. O. 2006. Fragmentation of the Golgi apparatus in neurodegenerative diseases and cell death. *J Neurol Sci*, 246, 21-30.
- GONATAS, N. K., STIEBER, A., MOURELATOS, Z., CHEN, Y., GONATAS, J. O., APPEL, S. H., HAYS, A. P., HICKEY, W. F. & HAUW, J. J. 1992. Fragmentation of the Golgi apparatus of motor neurons in amyotrophic lateral sclerosis. *Am J Pathol*, 140, 731-7.
- GORDON, J., AMINI, S. & WHITE, M. K. 2013. General overview of neuronal cell culture. *Methods Mol Biol*, 1078, 1-8.
- GORDON, P. H. 2013. Amyotrophic Lateral Sclerosis: An update for 2013 Clinical Features, Pathophysiology, Management and Therapeutic Trials. *Aging Dis*, 4, 295-310.
- GOSAVI, N., LEE, H. J., LEE, J. S., PATEL, S. & LEE, S. J. 2002. Golgi fragmentation occurs in the cells with prefibrillar alpha-synuclein aggregates and precedes the formation of fibrillar inclusion. *J Biol Chem*, 277, 48984-92.
- GOTHAM, S. M., FRYER, P. J. & PATERSON, W. R. 1988. The measurement of insoluble proteins using a modified Bradford assay. *Anal Biochem*, 173, 353-8.
- GROSSKREUTZ, J., VAN DEN BOSCH, L. & KELLER, B. U. 2010. Calcium dysregulation in amyotrophic lateral sclerosis. *Cell Calcium*, 47, 165-74.
- GRUNWALD, D. J. & EISEN, J. S. 2002. Headwaters of the zebrafish -- emergence of a new model vertebrate. *Nat Rev Genet*, 3, 717-24.
- GUEGAN, C. & PRZEDBORSKI, S. 2003. Programmed cell death in amyotrophic lateral sclerosis. *J Clin Invest*, 111, 153-61.
- GUERRERO, E. N., MITRA, J., WANG, H., RANGASWAMY, S., HEGDE, P. M., BASU, P., RAO, K. S. & HEGDE, M. L. 2019. Amyotrophic lateral sclerosis-associated TDP-43 mutation Q331K prevents nuclear translocation of XRCC4-DNA ligase 4 complex and is linked to genome damage-mediated neuronal apoptosis. *Hum Mol Genet*, 28, 3161-3162.

- GUNDOGDU, M., LLABRES, S., GORELIK, A., FERENBACH, A. T., ZACHARIAE, U. & VAN AALTEN, D. M. F. 2018. The O-GlcNAc Transferase Intellectual Disability Mutation L254F Distorts the TPR Helix. *Cell Chem Biol*, 25, 513-518 e4.
- GUO, B., PEARCE, A. G., TRAUlsen, K. E., RINTALA, A. C. & LEE, H. 2001. Fluorescence produced by transfection reagents can be confused with green fluorescent proteins in mammalian cells. *Biotechniques*, 31, 314-6, 318, 320-1.
- GURNEY, M. E., PU, H., CHIU, A. Y., DAL CANTO, M. C., POLCHOW, C. Y., ALEXANDER, D. D., CALIENDO, J., HENTATI, A., KWON, Y. W., DENG, H. X. & ET AL. 1994. Motor neuron degeneration in mice that express a human Cu,Zn superoxide dismutase mutation. *Science*, 264, 1772-5.
- GUSEL'NIKOVA, V. V. & KORZHEVSKIY, D. E. 2015. NeuN As a Neuronal Nuclear Antigen and Neuron Differentiation Marker. *Acta Naturae*, 7, 42-7.
- GYLYS, K. H., FEIN, J. A., YANG, F., MILLER, C. A. & COLE, G. M. 2007. Increased cholesterol in Abeta-positive nerve terminals from Alzheimer's disease cortex. *Neurobiol Aging*, 28, 8-17.
- HAAPANIEMI, E., BOTLA, S., PERSSON, J., SCHMIERER, B. & TAIPALE, J. 2018. CRISPR-Cas9 genome editing induces a p53-mediated DNA damage response. *Nat Med*, 24, 927-930.
- HAEUSSLER, M., SCHONIG, K., ECKERT, H., ESCHSTRUTH, A., MIANNE, J., RENAUD, J. B., SCHNEIDER-MAUNOURY, S., SHKUMATAVA, A., TEBOUL, L., KENT, J., JOLY, J. S. & CONCORDET, J. P. 2016. Evaluation of off-target and on-target scoring algorithms and integration into the guide RNA selection tool CRISPOR. *Genome Biol*, 17, 148.
- HAIDET-PHILLIPS, A. M., HESTER, M. E., MIRANDA, C. J., MEYER, K., BRAUN, L., FRAKES, A., SONG, S., LIKHTE, S., MURTHA, M. J., FOUST, K. D., RAO, M., EAGLE, A., KAMMESHEIDT, A., CHRISTENSEN, A., MENDELL, J. R., BURGHEs, A. H. & KASPAR, B. K. 2011. Astrocytes from familial and sporadic ALS patients are toxic to motor neurons. *Nat Biotechnol*, 29, 824-8.
- HALLORAN, M., RAGAGNIN, A. M. G., VIDAL, M., PARAKH, S., YANG, S., HENG, B., GRIMA, N., SHAHHEYDARI, H., SOO, K. Y., BLAIR, I., GUILLEMIN, G. J., SUNDARAMOORTHY, V. & ATKIN, J. D. 2019. Amyotrophic lateral sclerosis-linked UBQLN2 mutants inhibit endoplasmic reticulum to Golgi transport, leading to Golgi fragmentation and ER stress. *Cell Mol Life Sci*.
- HAMMOND, A. T., HEBERLE, F. A., BAUMGART, T., HOLOWKA, D., BAIRD, B. & FEIGENSON, G. W. 2005. Crosslinking a lipid raft component triggers liquid ordered-liquid disordered phase separation in model plasma membranes. *Proc Natl Acad Sci U S A*, 102, 6320-5.
- HANSON, D. A. & ZIEGLER, S. F. 2004. Fusion of green fluorescent protein to the C-terminus of granulysin alters its intracellular localization in comparison to the native molecule. *J Negat Results Biomed*, 3, 2.
- HARDIMAN, O., AL-CHALABI, A., CHIO, A., CORR, E. M., LOGROSCINO, G., ROBBERECHT, W., SHAW, P. J., SIMMONS, Z. & VAN DEN BERG, L. H. 2017. Amyotrophic lateral sclerosis. *Nat Rev Dis Primers*, 3, 17071.
- HARDIMAN, O. & VAN DEN BERG, L. H. 2017. Edaravone: a new treatment for ALS on the horizon? *Lancet Neurol*, 16, 490-491.
- HARRINGTON, H., HALLETT, M. & TYLER, H. R. 1984. Ganglioside therapy for amyotrophic lateral sclerosis: a double-blind controlled trial. *Neurology*, 34, 1083-5.

- HARRIS, N. J., READING, E., ATAKA, K., GRZEGORZEWSKI, L., CHARALAMBOUS, K., LIU, X., SCHLESINGER, R., HEBERLE, J. & BOOTH, P. J. 2017. Structure formation during translocon-unassisted co-translational membrane protein folding. *Sci Rep*, 7, 8021.
- HARSCHNITZ, O., JONGBLOED, B. A., FRANSSSEN, H., STRAVER, D. C., VAN DER POL, W. L. & VAN DEN BERG, L. H. 2014. MMN: from immunological cross-talk to conduction block. *J Clin Immunol*, 34 Suppl 1, S112-9.
- HAYASHI, H., KIMURA, N., YAMAGUCHI, H., HASEGAWA, K., YOKOSEKI, T., SHIBATA, M., YAMAMOTO, N., MICHIKAWA, M., YOSHIKAWA, Y., TERAO, K., MATSUZAKI, K., LEMERE, C. A., SELKOE, D. J., NAIKI, H. & YANAGISAWA, K. 2004. A seed for Alzheimer amyloid in the brain. *J Neurosci*, 24, 4894-902.
- HEAD, B. P., HU, Y., FINLEY, J. C., SALDANA, M. D., BONDS, J. A., MIYANOHARA, A., NIESMAN, I. R., ALI, S. S., MURRAY, F., INSEL, P. A., ROTH, D. M., PATEL, H. H. & PATEL, P. M. 2011. Neuron-targeted caveolin-1 protein enhances signaling and promotes arborization of primary neurons. *J Biol Chem*, 286, 33310-21.
- HEAD, B. P., PEART, J. N., PANNEERSELVAM, M., YOKOYAMA, T., PEARN, M. L., NIESMAN, I. R., BONDS, J. A., SCHILLING, J. M., MIYANOHARA, A., HEADRICK, J., ALI, S. S., ROTH, D. M., PATEL, P. M. & PATEL, H. H. 2010. Loss of caveolin-1 accelerates neurodegeneration and aging. *PLoS One*, 5, e15697.
- HEINO, J. 2007. The collagen family members as cell adhesion proteins. *Bioessays*, 29, 1001-10.
- HEINZ, S., ROMANOSKI, C. E., BENNER, C. & GLASS, C. K. 2015. The selection and function of cell type-specific enhancers. *Nat Rev Mol Cell Biol*, 16, 144-54.
- HENDEL, A., BAK, R. O., CLARK, J. T., KENNEDY, A. B., RYAN, D. E., ROY, S., STEINFELD, I., LUNSTAD, B. D., KAISER, R. J., WILKENS, A. B., BACCHETTA, R., TSALENKO, A., DELLINGER, D., BRUHN, L. & PORTEUS, M. H. 2015. Chemically modified guide RNAs enhance CRISPR-Cas genome editing in human primary cells. *Nat Biotechnol*, 33, 985-989.
- HENRIQUES, A., CROIXMARIE, V., PRIESTMAN, D. A., ROSENBOHM, A., DIRRIG-GROSCH, S., D'AMBRA, E., HUEBECKER, M., HUSSAIN, G., BOURSIER-NEYRET, C., ECHANIZ-LAGUNA, A., LUDOLPH, A. C., PLATT, F. M., WALTHER, B., SPEDDING, M., LOEFFLER, J. P. & GONZALEZ DE AGUILAR, J. L. 2015. Amyotrophic lateral sclerosis and denervation alter sphingolipids and up-regulate glucosylceramide synthase. *Hum Mol Genet*, 24, 7390-405.
- HENRIQUES, A., HUEBECKER, M., BLASCO, H., KEIME, C., ANDRES, C. R., CORCIA, P., PRIESTMAN, D. A., PLATT, F. M., SPEDDING, M. & LOEFFLER, J. P. 2017. Inhibition of beta-Glucocerebrosidase Activity Preserves Motor Unit Integrity in a Mouse Model of Amyotrophic Lateral Sclerosis. *Sci Rep*, 7, 5235.
- HENRIQUES, A., PITZER, C. & SCHNEIDER, A. 2010. Neurotrophic growth factors for the treatment of amyotrophic lateral sclerosis: where do we stand? *Front Neurosci*, 4, 32.
- HEWAMADDUMA, C. A., GRIERSON, A. J., MA, T. P., PAN, L., MOENS, C. B., INGHAM, P. W., RAMESH, T. & SHAW, P. J. 2013. Tardbp splicing rescues motor neuron and axonal development in a mutant tardbp zebrafish. *Hum Mol Genet*, 22, 2376-86.
- HIGHLEY, J. R., KIRBY, J., JANSWEIJER, J. A., WEBB, P. S., HEWAMADDUMA, C. A., HEATH, P. R., HIGGINBOTTOM, A., RAMAN, R., FERRAIUOLO, L., COOPER-KNOCK, J., MCDERMOTT, C. J., WHARTON, S. B., SHAW, P. J. & INCE, P. G. 2014. Loss of nuclear TDP-43 in amyotrophic lateral sclerosis (ALS) causes altered expression of splicing

- machinery and widespread dysregulation of RNA splicing in motor neurones. *Neuropathol Appl Neurobiol*, 40, 670-85.
- HINZ, F. I. & GESCHWIND, D. H. 2017. Molecular Genetics of Neurodegenerative Dementias. *Cold Spring Harb Perspect Biol*, 9.
- HORTON, A. C. & EHLERS, M. D. 2004. Secretory trafficking in neuronal dendrites. *Nat Cell Biol*, 6, 585-91.
- HOWE, K., CLARK, M. D., TORROJA, C. F., TORRANCE, J., BERTHELOT, C., MUFFATO, M., COLLINS, J. E., HUMPHRAY, S., MCLAREN, K., MATTHEWS, L., MCLAREN, S., SEALY, I., CACCAMO, M., CHURCHER, C., SCOTT, C., BARRETT, J. C., KOCH, R., RAUCH, G. J., WHITE, S., CHOW, W., KILIAN, B., QUINTAIS, L. T., GUERRA-ASSUNCAO, J. A., ZHOU, Y., GU, Y., YEN, J., VOGEL, J. H., EYRE, T., REDMOND, S., BANERJEE, R., CHI, J., FU, B., LANGLEY, E., MAGUIRE, S. F., LAIRD, G. K., LLOYD, D., KENYON, E., DONALDSON, S., SEHRA, H., ALMEIDA-KING, J., LOVELAND, J., TREVANION, S., JONES, M., QUAIL, M., WILLEY, D., HUNT, A., BURTON, J., SIMS, S., MCLAY, K., PLUMB, B., DAVIS, J., CLEE, C., OLIVER, K., CLARK, R., RIDDLE, C., ELLIOT, D., THREADGOLD, G., HARDEN, G., WARE, D., BEGUM, S., MORTIMORE, B., KERRY, G., HEATH, P., PHILLIMORE, B., TRACEY, A., CORBY, N., DUNN, M., JOHNSON, C., WOOD, J., CLARK, S., PELAN, S., GRIFFITHS, G., SMITH, M., GLITHERO, R., HOWDEN, P., BARKER, N., LLOYD, C., STEVENS, C., HARLEY, J., HOLT, K., PANAGIOTIDIS, G., LOVELL, J., BEASLEY, H., HENDERSON, C., GORDON, D., AUGER, K., WRIGHT, D., COLLINS, J., RAISEN, C., DYER, L., LEUNG, K., ROBERTSON, L., AMBRIDGE, K., LEONGAMORNLETT, D., MCGUIRE, S., GILDERTHORP, R., GRIFFITHS, C., MANTHRAVADI, D., NICHOL, S., BARKER, G., et al. 2013. The zebrafish reference genome sequence and its relationship to the human genome. *Nature*, 496, 498-503.
- HRUZ, T., WYSS, M., DOCQUIER, M., PFAFFL, M. W., MASANETZ, S., BORGHI, L., VERBRUGGHE, P., KALAYDJIEVA, L., BLEULER, S., LAULE, O., DESCOMBES, P., GRUISSEM, W. & ZIMMERMANN, P. 2011. RefGenes: identification of reliable and condition specific reference genes for RT-qPCR data normalization. *BMC Genomics*, 12, 156.
- HSIAO, C. T., CHENG, H. W., HUANG, C. M., LI, H. R., OU, M. H., HUANG, J. R., KHOO, K. H., YU, H. W., CHEN, Y. Q., WANG, Y. K., CHIOU, A. & KUO, J. C. 2017. Fibronectin in cell adhesion and migration via N-glycosylation. *Oncotarget*, 8, 70653-70668.
- HSIEH, Y. W. & YANG, X. J. 2009. Dynamic Pax6 expression during the neurogenic cell cycle influences proliferation and cell fate choices of retinal progenitors. *Neural Dev*, 4, 32.
- HU, R., CAO, Q., SUN, Z., CHEN, J., ZHENG, Q. & XIAO, F. 2018. A novel method of neural differentiation of PC12 cells by using Opti-MEM as a basic induction medium. *Int J Mol Med*, 41, 195-201.
- HUANG, C. Y., WU, T. C., HONG, Y. H., HSIEH, S. L., GUO, H. R. & HUANG, R. H. 2018. Enhancement of Cell Adhesion, Cell Growth, Wound Healing, and Oxidative Protection by Gelatins Extracted from Extrusion-Pretreated Tilapia (*Oreochromis* sp.) Fish Scale. *Molecules*, 23.
- HUANG, Y. F., GULKO, B. & SIEPEL, A. 2017. Fast, scalable prediction of deleterious noncoding variants from functional and population genomic data. *Nat Genet*, 49, 618-624.
- HUJOEL, M. L. A., GAZAL, S., HORMOZDIARI, F., VAN DE GEIJN, B. & PRICE, A. L. 2019. Disease Heritability Enrichment of Regulatory Elements Is Concentrated in Elements with Ancient Sequence Age and Conserved Function across Species. *Am J Hum Genet*, 104, 611-624.
- HUSSAIN, T. & MULHERKAR, R. 2012. Lymphoblastoid Cell lines: a Continuous in Vitro Source of Cells to Study Carcinogen Sensitivity and DNA Repair. *Int J Mol Cell Med*, 1, 75-87.

- IGLESIAS-BARTOLOME, R., TRENCHI, A., COMIN, R., MOYANO, A. L., NORES, G. A. & DANIOTTI, J. L. 2009. Differential endocytic trafficking of neuropathy-associated antibodies to GM1 ganglioside and cholera toxin in epithelial and neural cells. *Biochim Biophys Acta*, 1788, 2526-40.
- INGRE, C., ROOS, P. M., PIEHL, F., KAMEL, F. & FANG, F. 2015. Risk factors for amyotrophic lateral sclerosis. *Clin Epidemiol*, 7, 181-93.
- IQBAL, K., LIU, F., GONG, C. X. & GRUNDKE-IQBAL, I. 2010. Tau in Alzheimer disease and related tauopathies. *Curr Alzheimer Res*, 7, 656-64.
- IQBAL, S., GHANIMI FARD, M., EVEREST-DASS, A., PACKER, N. H. & PARKER, L. M. 2019. Understanding cellular glycan surfaces in the central nervous system. *Biochem Soc Trans*, 47, 89-100.
- ITO, H., NAKAMURA, M., KOMURE, O., AYAKI, T., WATE, R., MARUYAMA, H., NAKAMURA, Y., FUJITA, K., KANEKO, S., OKAMOTO, Y., IHARA, M., KONISHI, T., OGASAWARA, K., HIRANO, A., KUSAKA, H., KAJI, R., TAKAHASHI, R. & KAWAKAMI, H. 2011. Clinicopathologic study on an ALS family with a heterozygous E478G optineurin mutation. *Acta Neuropathol*, 122, 223-9.
- JAARSMa, D., ROGNONI, F., VAN DUJIN, W., VERSPAGET, H. W., HAASDIJK, E. D. & HOLSTEGE, J. C. 2001. CuZn superoxide dismutase (SOD1) accumulates in vacuolated mitochondria in transgenic mice expressing amyotrophic lateral sclerosis-linked SOD1 mutations. *Acta Neuropathol*, 102, 293-305.
- JAREB, M. & BANKER, G. 1997. Inhibition of axonal growth by brefeldin A in hippocampal neurons in culture. *J Neurosci*, 17, 8955-63.
- JARVIK, J. W. & TELMER, C. A. 1998. Epitope tagging. *Annu Rev Genet*, 32, 601-18.
- JIANG, F. & DOUDNA, J. A. 2017. CRISPR-Cas9 Structures and Mechanisms. *Annu Rev Biophys*, 46, 505-529.
- JIANG, J., ZHU, Q., GENDRON, T. F., SABERI, S., MCALONIS-DOWNES, M., SEELMAN, A., STAUFFER, J. E., JAFAR-NEJAD, P., DRENNER, K., SCHULTE, D., CHUN, S., SUN, S., LING, S. C., MYERS, B., ENGELHARDT, J., KATZ, M., BAUGHN, M., PLATOSHYN, O., MARSALA, M., WATT, A., HEYSER, C. J., ARD, M. C., DE MUYNCK, L., DAUGHRITY, L. M., SWING, D. A., TESSAROLLO, L., JUNG, C. J., DELPOUX, A., UTZSCHNEIDER, D. T., HEDRICK, S. M., DE JONG, P. J., EDBAUER, D., VAN DAMME, P., PETRUCCELLI, L., SHAW, C. E., BENNETT, C. F., DA CRUZ, S., RAVITS, J., RIGO, F., CLEVELAND, D. W. & LAGIER-TOURENNE, C. 2016. Gain of Toxicity from ALS/FTD-Linked Repeat Expansions in C9ORF72 Is Alleviated by Antisense Oligonucleotides Targeting GGGGCC-Containing RNAs. *Neuron*, 90, 535-50.
- JIANG, S., WANG, L. W., WALSH, M. J., TRUDEAU, S. J., GERDT, C., ZHAO, B. & GEWURZ, B. E. 2018. CRISPR/Cas9-Mediated Genome Editing in Epstein-Barr Virus-Transformed Lymphoblastoid B-Cell Lines. *Curr Protoc Mol Biol*, 121, 31.12.1-31.12.23.
- JIANG, Y. L., JIN, H., YANG, H. B., ZHAO, R. L., WANG, S., CHEN, Y. & ZHOU, C. Z. 2017. Defining the enzymatic pathway for polymorphic O-glycosylation of the pneumococcal serine-rich repeat protein PsrP. *J Biol Chem*, 292, 6213-6224.
- JINEK, M., CHYLINSKI, K., FONFARA, I., HAUER, M., DOUDNA, J. A. & CHARPENTIER, E. 2012. A programmable dual-RNA-guided DNA endonuclease in adaptive bacterial immunity. *Science*, 337, 816-21.
- JOHNSTON, A. D., SIMOES-PIRES, C. A., SUZUKI, M. & GREALLY, J. M. 2019. High-efficiency genomic editing in Epstein-Barr virus-transformed lymphoblastoid B cells using a single-stranded donor oligonucleotide strategy. *Commun Biol*, 2, 312.

- JOHRI, A. & BEAL, M. F. 2012. Mitochondrial dysfunction in neurodegenerative diseases. *J Pharmacol Exp Ther*, 342, 619-30.
- JOYCE, P. I., FRATTA, P., FISHER, E. M. & ACEVEDO-ARZENA, A. 2011. SOD1 and TDP-43 animal models of amyotrophic lateral sclerosis: recent advances in understanding disease toward the development of clinical treatments. *Mamm Genome*, 22, 420-48.
- JULIEN, J. P. 1997. Neurofilaments and motor neuron disease. *Trends Cell Biol*, 7, 243-9.
- KAAL, E. C., VLUG, A. S., VERSLEIJEN, M. W., KUILMAN, M., JOOSTEN, E. A. & BAR, P. R. 2000. Chronic mitochondrial inhibition induces selective motoneuron death in vitro: a new model for amyotrophic lateral sclerosis. *J Neurochem*, 74, 1158-65.
- KABASHI, E., LIN, L., TRADEWELL, M. L., DION, P. A., BERCIER, V., BOURGOUIN, P., ROCHEFORT, D., BEL HADJ, S., DURHAM, H. D., VANDE VELDE, C., ROULEAU, G. A. & DRAPEAU, P. 2010. Gain and loss of function of ALS-related mutations of TARDBP (TDP-43) cause motor deficits in vivo. *Hum Mol Genet*, 19, 671-83.
- KAISER, H. J., LINGWOOD, D., LEVENTAL, I., SAMPAIO, J. L., KALVODOVA, L., RAJENDRAN, L. & SIMONS, K. 2009. Order of lipid phases in model and plasma membranes. *Proc Natl Acad Sci U S A*, 106, 16645-50.
- KALUEFF, A. V., GEBHARDT, M., STEWART, A. M., CACHAT, J. M., BRIMMER, M., CHAWLA, J. S., CRADDOCK, C., KYZAR, E. J., ROTH, A., LANDSMAN, S., GAIKWAD, S., ROBINSON, K., BAATRUP, E., TIERNEY, K., SHAMCHUK, A., NORTON, W., MILLER, N., NICOLSON, T., BRAUBACH, O., GILMAN, C. P., PITTMAN, J., ROSEMBERG, D. B., GERLAI, R., ECHEVARRIA, D., LAMB, E., NEUHAUSS, S. C., WENG, W., BALLY-CUIF, L., SCHNEIDER, H. & ZEBRAFISH NEUROSCIENCE RESEARCH, C. 2013. Towards a comprehensive catalog of zebrafish behavior 1.0 and beyond. *Zebrafish*, 10, 70-86.
- KALUEFF, A. V., STEWART, A. M. & GERLAI, R. 2014. Zebrafish as an emerging model for studying complex brain disorders. *Trends Pharmacol Sci*, 35, 63-75.
- KANEHISA, M., FURUMICHI, M., TANABE, M., SATO, Y. & MORISHIMA, K. 2017. KEGG: new perspectives on genomes, pathways, diseases and drugs. *Nucleic Acids Res*, 45, D353-D361.
- KANG, M. J., SEO, J. S. & PARK, W. Y. 2006. Caveolin-1 inhibits neurite growth by blocking Rac1/Cdc42 and p21-activated kinase 1 interactions. *Neuroreport*, 17, 823-7.
- KAWASHIMA, I., NAGATA, I. & TAI, T. 1996. Immunocytochemical analysis of gangliosides in rat primary cerebellar cultures using specific monoclonal antibodies. *Brain Res*, 732, 75-86.
- KENNA, K. P., VAN DOORMAAL, P. T., DEKKER, A. M., TICOZZI, N., KENNA, B. J., DIEKSTRA, F. P., VAN RHEENEN, W., VAN EIJK, K. R., JONES, A. R., KEAGLE, P., SHATUNOV, A., SPROVIERO, W., SMITH, B. N., VAN ES, M. A., TOPP, S. D., KENNA, A., MILLER, J. W., FALLINI, C., TILOCA, C., MCLAUGHLIN, R. L., VANCE, C., TROAKES, C., COLOMBRITA, C., MORA, G., CALVO, A., VERDE, F., AL-SARRAJ, S., KING, A., CALINI, D., DE BELLEROCHE, J., BAAS, F., VAN DER KOOI, A. J., DE VISSER, M., TEN ASBROEK, A. L., SAPP, P. C., MCKENNA-YASEK, D., POLAK, M., ASRESS, S., MUNOZ-BLANCO, J. L., STROM, T. M., MEITINGER, T., MORRISON, K. E., CONSORTIUM, S., LAURIA, G., WILLIAMS, K. L., LEIGH, P. N., NICHOLSON, G. A., BLAIR, I. P., LEBLOND, C. S., DION, P. A., ROULEAU, G. A., PALL, H., SHAW, P. J., TURNER, M. R., TALBOT, K., TARONI, F., BOYLAN, K. B., VAN BLITTERSWIJK, M., RADEMAKERS, R., ESTEBAN-PEREZ, J., GARCIA-REDONDO, A., VAN DAMME, P., ROBBERECHT, W., CHIO, A., GELLERA, C., DREPPER, C., SENDTNER, M., RATTI, A., GLASS, J. D., MORA, J. S., BASAK, N. A., HARDIMAN, O., LUDOLPH, A. C., ANDERSEN, P. M., WEISHAUP, J. H., BROWN, R. H., JR., AL-CHALABI, A., SILANI, V.,

- SHAW, C. E., VAN DEN BERG, L. H., VELDINK, J. H. & LANDERS, J. E. 2016. NEK1 variants confer susceptibility to amyotrophic lateral sclerosis. *Nat Genet*, 48, 1037-42.
- KILPATRICK, D. C. 2002. Animal lectins: a historical introduction and overview. *Biochim Biophys Acta*, 1572, 187-97.
- KIM, S., KIM, D., CHO, S. W., KIM, J. & KIM, J. S. 2014. Highly efficient RNA-guided genome editing in human cells via delivery of purified Cas9 ribonucleoproteins. *Genome Res*, 24, 1012-9.
- KIM, S. M., KIM, H., KIM, J. E., PARK, K. S., SUNG, J. J., KIM, S. H. & LEE, K. W. 2011. Amyotrophic lateral sclerosis is associated with hypolipidemia at the presymptomatic stage in mice. *PLoS One*, 6, e17985.
- KIM, T. K. & EBERWINE, J. H. 2010. Mammalian cell transfection: the present and the future. *Anal Bioanal Chem*, 397, 3173-8.
- KIRCHER, M., WITTEN, D. M., JAIN, P., O'ROAK, B. J., COOPER, G. M. & SHENDURE, J. 2014. A general framework for estimating the relative pathogenicity of human genetic variants. *Nat Genet*, 46, 310-5.
- KITAZUME, S., TACHIDA, Y., OKA, R., SHIROTANI, K., SAIDO, T. C. & HASHIMOTO, Y. 2001. Alzheimer's beta-secretase, beta-site amyloid precursor protein-cleaving enzyme, is responsible for cleavage secretion of a Golgi-resident sialyltransferase. *Proc Natl Acad Sci U S A*, 98, 13554-9.
- KITAKA, D., ITOH, M., OHMI, Y., KONDO, Y., FUKUMOTO, S., URANO, T., TAJIMA, O., FURUKAWA, K. & FURUKAWA, K. 2008. Impaired hypoglossal nerve regeneration in mutant mice lacking complex gangliosides: down-regulation of neurotrophic factors and receptors as possible mechanisms. *Glycobiology*, 18, 509-16.
- KLUMPERMAN, J. 2011. Architecture of the mammalian Golgi. *Cold Spring Harb Perspect Biol*, 3.
- KNIGHT, E. M., WILLIAMS, H. N., STEVENS, A. C., KIM, S. H., KOTTWITZ, J. C., MORANT, A. D., STEELE, J. W., KLEIN, W. L., YANAGISAWA, K., BOYD, R. E., LOCKHART, D. J., SJOBERG, E. R., EHRlich, M. E., WUSTMAN, B. A. & GANDY, S. 2015. Evidence that small molecule enhancement of beta-hexosaminidase activity corrects the behavioral phenotype in Dutch APP(E693Q) mice through reduction of ganglioside-bound Abeta. *Mol Psychiatry*, 20, 109-17.
- KOCAK, D. D., JOSEPHS, E. A., BHANDARKAR, V., ADKAR, S. S., KWON, J. B. & GERSBACH, C. A. 2019. Increasing the specificity of CRISPR systems with engineered RNA secondary structures. *Nat Biotechnol*, 37, 657-666.
- KOCH, F., FENOUIL, R., GUT, M., CAUCHY, P., ALBERT, T. K., ZACARIAS-CABEZA, J., SPICUGLIA, S., DE LA CHAPELLE, A. L., HEIDEMANN, M., HINTERMAIR, C., EICK, D., GUT, I., FERRIER, P. & ANDRAU, J. C. 2011. Transcription initiation platforms and GTF recruitment at tissue-specific enhancers and promoters. *Nat Struct Mol Biol*, 18, 956-63.
- KOLLEWE, K., WURSTER, U., SINZENICH, T., KORNER, S., DENGLER, R., MOHAMMADI, B. & PETRI, S. 2015. Anti-ganglioside antibodies in amyotrophic lateral sclerosis revisited. *PLoS One*, 10, e0125339.
- KOMURA, N., SUZUKI, K. G., ANDO, H., KONISHI, M., KOIKEDA, M., IMAMURA, A., CHADDA, R., FUJIWARA, T. K., TSUBOI, H., SHENG, R., CHO, W., FURUKAWA, K., FURUKAWA, K., YAMAUCHI, Y., ISHIDA, H., KUSUMI, A. & KISO, M. 2016. Raft-based interactions of gangliosides with a GPI-anchored receptor. *Nat Chem Biol*, 12, 402-10.
- KOPPERS, M., BLOKHUIS, A. M., WESTENENG, H. J., TERPSTRA, M. L., ZUNDEL, C. A., VIEIRA DE SA, R., SCHELLEVIS, R. D., WAITE, A. J., BLAKE, D. J., VELDINK, J. H., VAN DEN BERG, L.

- H. & PASTERKAMP, R. J. 2015. C9orf72 ablation in mice does not cause motor neuron degeneration or motor deficits. *Ann Neurol*, 78, 426-38.
- KORKMAZ, O. T., AYTAN, N., CARRERAS, I., CHOI, J. K., KOWALL, N. W., JENKINS, B. G. & DEDEOGLU, A. 2014. 7,8-Dihydroxyflavone improves motor performance and enhances lower motor neuronal survival in a mouse model of amyotrophic lateral sclerosis. *Neurosci Lett*, 566, 286-91.
- KORN, H. & FABER, D. S. 2005. The Mauthner cell half a century later: a neurobiological model for decision-making? *Neuron*, 47, 13-28.
- KOSICKI, M., TOMBERG, K. & BRADLEY, A. 2018. Repair of double-strand breaks induced by CRISPR-Cas9 leads to large deletions and complex rearrangements. *Nat Biotechnol*, 36, 765-771.
- KOSTER, R. W. & FRASER, S. E. 2001. Tracing transgene expression in living zebrafish embryos. *Dev Biol*, 233, 329-46.
- KOTANI, M., KAWASHIMA, I., OZAWA, H., TERASHIMA, T. & TAI, T. 1993. Differential distribution of major gangliosides in rat central nervous system detected by specific monoclonal antibodies. *Glycobiology*, 3, 137-46.
- KOVALEVICH, J. & LANGFORD, D. 2013. Considerations for the use of SH-SY5Y neuroblastoma cells in neurobiology. *Methods Mol Biol*, 1078, 9-21.
- KOZAK, M. 1990. Downstream secondary structure facilitates recognition of initiator codons by eukaryotic ribosomes. *Proc Natl Acad Sci U S A*, 87, 8301-5.
- KRACUN, I., KALANJ, S., TALAN-HRANILOVIC, J. & COSOVIC, C. 1992. Cortical distribution of gangliosides in Alzheimer's disease. *Neurochem Int*, 20, 433-8.
- KRACUN, I., ROSNER, H., DRNOVSEK, V., HEFFER-LAUC, M., COSOVIC, C. & LAUC, G. 1991. Human brain gangliosides in development, aging and disease. *Int J Dev Biol*, 35, 289-95.
- KRAFT, A. D., RESCH, J. M., JOHNSON, D. A. & JOHNSON, J. A. 2007. Activation of the Nrf2-ARE pathway in muscle and spinal cord during ALS-like pathology in mice expressing mutant SOD1. *Exp Neurol*, 207, 107-17.
- KRIEG, R. C., DONG, Y., SCHWAMBORN, K. & KNUECHEL, R. 2005. Protein quantification and its tolerance for different interfering reagents using the BCA-method with regard to 2D SDS PAGE. *J Biochem Biophys Methods*, 65, 13-9.
- KUMAR, A., SINGH, P. K., PARIHAR, R., DWIVEDI, V., LAKHOTIA, S. C. & GANESH, S. 2014. Decreased O-linked GlcNAcylation protects from cytotoxicity mediated by huntingtin exon1 protein fragment. *J Biol Chem*, 289, 13543-53.
- KUMAR, P., NAGARAJAN, A. & UCHIL, P. D. 2018. Analysis of Cell Viability by the Lactate Dehydrogenase Assay. *Cold Spring Harb Protoc*, 2018.
- KWIATKOWSKI, T. J., JR., BOSCO, D. A., LECLERC, A. L., TAMRAZIAN, E., VANDERBURG, C. R., RUSS, C., DAVIS, A., GILCHRIST, J., KASARSKIS, E. J., MUNSAT, T., VALDMANIS, P., ROULEAU, G. A., HOSLER, B. A., CORTELLI, P., DE JONG, P. J., YOSHINAGA, Y., HAINES, J. L., PERICAK-VANCE, M. A., YAN, J., TICOZZI, N., SIDDIQUE, T., MCKENNA-YASEK, D., SAPP, P. C., HORVITZ, H. R., LANDERS, J. E. & BROWN, R. H., JR. 2009. Mutations in the FUS/TLS gene on chromosome 16 cause familial amyotrophic lateral sclerosis. *Science*, 323, 1205-8.
- LAGERLOF, O., HART, G. W. & HUGANIR, R. L. 2017. O-GlcNAc transferase regulates excitatory synapse maturity. *Proc Natl Acad Sci U S A*, 114, 1684-1689.
- LAGIER-TOURENNE, C., BAUGHN, M., RIGO, F., SUN, S., LIU, P., LI, H. R., JIANG, J., WATT, A. T., CHUN, S., KATZ, M., QIU, J., SUN, Y., LING, S. C., ZHU, Q., POLYMENIDOU, M.,

- DRENNER, K., ARTATES, J. W., MCALONIS-DOWNES, M., MARKMILLER, S., HUTT, K. R., PIZZO, D. P., CADY, J., HARMS, M. B., BALOH, R. H., VANDENBERG, S. R., YEO, G. W., FU, X. D., BENNETT, C. F., CLEVELAND, D. W. & RAVITS, J. 2013. Targeted degradation of sense and antisense C9orf72 RNA foci as therapy for ALS and frontotemporal degeneration. *Proc Natl Acad Sci U S A*, 110, E4530-9.
- LAIRSON, L. L., HENRISSAT, B., DAVIES, G. J. & WITHERS, S. G. 2008. Glycosyltransferases: structures, functions, and mechanisms. *Annu Rev Biochem*, 77, 521-55.
- LAMB, N. L. & PATTEN, B. M. 1991. Clinical correlations of anti-GM1 antibodies in amyotrophic lateral sclerosis and neuropathies. *Muscle Nerve*, 14, 1021-7.
- LANGHANS, M., HAWES, C., HILLMER, S., HUMMEL, E. & ROBINSON, D. G. 2007. Golgi regeneration after brefeldin A treatment in BY-2 cells entails stack enlargement and cisternal growth followed by division. *Plant Physiol*, 145, 527-38.
- LEBEDEVA, S., DE JESUS DOMINGUES, A. M., BUTTER, F. & KETTING, R. F. 2017. Characterization of genetic loss-of-function of Fus in zebrafish. *RNA Biol*, 14, 29-35.
- LEDEEN, R. 1966. The chemistry of gangliosides: a review. *J Am Oil Chem Soc*, 43, 57-66.
- LEE, E., GIOVANELLO, K. S., SAYKIN, A. J., XIE, F., KONG, D., WANG, Y., YANG, L., IBRAHIM, J. G., DORAISWAMY, P. M. & ZHU, H. 2017. Single-nucleotide polymorphisms are associated with cognitive decline at Alzheimer's disease conversion within mild cognitive impairment patients. *Alzheimers Dement (Amst)*, 8, 86-95.
- LEE, S., EMOND, M. J., BAMSHAD, M. J., BARNES, K. C., RIEDER, M. J., NICKERSON, D. A., TEAM, N. G. E. S. P.-E. L. P., CHRISTIANI, D. C., WURFEL, M. M. & LIN, X. 2012. Optimal unified approach for rare-variant association testing with application to small-sample case-control whole-exome sequencing studies. *Am J Hum Genet*, 91, 224-37.
- LEE, Y. B., CHEN, H. J., PERES, J. N., GOMEZ-DEZA, J., ATTIG, J., STALEKAR, M., TROAKES, C., NISHIMURA, A. L., SCOTTER, E. L., VANCE, C., ADACHI, Y., SARDONE, V., MILLER, J. W., SMITH, B. N., GALLO, J. M., ULE, J., HIRTH, F., ROGELJ, B., HOUART, C. & SHAW, C. E. 2013. Hexanucleotide repeats in ALS/FTD form length-dependent RNA foci, sequester RNA binding proteins, and are neurotoxic. *Cell Rep*, 5, 1178-86.
- LEK, M., KARCZEWSKI, K. J., MINIKEL, E. V., SAMOCHA, K. E., BANKS, E., FENNEL, T., O'DONNELL-LURIA, A. H., WARE, J. S., HILL, A. J., CUMMINGS, B. B., TUKIAINEN, T., BIRNBAUM, D. P., KOSMICKI, J. A., DUNCAN, L. E., ESTRADA, K., ZHAO, F., ZOU, J., PIERCE-HOFFMAN, E., BERGHOUT, J., COOPER, D. N., DEFLAUX, N., DEPRISTO, M., DO, R., FLANNICK, J., FROMER, M., GAUTHIER, L., GOLDSTEIN, J., GUPTA, N., HOWRIGAN, D., KIEZUN, A., KURKI, M. I., MOONSHINE, A. L., NATARAJAN, P., OROZCO, L., PELOSO, G. M., POPLIN, R., RIVAS, M. A., RUANO-RUBIO, V., ROSE, S. A., RUDERFER, D. M., SHAKIR, K., STENSON, P. D., STEVENS, C., THOMAS, B. P., TIAO, G., TUSIE-LUNA, M. T., WEISBURD, B., WON, H. H., YU, D., ALTSHULER, D. M., ARDISSINO, D., BOEHNKE, M., DANESH, J., DONNELLY, S., ELOSUA, R., FLOREZ, J. C., GABRIEL, S. B., GETZ, G., GLATT, S. J., HULTMAN, C. M., KATHIRESAN, S., LAAKSO, M., MCCARROLL, S., MCCARTHY, M. I., MCGOVERN, D., MCPHERSON, R., NEALE, B. M., PALOTIE, A., PURCELL, S. M., SALEHEEN, D., SCHARF, J. M., SKLAR, P., SULLIVAN, P. F., TUOMILEHTO, J., TSUANG, M. T., WATKINS, H. C., WILSON, J. G., DALY, M. J., MACARTHUR, D. G. & EXOME AGGREGATION, C. 2016. Analysis of protein-coding genetic variation in 60,706 humans. *Nature*, 536, 285-91.
- LEVO, M., ZALCKVAR, E., SHARON, E., DANTAS MACHADO, A. C., KALMA, Y., LOTAM-POMPAN, M., WEINBERGER, A., YAKHINI, Z., ROHS, R. & SEGAL, E. 2015. Unraveling determinants

- of transcription factor binding outside the core binding site. *Genome Res*, 25, 1018-29.
- LI, J., LI, X., ZHANG, S. & SNYDER, M. 2019. Gene-Environment Interaction in the Era of Precision Medicine. *Cell*, 177, 38-44.
- LI, X., LIU, D., MA, Y., DU, X., JING, J., WANG, L., XIE, B., SUN, D., SUN, S., JIN, X., ZHANG, X., ZHAO, T., GUAN, J., YI, Z., LAI, W., ZHENG, P., HUANG, Z., CHANG, Y., CHAI, Z., XU, J. & DENG, H. 2017. Direct Reprogramming of Fibroblasts via a Chemically Induced XEN-like State. *Cell Stem Cell*, 21, 264-273 e7.
- LI, Y., LUO, J., LAU, W. M., ZHENG, G., FU, S., WANG, T. T., ZENG, H. P., SO, K. F., CHUNG, S. K., TONG, Y., LIU, K. & SHEN, J. 2011. Caveolin-1 plays a crucial role in inhibiting neuronal differentiation of neural stem/progenitor cells via VEGF signaling-dependent pathway. *PLoS One*, 6, e22901.
- LI, Y. X., FARRELL, M. J., LIU, R., MOHANTY, N. & KIRBY, M. L. 2000. Double-stranded RNA injection produces null phenotypes in zebrafish. *Dev Biol*, 217, 394-405.
- LIANG, X., POTTER, J., KUMAR, S., ZOU, Y., QUINTANILLA, R., SRIDHARAN, M., CARTE, J., CHEN, W., ROARK, N., RANGANATHAN, S., RAVINDER, N. & CHESNUT, J. D. 2015. Rapid and highly efficient mammalian cell engineering via Cas9 protein transfection. *J Biotechnol*, 208, 44-53.
- LIAO, S., TAMMARO, M. & YAN, H. 2015. Enriching CRISPR-Cas9 targeted cells by co-targeting the HPRT gene. *Nucleic Acids Res*, 43, e134.
- LIAZOGHLI, D., PERREAULT, S., MICHEVA, K. D., DESJARDINS, M. & LECLERC, N. 2005. Fragmentation of the Golgi apparatus induced by the overexpression of wild-type and mutant human tau forms in neurons. *Am J Pathol*, 166, 1499-514.
- LIN, S., STAAHL, B. T., ALLA, R. K. & DOUDNA, J. A. 2014. Enhanced homology-directed human genome engineering by controlled timing of CRISPR/Cas9 delivery. *Elife*, 3, e04766.
- LING, J. P., PLETNIKOVA, O., TRONCOSO, J. C. & WONG, P. C. 2015. TDP-43 repression of nonconserved cryptic exons is compromised in ALS-FTD. *Science*, 349, 650-5.
- LINGWOOD, D., RIES, J., SCHWILLE, P. & SIMONS, K. 2008. Plasma membranes are poised for activation of raft phase coalescence at physiological temperature. *Proc Natl Acad Sci U S A*, 105, 10005-10.
- LIU, F., IQBAL, K., GRUNDKE-IQBAL, I., HART, G. W. & GONG, C. X. 2004. O-GlcNAcylation regulates phosphorylation of tau: a mechanism involved in Alzheimer's disease. *Proc Natl Acad Sci U S A*, 101, 10804-9.
- LIU, H. S., JAN, M. S., CHOU, C. K., CHEN, P. H. & KE, N. J. 1999. Is green fluorescent protein toxic to the living cells? *Biochem Biophys Res Commun*, 260, 712-7.
- LIU, M., REHMAN, S., TANG, X., GU, K., FAN, Q., CHEN, D. & MA, W. 2018. Methodologies for Improving HDR Efficiency. *Front Genet*, 9, 691.
- LIU, Y., LI, X., HE, S., HUANG, S., LI, C., CHEN, Y., LIU, Z., HUANG, X. & WANG, X. 2020a. Efficient generation of mouse models with the prime editing system. *Cell Discov*, 6, 27.
- LIU, Y., PATTAMATTA, A., ZU, T., REID, T., BARDHI, O., BORCHELT, D. R., YACHNIS, A. T. & RANUM, L. P. 2016. C9orf72 BAC Mouse Model with Motor Deficits and Neurodegenerative Features of ALS/FTD. *Neuron*, 90, 521-34.
- LIU, Y. J., MCINTYRE, R. L., JANSSENS, G. E. & HOUTKOOPEL, R. H. 2020b. Mitochondrial fission and fusion: A dynamic role in aging and potential target for age-related disease. *Mech Ageing Dev*, 186, 111212.

- LONGAIR, M. H., BAKER, D. A. & ARMSTRONG, J. D. 2011. Simple Neurite Tracer: open source software for reconstruction, visualization and analysis of neuronal processes. *Bioinformatics*, 27, 2453-4.
- LONGO, P. A., KAVRAN, J. M., KIM, M. S. & LEAHY, D. J. 2013. Transient mammalian cell transfection with polyethylenimine (PEI). *Methods Enzymol*, 529, 227-40.
- LUDEMANN, N., CLEMENT, A., HANS, V. H., LESCHIK, J., BEHL, C. & BRANDT, R. 2005. O-glycosylation of the tail domain of neurofilament protein M in human neurons and in spinal cord tissue of a rat model of amyotrophic lateral sclerosis (ALS). *J Biol Chem*, 280, 31648-58.
- MACCIONI, H. J., QUIROGA, R. & FERRARI, M. L. 2011. Cellular and molecular biology of glycosphingolipid glycosylation. *J Neurochem*, 117, 589-602.
- MACKENZIE, I. R., BIGIO, E. H., INCE, P. G., GESER, F., NEUMANN, M., CAIRNS, N. J., KWONG, L. K., FORMAN, M. S., RAVITS, J., STEWART, H., EISEN, A., MCCLUSKY, L., KRETZSCHMAR, H. A., MONORANU, C. M., HIGHLEY, J. R., KIRBY, J., SIDDIQUE, T., SHAW, P. J., LEE, V. M. & TROJANOWSKI, J. Q. 2007. Pathological TDP-43 distinguishes sporadic amyotrophic lateral sclerosis from amyotrophic lateral sclerosis with SOD1 mutations. *Ann Neurol*, 61, 427-34.
- MAGRANE, J., SAHAWNEH, M. A., PRZEDBORSKI, S., ESTEVEZ, A. G. & MANFREDI, G. 2012. Mitochondrial dynamics and bioenergetic dysfunction is associated with synaptic alterations in mutant SOD1 motor neurons. *J Neurosci*, 32, 229-42.
- MAJOUNIE, E., RENTON, A. E., MOK, K., DOPPER, E. G., WAITE, A., ROLLINSON, S., CHIO, A., RESTAGNO, G., NICOLAOU, N., SIMON-SANCHEZ, J., VAN SWIETEN, J. C., ABRAMZON, Y., JOHNSON, J. O., SENDTNER, M., PAMPHLETT, R., ORRELL, R. W., MEAD, S., SIDLE, K. C., HOULDEN, H., ROHRER, J. D., MORRISON, K. E., PALL, H., TALBOT, K., ANSORGE, O., CHROMOSOME, A. L. S. F. T. D. C., FRENCH RESEARCH NETWORK ON, F. F. A., CONSORTIUM, I., HERNANDEZ, D. G., AREPALLI, S., SABATELLI, M., MORA, G., CORBO, M., GIANNINI, F., CALVO, A., ENGLUND, E., BORGHERO, G., FLORIS, G. L., REMES, A. M., LAAKSOVIRTA, H., MCCLUSKEY, L., TROJANOWSKI, J. Q., VAN DEERLIN, V. M., SCHELLENBERG, G. D., NALLS, M. A., DRORY, V. E., LU, C. S., YEH, T. H., ISHIURA, H., TAKAHASHI, Y., TSUJI, S., LE BER, I., BRICE, A., DREPPER, C., WILLIAMS, N., KIRBY, J., SHAW, P., HARDY, J., TIENARI, P. J., HEUTINK, P., MORRIS, H. R., PICKERING-BROWN, S. & TRAYNOR, B. J. 2012. Frequency of the C9orf72 hexanucleotide repeat expansion in patients with amyotrophic lateral sclerosis and frontotemporal dementia: a cross-sectional study. *Lancet Neurol*, 11, 323-30.
- MALI, P., YANG, L., ESVELT, K. M., AACH, J., GUELL, M., DICARLO, J. E., NORVILLE, J. E. & CHURCH, G. M. 2013. RNA-guided human genome engineering via Cas9. *Science*, 339, 823-6.
- MANDYAM, C. D., SCHILLING, J. M., CUI, W., EGAWA, J., NIESMAN, I. R., KELLERHALS, S. E., STAPLES, M. C., BUSIJA, A. R., RISBROUGH, V. B., POSADAS, E., GROGMAN, G. C., CHANG, J. W., ROTH, D. M., PATEL, P. M., PATEL, H. H. & HEAD, B. P. 2017. Neuron-Targeted Caveolin-1 Improves Molecular Signaling, Plasticity, and Behavior Dependent on the Hippocampus in Adult and Aged Mice. *Biol Psychiatry*, 81, 101-110.
- MARSH, B. J. & HOWELL, K. E. 2002. The mammalian Golgi--complex debates. *Nat Rev Mol Cell Biol*, 3, 789-95.
- MARTINA, J. A., DANIOTTI, J. L. & MACCIONI, H. J. 2000. GM1 synthase depends on N-glycosylation for enzyme activity and trafficking to the Golgi complex. *Neurochem Res*, 25, 725-31.

- MARUYAMA, H., MORINO, H., ITO, H., IZUMI, Y., KATO, H., WATANABE, Y., KINOSHITA, Y., KAMADA, M., NODERA, H., SUZUKI, H., KOMURE, O., MATSUURA, S., KOBATAKE, K., MORIMOTO, N., ABE, K., SUZUKI, N., AOKI, M., KAWATA, A., HIRAI, T., KATO, T., OGASAWARA, K., HIRANO, A., TAKUMI, T., KUSAKA, H., HAGIWARA, K., KAJI, R. & KAWAKAMI, H. 2010. Mutations of optineurin in amyotrophic lateral sclerosis. *Nature*, 465, 223-6.
- MATSUMOTO, A., YOSHINO, H., YUKI, N., HARA, Y., CASHMAN, N. R., HANDA, S. & MIYATAKE, T. 1995. Ganglioside characterization of a cell line displaying motor neuron-like phenotype: GM2 as a possible major ganglioside in motor neurons. *J Neurol Sci*, 131, 111-8.
- MATUS, S., VALENZUELA, V., MEDINAS, D. B. & HETZ, C. 2013. ER Dysfunction and Protein Folding Stress in ALS. *Int J Cell Biol*, 2013, 674751.
- MCLAUGHLIN, R. L., SCHIJVEN, D., VAN RHEENEN, W., VAN EIJK, K. R., O'BRIEN, M., KAHN, R. S., OPHOFF, R. A., GORIS, A., BRADLEY, D. G., AL-CHALABI, A., VAN DEN BERG, L. H., LUYKX, J. J., HARDIMAN, O., VELDINK, J. H., PROJECT MIN, E. G. C. & SCHIZOPHRENIA WORKING GROUP OF THE PSYCHIATRIC GENOMICS, C. 2017. Genetic correlation between amyotrophic lateral sclerosis and schizophrenia. *Nat Commun*, 8, 14774.
- MELINO, G., THIELE, C. J., KNIGHT, R. A. & PIACENTINI, M. 1997. Retinoids and the control of growth/death decisions in human neuroblastoma cell lines. *J Neurooncol*, 31, 65-83.
- MENZIES, F. M., COOKSON, M. R., TAYLOR, R. W., TURNBULL, D. M., CHRZANOWSKA-LIGHTOWLERS, Z. M., DONG, L., FIGLEWICZ, D. A. & SHAW, P. J. 2002. Mitochondrial dysfunction in a cell culture model of familial amyotrophic lateral sclerosis. *Brain*, 125, 1522-33.
- MEYER, K., FERRAIUOLO, L., MIRANDA, C. J., LIKHTE, S., MCELROY, S., RENUSCH, S., DITSWORTH, D., LAGIER-TOURENNE, C., SMITH, R. A., RAVITS, J., BURGHESE, A. H., SHAW, P. J., CLEVELAND, D. W., KOLB, S. J. & KASPAR, B. K. 2014. Direct conversion of patient fibroblasts demonstrates non-cell autonomous toxicity of astrocytes to motor neurons in familial and sporadic ALS. *Proc Natl Acad Sci U S A*, 111, 829-32.
- MILLECAMPS, S., SALACHAS, F., CAZENEUVE, C., GORDON, P., BRICKA, B., CAMUZAT, A., GUILLOT-NOEL, L., RUSSAOUEN, O., BRUNETEAU, G., PRADAT, P. F., LE FORESTIER, N., VANDENBERGHE, N., DANIEL-BRUNAUD, V., GUY, N., THAUVIN-ROBINET, C., LACOMBLEZ, L., COURATIER, P., HANNEQUIN, D., SEILHEAN, D., LE BER, I., CORCIA, P., CAMU, W., BRICE, A., ROULEAU, G., LEGUERN, E. & MEININGER, V. 2010. SOD1, ANG, VAPB, TARDBP, and FUS mutations in familial amyotrophic lateral sclerosis: genotype-phenotype correlations. *J Med Genet*, 47, 554-60.
- MIRAT, O., STERNBERG, J. R., SEVERI, K. E. & WYART, C. 2013. ZebraZoom: an automated program for high-throughput behavioral analysis and categorization. *Front Neural Circuits*, 7, 107.
- MITSUMOTO, H., IKEDA, K., KLINKOSZ, B., CEDARBAUM, J. M., WONG, V. & LINDSAY, R. M. 1994. Arrest of motor neuron disease in wobbler mice cotreated with CNTF and BDNF. *Science*, 265, 1107-10.
- MIZUTA, I., OHTA, M., OHTA, K., NISHIMURA, M., MIZUTA, E. & KUNO, S. 2001. Riluzole stimulates nerve growth factor, brain-derived neurotrophic factor and glial cell line-derived neurotrophic factor synthesis in cultured mouse astrocytes. *Neurosci Lett*, 310, 117-20.

- MOHYUDDIN, A., AYUB, Q., SIDDIQI, S., CARVALHO-SILVA, D. R., MAZHAR, K., REHMAN, S., FIRASAT, S., DAR, A., TYLER-SMITH, C. & MEHDI, S. Q. 2004. Genetic instability in EBV-transformed lymphoblastoid cell lines. *Biochim Biophys Acta*, 1670, 81-3.
- MOJICA, F. J. M., DIEZ-VILLASENOR, C., GARCIA-MARTINEZ, J. & ALMENDROS, C. 2009. Short motif sequences determine the targets of the prokaryotic CRISPR defence system. *Microbiology*, 155, 733-740.
- MOLL, T., SHAW, P. J. & COOPER-KNOCK, J. 2020. Disrupted glycosylation of lipids and proteins is a cause of neurodegeneration. *Brain*, 143, 1332-1340.
- MOLLOY, M. P., HERBERT, B. R., WALSH, B. J., TYLER, M. I., TRAINI, M., SANCHEZ, J. C., HOCHSTRASSER, D. F., WILLIAMS, K. L. & GOOLEY, A. A. 1998. Extraction of membrane proteins by differential solubilization for separation using two-dimensional gel electrophoresis. *Electrophoresis*, 19, 837-44.
- MORI, K., WENG, S. M., ARZBERGER, T., MAY, S., RENTZSCH, K., KREMMER, E., SCHMID, B., KRETZSCHMAR, H. A., CRUTS, M., VAN BROECKHOVEN, C., HAASS, C. & EDBAUER, D. 2013. The C9orf72 GGGGCC repeat is translated into aggregating dipeptide-repeat proteins in FTL/ALS. *Science*, 339, 1335-8.
- MOROTZ, G. M., DE VOS, K. J., VAGNONI, A., ACKERLEY, S., SHAW, C. E. & MILLER, C. C. 2012. Amyotrophic lateral sclerosis-associated mutant VAPBP56S perturbs calcium homeostasis to disrupt axonal transport of mitochondria. *Hum Mol Genet*, 21, 1979-88.
- MORRICE, J. R., GREGORY-EVANS, C. Y. & SHAW, C. A. 2018. Animal models of amyotrophic lateral sclerosis: A comparison of model validity. *Neural Regen Res*, 13, 2050-2054.
- MORRISON, B. M., LEE, Y. & ROTHSTEIN, J. D. 2013. Oligodendroglia: metabolic supporters of axons. *Trends Cell Biol*, 23, 644-51.
- MOSMANN, T. 1983. Rapid colorimetric assay for cellular growth and survival: application to proliferation and cytotoxicity assays. *J Immunol Methods*, 65, 55-63.
- MOURELATOS, Z., GONATAS, N. K., STIEBER, A., GURNEY, M. E. & DAL CANTO, M. C. 1996. The Golgi apparatus of spinal cord motor neurons in transgenic mice expressing mutant Cu,Zn superoxide dismutase becomes fragmented in early, preclinical stages of the disease. *Proc Natl Acad Sci U S A*, 93, 5472-7.
- MUKAI, H., ISAGAWA, T., GOYAMA, E., TANAKA, S., BENICE, N. F., TAMURA, A., ONO, Y. & KOPITO, R. R. 2005. Formation of morphologically similar globular aggregates from diverse aggregation-prone proteins in mammalian cells. *Proc Natl Acad Sci U S A*, 102, 10887-92.
- NAGAI, M., RE, D. B., NAGATA, T., CHALAZONITIS, A., JESSELL, T. M., WICHTERLE, H. & PRZEDBORSKI, S. 2007. Astrocytes expressing ALS-linked mutated SOD1 release factors selectively toxic to motor neurons. *Nat Neurosci*, 10, 615-22.
- NAKAGAWA, K., KITAZUME, S., OKA, R., MARUYAMA, K., SAIDO, T. C., SATO, Y., ENDO, T. & HASHIMOTO, Y. 2006. Sialylation enhances the secretion of neurotoxic amyloid-beta peptides. *J Neurochem*, 96, 924-33.
- NAMSI, A., NURY, T., HAMDOUNI, H., YAMMINE, A., VEJUX, A., VERVANDIER-FASSEUR, D., LATRUFFE, N., MASMOUDI-KOUKI, O. & LIZARD, G. 2018. Induction of Neuronal Differentiation of Murine N2a Cells by Two Polyphenols Present in the Mediterranean Diet Mimicking Neurotrophins Activities: Resveratrol and Apigenin. *Diseases*, 6.
- NARAYANAN, R. K., MANGELSDORF, M., PANWAR, A., BUTLER, T. J., NOAKES, P. G. & WALLACE, R. H. 2013. Identification of RNA bound to the TDP-43 ribonucleoprotein

- complex in the adult mouse brain. *Amyotroph Lateral Scler Frontotemporal Degener*, 14, 252-60.
- NASEVICIUS, A. & EKKER, S. C. 2000. Effective targeted gene 'knockdown' in zebrafish. *Nat Genet*, 26, 216-20.
- NASSAR, N., SINGH, K. & GARCIA-DIAZ, M. 2010. Structure of the dominant negative S17N mutant of Ras. *Biochemistry*, 49, 1970-4.
- NASSIF, M., MATUS, S., CASTILLO, K. & HETZ, C. 2010. Amyotrophic lateral sclerosis pathogenesis: a journey through the secretory pathway. *Antioxid Redox Signal*, 13, 1955-89.
- NAUMENKO, N., POLLARI, E., KURRONEN, A., GINIATULLINA, R., SHAKIRZYANOVA, A., MAGGA, J., KOISTINAHO, J. & GINIATULLIN, R. 2011. Gender-Specific Mechanism of Synaptic Impairment and Its Prevention by GCSF in a Mouse Model of ALS. *Front Cell Neurosci*, 5, 26.
- NAYDENOV, N. G., HARRIS, G., MORALES, V. & IVANOV, A. I. 2012. Loss of a membrane trafficking protein alphaSNAP induces non-canonical autophagy in human epithelia. *Cell Cycle*, 11, 4613-25.
- NEITZEL, H. 1986. A routine method for the establishment of permanent growing lymphoblastoid cell lines. *Hum Genet*, 73, 320-6.
- NEUMANN, M., SAMPATHU, D. M., KWONG, L. K., TRUAX, A. C., MICSENYI, M. C., CHOU, T. T., BRUCE, J., SCHUCK, T., GROSSMAN, M., CLARK, C. M., MCCLUSKEY, L. F., MILLER, B. L., MASLIAH, E., MACKENZIE, I. R., FELDMAN, H., FEIDEN, W., KRETZSCHMAR, H. A., TROJANOWSKI, J. Q. & LEE, V. M. 2006. Ubiquitinated TDP-43 in frontotemporal lobar degeneration and amyotrophic lateral sclerosis. *Science*, 314, 130-3.
- NGAMUKOTE, S., YANAGISAWA, M., ARIGA, T., ANDO, S. & YU, R. K. 2007. Developmental changes of glycosphingolipids and expression of glycogenes in mouse brains. *J Neurochem*, 103, 2327-41.
- NGUYEN, D. K. H., THOMBRE, R. & WANG, J. 2019. Autophagy as a common pathway in amyotrophic lateral sclerosis. *Neurosci Lett*, 697, 34-48.
- NICCOLI, T., PARTRIDGE, L. & ISAACS, A. M. 2017. Ageing as a risk factor for ALS/FTD. *Hum Mol Genet*, 26, R105-R113.
- NICHOLS, A. J. & EVANS, C. L. 2011. Video-rate scanning confocal microscopy and microendoscopy. *J Vis Exp*.
- NILSSON, T., RABOUILLE, C., HUI, N., WATSON, R. & WARREN, G. 1996. The role of the membrane-spanning domain and stalk region of N-acetylglucosaminyltransferase I in retention, kin recognition and structural maintenance of the Golgi apparatus in HeLa cells. *J Cell Sci*, 109 (Pt 7), 1975-89.
- NISHIHARA, Y., TAN, C. F., ONODERA, O., TOYOSHIMA, Y., YAMADA, M., MORITA, T., NISHIZAWA, M., KAKITA, A. & TAKAHASHI, H. 2008. Sporadic amyotrophic lateral sclerosis: two pathological patterns shown by analysis of distribution of TDP-43-immunoreactive neuronal and glial cytoplasmic inclusions. *Acta Neuropathol*, 116, 169-82.
- NOLDUS, L. P., SPINK, A. J. & TEGELENBOSCH, R. A. 2001. EthoVision: a versatile video tracking system for automation of behavioral experiments. *Behav Res Methods Instrum Comput*, 33, 398-414.
- O'ROURKE, J. G., BOGDANIK, L., MUHAMMAD, A., GENDRON, T. F., KIM, K. J., AUSTIN, A., CADY, J., LIU, E. Y., ZARROW, J., GRANT, S., HO, R., BELL, S., CARMONA, S., SIMPKINSON, M., LALL, D., WU, K., DAUGHRITY, L., DICKSON, D. W., HARMS, M. B.,

- PETRUCELLI, L., LEE, E. B., LUTZ, C. M. & BALOH, R. H. 2015. C9orf72 BAC Transgenic Mice Display Typical Pathologic Features of ALS/FTD. *Neuron*, 88, 892-901.
- OATES, A. C., BRUCE, A. E. & HO, R. K. 2000. Too much interference: injection of double-stranded RNA has nonspecific effects in the zebrafish embryo. *Dev Biol*, 224, 20-8.
- OGAWA, M., SAWAGUCHI, S., KAWAI, T., NADANO, D., MATSUDA, T., YAGI, H., KATO, K., FURUKAWA, K. & OKAJIMA, T. 2015. Impaired O-linked N-acetylglucosaminylation in the endoplasmic reticulum by mutated epidermal growth factor (EGF) domain-specific O-linked N-acetylglucosamine transferase found in Adams-Oliver syndrome. *J Biol Chem*, 290, 2137-49.
- OHMI, Y., TAJIMA, O., OHKAWA, Y., MORI, A., SUGIURA, Y., FURUKAWA, K. & FURUKAWA, K. 2009. Gangliosides play pivotal roles in the regulation of complement systems and in the maintenance of integrity in nerve tissues. *Proc Natl Acad Sci U S A*, 106, 22405-10.
- OHMI, Y., TAJIMA, O., OHKAWA, Y., YAMAUCHI, Y., SUGIURA, Y., FURUKAWA, K. & FURUKAWA, K. 2011. Gangliosides are essential in the protection of inflammation and neurodegeneration via maintenance of lipid rafts: elucidation by a series of ganglioside-deficient mutant mice. *J Neurochem*, 116, 926-35.
- OHNMACHT, J., YANG, Y., MAURER, G. W., BARREIRO-IGLESIAS, A., TSAROUCHAS, T. M., WEHNER, D., SIEGER, D., BECKER, C. G. & BECKER, T. 2016. Spinal motor neurons are regenerated after mechanical lesion and genetic ablation in larval zebrafish. *Development*, 143, 1464-74.
- OKADA, M., ITOH MI, M., HARAGUCHI, M., OKAJIMA, T., INOUE, M., OISHI, H., MATSUDA, Y., IWAMOTO, T., KAWANO, T., FUKUMOTO, S., MIYAZAKI, H., FURUKAWA, K., AIZAWA, S. & FURUKAWA, K. 2002. b-series Ganglioside deficiency exhibits no definite changes in the neurogenesis and the sensitivity to Fas-mediated apoptosis but impairs regeneration of the lesioned hypoglossal nerve. *J Biol Chem*, 277, 1633-6.
- OKUYAMA, R. & MARSHALL, S. 2003. UDP-N-acetylglucosaminyl transferase (OGT) in brain tissue: temperature sensitivity and subcellular distribution of cytosolic and nuclear enzyme. *J Neurochem*, 86, 1271-80.
- PALLARES, L. F. 2019. Searching for solutions to the missing heritability problem. *Elife*, 8.
- PALMER, E. & FREEMAN, T. 2004. Investigation into the use of C- and N-terminal GFP fusion proteins for subcellular localization studies using reverse transfection microarrays. *Comp Funct Genomics*, 5, 342-53.
- PAMPHLETT, R., MORAHAN, J. M. & YU, B. 2011. Using case-parent trios to look for rare de novo genetic variants in adult-onset neurodegenerative diseases. *J Neurosci Methods*, 197, 297-301.
- PANDEY, A., SHIN, K., PATTERSON, R. E., LIU, X. Q. & RAINEY, J. K. 2016. Current strategies for protein production and purification enabling membrane protein structural biology. *Biochem Cell Biol*, 94, 507-527.
- PENNACCHIO, L. A., BICKMORE, W., DEAN, A., NOBREGA, M. A. & BEJERANO, G. 2013. Enhancers: five essential questions. *Nat Rev Genet*, 14, 288-95.
- PERSSON, K., LY, H. D., DIECKELMANN, M., WAKARCHUK, W. W., WITHERS, S. G. & STRYNADKA, N. C. 2001. Crystal structure of the retaining galactosyltransferase LgtC from *Neisseria meningitidis* in complex with donor and acceptor sugar analogs. *Nat Struct Biol*, 8, 166-75.
- PERSSON, R., SCHNELL, C. R., BORG, L. A. & FRIES, E. 1992. Accumulation of Golgi-processed secretory proteins in an organelle of high density upon reduction of ATP concentration in rat hepatocytes. *J Biol Chem*, 267, 2760-6.

- PESTRONK, A., ADAMS, R. N., CORNBLATH, D., KUNCL, R. W., DRACHMAN, D. B. & CLAWSON, L. 1989. Patterns of serum IgM antibodies to GM1 and GD1a gangliosides in amyotrophic lateral sclerosis. *Ann Neurol*, 25, 98-102.
- PESTRONK, A., CORNBLATH, D. R., ILYAS, A. A., BABA, H., QUARLES, R. H., GRIFFIN, J. W., ALDERSON, K. & ADAMS, R. N. 1988. A treatable multifocal motor neuropathy with antibodies to GM1 ganglioside. *Ann Neurol*, 24, 73-8.
- PETERS, O. M., CABRERA, G. T., TRAN, H., GENDRON, T. F., MCKEON, J. E., METTERVILLE, J., WEISS, A., WIGHTMAN, N., SALAMEH, J., KIM, J., SUN, H., BOYLAN, K. B., DICKSON, D., KENNEDY, Z., LIN, Z., ZHANG, Y. J., DAUGHRITY, L., JUNG, C., GAO, F. B., SAPP, P. C., HORVITZ, H. R., BOSCO, D. A., BROWN, S. P., DE JONG, P., PETRUCCELLI, L., MUELLER, C. & BROWN, R. H., JR. 2015. Human C9ORF72 Hexanucleotide Expansion Reproduces RNA Foci and Dipeptide Repeat Proteins but Not Neurodegeneration in BAC Transgenic Mice. *Neuron*, 88, 902-909.
- PETROSYAN, A., ALI, M. F. & CHENG, P. W. 2012. Glycosyltransferase-specific Golgi-targeting mechanisms. *J Biol Chem*, 287, 37621-7.
- PETROSYAN, A. & CHENG, P. W. 2013. A non-enzymatic function of Golgi glycosyltransferases: mediation of Golgi fragmentation by interaction with non-muscle myosin IIA. *Glycobiology*, 23, 690-708.
- PIAO, Y. S., WAKABAYASHI, K., KAKITA, A., YAMADA, M., HAYASHI, S., MORITA, T., IKUTA, F., OYANAGI, K. & TAKAHASHI, H. 2003. Neuropathology with clinical correlations of sporadic amyotrophic lateral sclerosis: 102 autopsy cases examined between 1962 and 2000. *Brain Pathol*, 13, 10-22.
- POLLARI, E., GOLDSTEINS, G., BART, G., KOISTINAHO, J. & GINIATULLIN, R. 2014. The role of oxidative stress in degeneration of the neuromuscular junction in amyotrophic lateral sclerosis. *Front Cell Neurosci*, 8, 131.
- POLYMENIDOU, M., LAGIER-TOURENNE, C., HUTT, K. R., HUELGA, S. C., MORAN, J., LIANG, T. Y., LING, S. C., SUN, E., WANCEWICZ, E., MAZUR, C., KORDASIEWICZ, H., SEDAGHAT, Y., DONOHUE, J. P., SHIUE, L., BENNETT, C. F., YEO, G. W. & CLEVELAND, D. W. 2011. Long pre-mRNA depletion and RNA missplicing contribute to neuronal vulnerability from loss of TDP-43. *Nat Neurosci*, 14, 459-68.
- PRADHAN, J., NOAKES, P. G. & BELLINGHAM, M. C. 2019. The Role of Altered BDNF/TrkB Signaling in Amyotrophic Lateral Sclerosis. *Front Cell Neurosci*, 13, 368.
- PRELICH, G. 2012. Gene overexpression: uses, mechanisms, and interpretation. *Genetics*, 190, 841-54.
- QUEST, A. F., GUTIERREZ-PAJARES, J. L. & TORRES, V. A. 2008. Caveolin-1: an ambiguous partner in cell signalling and cancer. *J Cell Mol Med*, 12, 1130-50.
- RAKHIT, R., CROW, J. P., LEPOCK, J. R., KONDEJEWSKI, L. H., CASHMAN, N. R. & CHAKRABARTTY, A. 2004. Monomeric Cu,Zn-superoxide dismutase is a common misfolding intermediate in the oxidation models of sporadic and familial amyotrophic lateral sclerosis. *J Biol Chem*, 279, 15499-504.
- RAMESH, T., LYON, A. N., PINEDA, R. H., WANG, C., JANSSEN, P. M., CANAN, B. D., BURGHESE, A. H. & BEATTIE, C. E. 2010. A genetic model of amyotrophic lateral sclerosis in zebrafish displays phenotypic hallmarks of motoneuron disease. *Dis Model Mech*, 3, 652-62.
- RAN, F. A., HSU, P. D., WRIGHT, J., AGARWALA, V., SCOTT, D. A. & ZHANG, F. 2013. Genome engineering using the CRISPR-Cas9 system. *Nat Protoc*, 8, 2281-2308.

- RAPPORT, M. M., DONNENFELD, H., BRUNNER, W., HUNGUND, B. & BARTFELD, H. 1985. Ganglioside patterns in amyotrophic lateral sclerosis brain regions. *Ann Neurol*, 18, 60-7.
- RATOVITSKI, T., CORSON, L. B., STRAIN, J., WONG, P., CLEVELAND, D. W., CULOTTA, V. C. & BORCHELT, D. R. 1999. Variation in the biochemical/biophysical properties of mutant superoxide dismutase 1 enzymes and the rate of disease progression in familial amyotrophic lateral sclerosis kindreds. *Hum Mol Genet*, 8, 1451-60.
- RATZ, M., TESTA, I., HELL, S. W. & JAKOBS, S. 2015. CRISPR/Cas9-mediated endogenous protein tagging for RESOLFT super-resolution microscopy of living human cells. *Sci Rep*, 5, 9592.
- RAYNAL, B., LENORMAND, P., BARON, B., HOOS, S. & ENGLAND, P. 2014. Quality assessment and optimization of purified protein samples: why and how? *Microb Cell Fact*, 13, 180.
- REAUME, A. G., ELLIOTT, J. L., HOFFMAN, E. K., KOWALL, N. W., FERRANTE, R. J., SIWEK, D. F., WILCOX, H. M., FLOOD, D. G., BEAL, M. F., BROWN, R. H., JR., SCOTT, R. W. & SNIDER, W. D. 1996. Motor neurons in Cu/Zn superoxide dismutase-deficient mice develop normally but exhibit enhanced cell death after axonal injury. *Nat Genet*, 13, 43-7.
- REDDY CHICHILI, V. P., KUMAR, V. & SIVARAMAN, J. 2013. Linkers in the structural biology of protein-protein interactions. *Protein Sci*, 22, 153-67.
- RENTON, A. E., CHIO, A. & TRAYNOR, B. J. 2014. State of play in amyotrophic lateral sclerosis genetics. *Nat Neurosci*, 17, 17-23.
- RENTON, A. E., MAJOUNIE, E., WAITE, A., SIMON-SANCHEZ, J., ROLLINSON, S., GIBBS, J. R., SCHYMICK, J. C., LAAKSOVIRTA, H., VAN SWIETEN, J. C., MYLLYKANGAS, L., KALIMO, H., PAETAU, A., ABRAMZON, Y., REMES, A. M., KAGANOVICH, A., SCHOLZ, S. W., DUCKWORTH, J., DING, J., HARMER, D. W., HERNANDEZ, D. G., JOHNSON, J. O., MOK, K., RYTEN, M., TRABZUNI, D., GUERREIRO, R. J., ORRELL, R. W., NEAL, J., MURRAY, A., PEARSON, J., JANSEN, I. E., SONDERVAN, D., SEELAAR, H., BLAKE, D., YOUNG, K., HALLIWELL, N., CALLISTER, J. B., TOULSON, G., RICHARDSON, A., GERHARD, A., SNOWDEN, J., MANN, D., NEARY, D., NALLS, M. A., PEURALINNA, T., JANSSON, L., ISOVIITA, V. M., KAIVORINNE, A. L., HOLTTA-VUORI, M., IKONEN, E., SULKAVA, R., BENATAR, M., WUU, J., CHIO, A., RESTAGNO, G., BORGHERO, G., SABATELLI, M., CONSORTIUM, I., HECKERMAN, D., ROGAEVA, E., ZINMAN, L., ROTHSTEIN, J. D., SENDTNER, M., DREPPER, C., EICHLER, E. E., ALKAN, C., ABDULLAEV, Z., PACK, S. D., DUTRA, A., PAK, E., HARDY, J., SINGLETON, A., WILLIAMS, N. M., HEUTINK, P., PICKERING-BROWN, S., MORRIS, H. R., TIENARI, P. J. & TRAYNOR, B. J. 2011. A hexanucleotide repeat expansion in C9ORF72 is the cause of chromosome 9p21-linked ALS-FTD. *Neuron*, 72, 257-68.
- RISS, T. L., MORAVEC, R. A., NILES, A. L., DUELLMAN, S., BENINK, H. A., WORZELLA, T. J. & MINOR, L. 2004. Cell Viability Assays. In: SITTAMPALAM, G. S., GROSSMAN, A., BRIMACOMBE, K., ARKIN, M., AULD, D., AUSTIN, C. P., BAELL, J., BEJCEK, B., CAAVEIRO, J. M. M., CHUNG, T. D. Y., COUSSENS, N. P., DAHLIN, J. L., DEVANARYAN, V., FOLEY, T. L., GLICKSMAN, M., HALL, M. D., HAAS, J. V., HOARE, S. R. J., INGLESE, J., IVERSEN, P. W., KAHL, S. D., KALES, S. C., KIRSHNER, S., LAL-NAG, M., LI, Z., MCGEE, J., MCMANUS, O., RISS, T., SARADJIAN, P., TRASK, O. J., JR., WEIDNER, J. R., WILDEY, M. J., XIA, M. & XU, X. (eds.) *Assay Guidance Manual*. Bethesda (MD).
- ROBBERECHT, W. 2000. Oxidative stress in amyotrophic lateral sclerosis. *J Neurol*, 247 Suppl 1, I1-6.

- ROBU, M. E., LARSON, J. D., NASEVICIUS, A., BEIRAGHI, S., BRENNER, C., FARBER, S. A. & EKKER, S. C. 2007. p53 activation by knockdown technologies. *PLoS Genet*, 3, e78.
- RODRIGUEZ-BOULAN, E. & MUSCH, A. 2005. Protein sorting in the Golgi complex: shifting paradigms. *Biochim Biophys Acta*, 1744, 455-64.
- RODRIGUEZ-PASCAU, L., COLL, M. J., CASAS, J., VILAGELIU, L. & GRINBERG, D. 2012. Generation of a human neuronal stable cell model for niemann-pick C disease by RNA interference. *JIMD Rep*, 4, 29-37.
- ROSEN, D. R. 1993. Mutations in Cu/Zn superoxide dismutase gene are associated with familial amyotrophic lateral sclerosis. *Nature*, 364, 362.
- RUPAIMOOLE, R., HAN, H. D., LOPEZ-BERESTEIN, G. & SOOD, A. K. 2011. MicroRNA therapeutics: principles, expectations, and challenges. *Chin J Cancer*, 30, 368-70.
- SACCON, R. A., BUNTON-STASYSHYN, R. K., FISHER, E. M. & FRATTA, P. 2013. Is SOD1 loss of function involved in amyotrophic lateral sclerosis? *Brain*, 136, 2342-58.
- SAHLENDER, D. A., ROBERTS, R. C., ARDEN, S. D., SPUDICH, G., TAYLOR, M. J., LUZIO, J. P., KENDRICK-JONES, J. & BUSS, F. 2005. Optineurin links myosin VI to the Golgi complex and is involved in Golgi organization and exocytosis. *J Cell Biol*, 169, 285-95.
- SAKAGUCHI, T., IRIE, T., KAWABATA, R., YOSHIDA, A., MARUYAMA, H. & KAWAKAMI, H. 2011. Optineurin with amyotrophic lateral sclerosis-related mutations abrogates inhibition of interferon regulatory factor-3 activation. *Neurosci Lett*, 505, 279-81.
- SAKOWSKI, S. A., LUNN, J. S., BUSTA, A. S., OH, S. S., ZAMORA-BERRIDI, G., PALMER, M., ROSENBERG, A. A., PHILIP, S. G., DOWLING, J. J. & FELDMAN, E. L. 2012. Neuromuscular effects of G93A-SOD1 expression in zebrafish. *Mol Neurodegener*, 7, 44.
- SALAZAR-GRUESO, E. F., ROUTBORT, M. J., MARTIN, J., DAWSON, G. & ROOS, R. P. 1990. Polyclonal IgM anti-GM1 ganglioside antibody in patients with motor neuron disease and variants. *Ann Neurol*, 27, 558-63.
- SANO, O., ITO, S., KATO, R., SHIMIZU, Y., KOBAYASHI, A., KIMURA, Y., KIOKA, N., HANADA, K., UEDA, K. & MATSUO, M. 2014. ABCA1, ABCG1, and ABCG4 are distributed to distinct membrane meso-domains and disturb detergent-resistant domains on the plasma membrane. *PLoS One*, 9, e109886.
- SAREEN, D., O'ROURKE, J. G., MEERA, P., MUHAMMAD, A. K., GRANT, S., SIMPKINSON, M., BELL, S., CARMONA, S., ORNELAS, L., SAHABIAN, A., GENDRON, T., PETRUCELLI, L., BAUGHN, M., RAVITS, J., HARMS, M. B., RIGO, F., BENNETT, C. F., OTIS, T. S., SVENDSEN, C. N. & BALOH, R. H. 2013. Targeting RNA foci in iPSC-derived motor neurons from ALS patients with a C9ORF72 repeat expansion. *Sci Transl Med*, 5, 208ra149.
- SASAKI, S., HORIE, Y. & IWATA, M. 2007. Mitochondrial alterations in dorsal root ganglion cells in sporadic amyotrophic lateral sclerosis. *Acta Neuropathol*, 114, 633-9.
- SASAYAMA, D., HORI, H., YAMAMOTO, N., NAKAMURA, S., TERAISHI, T., TATSUMI, M., HATTORI, K., OTA, M., HIGUCHI, T. & KUNUGI, H. 2014. ITIH3 polymorphism may confer susceptibility to psychiatric disorders by altering the expression levels of GLT8D1. *J Psychiatr Res*, 50, 79-83.
- SAWADA, A., WANG, S., JIAN, M., LEEM, J., WACKERBARTH, J., EGAWA, J., SCHILLING, J. M., PLATOSHYN, O., ZEMLJIC-HARPF, A., ROTH, D. M., PATEL, H. H., PATEL, P. M., MARSALA, M. & HEAD, B. P. 2019. Neuron-targeted caveolin-1 improves neuromuscular function and extends survival in SOD1(G93A) mice. *FASEB J*, 33, 7545-7554.

- SCHAEFER, K. A., WU, W. H., COLGAN, D. F., TSANG, S. H., BASSUK, A. G. & MAHAJAN, V. B. 2017. Unexpected mutations after CRISPR-Cas9 editing in vivo. *Nat Methods*, 14, 547-548.
- SCHMICK, M. & BASTIAENS, P. I. H. 2014. The interdependence of membrane shape and cellular signal processing. *Cell*, 156, 1132-1138.
- SCHMID, B. & HAASS, C. 2013. Genomic editing opens new avenues for zebrafish as a model for neurodegeneration. *J Neurochem*, 127, 461-70.
- SCHMID, B., HRUSCHA, A., HOGL, S., BANZHAF-STRAHMANN, J., STRECKER, K., VAN DER ZEE, J., TEUCKE, M., EIMER, S., HEGERMANN, J., KITTELMANN, M., KREMMER, E., CRUTS, M., SOLCHENBERGER, B., HASENKAMP, L., VAN BEBBER, F., VAN BROECKHOVEN, C., EDBAUER, D., LICHTENTHALER, S. F. & HAASS, C. 2013. Loss of ALS-associated TDP-43 in zebrafish causes muscle degeneration, vascular dysfunction, and reduced motor neuron axon outgrowth. *Proc Natl Acad Sci U S A*, 110, 4986-91.
- SCHMIDT, R., STRAHLE, U. & SCHOLPP, S. 2013. Neurogenesis in zebrafish - from embryo to adult. *Neural Dev*, 8, 3.
- SCHMITTGEN, T. D. & LIVAK, K. J. 2008. Analyzing real-time PCR data by the comparative C(T) method. *Nat Protoc*, 3, 1101-8.
- SCHNEIDER, J. S. 2018. Altered expression of genes involved in ganglioside biosynthesis in substantia nigra neurons in Parkinson's disease. *PLoS One*, 13, e0199189.
- SCHNEIDER, J. S., CAMBI, F., GOLLOMP, S. M., KUWABARA, H., BRASIC, J. R., LEIBY, B., SENDEK, S. & WONG, D. F. 2015a. GM1 ganglioside in Parkinson's disease: Pilot study of effects on dopamine transporter binding. *J Neurol Sci*, 356, 118-23.
- SCHNEIDER, J. S., KEAN, A. & DISTEFANO, L. 1995. GM1 ganglioside rescues substantia nigra pars compacta neurons and increases dopamine synthesis in residual nigrostriatal dopaminergic neurons in MPTP-treated mice. *J Neurosci Res*, 42, 117-23.
- SCHNEIDER, J. S., ROELTGEN, D. P., MANCALL, E. L., CHAPAS-CRILLY, J., ROTHBLAT, D. S. & TATARIAN, G. T. 1998. Parkinson's disease: improved function with GM1 ganglioside treatment in a randomized placebo-controlled study. *Neurology*, 50, 1630-6.
- SCHNEIDER, J. S., SEYFRIED, T. N., CHOI, H. S. & KIDD, S. K. 2015b. Intraventricular Sialidase Administration Enhances GM1 Ganglioside Expression and Is Partially Neuroprotective in a Mouse Model of Parkinson's Disease. *PLoS One*, 10, e0143351.
- SCHRODER, K. C., DUMAN, D., TEKIN, M., SCHANZE, D., SUKALO, M., MEESTER, J., WUYTS, W. & ZENKER, M. 2019. Adams-Oliver syndrome caused by mutations of the EOGT gene. *Am J Med Genet A*, 179, 2246-2251.
- SCHUMANN, K., LIN, S., BOYER, E., SIMEONOV, D. R., SUBRAMANIAM, M., GATE, R. E., HALIBURTON, G. E., YE, C. J., BLUESTONE, J. A., DOUDNA, J. A. & MARSON, A. 2015. Generation of knock-in primary human T cells using Cas9 ribonucleoproteins. *Proc Natl Acad Sci U S A*, 112, 10437-42.
- SCOTT, C. A., MARSDEN, A. N. & SLUSARSKI, D. C. 2016. Automated, high-throughput, in vivo analysis of visual function using the zebrafish. *Dev Dyn*, 245, 605-13.
- SEBASTIAN-SERRANO, A., SANDONIS, A., CARDOZO, M., RODRIGUEZ-TORNOS, F. M., BOVOLENTA, P. & NIETO, M. 2012. Palphax6 expression in postmitotic neurons mediates the growth of axons in response to SFRP1. *PLoS One*, 7, e31590.
- SENTMANAT, M. F., PETERS, S. T., FLORIAN, C. P., CONNELLY, J. P. & PRUETT-MILLER, S. M. 2018. A Survey of Validation Strategies for CRISPR-Cas9 Editing. *Sci Rep*, 8, 888.
- SEO, J. & LEE, K. J. 2004. Post-translational modifications and their biological functions: proteomic analysis and systematic approaches. *J Biochem Mol Biol*, 37, 35-44.

- SETHI, M. K., BUETTNER, F. F., KRYLOV, V. B., TAKEUCHI, H., NIFANTIEV, N. E., HALTIWANGER, R. S., GERARDY-SCHAHN, R. & BAKKER, H. 2010. Identification of glycosyltransferase 8 family members as xylosyltransferases acting on O-glycosylated notch epidermal growth factor repeats. *J Biol Chem*, 285, 1582-6.
- SEYFRIED, T. N., CHOI, H., CHEVALIER, A., HOGAN, D., AKGOC, Z. & SCHNEIDER, J. S. 2018. Sex-Related Abnormalities in Substantia Nigra Lipids in Parkinson's Disease. *ASN Neuro*, 10, 1759091418781889.
- SHARON, N. & LIS, H. 2004. History of lectins: from hemagglutinins to biological recognition molecules. *Glycobiology*, 14, 53R-62R.
- SHAW, M. P., HIGGINBOTTOM, A., MCGOWN, A., CASTELLI, L. M., JAMES, E., HAUTBERGUE, G. M., SHAW, P. J. & RAMESH, T. M. 2018. Stable transgenic C9orf72 zebrafish model key aspects of the ALS/FTD phenotype and reveal novel pathological features. *Acta Neuropathol Commun*, 6, 125.
- SHAW, P. J., INCE, P. G., FALKOUS, G. & MANTLE, D. 1995. Oxidative damage to protein in sporadic motor neuron disease spinal cord. *Ann Neurol*, 38, 691-5.
- SHEN, W. C., LI, H. Y., CHEN, G. C., CHERN, Y. & TU, P. H. 2015. Mutations in the ubiquitin-binding domain of OPTN/optineurin interfere with autophagy-mediated degradation of misfolded proteins by a dominant-negative mechanism. *Autophagy*, 11, 685-700.
- SHI, P., GAL, J., KWINTER, D. M., LIU, X. & ZHU, H. 2010. Mitochondrial dysfunction in amyotrophic lateral sclerosis. *Biochim Biophys Acta*, 1802, 45-51.
- SHIBATA, N. 2001. Transgenic mouse model for familial amyotrophic lateral sclerosis with superoxide dismutase-1 mutation. *Neuropathology*, 21, 82-92.
- SHOEMAKER, G. K., SOYA, N., PALCIC, M. M. & KLASSEN, J. S. 2008. Temperature-dependent cooperativity in donor-acceptor substrate binding to the human blood group glycosyltransferases. *Glycobiology*, 18, 587-92.
- SIMON-SANCHEZ, J., DOPPER, E. G., COHN-HOKKE, P. E., HUKEMA, R. K., NICOLAOU, N., SEELAAR, H., DE GRAAF, J. R., DE KONING, I., VAN SCHOOR, N. M., DEEG, D. J., SMITS, M., RAAPHORST, J., VAN DEN BERG, L. H., SCHELHAAS, H. J., DE DIE-SMULDERS, C. E., MAJLOOR-KRAKAUER, D., ROZEMULLER, A. J., WILLEMSSEN, R., PIJNENBURG, Y. A., HEUTINK, P. & VAN SWIETEN, J. C. 2012. The clinical and pathological phenotype of C9ORF72 hexanucleotide repeat expansions. *Brain*, 135, 723-35.
- SINGH, R. D., MARKS, D. L., HOLICKY, E. L., WHEATLEY, C. L., KAPTZAN, T., SATO, S. B., KOBAYASHI, T., LING, K. & PAGANO, R. E. 2010. Gangliosides and beta1-integrin are required for caveolae and membrane domains. *Traffic*, 11, 348-60.
- SINGH, R. D., PURI, V., VALIYAVEETIL, J. T., MARKS, D. L., BITTMAN, R. & PAGANO, R. E. 2003. Selective caveolin-1-dependent endocytosis of glycosphingolipids. *Mol Biol Cell*, 14, 3254-65.
- SLEIGH, J. N., ROSSOR, A. M., FELLOWS, A. D., TOSOLINI, A. P. & SCHIAVO, G. 2019. Axonal transport and neurological disease. *Nat Rev Neurol*, 15, 691-703.
- SMITH, R. G., HENRY, Y. K., MATTSO, M. P. & APPEL, S. H. 1998. Presence of 4-hydroxynonenal in cerebrospinal fluid of patients with sporadic amyotrophic lateral sclerosis. *Ann Neurol*, 44, 696-9.
- SOO, K. Y., HALLORAN, M., SUNDARAMOORTHY, V., PARAKH, S., TOTH, R. P., SOUTHAM, K. A., MCLEAN, C. A., LOCK, P., KING, A., FARG, M. A. & ATKIN, J. D. 2015. Rab1-dependent ER-Golgi transport dysfunction is a common pathogenic mechanism in SOD1, TDP-43 and FUS-associated ALS. *Acta Neuropathol*, 130, 679-97.

- SOWA, G., PYPAERT, M. & SESSA, W. C. 2001. Distinction between signaling mechanisms in lipid rafts vs. caveolae. *Proc Natl Acad Sci U S A*, 98, 14072-7.
- SREEDHARAN, J., BLAIR, I. P., TRIPATHI, V. B., HU, X., VANCE, C., ROGELJ, B., ACKERLEY, S., DURNALL, J. C., WILLIAMS, K. L., BURATTI, E., BARALLE, F., DE BELLEROCHE, J., MITCHELL, J. D., LEIGH, P. N., AL-CHALABI, A., MILLER, C. C., NICHOLSON, G. & SHAW, C. E. 2008. TDP-43 mutations in familial and sporadic amyotrophic lateral sclerosis. *Science*, 319, 1668-72.
- STATHOPOULOS, P. B., RUMFELDT, J. A., KARBASSI, F., SIDDALL, C. A., LEPOCK, J. R. & MEIERING, E. M. 2006. Calorimetric analysis of thermodynamic stability and aggregation for apo and holo amyotrophic lateral sclerosis-associated Gly-93 mutants of superoxide dismutase. *J Biol Chem*, 281, 6184-93.
- STERNBERG, S. H., REDDING, S., JINEK, M., GREENE, E. C. & DOUDNA, J. A. 2014. DNA interrogation by the CRISPR RNA-guided endonuclease Cas9. *Nature*, 507, 62-7.
- STEVENS, A., WELLER, M. & WIETHOLTER, H. 1993. A characteristic ganglioside antibody pattern in the CSF of patients with amyotrophic lateral sclerosis. *J Neurol Neurosurg Psychiatry*, 56, 361-4.
- STRONG, M. J., YANG, W., STRONG, W. L., LEYSTRA-LANTZ, C., JAFFE, H. & PANT, H. C. 2006. Tau protein hyperphosphorylation in sporadic ALS with cognitive impairment. *Neurology*, 66, 1770-1.
- SUKARDI, H., CHNG, H. T., CHAN, E. C., GONG, Z. & LAM, S. H. 2011. Zebrafish for drug toxicity screening: bridging the in vitro cell-based models and in vivo mammalian models. *Expert Opin Drug Metab Toxicol*, 7, 579-89.
- SUMMERTON, J. & WELLER, D. 1997. Morpholino antisense oligomers: design, preparation, and properties. *Antisense Nucleic Acid Drug Dev*, 7, 187-95.
- SUN, K. H., DE PABLO, Y., VINCENT, F., JOHNSON, E. O., CHAVERS, A. K. & SHAH, K. 2008. Novel genetic tools reveal Cdk5's major role in Golgi fragmentation in Alzheimer's disease. *Mol Biol Cell*, 19, 3052-69.
- SUNDARAMOORTHY, V., SULTANA, J. M. & ATKIN, J. D. 2015. Golgi fragmentation in amyotrophic lateral sclerosis, an overview of possible triggers and consequences. *Front Neurosci*, 9, 400.
- SUSUKI, K., BABA, H., TOHYAMA, K., KANAI, K., KUWABARA, S., HIRATA, K., FURUKAWA, K., FURUKAWA, K., RASBAND, M. N. & YUKI, N. 2007. Gangliosides contribute to stability of paranodal junctions and ion channel clusters in myelinated nerve fibers. *Glia*, 55, 746-57.
- SUZUKI, T., KITAJIMA, K., INOUE, S. & INOUE, Y. 1995. N-glycosylation/deglycosylation as a mechanism for the post-translational modification/remodification of proteins. *Glycoconj J*, 12, 183-93.
- SVAHN, A. J., DON, E. K., BADROCK, A. P., COLE, N. J., GRAEBER, M. B., YERBURY, J. J., CHUNG, R. & MORSCH, M. 2018. Nucleo-cytoplasmic transport of TDP-43 studied in real time: impaired microglia function leads to axonal spreading of TDP-43 in degenerating motor neurons. *Acta Neuropathol*, 136, 445-459.
- SVENNERHOLM, L., BRANE, G., KARLSSON, I., LEKMAN, A., RAMSTROM, I. & WIKKELSO, C. 2002. Alzheimer disease - effect of continuous intracerebroventricular treatment with GM1 ganglioside and a systematic activation programme. *Dement Geriatr Cogn Disord*, 14, 128-36.
- SWAMINATHAN, A., BOUFFARD, M., LIAO, M., RYAN, S., CALLISTER, J. B., PICKERING-BROWN, S. M., ARMSTRONG, G. A. B. & DRAPEAU, P. 2018. Expression of C9orf72-related

- dipeptides impairs motor function in a vertebrate model. *Hum Mol Genet*, 27, 1754-1762.
- SWENSON, E. S., PRICE, J. G., BRAZELTON, T. & KRAUSE, D. S. 2007. Limitations of green fluorescent protein as a cell lineage marker. *Stem Cells*, 25, 2593-600.
- SWINNEN, B., BENTO-ABREU, A., GENDRON, T. F., BOEYNAEMS, S., BOGAERT, E., NUYTS, R., TIMMERS, M., SCHEVENEELS, W., HERSMUS, N., WANG, J., MIZIELINSKA, S., ISAACS, A. M., PETRUCELLI, L., LEMMENS, R., VAN DAMME, P., VAN DEN BOSCH, L. & ROBBERECHT, W. 2018. A zebrafish model for C9orf72 ALS reveals RNA toxicity as a pathogenic mechanism. *Acta Neuropathol*, 135, 427-443.
- SYNOFZIK, M., FERNANDEZ-SANTIAGO, R., MAETZLER, W., SCHOLS, L. & ANDERSEN, P. M. 2010. The human G93A SOD1 phenotype closely resembles sporadic amyotrophic lateral sclerosis. *J Neurol Neurosurg Psychiatry*, 81, 764-7.
- TAKARADA, T., TAMAKI, K., TAKUMI, T., OGURA, M., ITO, Y., NAKAMICHI, N. & YONEDA, Y. 2009. A protein-protein interaction of stress-responsive myosin VI endowed to inhibit neural progenitor self-replication with RNA binding protein, TLS, in murine hippocampus. *J Neurochem*, 110, 1457-68.
- TAKOV, K., YELLON, D. M. & DAVIDSON, S. M. 2017. Confounding factors in vesicle uptake studies using fluorescent lipophilic membrane dyes. *J Extracell Vesicles*, 6, 1388731.
- TANG, Y., LIU, M. L., ZANG, T. & ZHANG, C. L. 2017. Direct Reprogramming Rather than iPSC-Based Reprogramming Maintains Aging Hallmarks in Human Motor Neurons. *Front Mol Neurosci*, 10, 359.
- TAYLOR, J. P., BROWN, R. H., JR. & CLEVELAND, D. W. 2016. Decoding ALS: from genes to mechanism. *Nature*, 539, 197-206.
- THOMAS, P. & SMART, T. G. 2005. HEK293 cell line: a vehicle for the expression of recombinant proteins. *J Pharmacol Toxicol Methods*, 51, 187-200.
- TONG, J., HUANG, C., BI, F., WU, Q., HUANG, B. & ZHOU, H. 2012. XBP1 depletion precedes ubiquitin aggregation and Golgi fragmentation in TDP-43 transgenic rats. *J Neurochem*, 123, 406-16.
- TUCK, E. & CAVALLI, V. 2010. Roles of membrane trafficking in nerve repair and regeneration. *Commun Integr Biol*, 3, 209-14.
- TULADHAR, R., YEYU, Y., TYLER PIAZZA, J., TAN, Z., RENE CLEMENCEAU, J., WU, X., BARRETT, Q., HERBERT, J., MATHEWS, D. H., KIM, J., HYUN HWANG, T. & LUM, L. 2019. CRISPR-Cas9-based mutagenesis frequently provokes on-target mRNA misregulation. *Nat Commun*, 10, 4056.
- TURNER, M. R., HARDIMAN, O., BENATAR, M., BROOKS, B. R., CHIO, A., DE CARVALHO, M., INCE, P. G., LIN, C., MILLER, R. G., MITSUMOTO, H., NICHOLSON, G., RAVITS, J., SHAW, P. J., SWASH, M., TALBOT, K., TRAYNOR, B. J., VAN DEN BERG, L. H., VELDINK, J. H., VUCIC, S. & KIERNAN, M. C. 2013. Controversies and priorities in amyotrophic lateral sclerosis. *Lancet Neurol*, 12, 310-22.
- UEMURA, S., SHISHIDO, F., KASHIMURA, M. & INOKUCHI, J. 2015. The regulation of ER export and Golgi retention of ST3Gal5 (GM3/GM4 synthase) and B4GalNAcT1 (GM2/GD2/GA2 synthase) by arginine/lysine-based motif adjacent to the transmembrane domain. *Glycobiology*, 25, 1410-22.
- ULIANA, A. S., GIRAUDO, C. G. & MACCIONI, H. J. 2006. Cytoplasmic tails of SialT2 and GalNAcT impose their respective proximal and distal Golgi localization. *Traffic*, 7, 604-12.

- VAJN, K., VILJETIC, B., DEGMECIC, I. V., SCHNAAR, R. L. & HEFFER, M. 2013. Differential distribution of major brain gangliosides in the adult mouse central nervous system. *PLoS One*, 8, e75720.
- VAN DER SPEK, R. A. A., VAN RHEENEN, W., PULIT, S. L., KENNA, K. P., VAN DEN BERG, L. H., VELDINK, J. H. & PROJECT MIN, E. A. L. S. S. C. P. S. 2019. The project MinE databrowser: bringing large-scale whole-genome sequencing in ALS to researchers and the public. *Amyotroph Lateral Scler Frontotemporal Degener*, 20, 432-440.
- VAN DIS, V., KUIJPERS, M., HAASDIJK, E. D., TEULING, E., OAKES, S. A., HOOGENRAAD, C. C. & JAARSMA, D. 2014. Golgi fragmentation precedes neuromuscular denervation and is associated with endosome abnormalities in SOD1-ALS mouse motor neurons. *Acta Neuropathol Commun*, 2, 38.
- VAN GALEN, J., CAMPELO, F., MARTINEZ-ALONSO, E., SCARPA, M., MARTINEZ-MENARGUEZ, J. A. & MALHOTRA, V. 2014. Sphingomyelin homeostasis is required to form functional enzymatic domains at the trans-Golgi network. *J Cell Biol*, 206, 609-18.
- VAN RHEENEN, W., SHATUNOV, A., DEKKER, A. M., MCLAUGHLIN, R. L., DIEKSTRA, F. P., PULIT, S. L., VAN DER SPEK, R. A., VOSA, U., DE JONG, S., ROBINSON, M. R., YANG, J., FOGH, I., VAN DOORMAAL, P. T., TAZELAAR, G. H., KOPPERS, M., BLOKHUIS, A. M., SPROVIERO, W., JONES, A. R., KENNA, K. P., VAN EIJK, K. R., HARSCHNITZ, O., SCHELLEVIS, R. D., BRANDS, W. J., MEDIC, J., MENELAOU, A., VAJDA, A., TICOZZI, N., LIN, K., ROGELJ, B., VRABEC, K., RAVNIK-GLAVAC, M., KORITNIK, B., ZIDAR, J., LEONARDIS, L., GROSELJ, L. D., MILLECAMPS, S., SALACHAS, F., MEININGER, V., DE CARVALHO, M., PINTO, S., MORA, J. S., ROJAS-GARCIA, R., POLAK, M., CHANDRAN, S., COLVILLE, S., SWINGLER, R., MORRISON, K. E., SHAW, P. J., HARDY, J., ORRELL, R. W., PITTMAN, A., SIDLE, K., FRATTA, P., MALASPINA, A., TOPP, S., PETRI, S., ABDULLA, S., DREPPER, C., SENDTNER, M., MEYER, T., OPHOFF, R. A., STAATS, K. A., WIEDAU-PAZOS, M., LOMEN-HOERTH, C., VAN DEERLIN, V. M., TROJANOWSKI, J. Q., ELMAN, L., MCCLUSKEY, L., BASAK, A. N., TUNCA, C., HAMZEIY, H., PARMAN, Y., MEITINGER, T., LICHTNER, P., RADIVOJKOV-BLAGOJEVIC, M., ANDRES, C. R., MAUREL, C., BENSIMON, G., LANDWEHRMEYER, B., BRICE, A., PAYAN, C. A., SAKER-DELYE, S., DURR, A., WOOD, N. W., TITTMANN, L., LIEB, W., FRANKE, A., RIETSCHER, M., CICHON, S., NOTHEN, M. M., AMOUYEL, P., TZOURIO, C., DARTIGUES, J. F., UITTERLINDEN, A. G., RIVADENEIRA, F., ESTRADA, K., HOFMAN, A., CURTIS, C., BLAUW, H. M., VAN DER KOOI, A. J., et al. 2016. Genome-wide association analyses identify new risk variants and the genetic architecture of amyotrophic lateral sclerosis. *Nat Genet*, 48, 1043-8.
- VAN TONDER, A., JOUBERT, A. M. & CROMARTY, A. D. 2015. Limitations of the 3-(4,5-dimethylthiazol-2-yl)-2,5-diphenyl-2H-tetrazolium bromide (MTT) assay when compared to three commonly used cell enumeration assays. *BMC Res Notes*, 8, 47.
- VANCE, C., ROGELJ, B., HORTOBAGYI, T., DE VOS, K. J., NISHIMURA, A. L., SREEDHARAN, J., HU, X., SMITH, B., RUDDY, D., WRIGHT, P., GANESALINGAM, J., WILLIAMS, K. L., TRIPATHI, V., AL-SARAJ, S., AL-CHALABI, A., LEIGH, P. N., BLAIR, I. P., NICHOLSON, G., DE BELLEROCHE, J., GALLO, J. M., MILLER, C. C. & SHAW, C. E. 2009. Mutations in FUS, an RNA processing protein, cause familial amyotrophic lateral sclerosis type 6. *Science*, 323, 1208-1211.
- VARCIANNA, A., MYSZCZYNSKA, M. A., CASTELLI, L. M., O'NEILL, B., KIM, Y., TALBOT, J., NYBERG, S., NYAMALI, I., HEATH, P. R., STOPFORD, M. J., HAUTBERGUE, G. M. & FERRAIUOLO, L. 2019. Micro-RNAs secreted through astrocyte-derived extracellular

- vesicles cause neuronal network degeneration in C9orf72 ALS. *EBioMedicine*, 40, 626-635.
- VASSALL, K. A., STATHOPOULOS, P. B., RUMFELDT, J. A., LEPOCK, J. R. & MEIERING, E. M. 2006. Equilibrium thermodynamic analysis of amyotrophic lateral sclerosis-associated mutant apo Cu,Zn superoxide dismutases. *Biochemistry*, 45, 7366-79.
- VASSYLYEVA, M. N., KLYUYEV, S., VASSYLYEV, A. D., WESSON, H., ZHANG, Z., RENFROW, M. B., WANG, H., HIGGINS, N. P., CHOW, L. T. & VASSYLYEV, D. G. 2017. Efficient, ultra-high-affinity chromatography in a one-step purification of complex proteins. *Proc Natl Acad Sci U S A*, 114, E5138-E5147.
- VEITIA, R. A. 2002. Exploring the etiology of haploinsufficiency. *Bioessays*, 24, 175-84.
- WAITE, A. J., BAUMER, D., EAST, S., NEAL, J., MORRIS, H. R., ANSORGE, O. & BLAKE, D. J. 2014. Reduced C9orf72 protein levels in frontal cortex of amyotrophic lateral sclerosis and frontotemporal degeneration brain with the C9ORF72 hexanucleotide repeat expansion. *Neurobiol Aging*, 35, 1779 e5-1779 e13.
- WANG, B. & BRAND-MILLER, J. 2003. The role and potential of sialic acid in human nutrition. *Eur J Clin Nutr*, 57, 1351-69.
- WANG, H. Y., LI, Y., XUE, T., CHENG, N. & DU, H. N. 2016. Construction of a series of pCS2+ backbone-based Gateway vectors for overexpressing various tagged proteins in vertebrates. *Acta Biochim Biophys Sin (Shanghai)*, 48, 1128-1134.
- WANG, I. F., WU, L. S. & SHEN, C. K. 2008. TDP-43: an emerging new player in neurodegenerative diseases. *Trends Mol Med*, 14, 479-85.
- WANG, Y., BRYANT, S., TATUSOV, R. & TATUSOVA, T. 2000. Links from genome proteins to known 3-D structures. *Genome Res*, 10, 1643-7.
- WANI, W. Y., OUYANG, X., BENAVIDES, G. A., REDMANN, M., COFIELD, S. S., SHACKA, J. J., CHATHAM, J. C., DARLEY-USMAR, V. & ZHANG, J. 2017. O-GlcNAc regulation of autophagy and alpha-synuclein homeostasis; implications for Parkinson's disease. *Mol Brain*, 10, 32.
- WARD, L. D. & KELLIS, M. 2012. Evidence of abundant purifying selection in humans for recently acquired regulatory functions. *Science*, 337, 1675-8.
- WARGELIUS, A., ELLINGSEN, S. & FJOSE, A. 1999. Double-stranded RNA induces specific developmental defects in zebrafish embryos. *Biochem Biophys Res Commun*, 263, 156-61.
- WASSLER, M. J., FOOTE, C. I., GELMAN, I. H. & SHUR, B. D. 2001. Functional interaction between the SSeCKS scaffolding protein and the cytoplasmic domain of beta1,4-galactosyltransferase. *J Cell Sci*, 114, 2291-300.
- WEBSTER, C. P., SMITH, E. F., SHAW, P. J. & DE VOS, K. J. 2017. Protein Homeostasis in Amyotrophic Lateral Sclerosis: Therapeutic Opportunities? *Front Mol Neurosci*, 10, 123.
- WEGORZEWSKA, I., BELL, S., CAIRNS, N. J., MILLER, T. M. & BALOH, R. H. 2009. TDP-43 mutant transgenic mice develop features of ALS and frontotemporal lobar degeneration. *Proc Natl Acad Sci U S A*, 106, 18809-14.
- WHITE, M. A., KIM, E., DUFFY, A., ADALBERT, R., PHILLIPS, B. U., PETERS, O. M., STEPHENSON, J., YANG, S., MASSENZIO, F., LIN, Z., ANDREWS, S., SEGONDS-PICHON, A., METTERVILLE, J., SAKSIDA, L. M., MEAD, R., RIBCHESTER, R. R., BARHOMI, Y., SERRE, T., COLEMAN, M. P., FALLON, J. R., BUSSEY, T. J., BROWN, R. H., JR. & SREEDHARAN, J. 2018. TDP-43 gains function due to perturbed autoregulation in a Tardbp knock-in mouse model of ALS-FTD. *Nat Neurosci*, 21, 552-563.

- WICKS, P., ABRAHAMS, S., PAPPS, B., AL-CHALABI, A., SHAW, C. E., LEIGH, P. N. & GOLDSTEIN, L. H. 2009. SOD1 and cognitive dysfunction in familial amyotrophic lateral sclerosis. *J Neurol*, 256, 234-41.
- WIEDAU-PAZOS, M., GOTO, J. J., RABIZADEH, S., GRALLA, E. B., ROE, J. A., LEE, M. K., VALENTINE, J. S. & BREDESEN, D. E. 1996. Altered reactivity of superoxide dismutase in familial amyotrophic lateral sclerosis. *Science*, 271, 515-8.
- WU, G., LU, Z. H., KULKARNI, N. & LEDEEN, R. W. 2012. Deficiency of ganglioside GM1 correlates with Parkinson's disease in mice and humans. *J Neurosci Res*, 90, 1997-2008.
- XI, Y., NOBLE, S. & EKKER, M. 2011. Modeling neurodegeneration in zebrafish. *Curr Neurol Neurosci Rep*, 11, 274-82.
- XICOY, H., WIERINGA, B. & MARTENS, G. J. 2017. The SH-SY5Y cell line in Parkinson's disease research: a systematic review. *Mol Neurodegener*, 12, 10.
- XU, X., DENIC, A., JORDAN, L. R., WITTENBERG, N. J., WARRINGTON, A. E., WOOLLA, B., PAPKE, L. M., ZOECKLEIN, L. J., YOO, D., SHAVER, J., OH, S. H., PEASE, L. R. & RODRIGUEZ, M. 2015. A natural human IgM that binds to gangliosides is therapeutic in murine models of amyotrophic lateral sclerosis. *Dis Model Mech*, 8, 831-42.
- XU, Y. F., GENDRON, T. F., ZHANG, Y. J., LIN, W. L., D'ALTON, S., SHENG, H., CASEY, M. C., TONG, J., KNIGHT, J., YU, X., RADEMAKERS, R., BOYLAN, K., HUTTON, M., MCGOWAN, E., DICKSON, D. W., LEWIS, J. & PETRUCELLI, L. 2010. Wild-type human TDP-43 expression causes TDP-43 phosphorylation, mitochondrial aggregation, motor deficits, and early mortality in transgenic mice. *J Neurosci*, 30, 10851-9.
- YAMAGUCHI, N. & FUKUDA, M. N. 1995. Golgi retention mechanism of beta-1,4-galactosyltransferase. Membrane-spanning domain-dependent homodimerization and association with alpha- and beta-tubulins. *J Biol Chem*, 270, 12170-6.
- YAMAGUCHI, T., YAMAUCHI, Y., FURUKAWA, K., OHMI, Y., OHKAWA, Y., ZHANG, Q., OKAJIMA, T. & FURUKAWA, K. 2016. Expression of B4GALNT1, an essential glycosyltransferase for the synthesis of complex gangliosides, suppresses BACE1 degradation and modulates APP processing. *Sci Rep*, 6, 34505.
- YAMAMOTO, N., FUKATA, Y., FUKATA, M. & YANAGISAWA, K. 2007. GM1-ganglioside-induced Abeta assembly on synaptic membranes of cultured neurons. *Biochim Biophys Acta*, 1768, 1128-37.
- YAMAMOTO, N., HIRABAYASHI, Y., AMARI, M., YAMAGUCHI, H., ROMANOV, G., VAN NOSTRAND, W. E. & YANAGISAWA, K. 2005. Assembly of hereditary amyloid beta-protein variants in the presence of favorable gangliosides. *FEBS Lett*, 579, 2185-90.
- YAMAMOTO, N., MATSUBARA, T., SATO, T. & YANAGISAWA, K. 2008. Age-dependent high-density clustering of GM1 ganglioside at presynaptic neuritic terminals promotes amyloid beta-protein fibrillogenesis. *Biochim Biophys Acta*, 1778, 2717-26.
- YAMANAKA, K., CHUN, S. J., BOILLEE, S., FUJIMORI-TONOU, N., YAMASHITA, H., GUTMANN, D. H., TAKAHASHI, R., MISAWA, H. & CLEVELAND, D. W. 2008. Astrocytes as determinants of disease progression in inherited amyotrophic lateral sclerosis. *Nat Neurosci*, 11, 251-3.
- YAMASHITA, K., HARA-KUGE, S. & OHKURA, T. 1999. Intracellular lectins associated with N-linked glycoprotein traffic. *Biochim Biophys Acta*, 1473, 147-60.
- YANAGISAWA, K. & IHARA, Y. 1998. GM1 ganglioside-bound amyloid beta-protein in Alzheimer's disease brain. *Neurobiol Aging*, 19, S65-7.

- YANAGISAWA, M., ARIGA, T. & YU, R. K. 2006. Cholera toxin B subunit binding does not correlate with GM1 expression: a study using mouse embryonic neural precursor cells. *Glycobiology*, 16, 19G-22G.
- YANG, C., WANG, H., QIAO, T., YANG, B., ALIAGA, L., QIU, L., TAN, W., SALAMEH, J., MCKENNA-YASEK, D. M., SMITH, T., PENG, L., MOORE, M. J., BROWN, R. H., JR., CAI, H. & XU, Z. 2014. Partial loss of TDP-43 function causes phenotypes of amyotrophic lateral sclerosis. *Proc Natl Acad Sci U S A*, 111, E1121-9.
- YANG, C. P., LI, X., WU, Y., SHEN, Q., ZENG, Y., XIONG, Q., WEI, M., CHEN, C., LIU, J., HUO, Y., LI, K., XUE, G., YAO, Y. G., ZHANG, C., LI, M., CHEN, Y. & LUO, X. J. 2018. Comprehensive integrative analyses identify GLT8D1 and CSNK2B as schizophrenia risk genes. *Nat Commun*, 9, 838.
- YANG, J. W., KIM, S. M., KIM, H. J., KIM, J. E., PARK, K. S., KIM, S. H., LEE, K. W. & SUNG, J. J. 2013. Hypolipidemia in patients with amyotrophic lateral sclerosis: a possible gender difference? *J Clin Neurol*, 9, 125-9.
- YANG, X. & QIAN, K. 2017. Protein O-GlcNAcylation: emerging mechanisms and functions. *Nat Rev Mol Cell Biol*, 18, 452-465.
- YANPALLEWAR, S. U., BARRICK, C. A., BUCKLEY, H., BECKER, J. & TESSAROLLO, L. 2012. Deletion of the BDNF truncated receptor TrkB.T1 delays disease onset in a mouse model of amyotrophic lateral sclerosis. *PLoS One*, 7, e39946.
- YAO, D., MCGONIGAL, R., BARRIE, J. A., CAPPELL, J., CUNNINGHAM, M. E., MEEHAN, G. R., FEWOU, S. N., EDGAR, J. M., ROWAN, E., OHMI, Y., FURUKAWA, K., FURUKAWA, K., BROPHY, P. J. & WILLISON, H. J. 2014. Neuronal expression of GalNAc transferase is sufficient to prevent the age-related neurodegenerative phenotype of complex ganglioside-deficient mice. *J Neurosci*, 34, 880-91.
- YIM, M. B., KANG, J. H., YIM, H. S., KWAK, H. S., CHOCK, P. B. & STADTMAN, E. R. 1996. A gain-of-function of an amyotrophic lateral sclerosis-associated Cu,Zn-superoxide dismutase mutant: An enhancement of free radical formation due to a decrease in Km for hydrogen peroxide. *Proc Natl Acad Sci U S A*, 93, 5709-14.
- YOSHIHARA, Y. 2002. Visualizing selective neural pathways with WGA transgene: combination of neuroanatomy with gene technology. *Neurosci Res*, 44, 133-40.
- YOSHIMURA, A., FUJII, R., WATANABE, Y., OKABE, S., FUKUI, K. & TAKUMI, T. 2006. Myosin-Va facilitates the accumulation of mRNA/protein complex in dendritic spines. *Curr Biol*, 16, 2345-51.
- YOUNG, J. J., LAVAKUMAR, M., TAMPI, D., BALACHANDRAN, S. & TAMPI, R. R. 2018. Frontotemporal dementia: latest evidence and clinical implications. *Ther Adv Psychopharmacol*, 8, 33-48.
- YU, R. K., TSAI, Y. T. & ARIGA, T. 2012. Functional roles of gangliosides in neurodevelopment: an overview of recent advances. *Neurochem Res*, 37, 1230-44.
- YUAN, A., RAO, M. V., VEERANNA & NIXON, R. A. 2012. Neurofilaments at a glance. *J Cell Sci*, 125, 3257-63.
- YUKI, N., SATO, S., MIYATAKE, T., SUGIYAMA, K., KATAGIRI, T. & SASAKI, H. 1991. Motoneuron-disease-like disorder after ganglioside therapy. *Lancet*, 337, 1109-10.
- YUKI, N., YANAKA, C., SUDO, M., FUNAKOSHI, M., ISHIDA, H., MORI, M., KANDA, F. & HIRATA, K. 2014. Lower motor neuron syndrome associated with IgG anti-GM1 antibodies revisited. *J Neuroimmunol*, 272, 62-6.
- ZHANG, H., TAN, C. F., MORI, F., TANJI, K., KAKITA, A., TAKAHASHI, H. & WAKABAYASHI, K. 2008. TDP-43-immunoreactive neuronal and glial inclusions in the neostriatum in

- amyotrophic lateral sclerosis with and without dementia. *Acta Neuropathol*, 115, 115-22.
- ZHANG, J., NUBEL, E., WISIDAGAMA, D. R., SETOGUCHI, K., HONG, J. S., VAN HORN, C. M., IMAM, S. S., VERGNES, L., MALONE, C. S., KOEHLER, C. M. & TEITELL, M. A. 2012. Measuring energy metabolism in cultured cells, including human pluripotent stem cells and differentiated cells. *Nat Protoc*, 7, 1068-85.
- ZHANG, X., GAO, F., WANG, D., LI, C., FU, Y., HE, W. & ZHANG, J. 2018. Tau Pathology in Parkinson's Disease. *Front Neurol*, 9, 809.
- ZHOU, Z., MOGENSEN, M. M., POWELL, P. P., CURRY, S. & WILEMAN, T. 2013. Foot-and-mouth disease virus 3C protease induces fragmentation of the Golgi compartment and blocks intra-Golgi transport. *J Virol*, 87, 11721-9.
- ZHU, Q., JIANG, J., GENDRON, T. F., MCALONIS-DOWNES, M., JIANG, L., TAYLOR, A., DIAZ GARCIA, S., GHOSH DASTIDAR, S., RODRIGUEZ, M. J., KING, P., ZHANG, Y., LA SPADA, A. R., XU, H., PETRUCELLI, L., RAVITS, J., DA CRUZ, S., LAGIER-TOURENNE, C. & CLEVELAND, D. W. 2020. Reduced C9ORF72 function exacerbates gain of toxicity from ALS/FTD-causing repeat expansion in C9orf72. *Nat Neurosci*, 23, 615-624.
- ZINSZNER, H., SOK, J., IMMANUEL, D., YIN, Y. & RON, D. 1997. TLS (FUS) binds RNA in vivo and engages in nucleo-cytoplasmic shuttling. *J Cell Sci*, 110 (Pt 15), 1741-50.
- ZITMAN, F. M., TODOROV, B., VERSCHUUREN, J. J., JACOBS, B. C., FURUKAWA, K., FURUKAWA, K., WILLISON, H. J. & PLOMP, J. J. 2011. Neuromuscular synaptic transmission in aged ganglioside-deficient mice. *Neurobiol Aging*, 32, 157-67.
- ZOLLER, I., BUSSOW, H., GIESELMANN, V. & ECKHARDT, M. 2005. Oligodendrocyte-specific ceramide galactosyltransferase (CGT) expression phenotypically rescues CGT-deficient mice and demonstrates that CGT activity does not limit brain galactosylceramide level. *Glia*, 52, 190-8.
- ZOLOV, S. N. & LUPASHIN, V. V. 2005. Cog3p depletion blocks vesicle-mediated Golgi retrograde trafficking in HeLa cells. *J Cell Biol*, 168, 747-59.
- ZU, T., LIU, Y., BANEZ-CORONEL, M., REID, T., PLETNIKOVA, O., LEWIS, J., MILLER, T. M., HARMS, M. B., FALCHOOK, A. E., SUBRAMONY, S. H., OSTROW, L. W., ROTHSTEIN, J. D., TRONCOSO, J. C. & RANUM, L. P. 2013. RAN proteins and RNA foci from antisense transcripts in C9ORF72 ALS and frontotemporal dementia. *Proc Natl Acad Sci U S A*, 110, E4968-77.

Appendices

Appendix 1. Mutations in EOGT found in ALS patients:

DNA change	Protein change	Allele frequency		Exon
		ALS	Controls	
c.1575T>G	p.Asp525Glu	0.001	0.0005	15
c.1546C>T	p.Pro516Ser	0.0001	0	15
c.1466C>T	p.Pro489Leu	0.0001	0	15
c.1459dupG	p.Glu487fs	0.0001	0	15
c.1456G>T	p.Gly486Trp	0.0001	0	15
c.1432G>A	p.Asp478Asn	0.0001	0	14
c.1417A>T	p.Lys473*	0.0001	0	14
c.1355G>A	p.Arg452His	0.0001	0	14
c.1342T>A	p.Cys448Ser	0.0001	0	14
c.1256C>T	p.Thr419Met	0.0001	0	13
c.1213A>G	p.Arg405Gly	0.01	0.006	12
c.1210T>A	p.Tyr404Asn	0.0001	0	12
c.1129C>T	p.Arg377Trp	0.0001	0	11
c.1114C>T	p.Arg372Trp	0.0001	0	11
c.1108C>T	p.Leu370Phe	0.0001	0	11
c.829A>G	p.Thr277Ala	0.0001	0	10
c.692T>C	p.Ile231Thr	0.0001	0	9
c.674C>T	p.Ala225Val	0.0001	0	9
c.647A>G	p.Gln216Arg	0.0001	0	9
c.563A>T	p.Lys188Ile	0.0002	0	8
c.562A>T	p.Lys188*	0.0002	0	8
c.430A>G	p.Ser144Gly	0.0002	0	7
c.314C>T	p.Thr105Met	0.0001	0	6
c.208A>G	p.Lys70Glu	0.0001	0	4
c.202C>G	p.Pro68Ala	0.0001	0	4
c.192C>G	p.Asp64Glu	0.0001	0	4
c.176C>G	p.Thr59Ser	0.0005	0.0003	4
c.169A>G	p.Ile57Val	0.0001	0	4
c.155A>G	p.His52Arg	0.0002	0	4
c.122G>T	p.Arg41Leu	0.0002	0	4
c.71C>G	p.Pro24Arg	0.0007	0.0003	4
c.9G>A	p.Met3Ile	0.0001	0	4

ALS-associated missense changes found within EOGT in 4493 sporadic ALS patients and 1924 controls. Mutations are listed 5' to 3'; EOGT has 15 exons and is encoded on the reverse strand of chromosome 3; exons 1 to 3 are non-coding.

Appendix 2. There is no significant ALS-association within *GLT8D1* when exon 4 is excluded.

DNA Change	Protein Change	Phenotype	ExAC Frequency	CADD Score	Exon
c.C1236T	p.R362Q	1 Control	0	33	10
c.A1178C	p.Y342X	1 Control	0.000008	35	10
c.C1089T	p.G313R	1 Control	0.000008	34	10
c.G894A	p.A248T	1 Control	0	31	8
c.C841T	p.R230H	1 Control	0.000008	29.9	8
c.G780A	p.R210C	1 Control, 2 ALS	0.00002	34	7
c.C481T	p.R110Q	1 Control	0.000008	34	4
c.G480A	p.R110W	1 Control	0.000008	29.5	4
c.G162A	p.R4C	1 Control	0.000008	29.4	2

Appendix 3. Aggregated enhancers linked to all genes within the 'amyotrophic lateral sclerosis' KEGG (Kyoto Encyclopaedia of Genes and Genomes) pathway.

Gene	p-value
BAD	0.02221442
BAX	0.32923386
BCL2	0.25897525
BCL2L1	0.38104716
BID	0.58361372
CASP3	0.32392291
CASP9	0.42946696
MAPK14	1
DAXX	0.07895007
GRIA1	0.68124886
GRIN2A	0.47640112
GRIN2C	0.16599534
GRIN2D	0.32923386
MAP3K5	0.7188191
NEFH	0.29623818
PPP3CA	0.91044659
PPP3CC	0.34407071
PPP3R1	0.28431081
MAPK13	0.05794358
PRPH2	0.62749869
SLC1A2	0.75739592
TNFRSF1A	0.89456041
TNFRSF1B	0.41763245
CCS	0.57698862
ALS2	0.15502367
CHP2	0.42141032
DERL1	0.89857213

Appendix 4. Genetic variation within *TBK1* enhancers is significantly associated with ALS.

Gene Target	Chromosome	Start	Finish
TBK1	chr12	64976982	64978649
TBK1	chr12	64849299	64852075
TBK1	chr12	64855048	64856317
TBK1	chr12	65194398	65194833
TBK1	chr12	65139887	65142519
TBK1	chr12	64349522	64350375
TBK1	chr12	64988381	64990575
TBK1	chr12	64852385	64854077
TBK1	chr12	65058182	65079989
TBK1	chr12	64479266	64484481
TBK1	chr12	64943421	64943781
TBK1	chr12	64953898	64955793
TBK1	chr12	64490881	64493995

Appendix 5. There is significant overlap between enhancers and ALS-associated variants linked to *CAV1* and *CAV2*.

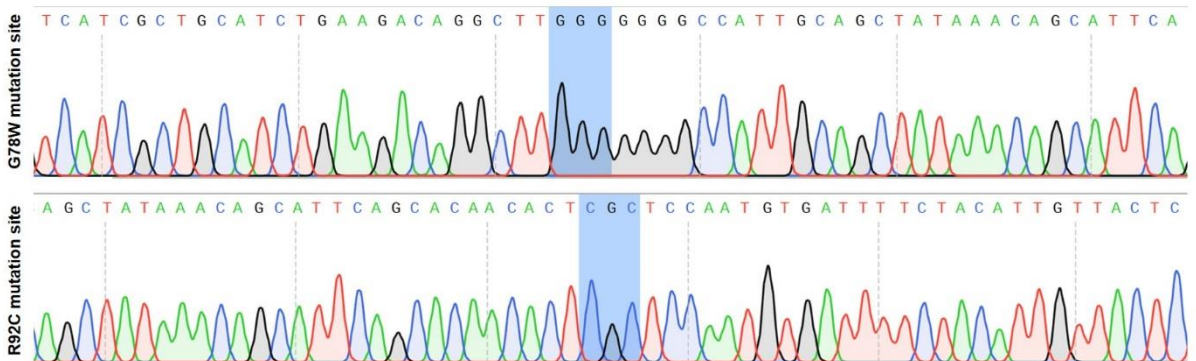
Variants	ALS Frequency	Control Frequency	Coding Gene
chr7:115899988:T:C	0.00022	0	CAV1:CAV2
chr7:115900605:A:G	0.00022	0	CAV1:CAV2
chr7:115994269:C:T	0.00044	0	CAV1:CAV2
chr7:115994303:G:A	0.00044	0	CAV1:CAV2
chr7:115994310:A:G	0	0.00052	CAV1:CAV2
chr7:115994595:T:G	0.00022	0	CAV1:CAV2
chr7:115994627:T:C	0.00022	0	CAV1:CAV2
chr7:115994719:G:A	0.00089	0.00104	CAV1:CAV2
chr7:115994770:C:G	0.00022	0	CAV1:CAV2
chr7:115994869:C:T	0.00022	0	CAV1:CAV2
chr7:115994875:C:T	0.00022	0	CAV1:CAV2
chr7:115995110:A:G	0.00044	0	CAV1:CAV2
chr7:115995386:G:A	0	0.00052	CAV1:CAV2
chr7:115995411:C:G	0.00022	0	CAV1:CAV2
chr7:115996247:A:G	0.00022	0	CAV1:CAV2
chr7:115996338:G:C	0.00022	0	CAV1:CAV2
chr7:115996639:T:G	0.00022	0	CAV1:CAV2
chr7:116034151:T:C	0.00022	0	CAV1:CAV2
chr7:116035733:C:A	0.00044	0	CAV1:CAV2
chr7:116152216:C:T	0.00022	0.00104	CAV1:CAV2
chr7:116198357:C:T	0.00089	0	CAV1:CAV2
chr7:116199522:T:C	0.00022	0	CAV1:CAV2
chr7:116200589:T:A	0.00022	0	CAV1:CAV2
chr7:116200705:C:T	0.00022	0	CAV1:CAV2
chr7:116200719:C:A	0.00022	0	CAV1:CAV2
chr7:116200953:A:T	0.00022	0	CAV1:CAV2
chr7:116200959:G:T	0	0.00052	CAV1:CAV2
chr7:116201160:T:C	0	0.00052	CAV1:CAV2
chr7:116201160:T:G	0	0.00052	CAV1:CAV2
chr7:116211360:G:A	0.00044	0.00468	CAV1:CAV2
chr7:116211574:C:T	0.00067	0.00052	CAV1:CAV2
chr7:116212628:A:G	0.00022	0	CAV1:CAV2
chr7:116212861:A:G	0.00022	0	CAV1:CAV2
chr7:116213876:A:T	0.00022	0.00104	CAV1:CAV2
chr7:116217283:C:G	0.00022	0	CAV1:CAV2
chr7:116222625:T:C	0.00044	0	CAV1:CAV2
chr7:116223328:A:G	0.00067	0.00052	CAV1:CAV2
chr7:116223448:C:T	0.00022	0	CAV1:CAV2
chr7:116224152:G:A	0.00200	0.00727	CAV1:CAV2
chr7:116474819:G:T	0.00067	0	CAV1
chr7:115957412:G:A	0.00022	0	CAV2
chr7:115957415:T:C	0.00022	0	CAV2
chr7:115957440:G:A	0.00022	0	CAV2
chr7:115957498:C:A	0.00022	0	CAV2
chr7:115957577:G:A	0.00022	0.00052	CAV2
chr7:116004321:G:A	0.00044	0	CAV2
chr7:116063605:A:G	0	0.00052	CAV2
chr7:116063624:T:C	0.00022	0	CAV2
chr7:116064199:T:C	0.00022	0	CAV2
chr7:116087637:G:A	0.00022	0	CAV2
chr7:116181928:T:C	0	0.00052	CAV2
chr7:116182530:A:G	0.00022	0	CAV2
chr7:116182646:A:G	0.00067	0.00312	CAV2
chr7:116182790:T:C	0	0.00052	CAV2
chr7:116184017:A:T	0.00912	0.00987	CAV2
chr7:116184130:T:A	0.00044	0	CAV2
chr7:116232009:G:C	0	0.00052	CAV2
chr7:116233640:T:C	0	0.00052	CAV2

Appendix 6. Sanger sequencing traces of pEGFP-N1_GLT8D1-eGFP vectors. Sequencing was performed using a CMV forward primer (sequence: CGCAAATGGGCGGTAGGCGTG).

pEGFP-N1_GLT8D1-WT clone

ATG start codon shown in green. Site of p.G78W mutation shown in purple (GGG codes for glycine), site of p.R92C mutation shown in red (CGC codes for arginine). Neither mutation are present.

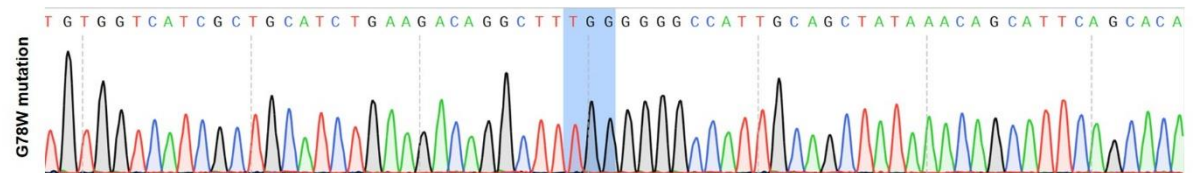
ATGTCATTCCGTAAGTAAACATCATCATCTTGGTCCTGGCTGTTGCTCTCTTCTTACTGGTTTTGCACCATAACTTCCTCAGCTTGAGCAGTTTGTTAAGGAATGAGGTTACAGATTAGGAATTGTAGGGCCTCAACCTATAGACTTTGTCCCAAATGCTCTCCGACATGCAGTAGATGGGAGACAAGAGGAGATTCTGTGGTCATCGCTGCATCTGAAGACAGGCTT**GGG**GGGGCCATTGCAGCTATAAACAGCATTACAGCACAACACT**CGC**TCCAATGTGATTTTCTACATTGTTACTCTCAACAATACAGCAGACCATCTCCGGTCTGGCTCAACAGTGATTCCCTGAAAAGCATCAGATACAAAATTGTCAATTTTGACCCTAACTTTTGAAGGAAAAGTAAAGGAGGATCCTGACCAGGGGGAATCCATGAAACCTTTAACCTTTGCAAGGTTCTACTTGGCCAAATTCTGGTCCCAGCGCAAAGAAGGCCATATACATGGATGATGATGTAATTGTGCAAGGTGATATTCTTGCCCTTTACAATACAGCACTGAAGCCAGGACATGCAGCTGCATTTTCAGAAGATTGTGATTGAGCCTCTACTAAAGTTGTCATCCGTGGAGCAGGAAACCAGTACAATTACATTGGCTATCTTGACTATAAAAAGGAAAGAATTCGTAAGCTTCCATGAAAGCCAGCACTTGCTCATTTAATCCTGGAGTT



pEGFP-N1_GLT8D1-G78W clone

ATG start codon shown in green. p.G78W mutation shown in purple (TGG codes for tryptophan).

ATGTCATTCCGTAAGTAAACNTNATCATCTTGGTCCTGGCTGTTGCTCTCTTCTTACTGGTTTTGCACCATAACTTCCTCAGCTTGAGCAGTTTGTTAAGGAATGAGGTTACAGATTAGGAATTGTAGGGCCTCAACCTATAGACTTTGTCCCAAATGCTCTCCGACATGCAGTAGATGGGAGACAAGAGGAGATTCTGTGGTCATCGCTGCATCTGAAGACAGGCTT**TGG**GGGCCATTGCAGCTATAAACAGCATTACAGCACAACACTCGCTCCAATGTGATTTTCTACATTGTTACTCTCAACAATACAGCAGACCATCTCCGGTCTGGCTCAACAGTGATTCCCTGAAAAGCATCAGATACAAAATTGTCAATTTGACCCTAACTTTTGAAGGAAAAGTAAAGGAGGATCCTGACCAGGGGGAATCCATGAAACCTTTAACCTTTGCAAGGTTCTACTTGCCAATTCTGGTCCCAGCGCAAAGAAGGCCATATACATGGATGATGATGTAATTGTGCAAGGTGATATTCTTGCCCTTACAATACAGCACTGAAGCCAGGACATGCAGCTGCATTTTCAGAAGATTGTGATTGAGCCTCTACTAAAGTTGTCATCCGTGGAGCANGAAACCAGTACAATTACATTGGCT

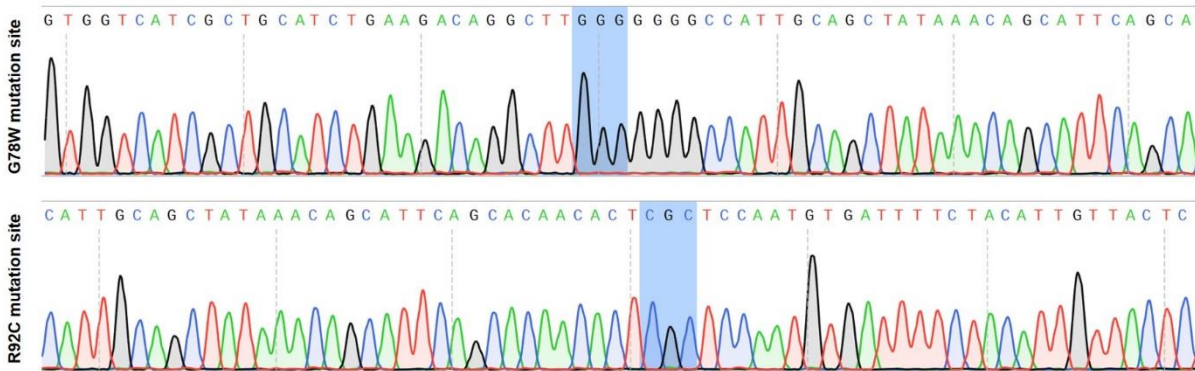


Appendix 8. Sanger sequencing traces of pcDNA5/FRT/TO_3xFLAG-GLT8D1 vectors. Sequencing was performed using a CMV forward primer (sequence: CGCAAATGGGCGGTAGGCGTG).

pcDNA/FRT/TO_3xFLAG-GLT8D1-WT clone

ATG start codon shown in green. Site of p.G78W mutation shown in purple (GGG codes for glycine), site of p.R92C mutation shown in red (CGC codes for arginine). Neither mutation are present.

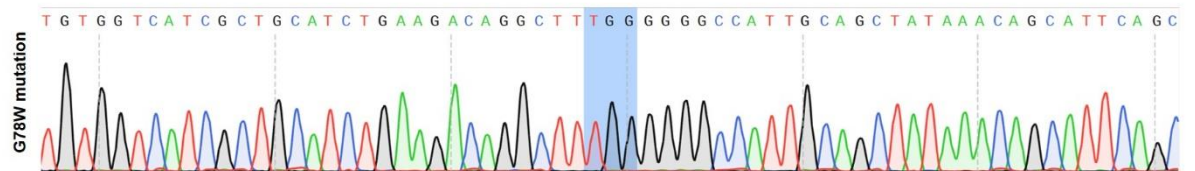
ATGGACTACAAAGACCATGACGGTGATTATAAAGATCATGACATCGATTACAAGGATGACGATGACAAGGGATCAATGT
 CATTCCGTAAAGTAAACATCATCATCTTGGTCCTGGCTGTTGCTCTCTTCTTACTGGTTTTGCACCATAACTTCCTCAG
 CTTGAGCAGTTTGTAAAGGAATGAGGTTACAGATTCAGGAATTGTAGGGCCTCAACCTATAGACTTTGTCCCAAATGC
 TCTCCGACATGCAGTAGATGGGAGACAAGAGGAGATTCTGTGGTCATCGCTGCATCTGAAGACAGGCTT**GGG**GGG
 GCCATTGCAGCTATAAACAGCATTTCAGCACAACACT**CGC**TCCAATGTGATTTTCTACATTGTTACTCTCAACAATACAG
 CAGACCATCTCCGGTCCTGGCTCAACAGTGATTCCCTGAAAAGCATCAGATACAAAATTGTCAATTTGACCCTAAAC
 TTTTGAAGGAAAAGTAAAGGANGATCCTGANACAGGGGGAATCCATGAAACCTTTAACCTTTGCAAGGT



pcDNA/FRT/TO_3xFLAG-GLT8D1-G78W clone

ATG start codon shown in green. p.G78W mutation shown in purple (TGG codes for tryptophan)

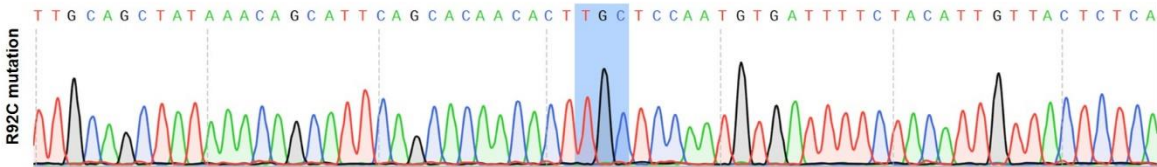
ATGGACTACAAAGACCATGACGGTGATTATAAAGATCATGACATCGATTACAAGGATGACGATGACAAGGGATCAATGT
 CATTCCGTAAAGTAAACATCATCATCTTGGTCCTGGCTGTTGCTCTCTTCTTACTGGTTTTGCACCATAACTTCCTCAG
 CTTGAGCAGTTTGTAAAGGAATGAGGTTACAGATTCAGGAATTGTAGGGCCTCAACCTATAGACTTTGTCCCAAATGC
 TCTCCGACATGCAGTAGATGGGAGACAAGAGGAGATTCTGTGGTCATCGCTGCATCTGAAGACAGGCTT**TGG**GGG
 GCCATTGCAGCTATAAACAGCATTTCAGCACAACACTCGCTCCAATGTGATTTTCTACATTGTTACTCTCAACAATACAG
 CAGACCATCTCCGGTCCTGGCTCAACAGTGATTCCCTGAAAAGCATCAGATACAAAATTGTCAATTTGACCCTAAAC
 TTTTGAAGGAAAAGTAAAGGAGGATCCTGACCAGGGGGAATCCATGAAACCTTTAACCTTTGCAAGGTTCT



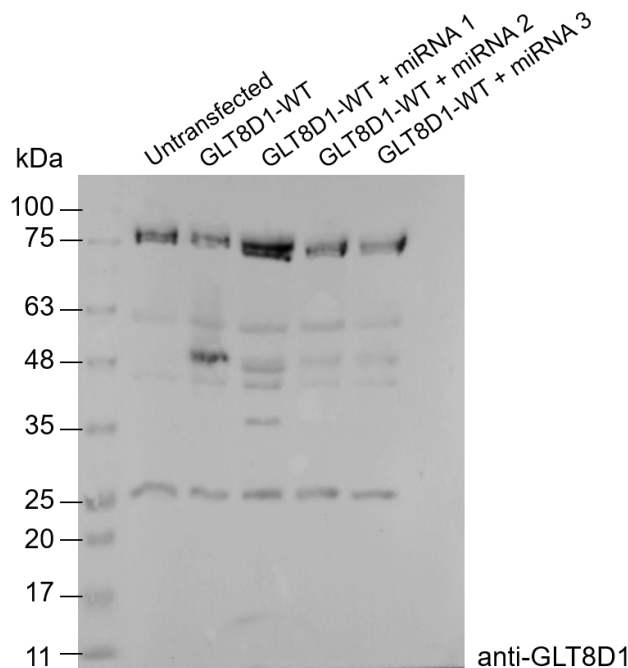
pcDNA/FRT/TO_3xFLAG-GLT8D1-R92C clone

ATG start codon shown in green. p.R92C mutation shown in red (TGC codes for cysteine)

ATGGACTACAAAGACCATGACGGTGATTATAAAGATCATGACATCGATTACAAGGATGACGATGACAAGGGATCAAT
GTCATTCCGTAAAGTAAACATCATCATCTTGGTCCTGGCTGTTGCTCTCTTCTTACTGGTTTTGCACCATAACTTCCT
CAGCTTGAGCAGTTTGTAAAGGAATGAGGTTACAGATTGAGGAATTGTAGGGCCTCAACCTATAGACTTTGTCCCAA
ATGCTCTCCGACATGCAGTAGATGGGAGACAAGAGGAGATTCTGTGGTCATCGCTGCATCTGAAGACAGGCTTG
GGGGGCCATTGCAGCTATAAACAGCATTGAGCACAACACT**TGC**TCCAATGTGATTTTCTACATTGTTACTCTCAAC
AATACAGCAGACCATCTCCGGTCTGGCTCAACAGTGATTCCCTGAAAAGCATCAGATACAAAATTGTCAATTTTGA
CCCTAAACTTTTGAAGGAAAAGTAAAGGAGGATCCTGACCAGGGGAATCCATGAAACCTTTAACCTTTGCAAGG
TTCTACTTGCCAATTCTGGTTCCAGCGCAAAGAANGCCATATACATGGATGATGATGTAATTGTGCAAGGTGATATT
CTTGCCCTTTACAATACAGCACTGAAGCCAGGACATGCAGCTGC



Appendix 9. Representative blot using a commercially available anti-GLT8D1 antibody (GeneTex; #GTX123636) to assess specificity following targeted knockdown of GLT8D1 in HEK293 cells using miRNAs. Antibody specificity is masked by the presence of multiple bands.

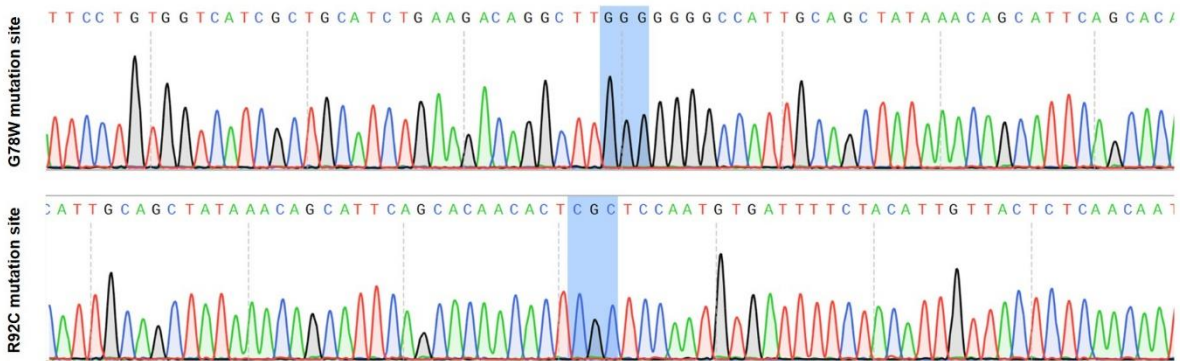


Appendix 10. Sanger sequencing traces of PCS2+_GLT8D1 vectors for the *in vitro* synthesis of capped mRNA for zebrafish embryo microinjection. Sequencing was performed using a CMV forward primer (sequence: CGCAAATGGGCGGTAGGCGTG).

PCS2+_GLT8D1-WT clone

ATG start codon shown in green. Site of p.G78W mutation shown in purple (GGG codes for glycine), site of p.R92C mutation shown in red (CGC codes for arginine). Neither mutation are present.

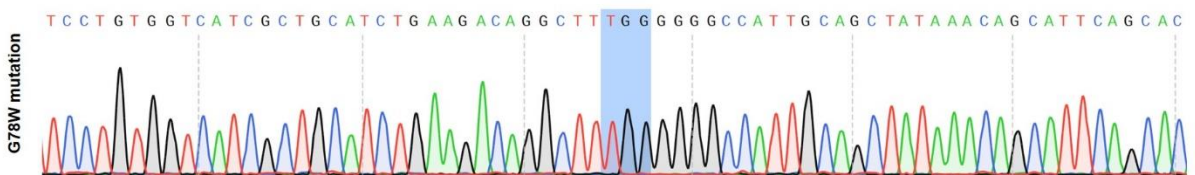
ATGTCATTCCGTAAAGTAAACATCATCATCTTGGTCCNGNCTGNTGCTCTCTTCTTACTGGTTTTGCACCATAAATTCTN
 AGCTTGAGCAGTTTGTAAAGGAATGAGGTTACAGATTACAGGAATTGTAGGGCCTCAACCTATAGACTTTGTCCCAAATGC
 TCTCCGACATGCAGTAGATGGGAGACAAGAGGAGATTCTGTGGTCATCGCTGCATCTGAAGACAGGCTT**GGG**GGGGC
 CATTGCAGCTATAAACAGCATTACGCACAACACT**CGC**TCCAATGTGATTTTCTACATTGTTACTCTCAACAATACAGCAGAC
 CATCTCCGGTCTCTGGCTCAACAGTGATTCCCTGAAAAGCATCAGATACAAAATTGTCAATTTTGACCCTAACTTTTGGAA
 GGAAAAGTAAAGGAGGATCCTGACCAGGGGGAATCCATGAAACCTTTAACCTTTGCAAGGTTTACTTGCCAATTCTGGT
 TCCCAGCGCAAAGAAGGCCATATACATGGATGATGATGTAATTGTGCAAGGTGATATTCTTGCCCTTTACAATACAGCACT
 GAAGCCAGGACATGCAGCTGCATTTTCAGAAGATTGTGATTCAGCCTCTACTAAAGTTGTCATCCGTGGAGCANGAAAC
 CAGTACAATTACATTGGCTATCTTGACTATAAAAAGGAAAGAATTCGTAAGCTTTCCATGAAAGCCAGCACTTGCTCATTTA
 ATCCTGGAGTT



PCS2+_GLT8D1-G78W clone

ATG start codon shown in green. p.G78W mutation shown in purple (TGG codes for tryptophan).

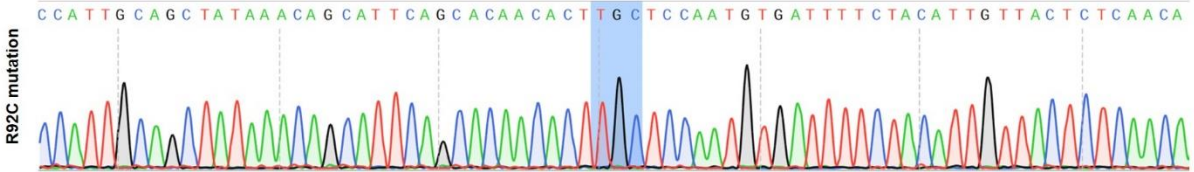
ATGTCATTCCGTAAAGTAAACATCATCATCTTGGTCCCTGGCTGTTGCTCTCTTCTTACTGGTTTTGCACCATAAATTCTCCT
 CAGCTTGAGCAGTTTGTAAAGGAATGAGGTTACAGATTACAGGAATTGTAGGGCCTCAACCTATAGACTTTGTCCCAAAT
 GCTCTCCGACATGCAGTAGATGGGAGACAAGAGGAGATTCTGTGGTCATCGCTGCATCTGAAGACAGGCTT**TGG**GG
 GGCCATTGCAGCTATAAACAGCATTACGCACAACACTCGCTCCAATGTGATTTTCTACATTGTTACTCTCAACAATACAG
 CAGACCATCTCCGGTCTCTGGCTCAACAGTGATTCCCTGAAAAGCATCAGATACAAAATTGTCAATTTTGACCCTAACT
 TTTGGAAGGAAAAGTAAAGGAGGATCCTGACCAGGGGGAATCCATGAAACCTTTAACCTTTGCAAGGTTTCTACTTGCC
 AATTCTGGTTCCAGCGCAAAGAAGGCCATATACATGGATGATGATGTAATTGTGCAAGGTGATATTCTTGCCCTTTACA
 ATACAGCACTGAAGCCAGGACATGCAGCTGCATTTTCAGAAGATTGTGATTCAGCCTCTACTAAAGTTGTCATCCGTGG
 AGCAGGAAACCAGTACAATTACATTGGCT



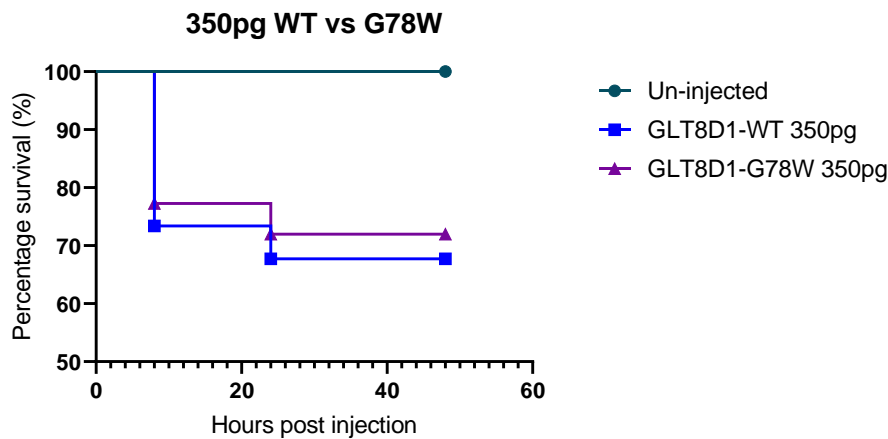
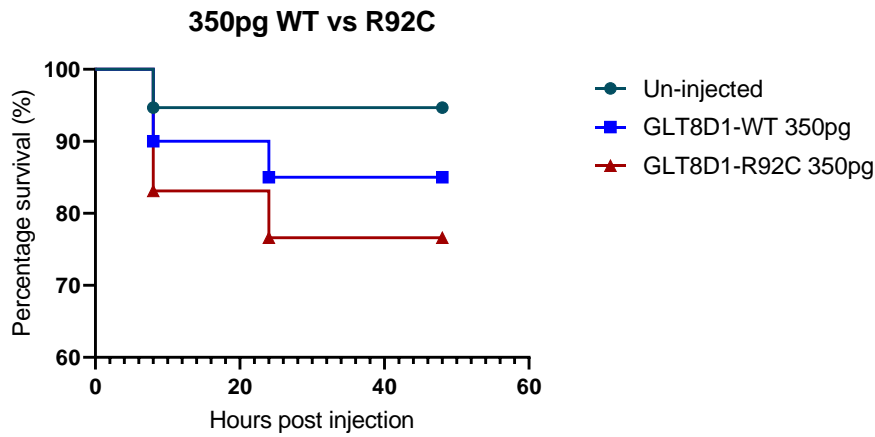
PCS2+ _GLT8D1-R92C clone

ATG start codon shown in green. p.R92C mutation shown in purple (TGC codes for cysteine).

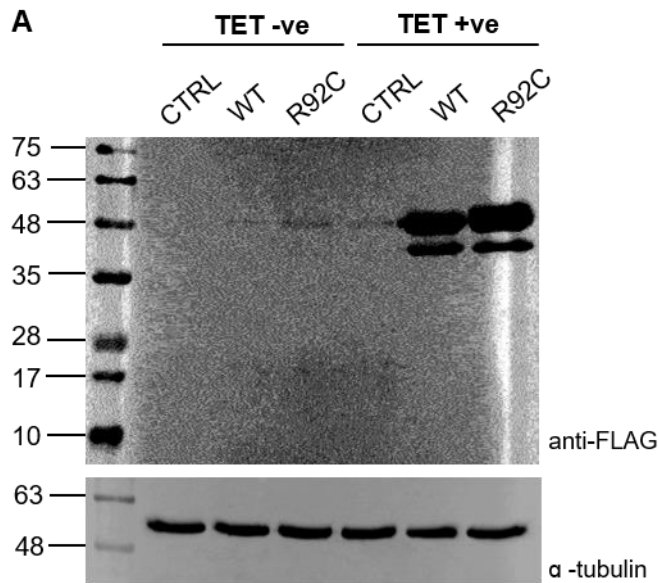
ATGCTCTCTTCTTACTGGTTTTGCACCATAACTTCCTCAGCTTGAGCAGTTTGTTAAGGAATGAGGTTACAGATTCAGG
 AATTGTAGGGCCTCAACCTATAGACTTTGTCCCAATGCTCTCCGACATGCAGTAGATGGGAGACAAGAGGAGATTCC
 TGTGGTCATCGCTGCATCTGAAGACAGGCTTGGGGGGGCCATTGCAGCTATAAACAGCATTACAGACAACACT**TGC**T
 CCAATGTGATTTTCTACATTGTTACTCTCAACAATACAGCAGACCATCTCCGGTCCTGGCTCAACAGTGATTCCCTGAA
 AAGCATCAGATACAAAATTGTCAATTTTGACCCTAACTTTTGAAGGAAAAGTAAAGGAGGATCCTGACCAGGGGGA
 ATCCATGAAACCTTTAACCTTTGCAAGGTTCTACTTGCCAATTCTGGTTCAGCGCAAAGAAGGCCATATACATGGAT
 GATGATGTAATTGTGCAAGGTGATATTCTTGCCCTTTACAATACAGCACTGAAGCCAGGACATGCAGCTGCATTTTCAG
 AAGATTGTGATTCAGCCTCTACTAAAGTTGTCATCCGTGGAGCANGAAACCAGTACAATTACATTGGCTATCTTGACTAT
 AAAAAGGAAAAGAAATTCGTAAGCTTTCCATGA



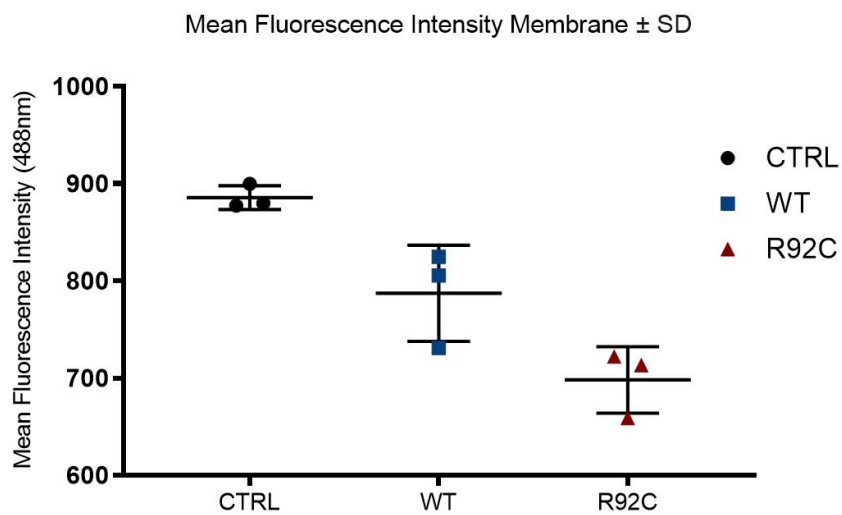
Appendix 11. Zebrafish survival data presented in the form of Kaplan-Meier survival curves.



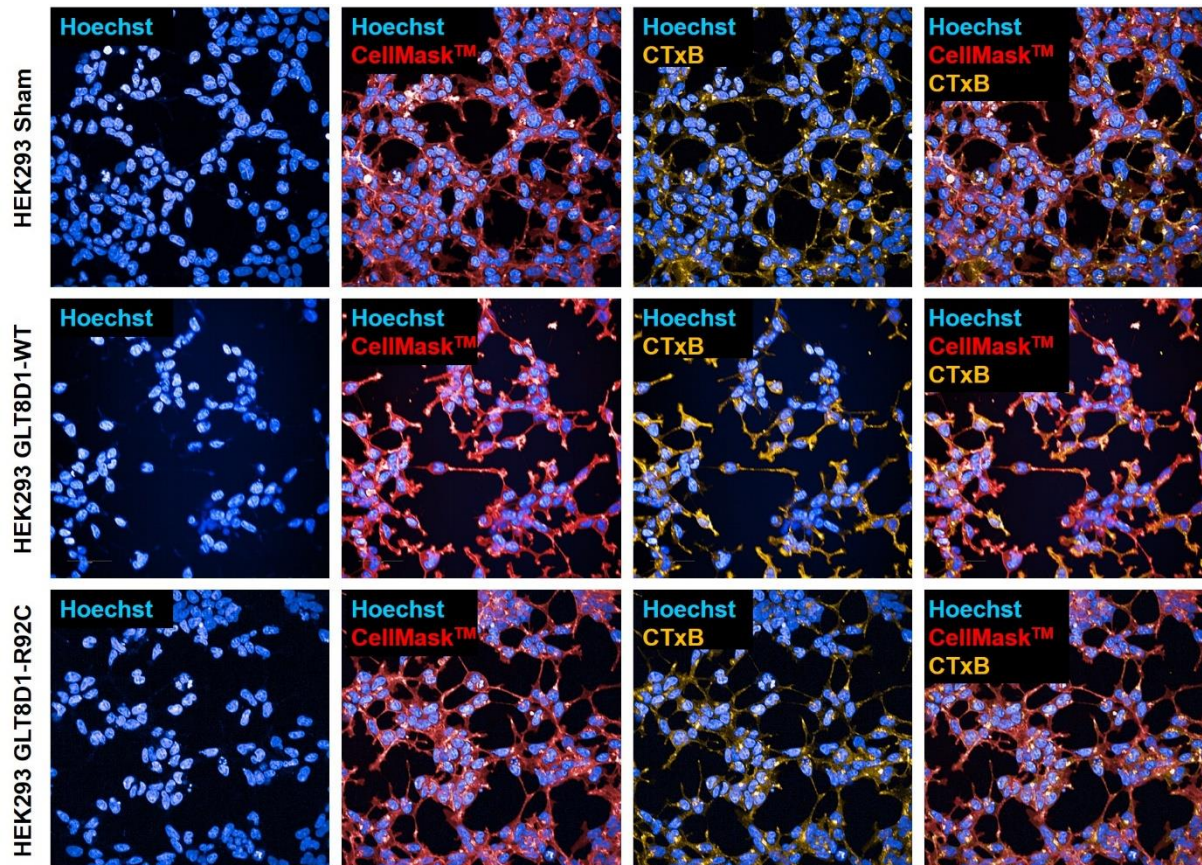
Appendix 12. Protein bands in un-induced stable HEK293 cells expressing GLT8D1-WT and GLT8D1-R92C were only made visible following overexposure of the image.



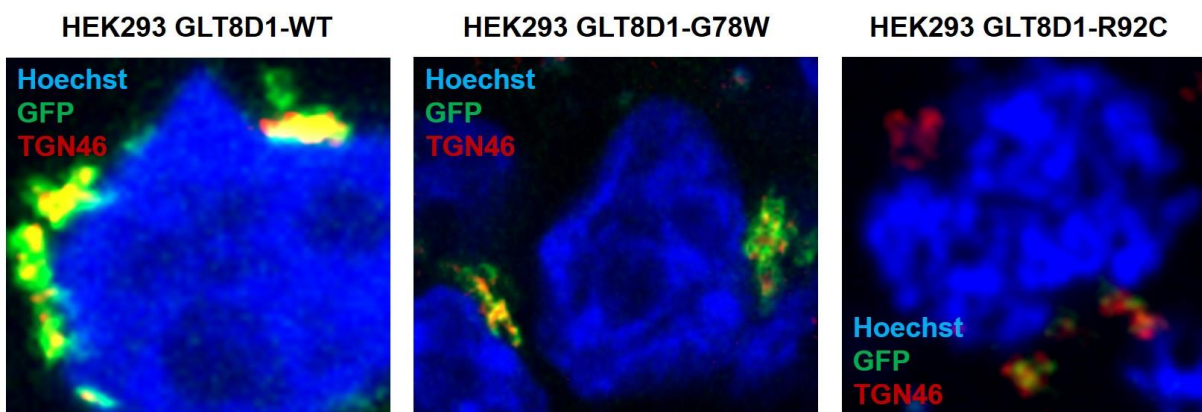
Appendix 13. WGA fluorescence intensity was also measured in the absence of tetracycline, showing a modest but non-significant decline in fluorescence intensity in the mutant line compared to WT (n=3, unpaired *t*-test $p > 0.05$).



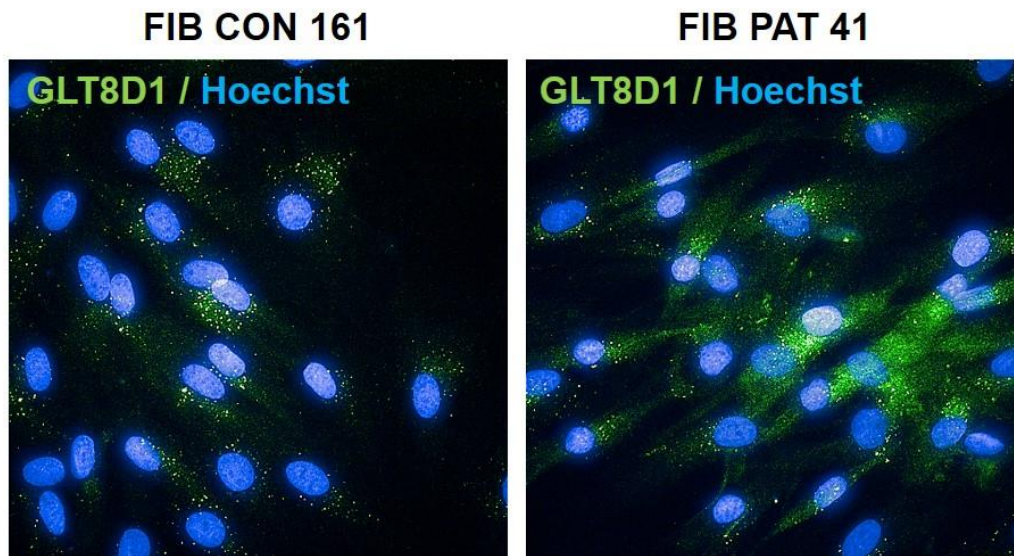
Appendix 14. Representative images of sham-transfected HEK293 cells, and stable isogenic HEK293 cells with tetracycline induced expression of GLT8D1-WT and GLT8D1-R92C. Cells were co-labelled with a CellMask™ plasma membrane stain (red) to identify cell regions and for accurate quantification of cell area.



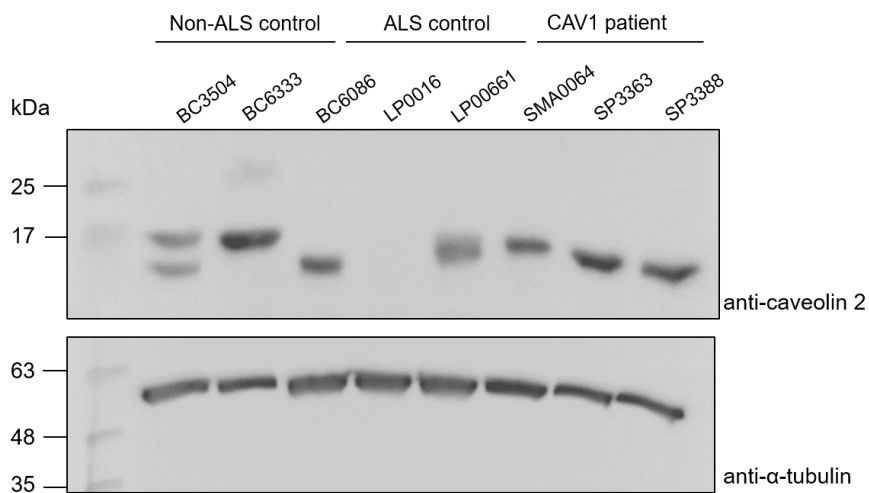
Appendix 15. The presence of either a G78W or R92C mutation in GLT8D1 does not affect the Golgi localisation signal.



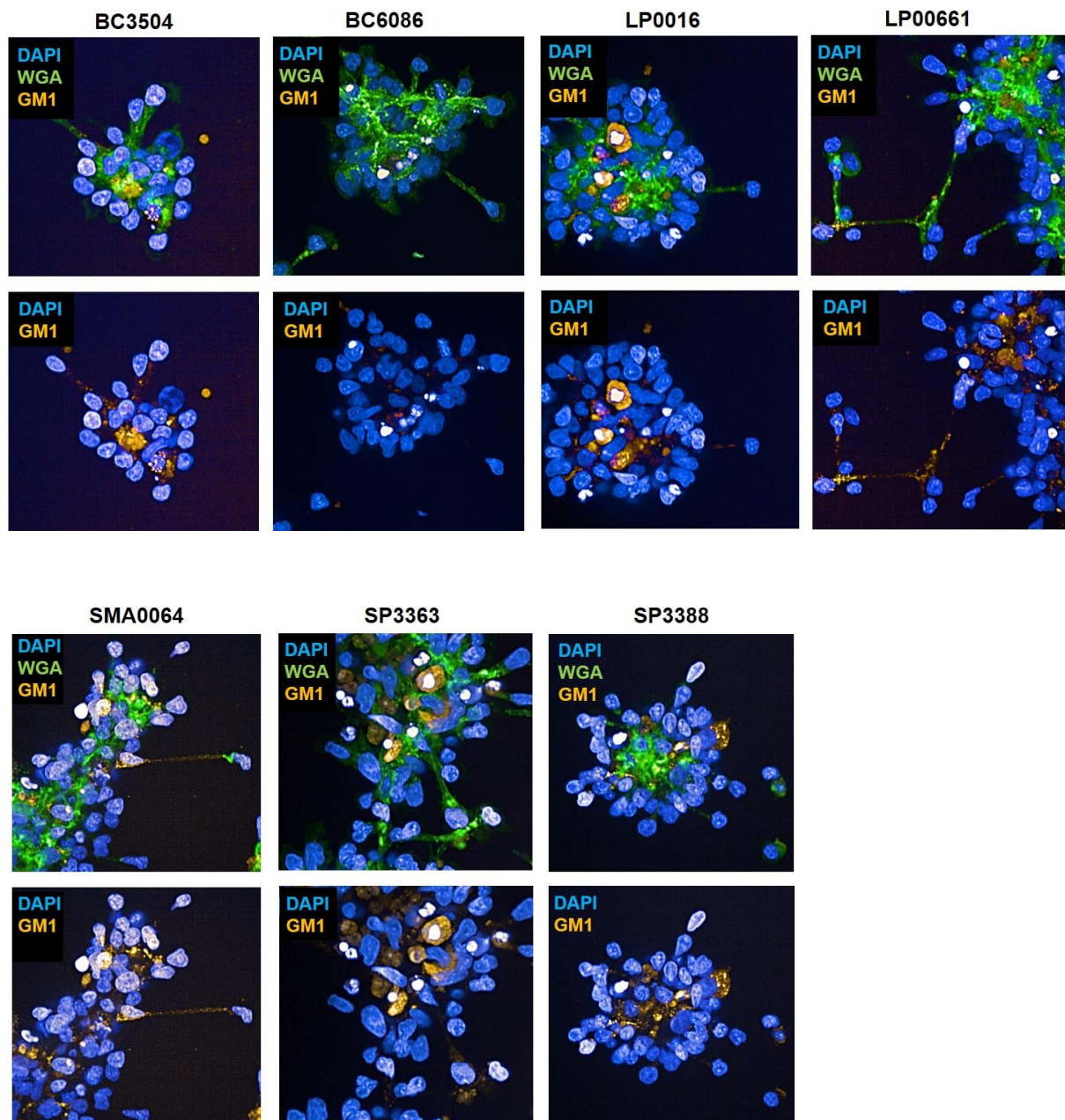
Appendix 16. Representative immunostaining of GLT8D1-ALS patient and age- and sex-matched control fibroblasts using a commercially available anti-GLT8D1 antibody (green) (GeneTex; #GTX123636). A weak fluorescence signal and diffuse staining suggests lack of antibody specificity.



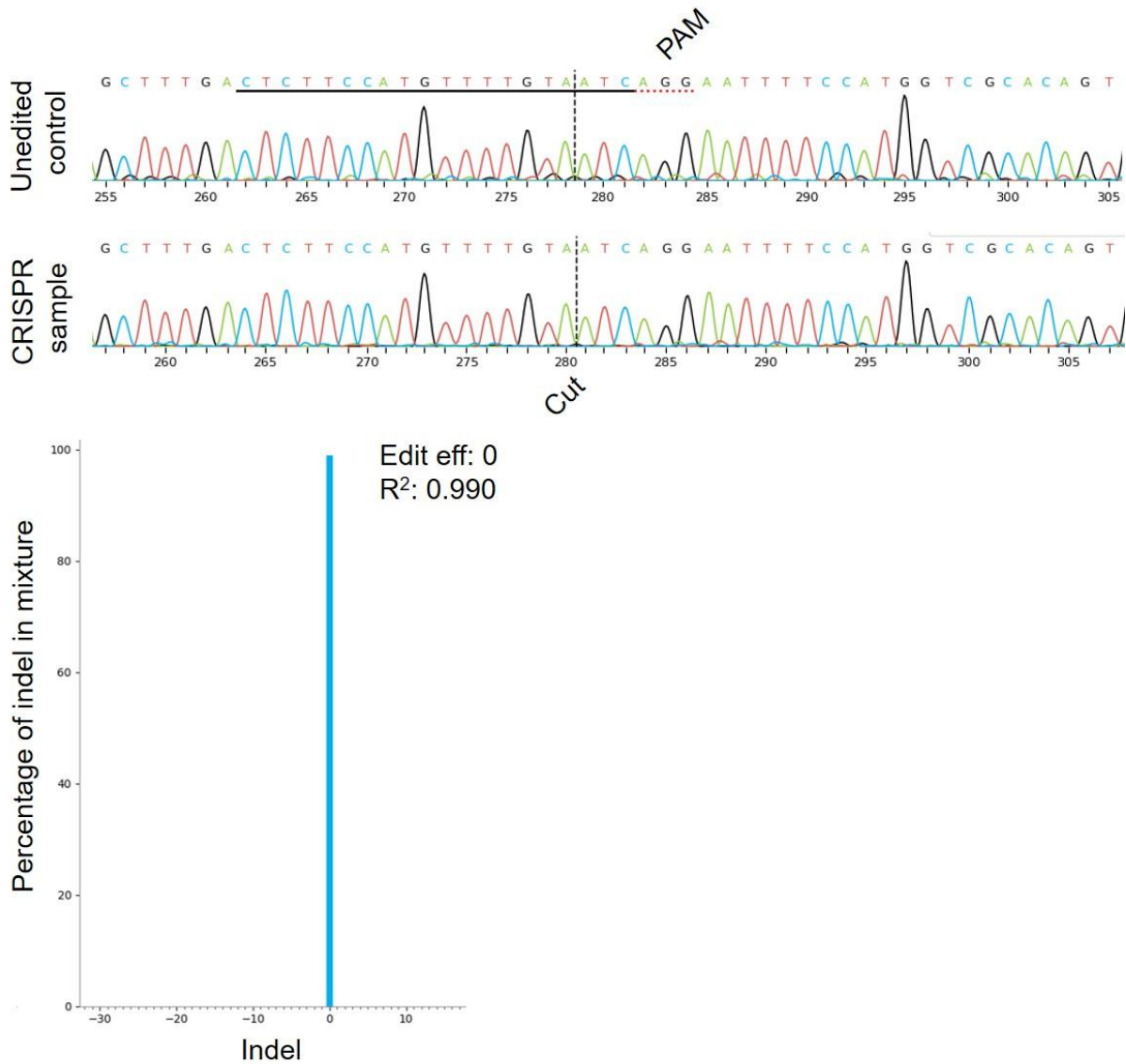
Appendix 17. Representative immunoblot for CAV2. Multiple bands detecting inconsistent molecular weights suggests a lack of antibody specificity.



Appendix 18. Representative images of all LCLs probed with CTxB and WGA.

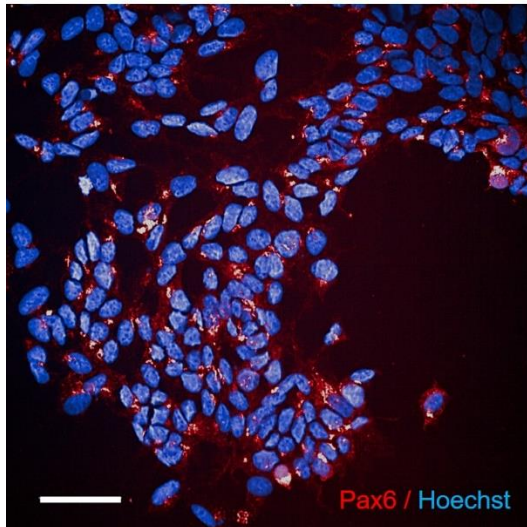


Appendix 19. CRISPR editing efficiency in LCLs using the PX459 plasmid. Sequencing traces for HPRT control and CAV1 mutant are shown. Analysis using ICE demonstrates 0% editing efficiency.

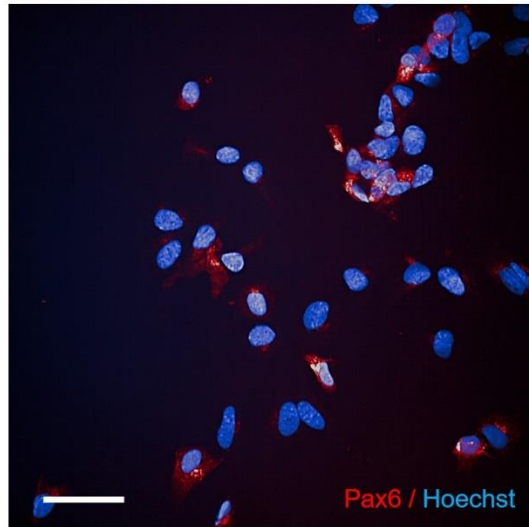


Appendix 20. Representative images of Pax6 staining in undifferentiated and differentiated SH-SY5Y cells. Images show unedited cells or cells with a CRISPR-mediated HPRT mutation.

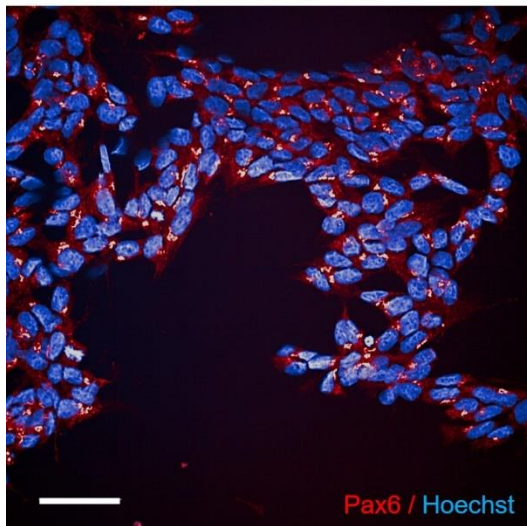
**SH-SY5Y undifferentiated
(CRISPR HPRT)**



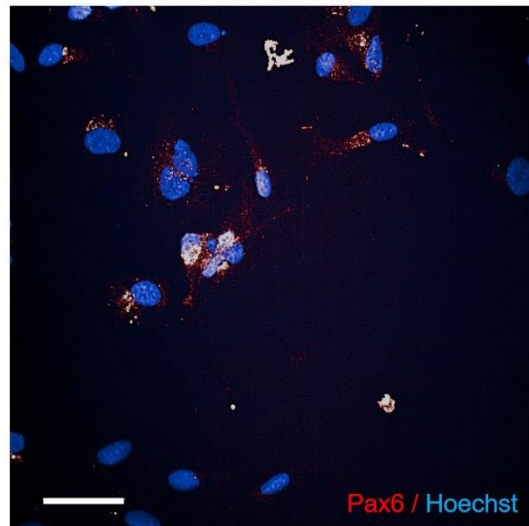
**SH-SY5Y differentiated
(CRISPR HPRT)**



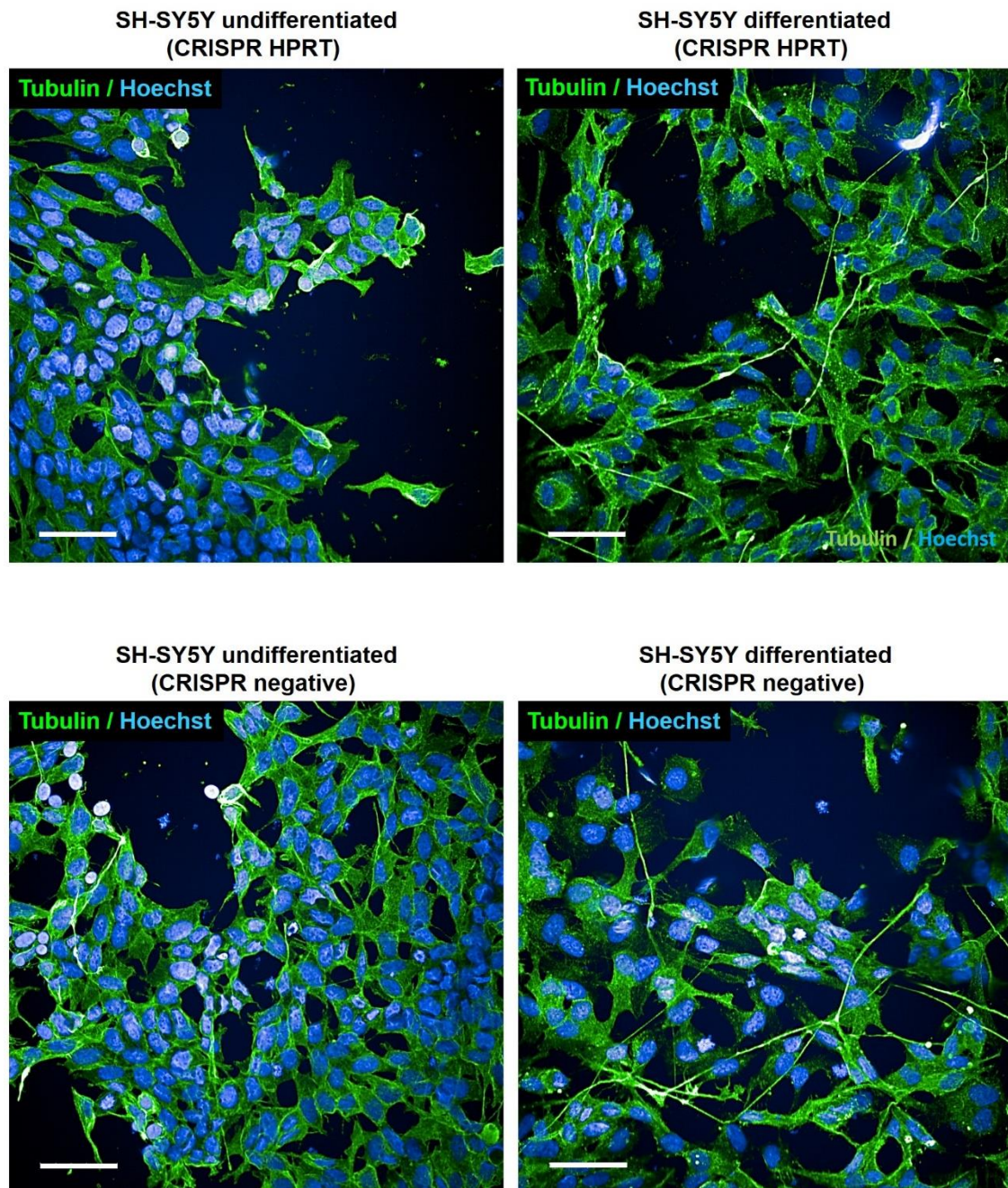
**SH-SY5Y undifferentiated
(CRISPR negative)**



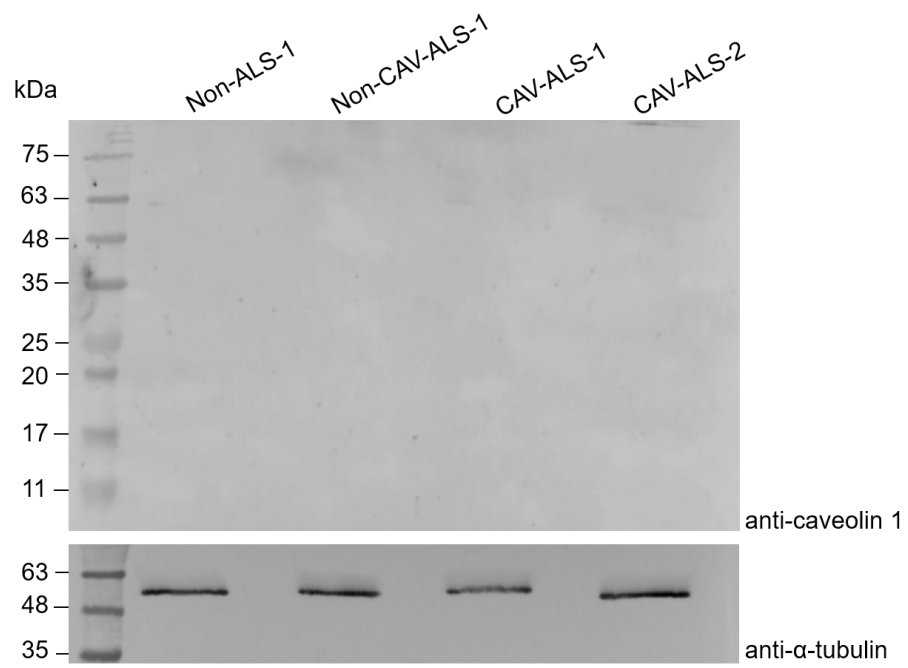
**SH-SY5Y differentiated
(CRISPR negative)**



Appendix 21. Representative images of α -tubulin staining in undifferentiated and differentiated SH-SY5Y cells. Images show unedited cells or cells with a CRISPR-mediated HPRT mutation.



Appendix 22. Representative blot following lysis of LCLs using IP lysis buffer. A signal was not detected when probed with a validated anti-caveolin-1 antibody.



Research outputs from the work of my PhD

Publications:

1. Moll, T., Cooper-Knock, J. & Shaw, P. (2020) Disrupted glycosylation of lipids and proteins is a cause of neurodegeneration, **Brain**. Awz358: 1-9.
2. Cooper-Knock, J., Moll, T. et al. (2019) Mutations in the glycosyltransferase domain of GLT8D1 are associated with familial amyotrophic lateral sclerosis, **Cell Reports**. 26(9): 2298-2306.

Submitted manuscripts:

1. Cooper-Knock, J., Zhang, S., Kenna, K., Moll, T. et al. (2020) Rare variant burden analysis within enhancers identifies *CAV1* as a new ALS risk gene. Available at https://papers.ssrn.com/sol3/papers.cfm?abstract_id=3606796

Conference presentations:

1. Moll, T., Cooper-Knock, J., Beer, A., Hobbins, H., Higginbottom, A., Hautbergue, G., Castelli, L., Ramesh, T., Kirby, J. and Shaw, P. **Mutations in the glycosyltransferase domain of GLT8D1 are associated with familial amyotrophic lateral sclerosis.** Motor Neurone Disease Association International Symposium, Perth (2019). Poster presentation.
2. Moll, T., Cooper-Knock, J., Beer, A., Hobbins, H., Higginbottom, A., Hautbergue, G., Castelli, L., Ramesh, T., Kirby, J. and Shaw, P. **Mutations in the glycosyltransferase domain of GLT8D1 are associated with familial amyotrophic lateral sclerosis.** Sheffield Medical School Research Meeting, Sheffield (2019). Platform presentation. Recipient of the 1st place oral presentation prize.
3. Moll, T., Cooper-Knock, J., Beer, A., Hobbins, H., Higginbottom, A., Hautbergue, G., Castelli, L., Ramesh, T., Kirby, J. and Shaw, P. **Mutations in the glycosyltransferase domain of GLT8D1 are associated with familial amyotrophic lateral sclerosis.** European Network to Cure ALS Meeting, Tours (2019). Poster presentation.
4. Moll, T., Cooper-Knock, J., Beer, A., Hobbins, H., Higginbottom, A., Hautbergue, G., Castelli, L., Ramesh, T., Kirby, J. and Shaw, P. **Mutations in the glycosyltransferase domain of GLT8D1 cause amyotrophic lateral sclerosis.** Motor Neurone Disease Association International Symposium, Glasgow (2018). Platform presentation.
5. Moll, T., Cooper-Knock, J., Beer, A., Hobbins, H., Higginbottom, A., Hautbergue, G., Castelli, L., Ramesh, T., Kirby, J. and Shaw, P. **Characterisation of a novel genetic variant of amyotrophic lateral sclerosis leads to a new disease pathway.**

European Network to Cure ALS Meeting, Oxford (2018). Poster presentation.
Recipient of a poster presentation prize.

Supervisory experience:

- **Think Ahead Sheffield Undergraduate Research Experience.** Experience designing a project and supervising an undergraduate student for an 8-week period. £3000 awarded in funding from the Wellcome Trust.
- **Nuffield Foundation Research Placement.** Experience supervising an A-level STEM student for a 5-week period.

Public engagement:

- Organiser of 'Soak a Scientist' to raise funding and awareness for ALS research (2018, 2019).
- Volunteer for the Sheffield Outreach Programme (2018-present).
- Volunteer for the Medical Research Council Festival at Sheffield Winter Gardens (2019).